Theoretical and Experimental Investigations on Critical Multiphase Flows in Safety Relief Valves and Nozzles

Supervisor: Dr. William Dempster

Author: Moftah Salem Moftah Alshaikh

A Thesis presented for the degree of Doctor of Philosophy

Department of Mechanical and Aerospace Engineering

University of Strathclyde,

Glasgow, UK

February, 2016

Dedicated to

My Father, My Mother,

My Wife, My Daughters

My Brothers, My Sisters

Abstract

Two-phase gas/liquid critical flows are in general complex due to the existence of mass, momentum and heat transfer between phases. In this study these processes have been investigated in a safety relief valve where the complex geometry introduces multiple choking points, shock waves, rapid accelerations involving rapid state changes of velocity, pressure and temperature and flow regime changes. These effects influence to a different degree the valve mass flowrate and the forces acting on the valve and thus the rating and dynamic response when in operation. At present no predictive tools are available for design evaluation of safety valves operating under two phase conditions. In this thesis the ability of the standard two fluid model to predict such processes is investigated.

Two fluid (Euler-Euler) multi-dimensional modelling approaches with a mixture k-Ɛ turbulence model to predict such conditions are investigated. The study has been divided into two stages: firstly, for fixed mass fraction conditions air-water two phase critical flows through a conventional spring loaded safety relief valve commonly used in the refrigeration industry have been carried out experimentally and computationally. Secondly, to extend the study to thermal non equilibrium conditions investigations of steam-water two phase flows through a converging-diverging nozzle have been performed computationally. In the first stage, experiments have been carried out for a range of pressures (4.8 - 13.8 bar), a wide range of water fractions (0 - 0.89) and for various different opening positions of the valve disc. Quasi steady flow has been assumed appropriate and valve flow-lift and force-lift characteristics have been obtained, which determine the capacity of the valve to control pressure, the sizing of the spring and the dynamics of the valve during operation. Comparison with the simplified homogenous mixture model will show that this model tends to underestimate mass flowrates for medium to high liquid mass fraction. Force and flow scaling parameters have been explored for use in valve design under various multiphase flow conditions. In the second stage, for thermal non equilibrium conditions the numerical calculations have been made for a range of pressures (1.34 - 1.89 bar), a range of water mass fractions (0 – 0.36). The computational predictions of mass flowrate compare well with experimental data from the literature.

In general, the two fluid model can adequately account for mechanical non equilibrium for these complex flow conditions with the use of simplified droplet sizing rules. Thus the CFD Euler-Euler model predictions have been found in good agreement with the experimental data. For thermal non equilibrium where phase changes dominate less progress was achieved and further investigated required.

Declaration

This thesis is the result of the author's original research. It has been composed by the author and has not been previously submitted for examination which has led to the award of a degree.

Acknowledgments

I would like to seize this unique opportunity to acknowledge my gratefulness concerning Dr. William Dempster's continuous support and co-operation. I would then like to express my sincere appreciation to him for his confidence in my ability to deliver this research work. I am very grateful to him for his encouragement through the years. I would like also to extend my thanks to my parents, brothers and sisters. Special thanks go to my beloved wife and also I wish her a success in her PhD. Last but not least, my thanks should go also to my lovely daughters Salsabil (Loly) and the wee one Sulaf (Saly)!

Table of Contents

List of Figures

Figure5-

Figure5-

List of Tables

Nomenclature

a Acceleration (m/s^2) a_s
Sound speed (m/s)
A Area (m^2)
C Constant (-)
C_D Drag coefficient (-)
d_p Droplet diameter (m)
E Total specific energy (J/kg)
f Drag factor (-) F
Force (N)
g Gravitational acceleration (m/s^2)
G Mass flux (kg/m^2.s)
G_k The generation of turbulence kinetic energy
due to the mean velocity gradients(J/kg)
G_b The generation of kinetic energy due to buoyancy
(J/kg)
k Turbulence kinetic energy (m^2/s^2)
K Thermal conductivity (W/m. K)
L Piston lift (mm) m Mass
(kg)
$\dot{m}$ Mass flowrate (kg/s)
M Mach number (-)
M_W Molecular weight (g/mol) N_{u_p}
Nusselt number (-)

P Pressure (Pa)

P_r Prandtl Number (-)

R Universal gas constant (J/mol. K)

Re Relative Reynolds number (-)

S The modulus of the mean rate-of-strain tensor

t Time (s)

T Temperature (K)

u Velocity component (m/s)

v Specific volume (m^3/kg) $\vec{V}$

Phase velocity (m/s)

x Coordinate direction

x_a Air mass fraction (-)

x_w Water mass fraction (-)

Y_M The contribution of the fluctuating dilatation in compressible turbulence to the overall dissipation rate (J/kg)

Greek Symbols

α Air volume fraction

$(1-\alpha)$ Water volume fraction

λ Volumetric heat transfer coefficient (W/m^3)

γ Heat capacity ratio (-)

c_P Specific heat at constant pressure (J/kg.k) δ_{ij} Kronecker delta

ε Turbulent dissipation rate (m^2/s^3)

η Pressure ratio (-)

μ Viscosity (kg/m.s)

ρ Density (kg/m^3)

σ Turbulent Prandtl number

τ Stress tensor (N/m^2)

τ_V Velocity response time (s)

τ_T Thermal response time (s)

ω Compressibility factor (-)

Subscript

a Air

atm Atmospheric

abs Absolute *crit*

Critical *d*

Discharge d_r

Drift *D* Drag eff

Effective G Gas

phase i Free

index j Free

index k

Turbulent kinetic

energy l Free

index L Liquid

phase m Mixture

N Normalised

o Stagnation condition

p Secondary phase

q Primary phase *seat*

Seat

t Turbulent w

Water

Ɛ Turbulent kinetic energy rate of dissipation

Chapter One

1 Introduction

1.1 Introduction and Project Rationale

In a wide variety of engineering systems such as heat exchangers, power systems, fluid transport systems and chemical plant, safe operation is achieved by the use of safety relief valves (SRV) to limit excessive pressure levels. The safety valve is normally closed to seal the pressurised system; however, it operates by discharging a volume of fluid from within the system as soon as a predetermined maximum pressure is reached. Two generic terms of

“safety valve” and “safety relief valve” are often used to describe this standard type of device utilized. The importance of safety valves operating correctly is reflected in the multitude of national standards that exist. These provide guidance on operating requirements, sizing, material quality etc. but largely leave the design process to the designer. Until recently this has been largely build and test based with final compliance to the standards through testing on accredited facilities. This indicates the need to guarantee the correct operation of the safety valves but also reflects the complexity of the device, particularly the flow physics. This study can be seen as one in a limited number that attempts to use correct developments in flow simulation techniques to improve the valve designer’s ability to design valves and reduce testing time. The particular focus is the two phase flow design of valves.

The flow path through the valve is complex and generally multi-dimensional distinguishing it from previous detailed modelling studies of critical flow where simple nozzles have been examined. This is on account of sharp edges and sudden curvature characterising the valve geometry. The complex behaviour of gas flows in safety relief valves is also associated with various flow phenomena such as turbulence, viscous effect, shock waves and critical flow conditions. Noise and vibration on most industrial applications can be allied to the aforementioned phenomena. Analysis of single phase flows and the determination of mass flows in safety valves is largely understood both experimentally and theoretically with CFD approaches having being successfully applied [15][88][113]. However, the more complex two phase flow also occurs in many industrial systems such as power plant, chemical and nuclear reactor vessels and results from cavitation, steam condensation and boiling, level swell and chemical reaction process occurring in the upstream components due to depressurisation. In fact, two phase flow becomes more complicated when encountered in small geometries such as safety valves with high velocity and high compressibility. The operation of safety valves under two-phase flow conditions is less well understood particularly when mechanical and thermal non equilibrium effects due to phase change occur. Here the rapid expansion in the valve often results in liquid flashing or droplet condensation depending on the upstream initial conditions. The resulting mass, momentum and heat exchange between the phases control the critical flow conditions which determine the valve flowrate. For two phase flow conditions, safety relief valve performance is significantly different from that of single phase flow conditions. The aforementioned non equilibrium effects make prediction of the two phase flow behaviour more difficult and complex.

To accomplish a level of valve performance required for safety relief valves deployed for two phase flow conditions, a procedure of safety valve design based only on experimental measurements and trial and error process are the norm. Due to the lack of knowledge and complexity of two phase flows, the experiment can be considered as a reliable procedure even though it is expensive and time consuming. Despite the existence of codes and standards for the selection and sizing of safety relief valves, there is no direct design methodology to be followed. At present the most widely accepted methods of predicting the relieving capacity of valves under two-phase flow conditions are the algebraic based homogenous equilibrium model (HEM) developed by Leung, [97] or the homogenous nonequilibrium model of Diener and Schmidt (HNEM-DS) proposed in ISO-4126-10,[106]. Unfortunately, most of the international standard design methods have led to either oversizing or undersizing of conventional safety relief valves [88]. In fact, this reflects an obvious uncertainty in safety relief valve design procedures and confirms that safety relief valve design is not an easy task. Furthermore, undersizing of the valve will lead to a deficiency in safety valve operation and results in a high risk; whereas the oversizing of the valve may lead to an over pressure in the downstream piping system, resulting in higher design cost. Moreover, an oversize valve may lead to a greater loss of system process fluid and also may result in valve stability issues.

Although the continuous improvement of two phase physical models and numerical methods makes simulations of the very complex flows in safety valves now possible, there are only a limited number of publications establishing their capability. According to the literature survey conducted, one attempt by Dempster and Elmayyah [115] -it is believed to be the first if not the only study- aimed at predicting the critical flow condition through a conventional safety relief valve using a simplified CFD mixture model for the multiphase airwater flows. The study showed good agreement between the CFD results and the experiments up to 40% liquid mass fraction. Interestingly the HEM method of Darby [84] and the CFD results also matched these conditions. However, an increasing discrepancy of the order of 15% under prediction was evident for larger liquid mass fractions from 40 to 90%. For the larger liquid mass fractions it was surmised that the effects of non-equilibrium increased due to the increase in liquid inertia, leading to an increase in velocity slip and an increase in liquid thermal inertia resulting in poorer mass flow predictions. This study investigates these issues further by examining the use of a CFD Euler-Euler two fluid model to account for the non-equilibrium effects and

investigate the capability of established closure models to predict the valve mass flows and forces exerted on the piston. The CFD simulations will provide detailed quantification and visualisations of the valve internal flow hence the impact of geometry variations in valve design could be assessed before the manufacturing process. A conventional spring loaded safety relief valve, depicted in Figure1.1, commonly used for refrigeration industry has been examined for both conditions of single and two phase flows. In addition, this type of safety relief valve is easy to install and use and provides an opportunity for low cost experimentation. To improve the design, control and selection of safety relief valves for various operating conditions, the mass flow exhausted and the associated net piston forces are the most relevant characteristics of a safety valve which should be well understood. The opening and closing process of the safety valve can be linked directly to the fluid forces and the spring resistance. As a consequence, the piston displacement along with the resulting discharge flowrate play a dominant role in determining the forces exerted on the piston. Hence, the most essential features of the valve performance will be obtained from the flow-lift and force-lift characteristics of the safety valve. The latter concept of the valve characteristics under steady state flow conditions is considered as the initial design approach for safety valves. Although experimental measurements will not provide much detail on the valve internal flow structure, they will be of importance to validate the CFD predictions. Thus an in-house test rig has been developed to generate multiphase flow conditions and facilitate the measurements of pressure, temperature, force and flowrate.

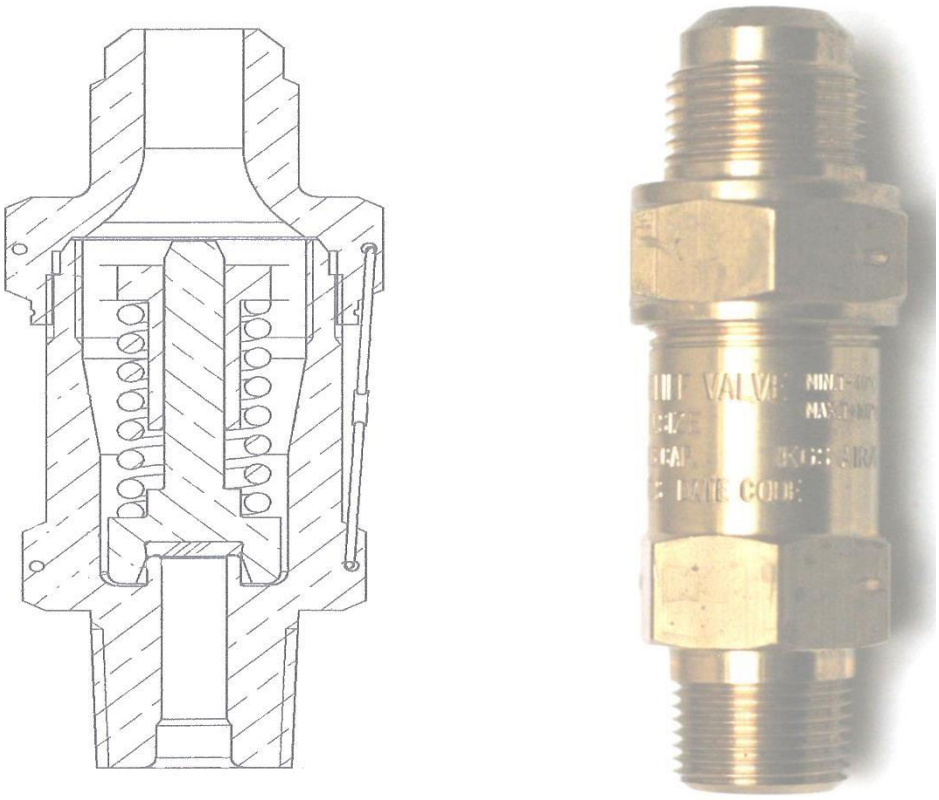

Figure1-1: Safety Valve Assembly

The operation of the valve is mainly a dynamic process therefore exceeding the opening pressure (the set pressure) leads to the piston lifting to allow mass to discharge via an available flow area. The piston lift relies essentially on the increasing system pressure which is expected to be limited due to the greater flow discharged. However, this work is simplified as quasi static conditions are postulated assuming that pressure waves can be ignored. Thus the flow in the valve is adequately represented by a series of steady state conditions. It is expected that this would be more appropriate for the closing operation of a safety relief valve than the opening phase.

Previous models for predicting valve two phase flow conditions tend to be based on simple algebraic approaches but have been effective at predicting mass flowrate and the sizing of discharge flow areas. However, the objective is valve design then a more detailed knowledge relating valve geometry to flow characteristics is required. Given the relative complexity of the flow geometry (Figure1.1) the approach most likely lead to success is multi-dimensional modelling using CFD techniques. In addition the question of appropriate two phase models

needs addressing. The flows in the valve result in high speed compressible conditions and generally result in a dispersed droplet flow possibly including liquid films. As will be discussed in Chapter 3, some success has been achieved in using reduced two-fluid models, particularly in high speed flows in turbine nozzles with condensing steam flows. In this study we have chosen to use full Euler-Euler models, partly because the mass fraction range is very wide but mainly because we seek a general two phase flow model for a safety relief valve that can be coupled to upstream vessel condition where a variety of two phase flow regimes are possible.

The modelling framework for investigating the two-fluid model will be the commercial CFD ANSYS FLUENT and will address two phase flows where no mass exchange is present, in a frozen flow. This will use air and water as the working fluids. Therefore, a number of models will be developed for a range of piston lifts at different single (air) and two phase (air-water) flow conditions to model the valve at various piston positions. The ANSYS CFD FLUENT Code will be implemented to solve the Euler-Euler two fluid model that represents the valve geometry and flow path using two dimensional axi-symmetric assumptions. In terms of experimental work, pressure, temperature, lift, force and air and water mass flowrate will be fundamentally the measured properties.

However, the study will be extended to flows where thermal non equilibrium dominates by investigating high speed flows in nozzles. At present the lack of additional studies using valve geometries that are available in the literature and practical limitations of time and resources in this study has prevented non equilibrium experiments in valves from being available. Furthermore, building a new rig facility related to mixtures of steam-water flows in a safety relief valve, even a small scale, were considered outwith the scope of the study. Therefore, modelling of two phase critical flashing flows of steam-water mixtures in a converging-diverging nozzle will be investigated instead. However detailed experimental data for nozzles provided by Charless [150] will be used to validate the two-fluid model developed and the associated evaporation-condensation mass transfer mechanisms.

1.2 Thesis Objectives

This study aims to achieve the following objectives:

- Investigate and develop CFD models for the prediction of single phase flow through safety valves.
- Investigate and develop CFD models for the prediction of two phase flow through safety valves for mechanical and thermal non equilibrium but with no mass exchange (frozen flows of air-water mixtures).
- Develop an experimental test rig to validate the above mentioned CFD models of single and two phase flow conditions, under frozen flow conditions using air and water.
- Define an approach to assist in safety relief valve scaling under multiphase flow conditions based on an analysis of the data obtained.
- Investigate and develop CFD models for the prediction of two phase flow through nozzles for non-equilibrium conditions with mass exchange (flashing flows of steamwater mixtures).

1.3 Thesis Layout

After an introduction to this study and the presentation of the studies objectives in Chapter1, Chapter2 presents a historical background to safety relief valves, valve function and definition, standards and approval authorities for safety valves, design and operation.

Chapter 3 reviews the literature of single phase flows of air and two phase frozen flows of air-water mixtures in safety relief valves. A literature review of two phase flashing flows of steam-water mixtures in nozzles and pipes, is also presented. The chapter provides a discussion on the relevant mathematical models, computational models as well as experimental works that are available in the literature.

Chapter 4 presents studies on compressible single phase flow of air in a conventional spring loaded safety relief valve. The chapter introduces details of the safety relief valve tested, test rig construction, experimental set up and the associated measurements, the computational model developed, results presented and discussed, and an approach to assist in safety relief valve design under single phase flow conditions using scaling parameters to normalise flow-lift and force-lift characteristics.

Chapter 5 presents studies on compressible two-phase flow of an air-water mixture in a conventional spring loaded safety relief valve. The chapter introduces details of the test rig construction and the associated water injection system developed, experimental procedure and the associated measurements, computational model developed, results presented and discussed, and an approach to assist in safety relief valve design under two phase flow conditions based on scaling parameters to normalise flow-lift and force-lift characteristics. The computational model is also validated against the homogenous mixture model, the analytical HEM model of Darby [84]and the HNE-DS model proposed by Diener and Schmidt [87]used by the international standards. The effects of mechanical and thermal non-equilibrium conditions of the two phase flows are addressed in detail.

Chapter 6 presents studies on compressible two-phase flashing flow of steam-water mixtures in a converging-diverging nozzle. The chapter introduces details of the nozzle and measurements required, computational model developed and the associated mass transfer model, the results are presented and discussed. The computational model is validated against the available experimental data of Charless [150].

Chapter 7 presents the conclusions and future work. The chapter is devoted to the concluding remarks and the future work of the three studies.

Chapter Two

2 Safety Relief Valves Background

2.1 Historical Background

As soon as mankind was able to boil water to create steam, the need for safety devices became evident. As long as 2000 years ago, the Chinese were using containers with hinged lids to allow relatively safer production of steam. Early in the 14th century, conical plugs and later compressed springs were used by chemists to act as safety devices on pressurised vessels. In 1680 and after several incidents of explosions, the French physicist Denis Papin successfully made the first counterweight safety relief valve for his high pressure cooker. The closing force of the safety relief valve is essentially dominated by a weight rather than a spring. Later, the counterweights were replaced by compression springs. Figure 2.1 depicts a more developed design for a simple counterweight [157]. The development of the effective safety relief valve was by Charles Retchie in 1848, who invented the

accumulation chamber that increases the compression surface, which allows the safety valve to open rapidly within a narrow overpressure margin [157]. The second successive attempt of developing safety relief valve was by William Naylor in 1863 [88].

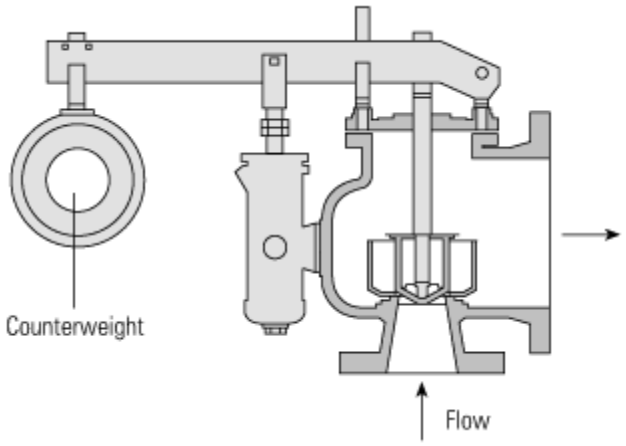

Figure 2-1: Counterweight safety relief valve

At the beginning of the 19th century, it was essential to figure out a practical way of introducing safety codes and standards. This was due to a series of boiler explosions on ships and locomotives caused by faulty safety devices. In 1911, the American Society of Mechanical Engineering (ASME) was urged to establish a design code. This was in response to 1300 deaths resulting from 1700 boiler explosions in the New England region of the USA in the period between 1905 and 1911 [157]. Thus the ASME Section VIII, Division 1, Appendix 11, Appendix M, was formulated by the Boiler and Pressure Vessels committee and became obligatory for all designers to follow. In Paragraph UG-125 (a), ASME specifically states "All pressure vessels within the scope of this division, irrespective of size or pressure, shall be provided with pressure relief devices in accordance with the requirement ofUG-125 throughUG-137." At present, every pressurised system has at least one safety relief valve. Therefore, most pressurised system users are obliged by local health and safety regulations to ensure that hazardous conditions are prevented.

2.2 Function and Definition

The fundamental function of a safety relief valve is to protect life, processes and property. The standard type of device utilized to protect pressurised systems against exceeding their maximum allowable pressure is the safety or safety relief valve. Although the safety valve is normally closed to seal the pressurised system, it operates by freeing a volume of fluid from within the system as soon as a predetermined maximum pressure is reached thereby reducing the excess pressure. At all times and for all possible over pressure conditions, the users of such safety devices should decisively assure that their safety valves are selfactuated to prevent catastrophic failure.

The terms **"safety valve"** and **"safety relief valve"** are considered to be generic terms to describe a wide range of different pressure relief devices that are deployed to protect industrial plants against excessive pressure. A variety of valves under different performance criteria are available for numerous industrial applications. These valves are designed to meet requirements of relevant national standards that govern the use of safety relief valves. However, the terms associated with safety and safety relief valves are differently defined in the available national standards. The terminologies used in Europe are noticeably different from those used in the USA. One of the most significant differences is that the term **"pressure relief valve"** denotes the safety valve in the USA whereas the term **"safety relief valve"** refers to the safety valve in Europe. However, the term "safety valve" is generally used in the USA to specifically refer to the full-lift type of safety valve in Europe.

"The ANSI PTC25.3 (American National Standards Institute)/ASME standards that are applicable to the USA defines the following generic terms:

- **Pressure relief valve -** A spring-loaded pressure relief valve which is designed to open to relieve excess pressure and to reclose and prevent the further flow of fluid after normal conditions have been restored. It is characterised by a rapidopening 'pop' action or by opening in a manner generally proportional to the increase in pressure over the opening pressure. It may be used for either compressible or incompressible fluids, depending on design, adjustment, or application. This general term includes the following generic terms:

- **Safety relief valve -** A pressure relief valve characterised by rapid opening or pop action, or by opening in proportion to the increase in pressure over the opening

pressure, depending on the application, and which may be used either for liquid or compressible fluid. In general, the safety relief valve will perform as a safety valve when used in a compressible gas system, but it will open in proportion to the overpressure when used in liquid systems, as a relief valve.

- **Safety valve -** A pressure relief valve actuated by inlet static pressure and characterised by rapid opening or pop action. Safety valves are primarily used with compressible gases and in particular for steam and air services. However, they can also be used for process type applications where they may be needed to protect the plant or to prevent spoilage of the product being processed.
- **Relief valve -** A pressure relief device actuated by inlet static pressure having a gradual lift generally proportional to the increase in pressure over opening pressure.

Relief valves are commonly used in liquid systems, especially for lower capacities and thermal expansion duty. They can also be used on pumped systems as pressure overspill devices".
"The European standard EN ISO 4126-1provides the following definition:

- **Safety valve -** A valve which automatically, without the assistance of any energy other than that of the fluid concerned, discharges a quantity of the fluid so as to prevent a predetermined safe pressure being exceeded, and which is designed to reclose and prevent further flow of fluid after normal pressure conditions of service have been restored" [157].

Table 2.1 presents the independent bodies for most countries who will examine the design and performance of a safety valve to ensure conformity with the relevant code to satisfy a customer requirement or a requirement of their insurance company before purchase. Table 2.2 shows the codes or standards that are associated with safety valves. In fact, the majority of these standards are sections within codes that are relevant to pressure containing vessels or boilers.

According to the piston lift, safety relief valves can be also classified into low, high and full lift safety relief valves. However, the aforementioned terms related to classification based lift vary for each standard or code.

The ASME classifies the pressure safety valves as follows:

- **Full lift safety valve**- for the situation where "The discharge area is not determined by the position of the disc".
- **Low lift safety valve**-for the condition when "The actual position of the disc determines the discharge area of the valve".

"The BS6759 (British Standard) defines the safety relief valves as follows:

- **Low lift safety valve** (ordinary class) - Valve member automatically lifts a distance of at least 0.042^{th} of the bore of the seating member, with an overpressure less than 10% of the set pressure.
- **High lift safety valve**- Valve member automatically lifts a distance of at least 0.083^{th} of the bore of the seating member, with an overpressure less than 10% of the set pressure.
- **Full lift safety valve**- Valve member automatically lifts to achieve a discharge area between 100% and 80% of the minimum area, with an overpressure less than 5% of the set pressure".

In addition, the safety relief valve could be classified according to its operation method into direct (loaded) and pilot operated safety relief valves. The most commonly used valves are the direct loaded safety relief valves where a direct mechanical load such as a spring or weight is inserted against a movable piston that directly acts based on an upstream fluid pressure. An auxiliary actuator to help in opening or closing the loaded safety relief valve might be employed. A pilot operated safety relief valve consists of a main valve to relieve the pressure, and a pilot to control the valve moving element that relies on the system pressure.

Typical examples of safety valves used on steam applications are illustrated in Figure 2.2. According to the work of Taras'ev and Kuzin reported by Elmayyah [88], they classified safety valves designs on their basic construction and operation, which provided a clear indication of the area of application for a wide range of safety valves.

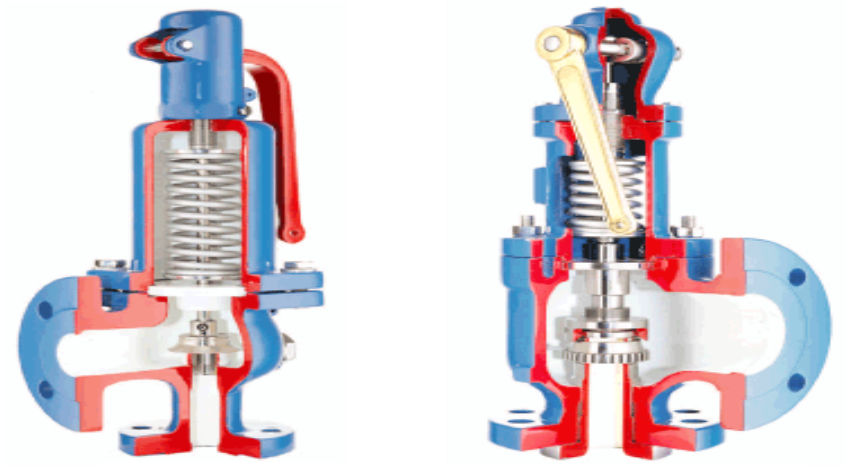

Figure2-2: Safety valves for steam

Table2-1: Approval authorities for safety valve [157]

Country	Abbreviation	Approval body
Belgium		Bureau Veritas
Canada		Ministry of Labour Canada
France		CODAP
		APAVE
Germany	TÜV	Association of Technical Supervision
	DSRK	Deutsche Schiffs-Revision und Klassifikation
Italy	ISPESL RINA	Institution of Prevention and Security Italian Register of Shipping
Korea		Ministry of Power and Resources Korean Register of Shipping
Netherlands		Dienst voor het Stoomwezen
Norway	DNV	Det Norske Veritas
UK	SAFed	Safety Assessment Federation Type Approval Service (STAS) formerly Associated Offices Technical Committee AOTC and British Engine
		Lloyds Register of Shipping
United States	NB	National Board of Boiler and Pressure Vessel Inspectors

Table2-2: Standards relevant to safety valve [157]

Country	Standard No.	Description
Australia	SAA AS1271	Safety valves, other valves, liquid level gauges and other fittings for boilers and unfired pressure vessels
European Economic Area	EN ISO 4126	Safety devices for protection against excessive pressure EN ISO 4126 is a harmonised European Standard and has replaced many National Standards of which British Standard BS 6759 and the French Standard AFNOR NFE-E 29-411 to 416 and 421 are examples.
Germany	AD-Merkblatt A2	Pressure Vessel Equipment safety devices against excess pressure - safety valves
	TRD 421	Technical Equipment for Steam Boilers Safeguards against excessive pressure - safety valves for steam boilers of groups I, III & IV
	TRD 721	Technical Equipment for Steam Boilers Safeguards against excessive pressure - safety valves for steam boilers of group II
Japan	JIS B 8210	Steam boilers and pressure vessels - spring loaded safety valves
Korea	KS B 6216	Spring loaded safety valves for steam boilers and pressure vessels
USA	ASME I	Boiler Applications
	ASME III	Nuclear Applications
	ASME VIII	Unfired Pressure Vessel Applications
	ANSI/ASME PTC 25.3	Safety and Relief Valves - performance test codes
	API RP 520	Sizing selection and installation of pressure-relieving devices in refineries
		Part 1 Design
		Part 2 Installation
	API RP 521	Guide for pressure relieving and depressurising systems
	API STD 526	Flanged steel pressure relief valves
	API STD 527	Seat tightness of pressure relief valves

Furthermore, other terms and definitions related mainly to safety relief valves operations could be presented as follows [158]:

- **Max allowable working pressure (MAWP)**

  Maximum allowable working pressure for operation, adopted as the basis for design, which varies in accordance with manufacturing standards.

- **Accumulation**

  Pressure increase over the MAWP magnitude, identified as percentage of MAWP that is allowed in the pressurised system. Maximum allowable accumulation is established by applicable codes for operating and fire incidents.

- **Set pressure (pset)**

  Predetermined pressure at which safety valves under operating conditions commence to open. It can be also defined as start of opening, opening pressure and start-to-leak pressure.

- **Cold-differential test pressure**

Pressure at which the valve is adjusted to open on the test bench, with the corrections for service conditions of back pressure and temperature are included.

- **Overpressure (ovp)**

Pressure increase over the set pressure and usually expressed as a percentage of the set pressure. The overpressure certifies the safety valves.

- **Relief pressure (p1)**

Pressure represents the sizing of a safety valve. Usually, it is greater than or equal to the set pressure plus overpressure.

- **Lift**

It defines the actual movement of the valve disc away from the closed position.

- **Coefficient of discharge**

It denotes the actual flow value from test (by manufacturer) divided by the theoretical flow value (from calculation).

- **Blowdown (bd)**

Usually, it is referred to as a percentage of the set pressure. It is the difference between the set pressure and the reseating pressure.

- **Back pressure (bd)**

Pressure on the reliving side of the safety valve (pressure in the downstream system). It represents the sum of the superimposed back and the built-up pressure.

- **Built-up back pressure**

Back pressure that caused by flow through the valve and the discharge system.

- **Superimposed back pressure**

It is constant or variable back pressure that exists at the time when the device is required to operate.

- **Flow area**

It is the minimum cross-sectional flow area between the inlet and the valve seat used to determine the value of the theoretical flow.

2.3 Design and Operation

The standard or conventional spring loaded safety valve is a simple, reliable self-acting device, which protects industrial applications against overpressure. Figure 2.3 depicts in detail the components of a safety relief valves based on the ASME and DIN standards. In reference to the figure, the presented safety relief valves have the same principle elements; however, the construction details are noticeably different. The fundamental elements of the construction comprise of a valve body, moving element (the disc), valve seat, spring and its adjuster. A nozzle representing the valve inlet is mounted directly on the pressurecontaining system. The valve inlet can be designed either as a semi-nozzle or a full-nozzle type, as shown in Figure 2.4. In addition, the valve inlet commonly referred to as “approach channel” which is the only element of the safety valve is normally exposed to the working fluid unless the valve is relieving. For process and high pressure applications, the full-nozzle inlet type is usually suggested whenever the fluid is corrosive. On the other hand, the seminozzle inlet type consists of a seating ring machined into the body, the top of which forms the seat of the valve that can be easily replaced, without replacing the entire inlet. However, the outlet of the valve could be either connected to a piped discharge system, or left open in order for the fluid to be atmospherically vented.

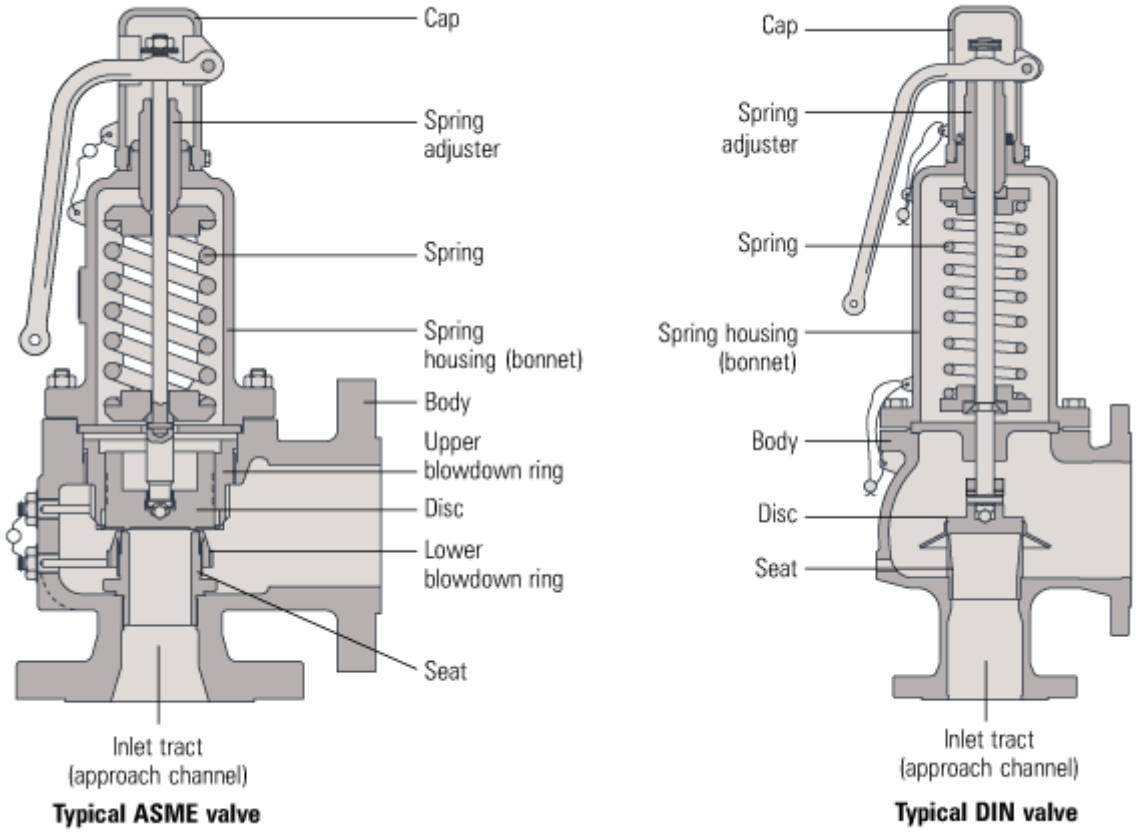

Figure2-3: Safety valves designs

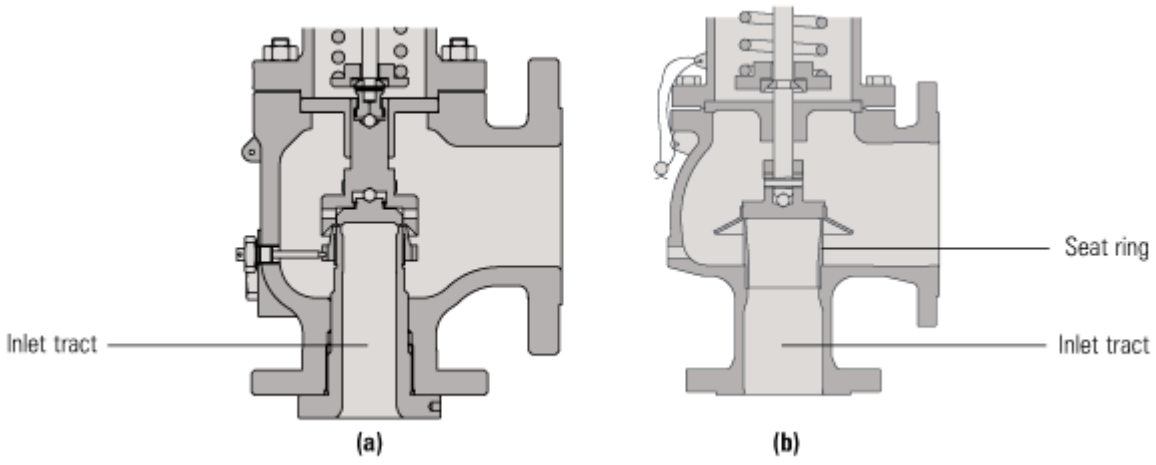

Figure2-4: A full-nozzle valve (a) & a semi-nozzle valve (b)

Under normal operating conditions, the valve spring holds the disc against the nozzle seat, which is kept in an open or closed spring housing arrangement (or bonnet) fitted on top of

the valve body. In rapid opening safety relief valves, referred to as pop type, there is a shroud or huddling chamber (disc holder), which surrounds the disc to produce the rapid opening characteristic, and also to ensure relatively small blowdown, as illustrated in Figure 2.5. The maximum allowable working pressure (MAWP) of a system determines where the safety valves should be installed. As soon as the inlet static pressure rises above the set pressure of the valve for one of the following reasons: supply of higher pressure gas or liquid, supply of external heat to the system, chemical reactions, and thermal expansion… etc.; the disc will start to lift off its seat. Concurrently the spring begins to compress resulting in a spring force increase, which means that the pressure would have to continue to rise before any further lift could occur. In order for the safety valve to commence relieving, an additional pressure rise, referred to as overpressure, is required. The overpressure is always predetermined by the standards being followed. It relies also on the particular industrial application. Hence for liquids, it is normally between10% and 25%, and for compressible fluids between 3% and 10%. The lifting magnitude of the safety relief valve is basically proportional to the pressure force that pushes the moving element against the spring force and opens the valve. This will never occur unless the fluid pressure exceeds the maximum allowable pressure of the industrial system. The movement (lifting) allows an amount of fluid to be relieved, which causes a pressure reduction of the system. The full opening (full lift) can be achieved from small overpressure by using the shroud (the hood around the disc).

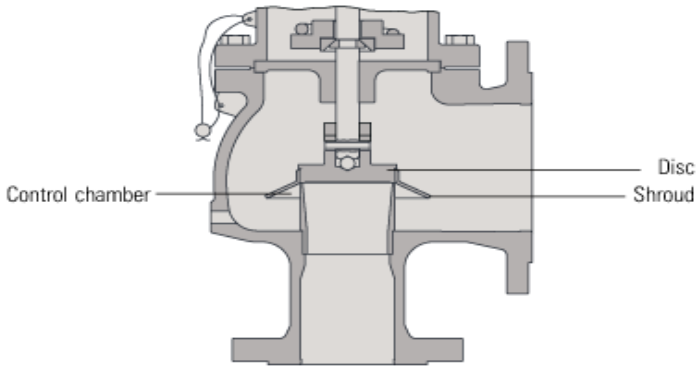

Figure2-5: Typical disc and its holder used on pop type safety relief valve

Conversely, there is a reseating stage that should occur once the relief pressure has reduced below the set pressure. At this stage, the spring force becomes greater than the fluid force and closes the valve. The pressure that the valve closes is defined as the **reseat pressure**. The difference between the set pressure and the reseat pressure is called the **blowdown**

pressure. Basic operation of a conventional safety valve is illustrated in Figure 2.6. The figure is divided into three conditions a, b and c. In condition a, the valve is closed as the disc is attached to its seat (sealing position), due to the pressure force exerted on the disc being less than the spring force. In condition b, the valve begins to open as the fluid pressure force becomes greater than the spring force at and slightly above the set pressure. At condition b fluid is being released from the system. In condition c, a much higher fluid flow exists as the valve disc lifts further due to a higher force produced by the increase in exposed disc area.

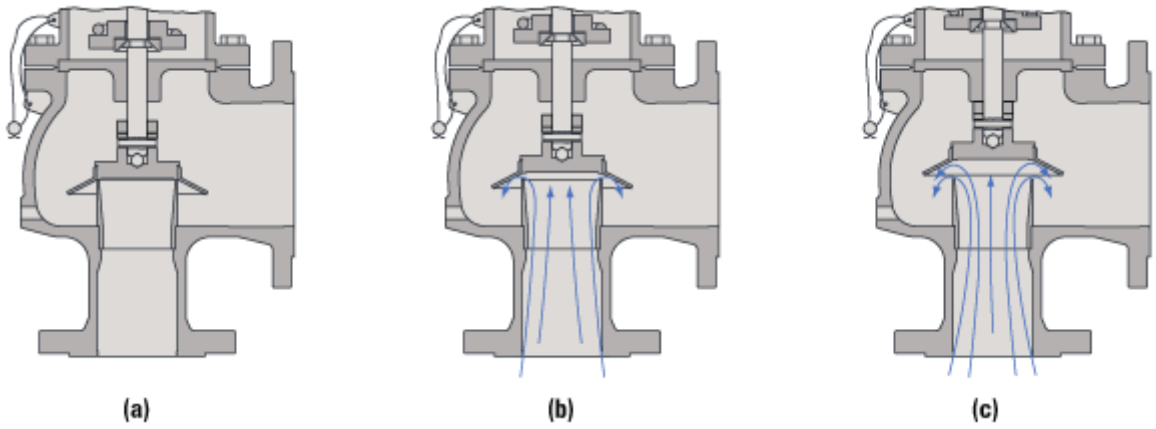

Figure2-6: Basic operation of a typical safety valve

Figure 2.7 shows the relationship between pressure and lift for a typical safety valve at opening and closing conditions. It also clarifies opening and closing condition with an overpressure and the blowdown of 10% of the set pressure.

According to the outlet flow direction, safety relief valves are classified into two types. The first type is the 90^{0} angle valve that denotes the right angle between the inlet and the outlet of the valve. This is the most appropriate to prevent valve components (the spring, gland …etc.) from a corrosive or erosive flow and will be reflected an increase in valve lifetime. The second type has a flow path through the valves and results in the valve components (spring, spring holders, spring adjusting), being exposed to the fluid flow. In terms of valve design, it is much more complicated and dependant on more factors compared to the first one. It is also very sensitive to the downstream pressure, which is influenced by the valve geometry.

The downstream pressure significantly affects the forces exerted on the piston and the opening and closing characteristics.

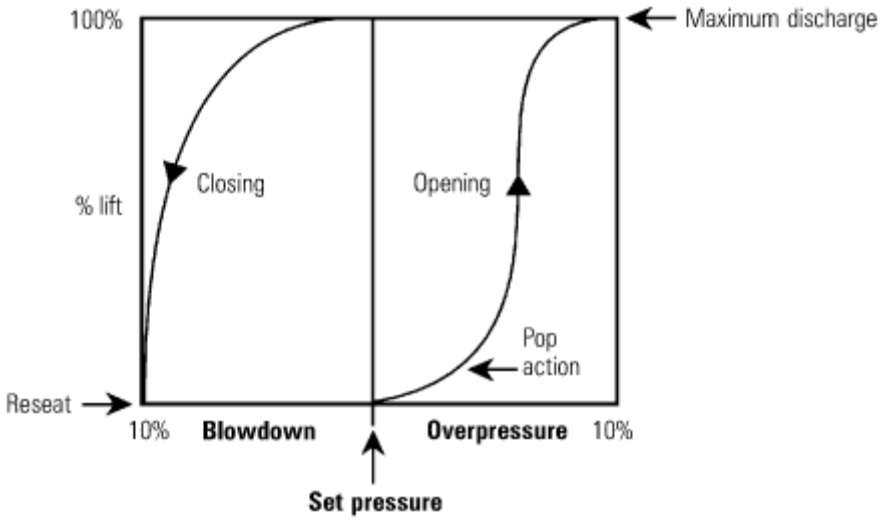

Figure2-7: Pressure-lift relationship for a conventional safety valve

The safety relief valve investigated in this study is a full lift safety relief valve of a through flow type. The valve construction and components are detailed in Section 4.2.

Chapter Three

3 Literature Review

3.1 Safety Relief Valve Design Requirements

The main purpose of safety systems in processing plants is to prevent damage to equipment, avoid injury to workers and to eliminate hazards in the community. In emergency situations, a sufficient mass must be vented to reduce the pressure to a safe level. The function of a safety relief valve is to protect piping systems, pressure vessels, and other equipment from

pressures exceeding a fixed predetermined amount (pressure design). This allowable amount is different from one equipment to another and depends upon the conditions causing the overpressure, which is covered throughout various codes and standards. The safety relief valve is not a control or regulating valve.

In industry, the well-established design and operation of safety relief valves are now available to cover a wide range of pressures, temperatures and fluids. In fact, this requires a variety of design solutions, which most likely include important issues such as sealing, spring design, pressure integrity, material selection, etc. The aforementioned issues are very significant but will not be considered in this study. The main issues that will be taken into consideration are the opening and closing of the valve, and the flow related design issues of flow rate, i.e. the primary functions of a safety relief valve. At present experimental design methods, with trial and error procedures play the major role of the design of safety relief valves to accomplish a required level of performance. However, the basic requirements for a satisfactory design have already existed in national and international standards since the early 1900's.Thus to achieve an adequate relief flow, a semi-empirical approach for the sizing of the flow areas can be implemented. Although there are no clear guidelines for the achievement of the valves opening and closing conditions, the current standards i.e. (ENISO-4126-1) require that the valve open and close within +10% and -15% of the set pressure respectively. However, an understanding of how the forces and mass flow vary with lift on the main moving element of the valve (the piston) leads to a general methodology, which is based on quasi- steady assumptions. The valve piston responds to an imbalance between the fluid dynamic and the spring forces. These forces noticeably vary with the valve opening (valve lift) and pressure as shown in Figure 3.1. Opening of the valve implies that the fluid dynamic force is greater than the opposing spring force. On the other hand, a balance of the fluid dynamic and spring forces after the initial piston motion possibly occurs if the upstream pressure remains steady and will lead to a constant opening of the valve at L_{max} (full lift) at some pressure above the set pressure.

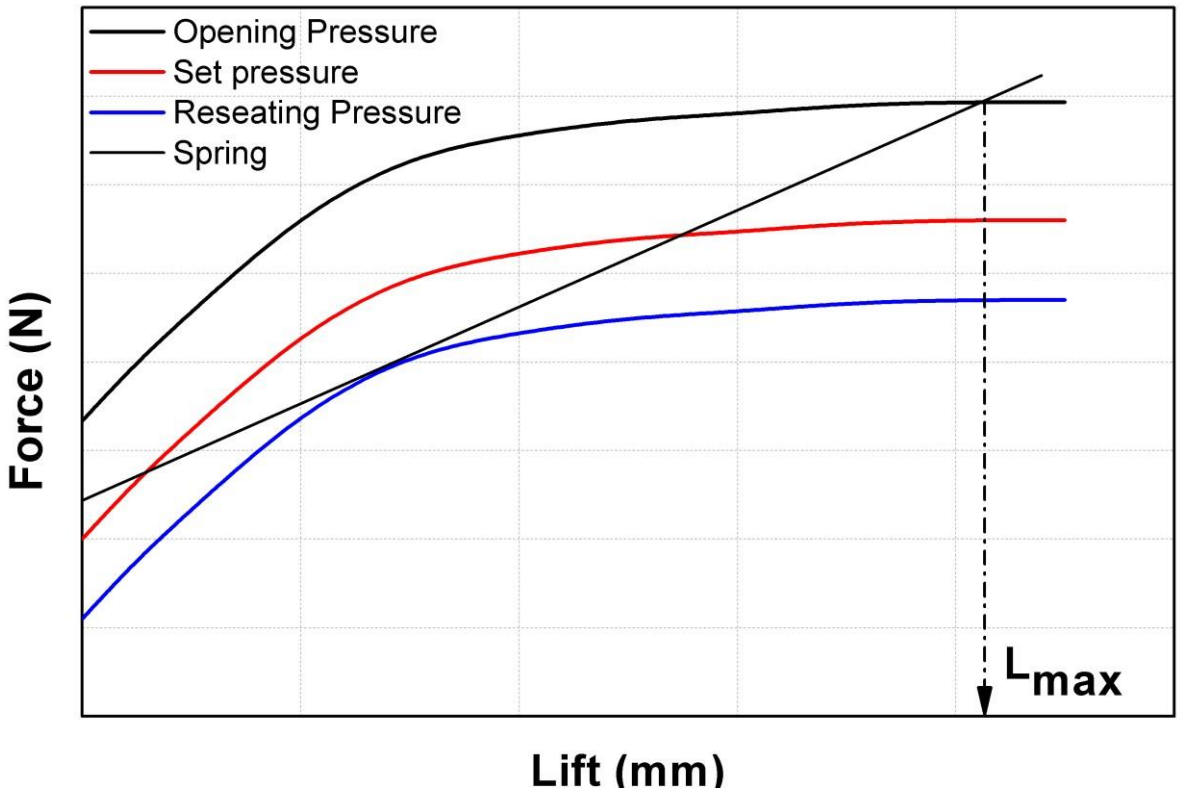

Figure3-1: Force-Lift curve to represent the general opening and closing characteristics for a safety relief valve

The discharge mass flow can be obtained from the mass flow characteristics at full lift (L_{Max}) for a relieving pressure corresponding to a set pressure. The mass flow should be approximately the same calculated value in the International Standards especially, if a proper flow area is selected. Hence, a noticeable reduction in system pressure leads to lower piston forces. The EN-ISO-4126-1:2004 calculates the mass flow (W) based on Eq.3.1. This formula is used with different set pressures and various flow areas. It is noted that the standard is applicable to safety valves with a set pressure of 0.1 bar gauge or above and a flow diameter of at least 6mm. However, the sizing formulas in Section 7.5 of the ISO4126-1 are explicitly solved in terms of the minimum required flow area (A) at different fluids such as critical or subcritical gases and vapours, liquids and steam. Moreover, other codes and standards such as ASME VIII, API PR 520, EN-ISO 4126-1 and AD Merkblatt 2000-A2 are also published throughout the world, which contain the main sizing formulas to address the design and application of safety relief valves. The ASME code is the most widely used and recognized among those codes.

$$W = P_0 \,.\, C \,.\, A \,.\, K_{dr} \,.\, \sqrt{\frac{M}{ZT_0}} [\text{kg/s}] \qquad (3.1)$$

Where:

P_0 : Relieving pressure [bar].

C : Function of the isentropic coefficient [-].

K_{dr} : certified derated coefficient of discharge [-].

A: Flow area of the safety valve [mm^2].

M: Molar mass [kg/k_{mol}].

Z: Compressibility factor at actual relieving pressure and temperature [-].

T_0: Relieving temperature [K].

The fluid dynamic force-lift curve can be established for each pressure. Figure3.1 shows the force-lift curve at a reseating pressure (blue line) where the spring forces are now greater than the fluid dynamic forces. This allows the valve to close and represents the upper limit of the valve pressure. This also should be used to indicate the performance of the valve closing and to ensure its ability to meet the requirements of the International Standards. Figure 3.2 shows the flow-lift curve at various piston lifts, and indicates the maximum mass flowrate discharged at the maximum lift. Hence this will lead to the proposed calculation of the flow area in the standard, which is mainly dependent upon the maximum mass flow discharge determined as shown in Figure 3.2. This primarily requires the piston force-lift and mass flow-lift characteristics to be emphasised. This approach is fundamental for valve sizing design and will be assumed in this research study, even though it is poorly discussed throughout the literature. In brief, the main methodology of this study will be divided into two parts. The first part is an experimental study, which will be carried out based on an inhouse test facility, to generate the mass flow and force characteristics of the valve. The second part is a theoretical approach and will be the main focus of this research study, with the objective of predicting these characteristics by implementing the available techniques of Computational Fluid Dynamics (CFD). The following sections of this Chapter will review available published studies and will be divided into two separate sections examining single and two phase flow conditions.

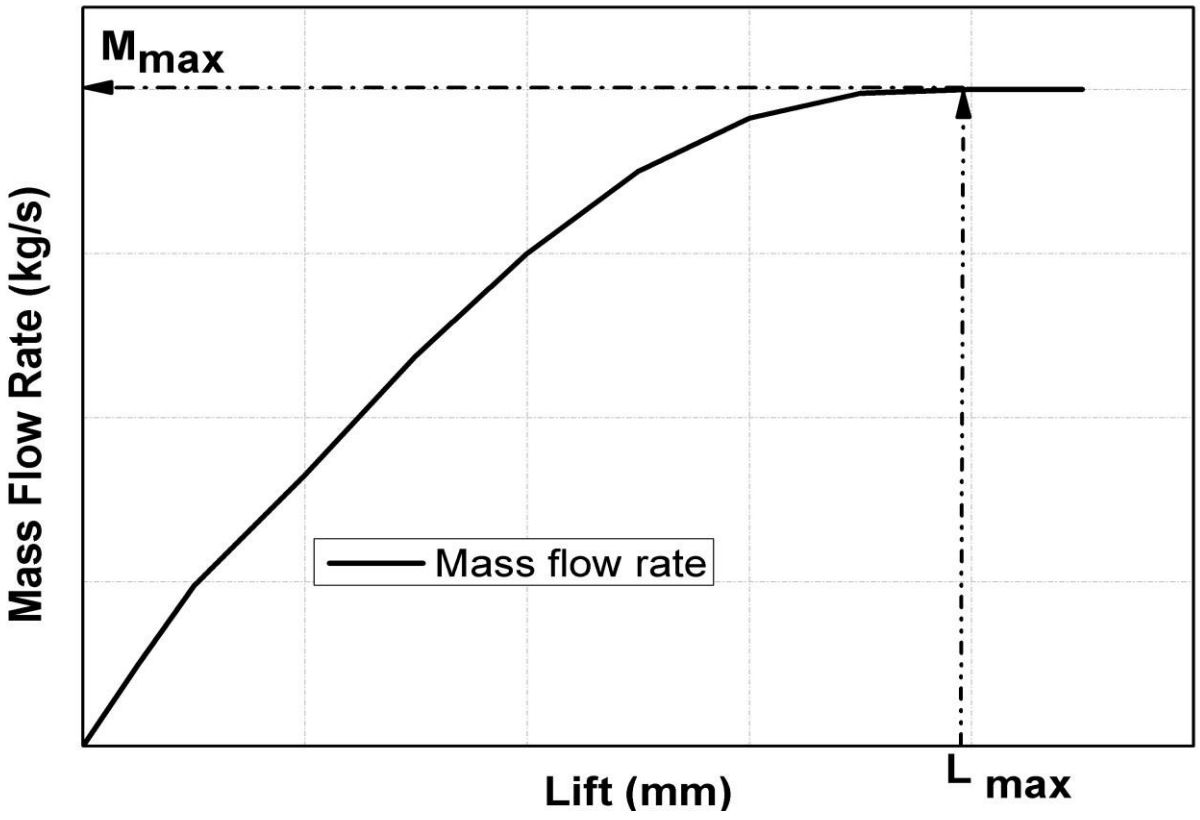

Figure3-2: Flow-Lift curve to represent the general opening and closing characteristics for a safety relief valve

3.2 Single Phase Applications

This section will review the available literature for safety valves operating under single phase flows as the majority of applications are with this condition. A thorough understanding of single phase flow will pave the way for understanding two phase flow. This will include a discussion of International Standards requirements and available sizing methods. Following that, theoretical methods for predictions of mass flowrate and forces will be presented, which will include the quasi one-dimensional modelling approach and the use of Computational Fluid Dynamics (CFD) techniques. Furthermore, the complexity of the three dimensional geometry of the valve will be highlighted since simplifications are generally assumed. Moreover, studies on safety relief valves under single phase transient conditions will be presented. Ultimately, there will be also a brief review of the most common safety valve operation problems (instabilities on valves)

3.2.1 International Standards Requirements for Safety Relief Valves under Compressible Single Phase Flow

The main purpose of this section of the study is to provide a brief review to some of the codes and standards that are applicable to safety relief valve. Those codes and standards govern the design parameters and use of pressure safety relief valves and also to ensure operating performance in a consistently smooth manner on a variety of fluid phases. On the other hand, testing and evaluation work of a new safety relief valve design are very significant *but* will not be presented since this is beyond the scope of this study. In addition, the most common applicable International Standards are ISO, API, ASME, AD and TRD. In fact, these standards consist of many sections associated with pressure vessels and boilers, which deal with different design issues. One of these sections should be related to the safety relief valve, as illustrated in Table 3.1. These International Standards contain different formulas, which accomplish various results. The so called "Type test" is significant and should be taken into account as this test is to check set pressure, overpressure, reseating pressure, lift at overpressure, mechanical characteristics such absence of chatter, flutter, sticking and harmful vibration and eventually the reproducibility of valve performance. The tolerances accepted in the type test for operating pressures are different from one standard and code to another.

According to the international standards, a calculation method for the discharge area at the operation conditions is proposed to ensure the discharge mass flowrate is achieved. A study was carried out by Follmer and Schenttler [1], who carried out a comparison between the related international standards for safety relief valves. Table 3.1 presents the results of the comparison which shows that, despite the ASME I limits the tolerance for maximum overpressure value to 3%; the other standards give a maximum opening overpressure limit of 10%. The comparison also shows no agreement between the standards of the maximum closing pressure tolerance. For the EN ISO 4126-1, the closing tolerance for the maximum overpressure value is relatively high. Based on new requirments for reducing greenhouse gas emissions, this value should be changed to a lower value [21]. It should be noticed that, for the valve operation worldwide, there are no common requirements. Thus consistent conditions could be clearly imposed.

Table3-1: Comparison: Required function values for pressure safety relief valves, gas &steam, [88]

CODES & STANDARDS	AD A2 / TRD 421	EN ISO 4126-1	ASME VIII	ASME I
The Fluid Type	Gas/Vapour/Steam	Gas/Vapour/Steam	Gas/Vapour/Steam	Steam
Open	Max. 5% / 10% Or 0.1 bar.	Manufacture indication max. 10% or 0.1 bar.	Max. 10% or 0.2 bar.	3%
Close	Max. 10% or 0.3 bar.	Manufacture indication max. 15% or 0.3 bar.	Max. 7% or 0.2 bar.	Max. 4% or 0.28 bar.

"Note: all the percentages presented in Table 3.1 are based on the set pressure of the valve"

3.2.2 Simplified Models for Safety Relief Valve

In the literature, common assumptions are often proposed to simplify the complexity of dimensional geometry and flow through safety relief valves. For example, reducing the three dimensional unsteady flow to a quasi-one-dimensional flow is one of the most common assumptions [21]. With regards to the simplified geometry, the majority of research studies consider the valve as a convergent divergent nozzle.

A study was carried out by Gringberg and Krichker [2] with an assumption of steady one dimensional flow. The fluid force was calculated based on the opening pressure (Working Pressure) and maximum flow. Based on a force balance particularly between the fluid forces, the friction force and the spring force; the setting and reseating pressure can be estimated. From this the inner diameter of the valve could be easily determined.
Similarly, Sterland [3] adopted the same method of assumptions and simplified the valve geometry to a convergent divergent nozzle. An experimental investigation was performed to present a dimensionless force-lift characteristics.

A study was carried out by Sharma [4], who calculated the mass flowrate by implementing an empirical formula and simplified the valve geometry to an ideal convergent divergent nozzle.

Although the study failed to provide a full model, empirical formulas were utilized to design the valve seat,the spring and the spindle. On the one hand, most of the research studies present the general background knowledge of opening pressure, set pressure, flowrate as well as force that are related to several aspects of the valve operation. On the other hand, the compressible flow conditions that occur within the valve have not been well-established. This is clearly due to the lack of theoretical and experimental facilities to provide general technique in dealing with the existing complex flow conditions. Accordingly, industry has merely depended upon both; the gained experience of experiments and methods of trial and error [21]. One dimensional fluid models to investigate the compressible flow through safety relief valves were developed by many successful attempts.Thus, the aforesaid general background information was established to emphasise how the force and mass flow vary with lift and how they could affect the valve performance.Simplifying the valve geometry to a convergent divergent nozzle was the main part of the models achievement [21].

Parker [5] was one of the early attempts to theoretically determine the pressure-lift characteristics with the aid of a one dimensional flow model. The study determined the opening and closing of the valve based on spring charactristics. The comparison of model prediction with experimental data showed good agreement.

Francis J. [8] calculated the pressure around the disc after dividing the flow regions into different zones then determined the force-lift characteristics. The study compared the predictions with published expirements and showed a good comparison.

A study was performed experimentally by Bett and Francis [6] to determine the pressure distribution on the back side of a safety relief valve. This was achieved by inserting pressure tappings under the valve piston at different circumferential locations. This also was to check the axisymmetric flow properties, by means of measured pressures.The study suggested that the 2D-axisymmetric model is acceptable for pressure prediction and can determinethe critical (choked) area. By the same authors, dimensionless coefficients were introduced to determine the flow rate , force and lift in safety relief valves with the assumption of a convergent divergent nozzle [7]. The study aimed to present the safety valve characteristics regardless of the valve geometry and the operating pressure.

The above-mentioned attempts were a good start in dealing with the compressible flow through safety relief valves.The aformentioned methods were affected by those assumptions

of simplification, therefore, they showed a clear limitation of application as well as accuracy. On the other hand, recommended sizing methods of the international standards for safety relief valves under single phase flow conditions were based on these methods.

3.2.3 Sizing of Safety Relief Valves for Single Phase Flow

In the literature, most of the research studies on relief valves have dealt with sizing rather than design. Calculating the mass flow rate through a safety relief valve is the main objective in selecting the right valve. Using the simple theory of flow through convergentdivergent nozzles in calculating the effective discharge area leads to sizing and selection of safety relief valves. This procedure requires a correction factor in the form of a discharge coefficient (k_d), which is determined experimentally. The valve manufacturer is responsible for supplying customers with the discharge coefficient. There are slightly different sizing formulas, which are based on the following editions of codes and standards: the ASME VIII (2008), the American Petroleum Institute API RP 520, the international standard EN ISO 4126-1 (2004) and AD Merkblatt2000-A2 (2006). The formulas used in the standards use the ideal gas equation for sizing safety relief valves. In spite of these limitations, the semiempirical approach provides reasonable accuracy in determining the discharge coefficient with some limitations. Gases behave in a real manner particularly at a very high pressure or a low temperature therefore friction, heat exchange with walls and intermolecular forces are no longer negligible [21].

Based on the theory of flow through a convergent-divergent nozzle, Luft G. et al [9] carried out an experimental study to examine the validity of international standard ISO 4126-1 and the American Petroleum Institute API 520 methods for sizing safety relief valves at high pressures conditions. The study was performed over a wide range of pressures (150-300 MPa) and temperature with a large reactor capacity of ethylene. Although there was a major concern due to a decomposition reaction, the calculation methods of the standards could be highly recommended. However, these methods should use the thermodynamic data of ideal gases when sizing safety relief valves at high pressure conditions. The study also concluded that the evaluation of the discharge coefficient should be based on relief measurements under real operating conditions. Thus, in this case, a factor must be added in the equation of the mass flow during relief to account for the chemical decomposition. Following

incorporation of the aforementioned recommendations during laboratory experiments led to a good agreement with industrial experience.

Schmidt J. et al [10] carried out a study by adapting the same procedure, but this time, the authors calculated the discharge mass flow by taking into consideration the real gas factor using their own derived equation. A comparison between the results of this equation and the ISO model, CFD simulation and experimental work was made at high pressure. The comparison showed that, in the case where a thermodynamic critical point occurs, the ISO model is not sufficient to determine the mass flow rate at high pressures due to ideal gas assumption. Accordingly, the sizing models of the international standards are not precise enough and have limits in some applications. Consequently, more accurate models with a wide range of applications are required, which could be found by focusing on CFD models.

An extensive experimental research study on safety relief valves was carried out by Dossena et al [37] to clarify the influence of valve size and the associated back pressure on the valve flow discharge. Valve operating characteristics in association with a reduction in flow rate due to the occurrence of a subsonic flow regime in the flow along with adequate piston lift, can be significantly affected by the resulting back pressure. The movement of the piston valve can lead to the well-known non-exact geometrical scaling, which will result in a different orifice diameter within the same valve size. For example, the API standard 526 requires for "the valve inlet, valve outlet and face to face dimension" not to be exactly scaled with respect to the orifice diameter, which induced altered safety relief valve performances. The study evaluated the impact of the aforementioned parameters on the flow discharge capacity of the safety relief valve under different operating conditions.
Although this work required an extensive number of experimental tests as well as a sensitivity analysis on these effects, an experimental correlation to predict the non similarity effects was proposed to minimize and limit the experimental efforts.

3.2.4 CFD in Modelling Safety Relief Valve

Since the mid 70's, the application of computational fluid dynamic techniques (CFD) has extensively been used in the aerospace industry. Nowadays, the use of CFD is of growing interest and extending to other industries. This is clearly due to the rapid development of powerful mini computers. Greater accuracy for a wide range of applications in sizing and

design of safety relief valves could be achieved when utilizing CFD techniques. However, only recently, have investigations of the complex multi-dimensional compressible flow in safety relief valves been made and is a result of the rapid development in computational fluid dynamic techniques for complex geometries. There are many attempts in the literature aimed to use CFD for sizing and design of safety relief valves under single phase flow conditions, these are discussed below.

A simulation study was performed by Sethi and Lai [11] to determine the opening and closing performance of a safety relief valve by using a dynamic model. The model mainly used a simple force balance, which included force coefficients accounting for influences of the fluid dynamics. Although there was no clear description of the mathematical model in determining the force coefficient with the aid of experiments, the CFD was a good start.

A numerical study was adopted by Berger [13], who presented the theoretical framework and the numerical capabilities of the so-called Navier-Stokes CFD code TASCflow. The study investigated the behaviour of a compressible gas flow through pneumatic components. The study summarized the numerical methods for solving the mass-averaged Navier-Stokes equations in connection with the standard k-ε turbulence model. The study showed that, it is neither possible nor profitable to perform flow measurements due to geometrical dimensions of most pneumatic components being very small. A very simple geometry of a pneumatic vacuum ejector and a pipe-nozzle-pipe configuration were simulated and solved based on 2-D axisymmetric model. The study showed how the predicted results could be influenced by the mesh type. The study proved that the CFD technique is an effective tool in designing pneumatics. The study concluded that the predicted mass flow exactly matched the measured mass flow hence the CFD technique was recommended in such conditions.

As part of his PhD studies, Elmayyah [88] investigated the performance of a safety relief valve under a compressible flow of air. The study aimed to determine the predictive capability of a CFD approach. In general, the force-lift and mass flow-lift characteristics were determined based on experimental facilities. The commercially available code FLUENT 6.3.26 was used. The predicted results were in very good agreement with the experiments and gave better understanding to the compressible flow behaviour through a spring loaded safety valve.

However, the study was limited in the operating conditions studied to a pressure of no more than 200 psi (13.8 bar).

A study was carried out theoretically and experimentally by Dempster and Elmayyah [14] to investigate the flow-lift and force-lift characteristics of a safety relief valve designed for the refrigeration industry and was extended to include pneumatic systems as air represented the compressible fluid. The valve forces and the discharge mass flow were measured and predicted at different valve lift conditions. The model was presented as a 2-D axisymmetric RANS approach implementing the standard k-ε turbulence model. The CFD code FLUENT predicted the discharge mass flow rates, valve forces and the flow conditions such as Mach number, pressure and temperature. The study also aimed to investigate the CFD capability in safety relief valves design and improvement. The predicted results showed very good agreement with the experimental measurements.

A computational study was performed by Kim et al [18] to investigate the gas flow through a LNG safety valve used in ship engines. The study was conducted to simulate mainly the gas flow between the valve seat/disk and the nozzle exit. A CFD model using 2-D, axisymmetric, compressible Navier-Stokes equations, was deployed for the aforementioned simulation. The predicted results obtained at different lift (various distances between the valve disk and nozzle exit) to radius ratio (L/R) and operating pressure (P_0/P_a). The CFD results were in reasonable agreement with theoretical results, which were obtained by a 1-D, isentropic flow calculation using the equation of state for an ideal gas. Moreover, there was no experimental work and the grid size influenced the accuracy of the CFD calculations.

A study was carried out by Moncalvo et al [17], who investigated the influence of the flow volume discretization and the selected turbulence model on the accuracy of the numerical solution and the duration of the calculations. The mass flow rates of air in two safety valves (type 441 DN 25/40 and type 459 DN 15/25) were predicted by using the commercial code ANSYS CFX-flo. The valves were presented in a three-dimensional geometry with different types of a grid size such as coarse, fine and very fine. Likewise, different types of turbulence model were investigated such as SST, k-ε, k-ω and Reynolds stress, for relieving pressures between 4.4 and 35.2 bar. The experiments were based upon old measurements at the test

facility of LESER GmbH & Co. KG. The study showed that the degree of the discretization was the most significant factor affecting both; the duration and accuracy of calculations. The predicted results of the air mass flow rates in comparison to the experiments, gave slightly better accuracy when using either the SST model or the standard k-ω model.

A study was carried out by Dempster et al [15] to develop a design methodology for the safety relief valves using available CFD techniques. The study was the first publication using CFD in safety relief valve design. The authors predicted the mass flow and force characteristics of 2-D axisymmetric model of a safety relief valve. The turbulence effects of the model were taken into consideration by implementing RANS equations in conjunction with the standard k-ε and Energy Equation. The study considered the air as an ideal gas and solved the model which was based upon the commercial code CFD-FLUENT 6.3.2. In spite of the mass flow rates and forces being in excellent agreement with the predicted results, the study showed a significant sensitivity to valve geometry.

D'Alessandro [19] and Muschelknautz and Wellemhofer [20] performed CFD studies to predict mainly the mass flow rates in safety relief valves. The two studies also predicted some reaction forces and did not include any prediction of the valve forces. The studies provided information relating to using CFD in valve force predictions.
Sethi and Sabet [12] developed a model of fluid flow through a pressure relief valve using the code CFD-PHOENICS. Air as a perfect gas represented the abovementioned fluid flow through the pressure valve. Predicted results of the mass flow and disk force at different lift were presented based upon steady-state Euler equations. The study showed good acceptance of the CFD predicted results. However, a more general and realistic prediction could be obtained if the viscosity and transient terms of Navier Stokes equations were included.

A study was carried out by Bilanin and Teske [16], who investigated safety relief valve performance. Hence, the full Navier Stokes equations were applied to examine and improve fluid flow through a spring loaded safety relief valve. Despite no experimental work for validation of the prediction, a calibrated model called ''COUPLE'' was used to verify the accuracy of the presented model.

Bassi et al [35] developed a code based on Discontinuous Galerkin (DG) discretization of the compressible RANS and k-ω turbulence model equations for 2D axisymmetric flows, which was applied to a transonic flow in safety relief valves. The model was implemented to determine the flow in a spring-loaded safety relief valve for a wide range of different back pressures and piston lifts. Although an "exact" Riemann solver was applied to determine the interface numerical inviscid flux, the BRMPS scheme was used for the viscous flux discretization. A shock-capturing technique evaluated by the EU ADIGMA project was of significance, hence; obtaining control of a high-order oscillation solution through the shocks. Experimental data of the valve flowrate and pressure inside its bonnet were used to validate the CFD prediction, which allowed the complex behaviour incurred to be clarified.

Bassi et al [36] extended their work of [35] to develop an accurate Discontinuous Galerkin solver to ensure proper functional operation with both compressible and incompressible flows. A spring loaded safety relief valve used in shell-type water-gas heat exchanger was examined under both conditions of water and air separately. The study showed that the valve performance can significantly vary when operating with different working fluids. A fully implicit high-order DG discretization of the RANS and k-ω turbulence model equations was used for the incompressible flows. The study was aimed at investigating possibly different behaviour of the same safety relief device when operating in air or water. The study concluded that the discharge coefficient in water is smaller than in air due to compressibility effects and the relevance of viscous losses up to the sonic throat. The valve manufacturers have started testing their valves in air and water, hence, the normal practice applied by valve manufactures in testing the valve in air first then an empirical reduction factor to the discharge coefficient in case of the working fluid is water, can be now considered outdated.

Beune [28] developed a valve sizing method of the real-average and the real-integral, and a numerical CFD approach to predict the opening characteristics of a safety relief valve at high pressures up to 3600 bar. In fact, this was intended to extend existing former CFD studies, whose valve capacities were validated at a working pressure up to 35 bar. The "Soave Redlich-Kwong" real-gas equation of state is applied to a test fluid of nitrogen. The results were compared against experimental data hence a discrepancy of less than 5% was found for reduced temperatures larger than 1.5.

Beune et al [60] repeated the previous work of [28]; however, it was carried out this time for an incompressible flow of water for a testing pressure of up to 600 bar. The work was performed for the prediction of the discharge capacity in accordance to the valve sizing method of EN ISO 4126-1 standard. Although the experimental and the computational mass flowrates agreed with a slight deviation of 3%, the discrepancy between the ANSYS CFX modeling and the experiment of the flow forces was approximately 12%. Therefore, a successful attempt was made by including a model to account for cavitation, which reduced the overpredictions in flow force to 7%. In addition, the study concluded that at higher piston lift, the influence of cavitation was less and a 4% discrepancy in forces observed.

Dossena et al [29] carried out a numerical and experimental analysis to evaluate the behaviour of a safety relief valve using different gases. Air, argon and ethylene were the considered gases, for a wide range of specific heat ratios. The first experiment was achieved in air and argon for a safety relief valve with an orifice of 10 mm diameter, designed using the API 526 standard. However, a very significant reduction in lift and in mass flowrate discharge at a normal overpressure was noted when operating with argon. A deeper insight into the physics was obtained based on an extensive testing, using a novel CFD code of discontinuous Galerkin formulation. Good agreement between the CFD results and experiments were achieved when operating with air. The same computational grid was used for the testing fluid with argon and ethylene, which were considered to be perfect gases. The observed trends were critically discussed based on the numerical results to identify the fluid dynamic and physical reasons in the opening force and mass flow discharge. The study concluded that attention must be paid to safety relief valves operating with a fluid of a specific heat ratio greater than the one of the gas.

3.2.5 Safety relief valves under transient flow conditions

A model for the opening dynamic response of a direct spring loaded safety relief valve used for gas or vapour applications, was developed by Darby [31] to account for the opening characteristics of the valve. The model consists of a set of five coupled nonlinear algebraic/differential equations, which are solved based on a numerical method. The solution procedure allows this mathematical model to be implemented on a spreadsheet to forecast

the position of the valve piston as a time-dependent function. However, the model was successful and incorporated the impact of various parameters on the valve stability.

The work of Darby [31] was extended by Aldeeb at al [32], who designed an experimental test facility to determine the opening characteristics of three different valve sizes from three different manufacturers at two different set pressures. The working fluid was nitrogen and the valves were examined with and without discharge piping as well as with several different lengths of inlet piping system. National Instruments hardware and Labview 8.2 software conducted on a laptop computer were used for data acquisition. The purpose, however, was to validate the mathematical model derived by Darby [31].

Darby and Aldeeb [33] carried out a third study that is related to the aforementioned studies of Darby [31] and Aldeeb et al [32]. The study discussed a comparison of the mathematical model predictions presented in [31] with the measured dynamic opening response data presented in [32]. The study showed that the mathematical model is quite reasonable in predicting the dynamic response of all valves tested.

Hős et al [34] derived a model of an in-service direct-spring loaded safety relief valve based on the API (American Petroleum Institute, 2009) guideline, which proposes that the irreversible pressure loss in the inlet line should be limited to a pressure relief of 3% of the valve set pressure. Three different commercially available valves were tested based on existing laboratory experiments. The test conditions were for a wide range of different mass flowrates and lengths of the inlet pipe, for a test fluid of gas. The study disclosed that violent oscillations can occur beyond a critical pipe length, which might result either in the valve opening or closing. Hence the industry standard of 3% inlet loss criterion could not be generalized. However, the accuracy of the model was evaluated by using the test data and was of interest. One of the advantages of this mathematical model is that, this mathematical approach would be extended to capture other effective parameters such as the dynamics of the fluid upstream of the valve, the flow-lift characteristics, the piston net forces, the pressure drop in the discharge line. On the other hand, the study revealed that the conclusions on the mechanisms of instability should be only valid for the tested valves.

Beune et al [55] developed a 2D axially symmetric multi-mesh numerical model to investigate the opening characteristic of high pressure safety relief valves. The movement of the piston of a spring loaded safety relief valve was simulated based on Newton's law and the flow force CFD software package ANSYS CFX results. The valve was examined under two different working fluids of water and air, respectively. The study was aimed at investigating the influence of valve dynamics on steady-state flow by using a fluid-structure interaction (FSI) based on CFD calculations of the flow through the safety valve, hence, the opening characteristic of a high pressure safety relief valves under different flow conditions was distinguished. A redirection of the bulk incompressible transient flow results in a large force increase and collapse, therefore the assumption of a quasi-steady methodology might be no longer applicable. On the other hand, high oscillations at a 40 bar set pressure were observed during the valve closing phase, particularly for real gases flows.

A study of the dynamic characteristics of a spring loaded safety relief valve carrying an incompressible turbulent fluid of water was performed by Pateriya and Khan [56], who used 2D ANSYS simulations. The concept of mesh deformation resulted from the fluid-solid interaction between the valve piston and the surrounding fluid, was applied to account for the valve piston motion. The study was specifically aimed to identify the region that would significantly affect the transient response of the system. The velocity and pressure distribution inside the valve were obtained for different time step as well as different upstream inlet pressure conditions. Thus, results presented were of significance to contribute to the safety relief valve design process. On the other hand, the study also reviewed some of the existing researches ([52], [58], [59], [60], and [61]) that are focused on the opening characteristics of pressure relief valves by means of developing a dynamic model to investigate the performance of various SRVs.

Song et al [39][42] and [40][41] developed a successful 2D and 3D model, respectively, to investigate dynamic characteristics of a direct operated relief valve (spring loaded safety relief valve) by means of understanding the transient flow behaviour and the valve disc performance. CFX Expression Language (CEL) was used to solve a 1D dynamic equation of the valve piston. This was in combination with the moving mesh technique implemented by the commercial software program ANSYS CFX (Version 11.0, ANSYS, Inc.,) to study the fluidsolid

interaction between the valve disc and the surrounding turbulent flow of air. The influence of different over pressure conditions on the dynamic behaviour of the valve disc was examined. The 2D convergence was achieved at each time step due to high-quality mesh, hence a better insight into the flow visualization aspects of velocity, pressure distribution…etc. were recorded. The 3D transient flow field through the valve provided greater visualization, which might overcome the limitation and difficulty of the experimental and steady CFD analysis.

Song et al [43] developed a simplified dynamic model (SDM) for the prediction of the dynamic characteristics during the reclosing process and blowdown of a spring loaded safety relief valve. The equation of motion for a single degree of freedom system was fundamental to the SDM model. This was in combination with the steady state CFD analysis that determined the force-lift characteristics of the valve at different fixed piston position. It is worth mentioning here that the damping influence was ignored as a result of its minor impact on the blowdown time. Even though pressure drop conditions were obtained from several experiments, the study showed a well-pronounced method of prediction for the dynamic behaviour and the blowdown of the valve since the SDM model was very reliable.

Song et al [44] extended the previous work of [40] to examine the effect of mesh fineness and the sensitivity of turbulence modelling on the valve piston force. A range of two equation turbulence models was investigated: the standard k-Ɛ, the RNG k-Ɛ model, the SST model, the k-ω and BSL model. The results of the study indicated that the overall variation for different mesh densities and different models for turbulence was less than 18%. Using fine and very fine mesh densities, however, reduced the aforementioned discrepancy of the predictions to 4%. On the other hand, more CPU time was required when using the very fine mesh to achieve relative independence of the turbulence model and mesh densities.

3.2.6 Stability on safety relief valve

Many problems might occur during safety relief valve operation, and can be defined by the various modes of valve dynamic response (the time-dependent position of the valve piston (lift) as soon as the valve set pressure is reached) [31]. These problems are chatter (the piston opens and re-closes at sufficiently high frequency and amplitude), flutter (the response is oscillatory but with a low amplitude), the improper sealing after opening, exceeding an allowable noise level, no seat impact and the rapid wear of the valve seat sealing material.

Chatter arises by rapid opening and closing of the valve due to a lower flowrate than design, is one of the most significant problems. Dynamic instability of the valve results in this chatter during opening, which usually causes major damage to the valve due to seat impact. Therefore, a minimum flowrate through safety relief valves should be maintained while the valve opens. Accordingly, a mismatch between valve geometry and spring stiffness with operational conditions such as mass flowrate, set pressure and back pressure lead easily to chatter. Given that destruction of the valve could be caused by chatter, several studies were conducted to investigate the mechanism of valve instabilities.

Funk [22] carried out one of the earliest studies to account for valve stability derived from its design parameters and the operation conditions. On one hand, the study was performed based upon an incompressible fluid. On the other hand, basic knowledge of the analysis and understanding of the valve stability was acquired.
An experimental study was carried out by Föllmer [23] to investigate oscillations in safety relief valves, due to inlet geometry effects. The flow was visualized by a high resolution camera and the oscillation frequency recorded.

Available published sizing rules to prevent chatter were investigated by Cremers and Friedel [24]. The commonly recommended rule of 3% pressure loss (API PR 520/AD A2) for the allowable inlet pipe pressure drop is applicable. Another recommendation is based on the transmission time and the amplitude of the pressure waves generated by the abrupt safety valve opening and closing. According to the investigation results, the published sizing rules did not precisely predict the safe inlet pipe length. Subsequently, a new sizing criterion was developed based on the pressure surge criterion. The study proved that the flow separation could possibly occur in a sharp edged valve inlet.

A study was carried out by Macleod [25] to predict chatter conditions in a wide range of applications. A dynamic model with the aid of an ideal gas law for the fluid flow was developed to examine the dynamic stability of the valve closing. The method of the study should be presented in a general form.

A literature review was recently presented by Darby [31] to identify previous studies, which dealt with issues of stability. Accordingly, more than 50 references were found; however, only 35 of these contain significant information relevant to valve stability issues [31]. Darby reported that, despite a number of factors contributing to the instability of the valve response being identified, significant factors such as the spring-mass-damping characteristics of the moving parts, the net forces exerted into the piston, the setting of the blow-down ring, the dynamics of the fluid upstream of the valve, the pressure drop in the discharge line and the associated backpressure, the characteristics of the flow against the piston lift; were not considered [31].

A considerable review of scientific literature relevant to valve instabilities was performed by Hős et al [34]. Five different effects on valve stabilities were found and included: "the interaction between the poppet and other elements, flow transition from laminar to turbulent, a negative restoring force, hysteresis of fluid force, fluctuating supply pressure" [34]. However, the study was only focused on the first of these effects.

Avtar [51] developed a 1D model to study the relative influences of spring-mass characteristics, geometry of internal parts and adjusting gland settings on the stability of the safety relief valve. This was by means of investigating the effects of these parameters on the blowdown, maximum lift as well as the valve opening time over a wide range of steam conditions. The analytical results of the study showed that the stability, longer blowdown and shorter opening time of the valve can be obtained by "lowering of the guide adjusting gland position or raising the nozzle adjusting ring ". In addition, the impact of damping on the valve stability was considered to eliminate unstable dynamic behaviour of the safety relief device.

3.2.7 Summary

- For single-phase flow, the proper method for sizing the relief valve is straightforward, since the fluid properties are simple and measured values of K_d are available.
- The current standards contain reliable recommendations for single phase fluids therefore they are adequately accurate for the sizing of safety relief valves for single phase flow.

- The recommended methods presented in international codes and standards for sizing safety relief valves have dealt with safety relief valves to ensure only safe operations instead of assisting their design process.
- The quasi steady state model is an essential step in understanding the compressible flow through safety relief valves. This should be extended to account for the opening and closing characteristics of safety relief valves under transient conditions.
- Very few recent publications investigated the valve performance on opening and closing under transient compressible single phase flow conditions.
- "According to the academic studies modelling safety valve flow should be possible with sufficient accuracy. However, the industry has not published accurate validation data yet. The capability of a numerical tool for the highly complex safety valve flow can be judged only when it is also focused on the individual flow phenomena that occur in safety valve flows" [60].
- Detailed information of a compressible single phase flow through safety relief valves is obtainable by CFD, but more experiments should take place for validations. However, the experimental procedure is very expensive, power man and time consuming.
- There are few publications where CFD is used to study the forces acting on safety relief valves under transient conditions.
- The CFD studies have provided more analysis of the flow inside the safety relief valves and addressed some limitations of the experiments.
- More research work should be devoted to further investigation on valve instability issues.

3.3 A review of the current modelling approaches of two phase flow through safety relief valves

3.3.1 Overview

The existence of liquid-gas or vapour mixtures is a common feature of processes found in heat transfer, power or chemical engineering systems. The use of safety valves to maintain adequate levels of pressure is common. However, ensuring sufficient designs is a more onerous task for two phase flows since the fundamental flow physics is less well understood. The majority of previous work has focused on determining methods for the sizing of valve discharge areas and this has been incorporated into national standards; the ISO standard organisation only recently issuing this in 2010. These aspects will be discussed in this part of the literature review but will also address the more current published work and detailed studies of two phase flow in safety valves, which can be used in the overall design process.

3.3.2 Classification of two-phase flows:

For modelling purposes, classification of the large variety of two-phase flows is very useful. The classification is mainly based on both; the flow structure and the phase state of the twophases. With regards to the physical state, four combinations are established: gas-solid, liquid-solid, gas-liquid and liquid-liquid mixtures. In terms of the flow structure, and particularly the interface topology, it is rather difficult to classify the flows due to changes that might be continually occurring. However, following the work of Ishii [63], who generally

classified two-phase flows into three categories based on the shape of the interface: separated flows, mixed flows and dispersed flows. , as depicted in Figures 3.3, 3.4 and 3.5.

Briefly, in separated two-phase flow modelling, there is no modelling approach to fully capture the interface topology. Hence, a symmetrical role is assumed separately for each phase. This flow can be described through two mathematical approaches: either by tracking the interface between the two phases or by utilizing an averaging procedure to derive a set of conservations equations. The first approach is deployed by means of solving NavierStokes equations in each phase (Volume of fluid [64] and a Level-Set Approach [65]).Although the second approach is implemented with an assumption that each phase might be present simultaneously at any point, the two-phase flow should be described as a whole entity. According to the second approach, the smallest scales of the interface are modelled but not resolved by using the averaging procedure. One of these well-known models is the Baer-Nunziato system of 7 equations [67] and [66], and its reduced models are also applicable, as in [68] and [69].

In the case of dispersed flows, however, one phase should have typical values of the volume fraction in the range 10-5 and 10-2 (dilute phase). Typically, this phase is composed of very tiny spherical inclusions- if they are compared to the macroscopic scale of the system- such as (droplets, particles or bubbles), which are dispersed inside the carrier phase (the second phase of the flow). Accordingly, the computing procedure of the flow inside and around the particle is not necessary. In addition, the carrier phase can be easily affected by those spherical inclusions; therefore, additional source terms in the right hand side of the transport equations should be taken into consideration.

Figure3-3: Separated two-phase flow: film flow, annular flow and jet flow [62]

Figure3-4: Mixed two-phase flow: slug or plug flow, bubbly annular flow and droplet annular flow [62]

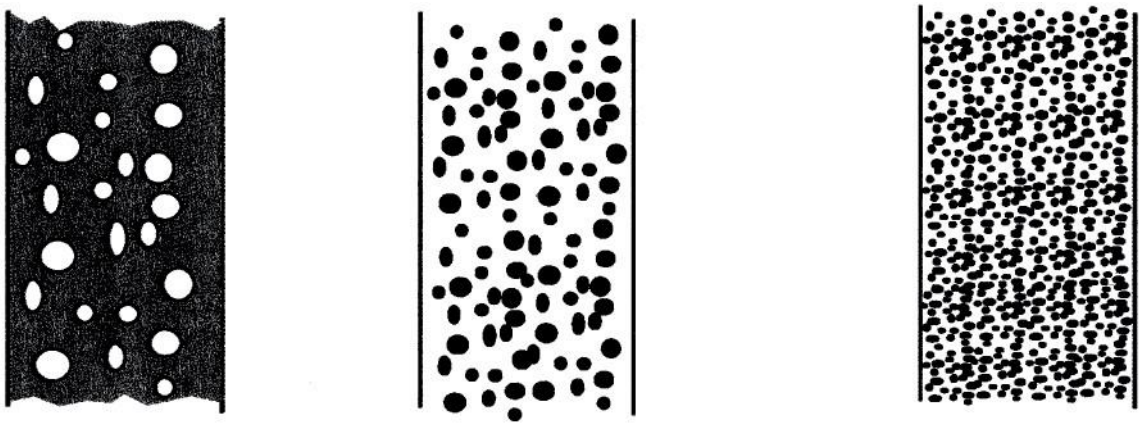

Figure3-5: Dispersed two-phase flow: bubbly flow, droplet flow and particulate flow [62]

3.3.3 The most commonly proposed approaches of two-phase flow modelling are as follows:

This section reviews approaches that are currently used in engineering design calculations to predict the discharge flowrate of a safety relief valve under various two-phase flow conditions. Commonly, the most widely accepted methods of predicting the relieving capacity of a safety relief valve under two-phase flow conditions are: the homogenous equilibrium model (HEM) developed by Leung, the homogenous non-equilibrium model of
Diener and Schmidt (HNEM-DS) proposed in ISO-4126-10, and the latest version of the Recommended Practice (RP) 520 two-point ω-model of the American Petroleum Institution (API) [106]. In addition, other various published empirical models namely slip models are: Homogenous model, Lockhart and Martinelli (1949), Fauske (1962), Thom (1964) correlation, Zivi (1964) model, Baroczy (1965) correlation, Moody (1965) and eventually, Wallis (1965) separate cylinder model [109].

Following the recent work of Kourakos, the two-phase flow models are classified as follows: [113]:

- **The Homogenous Equilibrium Model**

It is the simplest approach and its validity largely relies on the degree of mixing of gas and liquid. The highest accuracy of the model can be obtained from the greatest phase mixing. This model considers two-phase flow like a single-phase flow, which has average fluid properties depending essentially upon the mass quality. In addition, the calculation of the frictional pressure drop is mainly dependent on an assumption of constant friction coefficient between the inlet and outlet sections. Moreover, this model is based on the assumption of no velocity slip between the phases. The two-phases of this model should be also at the same temperature to account for the thermal equilibrium assumption. The accuracy of the model is improved for high pressure and flowrate conditions.

- **Thermal equilibrium mixture model with mechanical non-equilibrium**

Based on a category that depends upon the slip ratio (an algebraic relation between velocities of the two phases), the drift-flux model is the most commonly used one. The socalled IS model

is more applicable particularly for low pressure and/or low flowrates under quasi-steady-state conditions

- **Separated two-phase flow model**

Thermal and mechanical non-equilibrium of the phases are addressed by the separated two phase flow model. Three independent conservation equations of mass, momentum and energy for each phase are solved. The correlations to close the models belonging to this type of model are mostly formulated without any particular reference to the physical properties or the flow regime of the system. In addition, the assumption of thermodynamic equilibrium between the two phases is assumed. In contrast to the homogenous flow model, these models are also named the slip flow models. The first and most commonly applied method based on the category of the separated two phase model was proposed by Lockhart and Martinelli (1949) for subsonic flows. They conducted their work using Air and

Water in a straight pipe with the purpose of calculating two-phase frictional pressure drop. However, it is the simplest model with an accuracy that is considered to be relatively low owing to ignoring the effects of the flow patterns.

3.4 A review of the available literature of two-phase frozen flow through safety relief valves

In general, selection of the proper safety relief valve for two-phase flow is not an easy objective due to the complexity of two-phase flows. The complexity is due to the lack of available correlations used to determine the flow behaviour. Flow geometry, phase distributions and interfacial stresses can easily result in the occurrence of this complexity. There are no design methods which should be followed to ensure the accurate design of the safety relief valve under two-phase flow conditions. In addition, dealing with safety relief valves in two-phase flow by either prediction or analytical description depends upon a number of parameters which are not straightforwardly linked to the properties of the fluid itself, fluid flow and the interaction between phases, etc. These parameters are phase volume fraction, temperature, pressure, mass, relative velocity, momentum and heat transfer [88].

The thermal and fluid dynamic phenomena such as interfacial drag and interfacial heat and mass transfer are the main reasons for the aforementioned complexity. Therefore, the flow conditions are normally affected by the variation of these parameters particularly with

different operating conditions of the valve. Depending on the extent of phase change due to pressure drop, there are two types of two-phase flow which are called flashing flow (phase change) and non-flashing flow (no phase change). Other types of two-phase flow are classified as critical, sub-critical, separated, homogenous...etc. However, there are three main approaches that have been deployed throughout the literature which should be followed to model, and analyse safety relief valves. These approaches are the analytical approach, computational approach and finally the experimental approach [88].

The analytical approach consists of equations that have been formulated to deal with the study of the two-phase flow characteristics through safety relief valves but unfortunately, this stated method has been affected by the complexity of the two phase flow and misrepresents the precise flow conditions. Besides, the two phase formulations have been developed from single-phase methods by implementing appropriate assumption to suit the two-phase flow conditions [88]. These simplified models are recognised to be the most common description of two-phase flow conditions in safety relief valves [107].

The second technique uses “computational fluid dynamics” (CFD) for dispersed two phase flows. This consists of two major approaches, which are the Eulerian-Lagrangian and the Eulerian-Eulerian approaches. The Eulerian-Lagrangian approach treats the continuous phase as a continuum and the velocity, mass and temperature of each particle or droplet are calculated separately using Newton 2nd law. It has been extended to include the effect of the dispersed phase on the continuous phase; by means of determining mass, momentum and heat transfer between the two phases. It is applicable to both dense and dilute dispersed flows. On the other hand, the Eulerian-Eulerian approach treats both phases as a continuum hence; each phase has its own set of transport equations in addition to the interfacial interaction equations. These approaches are used to predict the two-phase flow characteristics. Recently, the advances in the available computational power has been deployed to ensure ability of the CFD models in resolving the energy equations, the interfacial equations for the whole phases, momentum and continuity equation. Generally, there is more accuracy when using CFD models and this is considered to be due to the CFD models having fewer assumptions. The benefit of having fewer assumptions is to ensure the reduction on the computational effort. Furthermore, dealing with the two fluid flows as one mixture is agreed to be one of the main common hypotheses particularly in case of a dilute flow.

The third approach is empirical based methods using experimental testing. The purpose of this approach is to investigate the majority of the flow properties which are mainly identified to be: the velocities, pressure, temperature, phase volume fraction and the flow rate. Therefore, from these properties, the common features and validation of these modelling methods could be obtained but it does not mean the characteristics are correct. Also, empirical or semi-empirical methods are allowed to be utilised as well. The most common place of investigating the performance of the safety relief valves is the international standards even though these standards deal with the specifications of the safety valves and their limits based on the simplified methods. There then follows a discussion of others' consistent literature for the sizing of safety relief valves under twophase flow conditions [88].

3.4.1 Simplified models used for the sizing of safety relief valves under two-phase flow

Using the international standards has led to many limitations although the majority of these limits have disappeared under single-phase flow conditions. One of these restrictions emerged in ISO 4126-10 [92] as the study is limited to cover the sizing of safety relief valves using restricted simplifying models for the two-phase flow with recommendations for categorising both quality and flow regime at the inlet of the valve itself. Also, there are no guiding principles regarding the opening and closing pressure and there is no clear procedure which should be followed for different operating requirements. The discharge mass flow rate has introduced to maintain the system pressure below a certain design pressure [88].

The international standards such as ASME, API and ISO have adopted simplified models particularly in dealing with both the selection and sizing of safety relief valve under two phase flow conditions. To understand these models, four standard approaches should be understood. Firstly, the Homogenous Equilibrium Model (HEM), a pseudo single-phase flow approach assumes well-mixed flow so that mechanical and thermal equilibrium exists. This also implies that the velocity or temperature of the two components is the same. Secondly, there is a Non-Homogenous Equilibrium Model (NHEM) that accounts for slip between the two components. Furthermore, the two mentioned models are considered as the most reliable and most appropriate for use on safety relief valves. Thirdly, there is a Homogenous Non-Equilibrium Model (HNEM) which is equivalent to the HEM but accounts for temperature difference between the two components. Lastly, there is a Non-Homogenous Non-Equilibrium Model (NHNEM) that accounts for slip and temperature difference between

the two components. The models differ by accounting for energy transfer, momentum and interfacial mass between the phases to extend their capability. The noteworthy hypothesis in these models is to represent the safety relief valve as an ideal convergent-divergent nozzle and also to determine empirically a discharge coefficient to account for model discrepancies. The mass flux is required to be determined to allow sizing of the relief valve. The discharge area of the valve could be determined by dividing the desired mass flow rate by the mass flux and the discharge coefficient. Hence, the discharge coefficient represents the major challenge in the application of the standards in sizing a safety valve.

Leung [98] considered the safety relief valve as a sharp-edged orifice for compressible twophase flow at different flow conditions. This modelling approach dealt with determining the discharge coefficient of two-phase flow. On one hand, there is a published experimental work on safety relief valves corresponding with the development of the discharge coefficient by Leung [98] which introduced a great satisfaction. On the other hand, this approach needs an initial guess value for the two-phase flow discharge coefficient by applying a trial and error procedure. Obviously, the considered geometry of the valve is to be the nozzle shape in order for the simplification of two-phase flow to be applied.

Leung [97] developed the ω Method in 1986 which is considered to be a special case of the HEM, then in 1996 was further modified by Leung himself. In addition, the ω Method is essentially based on a compressibility factor approach which can be used to define analytically the state of the two-phase flow. The so-called factor accounts for the density variation with respect to pressure change between the stagnation and the throat location. Further research has been conducted to investigate the working conditions, the limitations of this method and to find appropriate modifications for better accuracy.

$$\omega = \frac{\Delta\rho}{\Delta P} \cdot \frac{P_0}{\rho_0} \tag{3.2}$$

$$\omega = \frac{\frac{v}{v_0} - 1}{\frac{P_0}{P} - 1} = \frac{x_0 \cdot v_{G,0}}{v_0} + \frac{C_{P_L} \cdot T_0 \cdot P_0}{v_0} \left(\frac{v_{G,0} - v_{L,0}}{L_0}\right)^2 \tag{3.3}$$

Hence:

For critical conditions:

$$P_1 < n_{crit} \cdot P_0 \rightarrow G = \sqrt{} \tag{3.4}$$

Where:

$$n_{crit} = \frac{P_1}{P_0} \tag{3.5}$$

Whilst for subcritical conditions:

$$\rightarrow G = \frac{\sqrt{}}{()} . \sqrt{} \tag{3.6}$$

Where:

n_1 : The back pressure ratio $\frac{P_1}{P_0}$

The critical pressure ratio is established by Epstein, 1983 [113] for the case of $\underline{\omega \geq 2}$ as the following:

$$n_{crit} = 0.55 + 0.217 \ln(\omega) - 0.046(\ln(\omega))^2 + 0.004(\ln(\omega))^3 \tag{3.7}$$

And for the case of $\underline{\omega \leq 2}$, the following equation should be solved iteratively:

$$n_{crit} + (\omega^2 - 2\omega)(1 - n_{crit})^2 + 2\omega^2 \ln(n_{crit}) + 2\omega^2(1 - n_{crit}) = 0 \tag{3.8}$$

In addition, an explicit solution for n_{crit} proposed by Tyco, 2008 is as follows:

$$n_{crit} = [1 + (1.0446 - 0.0093431\ \omega^{0.5})\omega^{-0.56261}]^{(-0.70356 + 0.014685 \ln \omega)} \tag{3.9}$$

Derlien and Friedel [85] and [86] showed that, despite the ISO recommendations leading to oversized valves throughout the whole working conditions, the sizing of the safety relief valve under the two-phase flow conditions was precisely achieved at different working conditions by applying the ω Method.

Moncalvo and Friedel [99] carried out a study in two-phase flow under a wide variety of liquid phase viscosities to investigate the accuracy of the models especially for the process of sizing safety relief valves. The vast majority of the models which are used in the industry such as the ω Method and the ISO were also compared. Based on the previous studies, the ISO model was highly advised to be used in valve sizing. There is also a noticeable lack of knowledge concerning the characteristics of valve force-lift and flow-lift which are significantly required in understanding the closing and opening characteristics of the valves under two-phase flow conditions.

Darby [84] proposed that the discharge coefficient of two-phase flow for constant mass quality is equal to the gas discharge coefficient especially in the case of choked flow whereas in the case of non-choking flow: the discharge coefficient of the two-phase flow is equal to the discharge coefficient of the liquid component. In this model, the good mixing of the two phases is a major hypothesis (pseudo single-phase); hence, the fluid should have weighted average properties of each phase. In addition, mechanical and thermal equilibrium between the two phases is necessarily supposed. A vapour-liquid equilibrium could be assumed for a flashing thermodynamic system. For the case of no mass transfer between the two components (the so-called non-flashing flows), equilibrium assumes no difference in temperature between the two-phases. Herein the frozen flow could be easily emphasised if there is no heat transfer between the two phases. Accordingly, for frictionless isentropic choked flow through a nozzle, the mass flux (G) can be derived:

$$G = \rho . \sqrt{-2 . \int_{P_0}^{P_1} \frac{dP}{\rho^*}} \qquad (3.10)$$

The associated parameters of the above expression are further explained in Section 5.5.2.

Boccardi et al. [78] modified the discharge coefficient by attaining good results from carrying out experimental work. This experimental work was accomplished by a mathematical model. The implementation of this method showed that the equation underestimates the flow rate for the majority of the tested conditions. Despite the aforementioned limitations, the simplified models are used to determine principally the critical mass flow through the valve, particularly at the maximum lift position. This calculation of the critical mass flow rate requires the appropriate discharge area to be known in order for the correct valve to be selected for the required duty.

Boccardi et al. [79] conducted experimental work to investigate the required critical flow characteristics for the same diameter of two safety relief valves with different inlet geometry and also different discharge coefficients. The experimental results compared precisely with the ω Method and showed how the geometry can affect the sizing of the valve. Hence, undersized valves could easily result from the application of the ω Method particularly with a lower quality.

Lenzing et al. [95] investigated different safety relief valves experimentally and then compared the results with available models such as the HEM, the Homogenous Frozen and the ω model developed by the Design Institute for Emergency Relief Systems (DIERS). Lenzing et al. improved the prediction of the mass flow rate in their homogenous equilibrium model by defining a simple volume of the two phases and also by applying an equation to identify the discharge coefficient.

Diener and Schmidt [87] developed a new technique using the Homogenous NonEquilibrium Model Diener-Schmidt (HNE-DS) to eliminate some of the limitations of the ω Method. The improvement of the HNE-DS model was obtained by creating a new coefficient which is named the boiling delay (N). This coefficient was introduced at the critical cross section based on the mass quality to give a better description of thermal nonequilibrium cases for low mass fractions flows of vapour at the start of nucleation. The parameter N is in the range between the frozen flow (non-flashing) (N=0) and the homogenous equilibrium flow (N=1). There are a number of parameters that play a major role in determining the boiling delay. These parameters are: the inlet mass quality (x_0), the pressure drop and the relaxation time

between the inlet and the narrowest cross section. However, the same authors introduced a correlation for the slip velocity by modifying the model to take into account the friction between phases which is responsible for producing mechanical non-equilibrium. The final form of boiling delay factor is expressed as:

$$N = (x_0 + \left(\frac{C_{PL} T_0 P_0 (v_{G,0} - v_{L,0})}{L_0^2}\right) . ln \left(\frac{P_0}{P_{crit}}\right))^{\wedge} \alpha \quad (3.11)$$

So, Henry and Fauske (1971) recommended a value $\alpha = 0.4$for safety valves.
Hence, the ω_{DS}parameter as defined from this model becomes:

$$\omega_{DS} = \frac{x_0 v_{G,0}}{v_0} + \frac{C_{P_L \cdot T_0 \cdot P_0}}{v_0} \left(\frac{v_{LG,0}}{L_0}\right)^2 . N \quad (3.12)$$

The equation for the critical mass flux developed by Henry and Fauske (1971) is given by:

$$\frac{\sqrt{\quad (\text{——}) \quad (\quad)(\quad)}}{(\text{——} \quad) \quad]} \quad \sqrt{\text{—}} \quad (3.13)$$

The HEN-DS model was applied by Diener and Schmidt to different operating conditions to a lesser DN $25/40$ valve. The results, particularly at low mass quality achieved good accuracy compared to the experimental work, HEM and the ω Method whilst the same degree of accuracy was achieved with the three stated models at high mass qualities.

Fauske [89] and [90] determined the mass flux of the two phases by identifying individually the mass flux of the liquid and the mass flux of the gas followed by a mass weighted average of those two mass fluxes. Although the two previous methods applied by Fauske and Lenzing et al. led to reasonable prediction of the mass flow, those methods are affected by the real case of a critical mixture flow where it is postulated that the liquid phase must be identified under its non-critical conditions, and the gas phase should be calculated under its critical conditions.

Tran and Reynolds [109] proved the possibility of determining sizing for safety relief valves under the HEM. The study was based on research that was carried out by the DIERS (The

Design Institution for Emergency Relief System). The researchers applied different types of safety relief valves sizing methods to predict relief discharge rates. The predicted results based on the HEM, the recommended practice of API 520 and the so-called slip models were compared with experimental data. The study concluded that the API method leads to undersized relief valves in comparison with HEM. According to the API method and for the case of low pressure fluids, measured relief discharge rates were observed to be as high as a factor of three times in comparison to those predicted by HEM. Even though the slip models include several correlations for slip ratio, the predicted results of these slip models were in good agreement with the experiments. However, the recommended practice (RP 520 (2000)) by American Petroleum Institute (API) was found to be applicable to the proper selection and sizing of safety relief valves whose maximum allowable pressure is greater than 15 psig. Accordingly, the discharged mass flux based on using the drift-flux separated two-phase flow models of Wallis (1969) can be determined from the following equation:

$$G = \left[\frac{X\,A_G}{M_G} + \frac{(1-X)A}{M_L}\right]^{-1} \quad (3.14)$$

Where A_G and A_L are the areas occupied by the gas and liquid respectively. The sum of those two areas represents clearly the total flow area (A= A_G +A_L). The mass fluxes of the gas phase and the liquid phase are respectively written as:

$$G_G = K_d\, K_b\, P^0 \sqrt{\frac{M}{RTZ}} \sqrt{\left[k\left(\frac{2}{k+1}\right)^{(k+1)/(k-1)}\right]} \quad (3.15)$$

And

$$G_L = K_d\, K_W\, K_V \sqrt{2\rho_L(P_0 - P_1)} \quad (3.16)$$

Where: Kb, Kw and KV are correction factors, as reported in [109].

However, the non-equilibrium influences are not considered within the API 520 nor are the method acceptable at low mass flow qualities.

Friedel [71] made the first attempt to calculate the total pressure drop between the inlet and the outlet of the safety valve for two-phase two-component flow.

As far as the ω Method is concerned, this is dependent primarily upon the inlet stagnation condition but the discharge coefficients of both the liquid and the gas for single-phase flow are needed in order to make use of this approach. These discharge coefficients can be obtained either from the experimental work or from the manufacturer himself. Also, the aforementioned models are highly recommended approaches by all of the international standards for safety relief valves under two phase flow. Examples of these are: the HNE-DS model, adopted by the ISO 4126-10 with an assumption of mechanical equilibrium, and the ω Method adopted for use by API 520. Significantly, the capability of these models has been investigated widely by a large number of research studies especially in the prediction of the flow rate at different flow conditions.

The ISO recommended model, the API recommended model, the ω Method by Leung [97], and the HEM were compared for many cases in studies by Schmidt and Egan [106]. According to the comparison, the flows for smaller valve sizes could be predicted by both HNE-DS and ISO particularly for inlet pressures less than the thermodynamic critical pressure and non-equilibrium conditions. On the other hand, other models such as the HEM and that recommended by API 520 standards are used for large sized valves. In addition, Lenzing et al. [96] verified both deviation and limits of the models at different working circumstances and gases for different cases by comparing the HEM and the ω Method.

Furthermore, the modified ω Method compared well with the HEM.

3.4.2 Experiments on safety relief valves under two-phase flow

Although there are few published experimental studies investigating two phase flow or force-lift characteristics, experimental techniques can produce a good understanding of the major flow-force characteristics of two-phase flows through the safety relief valves. Accordingly, the calculation of the discharge coefficient is still thoroughly dependent upon experimental measurements as can be observed in the majority of the models and the standards. In many cases, the main purpose of the experiments is to support the validation of the analytical models.

A study was carried out by Narabayashi et al. [104], who concluded that the piston force could be influenced by the inlet void fraction. The study used a special test facility to investigate a wide range of two phase flow conditions. This study showed satisfactory results in the opening and the closing of the valve.

An experimental work was carried out by Kendoush et al. [93] and the main target of this study was to investigate the thermodynamic performance upstream of the safety relief valve under two-phase flow conditions using five different safety relief valves. Also, this study applied a wide range of pressures and good techniques of measurements were used such as a turbine flow meter to measure the mass flow rate and a gamma ray densitometer to measure the void fraction. Despite obtaining the aforementioned parameters and also the back pressure of the valves, the authors did not deliver abundant information which is essential to the characterisation of the valves. Thus, significant changes were noticed in the flow through the safety relief valves (SRVs) under the two-phase flow with providing a good numerical solution for the two-phase flow transient one-dimensional type under a wide range of pressure. This was selected to be between 4.5 to 75 bars and to present also good experiments.

Another study was carried out experimentally by Benbella [77], who applied different flow conditions on different safety relief valve types, as well as theoretically applying the Darcy equation and developed an empirical correlation to investigate the loss coefficient. This study considered some significant influencing parameters such as the Reynolds number, the void fraction, the geometry of the safety relief valve and high viscosity fluids. In addition, a good agreement was pointed out by using approximately 2000 measured data to ensure an adequate comparison for the proposed model. A standard deviation of 27% was calculated. This study also represented a vital improvement in the safety design particularly in nuclear power plants.

Another study was carried out experimentally by Moncalvo and Friedel [100] to examine how the void fraction at the inlet of a safety relief valve could be affected by the physical properties of the liquid component. This was by developing a test rig to help in measuring the required characteristics of the two-phase flow throughout the aforementioned device.

Bolle et al. [80] and [81] conducted experiments for flashing and non-flashing water flow in a CROSBY safety valve model. The study mainly measured and investigated the mass flow rate, the distribution of the pressure inside the valve and the inlet and outlet temperatures.

The mass-flow rate based on the geometry of the valve was presented as a function of the square root of the pressure drop. This study is highly appreciated due to providing a thorough base for a better understanding of two phase flow through safety relief valve. The experimental data was compared with developed and existing methods such as the HEM and the HRM (Relaxation model). The study emphasized that the two-phase flow behaviour can be substantially influenced as a result of the non-equilibrium character of rapid evaporation. The study showed that the Bernoulli equation based on the nozzle crosssection area might be a good choice for estimating the cold non-flashing water flow. The critical mass-flow rate and the pressure profile along the nozzle were accurately predicted through the relaxation model. Once the flow is choked in the injection nozzle the HRM seems to be sufficient to describe the flashing flow for high lifts. In the case of small inlet sub-cooling, the critical mass-flow rates were generally underestimated for more than 20% through the HEM. At the same inlet conditions and also with following the aforementioned assumption, the critical mass flow rate was calculated by using both models of HEM and HRM. Although there was a clear discrepancy between measured and predicted results, good agreement was observed for highly sub-cooled inlet conditions, especially when the flow was choked.

A study in safety relief valves consisted of both experimental work and CFD modelling was carried out by Elmayyah [88] in order to investigate the performance of the safety relief valve under two-phase flow conditions. The two-phase flow was a mixture of water and air with the assumptions of using the standard K-Ɛ turbulence model and the quasi-steady flow to cover the characteristics of mass flow-lift and force-lift. Also, the scaling parameters of both mass flow and piston force were proposed under a wide range of pressures and mass flow rates. The study also investigated the prediction of these stated characteristics by utilizing CFD techniques. On one hand, the experimental study provides a good contribution to knowledge in two phase flow through safety relief valves by means of investigating the mass fraction, back pressure and their effects on the discharged mass flow of the valve. Additionally, the experiment has been used to assist validation of relevant computational models which may lead to either improving or enlarging the applications of the existing models. On the other hand, this experimental work consumes time and is also expensive.

A recent study was carried out by Kourakous [113], who investigated the behaviour of a safety relief valve under various two-phase flow conditions. An industrial $1\ 1/2"\ G\ 3"$ safety relief valve was examined under two-phase flow conditions. Static behaviour of the valve was studied and a transparent model of the valve was constructed to visualise cavitation phenomenon. The transparent model was built with the same inlet and outlet dimensions but with small discrepancies from the core and seat disk of the industrial valve. The results from the transparent model of the valve tended to build the pressure drop correlation of two-phase flows. Also, different methodologies of predicting mass flux for non-flashing and flashing scenarios such as the ω method, $\mathrm{RP\ API520}$ and $\mathrm{HNE\text{-}DS}$ method were tested. Interestingly, the void fraction and bubble size and velocity were optically measured. A dual optical probe was placed perpendicular to the flow. Several measurement techniques were also employed and their working principles, their assumptions and limitations were extensively reported. The water and air flow rate were measured by using electronic flow meters and in the case of high flow rates, a rota-meter was utilized. The pressure evolution at several locations of the transparent model was measured by variable differential pressure transducers. There was also a force sensor to measure flow-force of the air and water. Statistical analysis of those measured parameters proved that all the bubbles are spherical and having the same diameter particularly those that are running at the same velocity. The study proved that the $\mathrm{HNE\text{-}DS}$ methodology is the most precise method in determining the discharged mass flow rate of two-phase flows. Even though the study concluded that the two-phase flow of air-water with cavitation phenomena could be modelled by deploying the so-called $\mathrm{CF\text{-}HNE\text{-}DS}$, further validation is still required.

3.4.3 CFD modelling of the safety relief valves under two-phase flow

Although the majority of the applicable CFD models were presented during many studies of the safety relief valve under single-phase flow conditions, a few publications of direct application of the CFD in safety relief valves under two-phase flow were introduced. This is fortunately due to the constant improvement of the physical models and capability of CFD codes. Previous CFD studies of two-phase flow have been carried out to predict the twophase flow via jets, pipes, ducts and so on but it will be readily seen that there are *not enough CFD publications* related to the safety relief valve under two-phase flow.

A study to predict a high volume fraction flow through a convergent divergent nozzle under two-phase flow of water and air was presented by Pougatch [105]. The two components of the fluid were represented as a compressible dispersed phase bubbly flow (air) and an incompressible continuous phase (water). During this study the use of a two fluid EulerianEulerian model was made by means of neglecting the mass and heat transfer between the two phases. The model consisted of momentum equations, energy equations, two sets of continuity and the standard k-Ɛ turbulence model. Good agreement with the experimental results of the mass flowrate was achieved.

A two-phase mixture model was implemented by Elmayyah [88] to predict the critical flows of air and water through an industrial refrigeration safety relief valve of ¼'' inlet bore size. The continuity equation, momentum equation and energy equation for the mixture in addition to the volume fraction of the secondary phase were numerically solved based on a 2D axisymmetric mixture model. This work followed an experimental study that was carried out for the same safety relief valve. This was for air mass qualities from 0.23 to 1, a pressure range of 6-15 barg. The two-phase mixture was vented to the atmosphere for different positions of the valve lift. The standard k-Ɛ turbulence model was used to account for the mixture turbulent transport through the valve. Predicted results of the mixture model were compared with some existing and developed models of the HEM and the HNEM adopted by international standards (ISO 4126-10). The study concluded that, the mixture model can be implemented satisfactorily to predict the flow force characteristics for the given conditions. Accordingly, this study provided a prediction accuracy, which is considered to be much better than the ISO 4126-10 sizing model with a slight deviation of 15%.

Höhne et al [76] used ANSYS CFX for simulating the flow in a safety relief valve. ANSYS CFX is an element-based finite-volume method with second-order discretisation schemes in space and time. In this case, the CFX worked with unstructured hybrid grids consisting of around one million nodes. It applied a coupled algebraic multi-grid algorithm to solve the linear systems arising from discretisation. Computational fluid dynamics (CFD) codes can help to improve design and sizing of safety valves. The ANSYS CFX code was validated based on twophase flow measurements that were carried out at the Institut für Strömungsmechanik of the TU Hamburg-Harburg (TUHH). The effects of turbulence on the flow were modelled based on a ω-based length scale equation (BSL) in conjunction with the so-called nonisotropic Reynolds model (RSM), which was extracted from the Reynolds Averaged NavierStokes

Equations (RANS). Although steady state calculation using inlet and outlet different pressure conditions was conducted based on FZD LINUX cluster with a parallel mode of four processors, the calculation was completed in 2 weeks' time. The safety valve selected in this study was modelled on 3D using the CFX code hence, an exact representation of the sensitive parts of the valve such as inlet, seat and disc and shape of the valve body was carefully achieved. In addition, different mesh densities were examined during the study. The experimental work consisted of four different types of fluid compositions with a 5.5 mm disc hub. Interestingly, one of these compositions was an air/water two phase mixture at a stagnation pressure range from 5.52 bars to 8.55 bars with a temperature range from 18.96°C to 19.57°C. The study concluded that, even though the calculation was in a good agreement with the measured mass flow rates particularly at low stagnation pressures, a clear discrepancy with a maximum of 27% was shown at higher stagnation pressures values.

Yoon et al. [110] developed a mechanistic model in order to investigate choking in twophase flow by considering only mechanical non-equilibrium. Hence, the momentum equation combined with the choking definition determined the critical mass flux. The choking mass flow was determined as a function of other parameters such as pressure, quality and slip ratio. The proposed model was assessed experimentally using air-water data and the assessment ensured up to 80% of the experimental data were well matched to predictions with a small error.

By the same authors, Yoon et al. [111], the previous study was repeated with modifications to account for thermal non-equilibrium of the two-phase flow, the development of the Bernoulli choking model and the bubble conduction time. The research eventually presented a better prediction over a wide range of pressures.

Recently, Kourakous [113] performed numerically a simple 2D axisymmetric model to extract the flow behaviour and interaction between disc-disc seat and valve body. The CFD computations followed experiments that were carried out by the same author. The numerical results of the air and water flow-force were in very good agreement with experiments with a slight deviation related to experimental uncertainty of the adjustment ring location.
Kourakous et al [114] conducted a study on a 1 ½ in. G 3in. spring loaded safety relief (SRV) to investigate valve opening characteristics associated with flow forces applied on the valve piston. A steady-state transparent model was tested for a wide range of compressible and

incompressible single and two phase flow conditions. The spring was removed and forces exerted into the valve piston were measured at different lift positions as well as different upstream inlet pressures. The experimental work was for validation purposes based on developing of a 2D axisymmetric CFD model, which was used for flow force prediction. Results of the study showed that, in terms of forces exerted on the piston, the single phase flow behaviour approached the two phase mixtures for 5-10% liquid mass fractions, particularly at higher piston lift positions. This is in addition to obtaining the physical phenomenon occurred on the fluid domain.

A successful attempt was conducted by Dempster and Elmayyah [115] who did predict the critical flow condition through a conventional safety relief valve by developing a simplified CFD mixture model for the multiphase air/water flows. The mixture model was examined by using a commercial code Fluent 6.3.2. This mixture model assumes that both phases are running at mechanical and thermal equilibrium conditions. Furthermore, the study showed very good agreement between the CFD results and the HEM method of Darby [84]. The CFD results were in good agreement with the experiments up to 40% liquid mass fraction. For larger liquid mass fractions up to 90%, a discrepancy of around 15% was evident. Unfortunately, the study does not distinguish between the types of flow regimes which are either dispersed or annular flows

3.4.4 Summary

- According to the International Standards, there are no clear design procedures regarding the opening and closing pressure of safety relief valves. Most of the international standard design methods have led to either oversizing or undersizing of conventional safety relief valves.
- There are few publications on two-phase flow through safety relief valves that have been performed based on CFD techniques.
- Although experimental facilities for investigating two-phase flows characteristics are assuredly expensive and time consuming, more experimental studies are still required to ensure more accurate validation for existing CFD models.
- After a thorough literature review, a lack of understanding in the field of heat and mass transfer mechanisms that are involved in either dispersed or annular twophase

flows through safety relief valves. Thus, a model of two-phase flow should be proposed to investigate the heat and mass transfer between phases in both cases of mechanical and thermal non-equilibrium of flashing (phase change) and non- flashing (no phase change) flows. Hence, a more accurate Eulerian model for a more realistic prediction is mainly agreed to represent the two phases (Eulerian –Eulerian).

- The modelling and investigating of the two-phase flows is to include both; firstly, an experimental work to validate the CFD model should take place based on a test rig that is based in the University of Strathclyde laboratory. Secondly, a 3D safety relief valve model should be simulated based on a commercial code of ANSYS CFD with its fluent solver. This possibly could pave our way for a better understanding of twophase flows through safety relief valves under various operating conditions.
- Large mechanical and thermal non-equilibrium condition is expected in nozzles with small area ratio since a rapid depressurization occurs in a short length path ($\mathrm{N} << 1$). The time for heat transfer between the two phases is very short. In contrast, in safety valves a more important boiling delay might occur with enough time for heat exchange between the two phases reaching almost thermodynamic equilibrium conditions [113].
- According to Bocarrdei, however, the HNE methods proposed by Fischer et al (1992) are mainly used in the case of short nozzles (less than 10 cm) where the fluid residence time could be too short for a significant vaporisation.
- The recent study by Kourakous [113] proved that the $\mathrm{HNE\text{-}DS}$ methodology is the most precise method in determining the discharged mass flow rate of two-phase flows.
- The continuous improvement of the physical models and numerical methods makes simulations of the very complex flows in safety valves now possible.
- In the Eulerian approach, the particle or droplet cloud is treated as a continuum medium with properties analogous to those of a fluid. The continuous phase is considered to be a fluid hence utilizing of the Eulerian approach for the dispersed phase is commonly referred to as the two-fluid or the Eulerian-Eulerian approach.

3.5 A review of the available literature of mechanical and thermal nonequilibrium studies on two-phase flashing flows

3.5.1 Overview

In many situations the discharge of mass through a safety valve will involve the flashing, boiling or condensation of the fluid as it expands in the valve. This may involve the nucleation of liquid or vapour and subsequent growth of the phase and will influence the vapour/liquid content and thus the critical flowrate and the dynamics of the valve. In this chapter the modelling of such processes will be reviewed via the existing literature with a particular focus

of high vapour fraction flows when occurring in a high speed, expanding condition, such as in valves, nozzles and free discharge pipe exits.

3.5.2 Existing attempts for a two-phase flow (liquid and gas) with evaporation or condensation

Condensation is a thermodynamic non-equilibrium process of phase change from the gaseous to the liquid phase. For the conditions studied in this thesis the non-equilibrium is created by the rapid temperature variation due to the acceleration of the fluid. In response to this, two mechanisms of phase change can be distinguished: the creation of new droplets per unit volume (nucleation) and the evaporation or growth of the existing droplets. Eventually, the appearance of new droplets with the size of a critical radius $\mathrm{r_c}$ starts when the vapour temperature falls to particular value below the saturation temperature (steam starts to nucleate for sub-cooling temperatures between 30 and $40\mathrm{K}$) [136]. As a result, a wide variety of industrial applications have been investigated for many decades. In the energy sector and in terms of the efficient production of power, condensation in the steam turbines of conventional power plants remains one of the important issues. It is a very serious problem, particularly in the low pressure turbine stages, since they are responsible for generating the largest portion of the power amongst all of the stages. This is mainly due to additional losses and blade erosion that are encountered as a consequence of condensation induced droplets.

Extensive experimental and theoretical publications dealing with steam-water mixture flows were found throughout the literature. The majority of these were focused on bubbly flows where initially saturated or subcooled liquid was the test fluid [119] [120] [121] [122] [123] [124] [125]. In addition, the vast majority of these studies were conducted to examine mainly the critical mass flowrates of two-phase flashing flows in nozzles and pipes.

An extensive review of the various analytical methods proposed for two-phase critical flows was introduced by Graham and Wallis [123]. The review was aimed to include other aspects of the two-phase critical flow issues that have not been addressed through previous review articles of “Simon (1973), Hutcherson (1975), Lahey & Wallis (1975), Ardron & Furness (1976), Boure (1977) and Jones & Saha (1977”. The review also reported that mathematical expressions for critical flowrate derived by Moody, Fauske, Henry and Fauske can be found in the paper presented by Henry (1979). These algebraic formulas were found to cover a wide

range of homogenous equilibrium and frozen models; however, the non-equilibrium two-fluid models were presented in the paper by Wendroff (1979).

A systematic evaluation of the existing data and theoretical models used for determining the critical flowrate was conducted by Elias and Lellouche [122]. The main purpose was to provide a general overview of two-phase critical flow and to establish useful codes for thermal-hydraulic systems.

A valuable review relevant to modelling of steam-water mixture flows in nozzles and pipes was carried out by Schwellnus and Shoukri [124], who presented the available models for simple semi-empirical, mixture and two-fluid approaches.

An experimental study based on steam-water flows in a rectangular cross-section converging-diverging nozzle was carried out by Alger [118]. The study aimed at determining the droplet size distribution, the droplet spatial distribution as well as the mean droplet velocity. Unfortunately, crucial details of the numerical method and dimensions of the experiential nozzles were not clearly apparent in the available copy of the thesis.

An analytical and experimental study was performed by Charless [150], who examined the flow of air-water and steam-water mixtures at low liquid fractions for a 2D convergingdiverging nozzle. A 1D flow model was developed to explicitly include the mass, momentum and energy transfer between the two phases, hence to calculate the critical flowrates and the pressure distribution along the nozzle length. The study ignored the condensation effects (due to the formation of nucleation) within the vapour phase; therefore a discrepancy between the analytical model and the experiments was observed particularly in the divergent section.

A good attempt at modeling the two-phase turbulent flows (a condensing-flow problem) in a horizontal constant-cross section tube was conducted by Dunn [135]. The study focussed on the development of a one-dimensional framework for two-fluid modeling, to identify issues related to two-phase phenomena and to implement the model on a computer code. Accordingly, important models were required for the distribution of the vapour and liquid in the cross-section along the axial direction plane of the tube. At the boundaries of each phase, models for the transport of mass, momentum and heat were proposed. The study showed that the interfacial shear stress, associated with the dissipative effect of wave generation and

decay, was more significant than the shear stress at the wall. The singlephase heat transfer coefficient approach was implemented to highlight the possibility of modeling heat fluxes between the two phases and also from each phase to the wall. The mass transfer flux at the interface was identified by utilizing two different approaches. The first approach was based on a temperature jump assumption at the interface by employing the kinetic theory of gases, and the second one was based on determining the difference between the vapour and liquid heat fluxes at the interface. The study presented some unresolved issues such as (1) the two-fluid equations that have been implemented to resolve the problem do not distinguish between different flow regimes (2) there is no clear method for predicting the temperature jump at the interface.

A study was conducted by Karkoszka [134], who investigated numerically and analytically the water vapour condensation from the multicomponent mixture of condensable and noncondensable gases. In terms of application, the study was performed on pressure water reactor containments (PWR). An informative comprehensive literature review in the area of the nuclear reactor thermal-hydraulic safety was well-presented. A general mathematical description of simplified physical models was developed to appropriately treat both liquid and vapour as Newtonian fluids and the pressure tensor fulfils Stokes hypothesis. In terms of heat and mass transfer phenomena, the analytical solution was identified by employing *the boundary layer approximation and the similarity variables method* to a system of film and mixture conservation equations. The numerical solution was achieved by using an inhouse developed code and commercial CFD software. The study showed that the heat transfer enhancement was due to the presence of waves, resulting from liquid film instabilities. This heat transfer development was straightforwardly allied to the internal film hydrodynamics "(As reported, Banerjee et al (1967) was one of the first who investigated theoretically the influence of the wave hydrodynamics on the mass transport phenomena)". Three approaches for the modeling of the condensation phenomenon were reviewed: Empirical correlations, Analogy between heat and mass transfer (namely, the Nusselt number and Sherwood number), Diffusion layer model or thermal resistance model (DLM or TRM) and eventually Boundary layer approximations and fully mechanistic model. Although the aforementioned model was applicable for two or even three-dimensional fully coupled system of conservation equations, it included enough information about the investigated phenomenon and its general applicability were the downsides.

An article authored by Gerber and Kermani [136], described a model for homogenous nucleation in transonic turbulent flow applicable to the wet stages of a steam turbine. In particular, the model was to predict the moisture distribution in high-and low pressure steam flow in a 2D rotor-tip section of a single stage turbine and a Laval nozzle. A full Navier-Stokes viscous flow solution procedure was implemented based on employing a pressure based finite-volume/finite-element discretization of the governing equations of fluid motion. Eulerian multiphase equations were formulated to govern both the vapour and liquid phases. Classical nucleation theory of Macdonald in 1963 "cited in [136]", and the concept of the droplet interfacial area density (IA) were utilized to formulate the multiphase governing equations. A scalar transport equation accounted for the mass conservation of liquid droplets, which were assumed to be very small and travelled at the vapour velocity allowing one of the momentum equations to be used to determine the liquid velocity. The volume occupied by the liquid phase was small due to low mass fractions of liquid, which led to the volume fraction equation being neglected and made the computational solution less expensive. The droplet temperature was assumed to be uniformly distributed due to their small size and fortunately led to eliminating the need for a mass transfer model. The highReynolds number k-Ɛ turbulence model was employed with an assumption that the liquid droplet has no direct influence on the velocity field. Only the turbulence in the vapour phase has an effect on the droplet dispersion. An obvious solution strategy was followed by applying an implicit time integration scheme without any constraints on time-step selection (Large time step can be easily applied). An algebraic multi-grid (AMG) approach was used to resolve the discrete equations, along with the use of the popular SIMPLE method of segregated iterative procedures to solve the pressure-velocity coupling in the flow. Convergence strategies with the highly non-linear homogenous nucleation process were described. The model was implemented within the commercial CFD code CFX-TASCflow.

A study was presented by Simpson and White [139], who calculated spontaneously nucleating flows of wet-steam through different converging-diverging nozzles. A twodimensional calculation of the Reynolds-averaged Navier-Stokes equations for a two-phase mixture was solved, using a Jameson-style finite volume method based on an unstructured triangular mesh that was adapted in the rapidly changing condensation zone. The numerical scheme was similar to an unstructured tetrahedral flow solver that was developed by Dawes in 1992 "cited in [139]". The mixture consisted of vapour at a pressure$P$and temperatureT_v, and spherical

liquid droplets with sufficiently small sizes at temperatureT_l. This also was in the absence of velocity slip as the small droplets were to travel at the same vapour velocity. All the quantities were averaged, with pressures and densities taken as time averages, whilst other variables such as internal energy, enthalpy and velocities were described as density weighted averages. With regards to turbulence modeling, the stress tensor components consisted of laminar and turbulent contributions which were calculated by means of laminar and turbulent viscosities μ_L and $\mu_T$respectively. Thus, the laminar viscosity of the mixture was sufficiently quantified by its vapour phase due to a practical fact that the volume fraction of the liquid phase for the majority of wet-steam flows is too small (in order of 10^{-5}). On the other hand, the calculation of the turbulent viscosity was based on a standard$\mathrm{k}$-$\mathrm{\varepsilon}$ model of Yang and Shih in 1993 "cited in [139]". Two approaches were followed: firstly, a numerical scheme was implemented to identify steady viscous flow and based on that, a significant influence of boundary layer growth on a stream-wise pressure distribution and droplet sizes was shown. Secondly, the same numerical simulation was applied to calculate unsteady inviscid flows in different nozzle geometries with a variety of inlet conditions. In this study the first predictions of *an asymmetric oscillation mode* in pure steam was made. In fact, the first detection of an asymmetric oscillation mode was by Adam and Schnerr in 199 "cited in [139]" and the poly-dispersed nature of droplet size distribution was adapted by the author here based on a moment-based method (MOM) as it was introduced first by Hill in 1966 "cited in [139]".

A study was performed by Guha and Young [140], who developed a one dimensional timemarching technique that can be employed for a wide variety of pure steam flows in convergent-divergent nozzles. An accurate, fast and simple model was described and applicable for the simulation of steady or unsteady, nucleating or non-nucleating, and subcritical or supercritical flows of wet steam. The developed model was based on a novel technique that involves the integration of the droplet growth equations along the fluid path lines, instead of freezing the gas dynamic flow field instantaneously in preforming the integration. Thus, accurate coupling was maintained to simulate the relevant equations of the vapour phase gas-dynamics and the relaxation effect of the droplets. A poly-dispersed droplet spectrum was maintained by the scheme to model the nucleation zone precisely. The steady and unsteady results of this study achieved much closer agreement with reported experimental measurements. The study showed that the poly-dispersed droplet spectrum might be augmented due to supercritical heat addition caused by an unsteady condensation.

Unfortunately, this scheme could not predict this phenomenon. Supercritical heat addition can easily result in a compressive wave causing unsteady operation. This wave can propagate towards the nozzle throat resulting in a pressure rise causing a reduction in nucleation rate. It is worth mentioning here that the process can easily repeat itself. In 1962, Schmidt "cited in [140]" was the first in reporting such types of instability resulting from supercritical heat addition. The study was well-presented particularly in modeling the nucleation rate of droplets and the subsequent growth of the liquid phase. One of the drawbacks of this study is that there was no clear difference between the presented scheme of heat and mass transfer and the other scheme, which is mainly dependent upon the difference between the surface temperature of the droplet liquid phase and the fluid path line of the gas phase.

Bakhtar et al [141] discussed the classical theory of homogenous nucleation of liquid droplets from supersaturated vapour and its application in predicting condensation in steam nozzles. A review of classical nucleation theory focused on the up-to-date modifications that were made to the original theory of Becker-Döring. The study showed that the required accuracy of the new modified correlations, which are derived from first principles, has not been attained yet. All of the accomplished calculations were based on the implementation of the numerical integration of the droplet growth equations through the nucleation zone. It is interesting to refer to the simplifications that were made by the authors, who applied both tabular and analytical methods. During the study, more attention was drawn to the tabular methods, where the data for the resulting mean droplet size and vapour behaviour for a given degree of super-cooling on the steam, were pre-computed to avoid undertaking more extensive numerical calculations. However, it is worth mentioning here that the original equation of the nucleation rate with the Courtney and Kantrowitz modification is the most successful form. Based on the latter crucial form of nucleation rate and the combination of a standard droplet growth model and a suitable equation of state for steam, the sauter mean droplet radii and the nozzle pressure distributions over a range of conditions can be predicted. On the one hand, the study addressed homogenous nucleation rate at the inlet to high-pressure (HP) turbines of pressurized water reactors of nuclear power stations. On the other hand, the study was not successful for very low pressures as the droplet growth rate in the nucleation zone was underestimated.

A study was conducted by Guha [142], who investigated numerically and analytically the internal structures of partly dispersed shock waves in pure vapour-droplet system. "This type

of shock wave was described as a steep-fronted discontinuity that is dominated by viscous dissipation and thermal conduction, followed by a relaxation zone". It can be readily noticed in a flow field whose upstream velocity is greater than the local frozen sonic speed. The relative effects of different flow variables (the droplet radius, wetness fraction, and frozen Mach number) on the structure and thickness of the shock wave were systematically analysed. The study also identified the occurrence of complete evaporation far upstream and far downstream of the shock wave. The study proved that if the upstream liquid mass fraction is sufficiently high the liquid phase might be completely evaporated after a strong frozen shock. For the case of a vapour-droplet mixture in equilibrium, it was noted that the two-phase flow was converted to a single-phase system downstream of the shock wave. This does not occur for solid-particle-laden gas flow. The assumptions were made; the droplet temperature is equal to the saturation temperature hence, the change in enthalpy was ignored and the effective mass transfer was neglected. The three linear simultaneous differential equations consisting of the three quantities of the velocity, pressure and temperature were solved. These equations were incomplete therefore; three supplemented equations were necessary to close the procedure. The latter equations represent the interphase transport of mass, momentum and energy. The interphase mechanisms were of great importance to account for the rate at which the two-phase mixture reverts to equilibrium. These were mainly based on a process of three different relaxation times. The study showed that the droplet could not drag the vapour even though the liquid phase velocity was moving relatively faster than the vapour. The study also concluded that the linearized analysis was unsuccessful in such cases although the procedure was often presented for relaxing flows downstream of frozen shocks but it was of limited capability to vapour-droplet flows.

By the same author [143], the previously mentioned work was extended to form a unified theory for different types of discontinuities, which can occur in a steam-water droplet mixture with or without a carrier gas, through a broad variety of operating conditions. This is based on a control-volume analysis that is similar to that of an adiabatic shock wave in an ideal gas. In reality, the vapour-droplet mixture does not have a unique sonic speed and when the non-equilibrium exchanges of mass, momentum and energy between the two phases are substantial, the analysis procedure becomes more complicated than in an ideal gas. The two types of discontinuity presented were aerodynamic and condensation shock waves.

Surprisingly, these types of shock waves were modelled by applying the same conservation equations. Approximate, explicit analytical jump conditions across these discontinuities were derived and found to be applicable to several boundary conditions. The latter procedure might be named the generalized Rankine-Hugoniot approach and is also applicable for pure vapour-droplet flows where the mass fraction of the carrier gas is equal to zero. The presented integral analysis contributed to more physical insight and showed four different types of aerodynamic shock wave: equilibrium partly dispersed, equilibrium fully dispersed, partly dispersed with complete evaporation, and fully dispersed with complete evaporation. The study also specified the conditions for each type of shock wave to occur and derived the appropriate jump conditions. This research work deduced a flow map for different types of condensation shock wave to occur. Same jump conditions were successfully applied to most supersonic and subsonic condensation of both homogenous and heterogeneous flows. In addition, time-marching solutions for different types of condensation shock waves in convergent-divergent nozzles were presented and novel solutions were obtained.

A study was recently presented by Zhu et al [144], who developed a numerical method within an Eulerian-Eulerian framework for the purpose of modelling non-equilibrium condensing flows in nozzles and a cascade of steam turbines. The above-mentioned framework was based on the so-called Jacobian matrix where a Roe convective flux was featured with real steam properties considered with fully coupled wetness fraction along with other conservative variables. Therefore, right and left side eigenvectors of the analytical expression were deduced and the treatment of real steam properties was accounted for via the original two-dimensional Tabular Taylor Series Expansion method (TTSE). The latter was extended to cover the three dimensions and contribute to a more convenient Euler-Euler model. During the study, one of the greatest challenges was modelling of the poly-dispersed droplet spectrum, which was addressed by implementing the Quadrature Method of Moments (QMOM). For steady state problem, however, stability issues were encountered due to moment corruption. At early stages, during a time marching scheme, difficulties of disturbed flow field and corrupted moments data were incurred; henceforward an elegant correction scheme was applied to overcome these vital problems. The model was applied to two nozzles and one cascade cases and the results were good particularly for the nozzle pressure. On the other hand, prediction of the sauter radius was more difficult as it was strongly dependant on

droplet number and droplet distribution. The study revealed clearly that “it is hard to tell whether the QMOM method provided better results than the method of moments (MOM)”.

Ju et al [145] performed a study on nozzles and a 2D cascade, carrying a two-phase wet steam flow with spontaneous condensation. Experiments and flow analysis on a nozzle were accomplished for the validation of the numerical model. A three-dimensional ReynoldsAveraged gas-liquid two-phase flow solver was applied with a swirl modified k-Ɛ turbulence model. The study also included a development of a 3D numerical calculation on the last stage stator of a steam turbine. The study concluded that the droplet growth rate following a nucleation process can significantly cause a sudden pressure rise particularly on blade suction surface. In the rear of the cascade passage, the sudden pressure rise was not of significance although there was noticeable condensation. This work also showed that the maximum under-cooling and the number of droplets per unit volume resulted most likely from a bulk nucleation rate. An obvious influence on the outlet parameters of the blade cascade was due to an interaction of a weak condensation wave and a strong aerodynamic shock wave. During the condensation process near a blade surface, there was a reduction of the flow velocity due to an increase in liquid momentum that was delivered from the gas phase momentum.

Senoo and White [146] presented numerical techniques for non-equilibrium condensation in low pressure steam turbines. They described a finite volume method based on conservation equations for homogenous gas-liquid two-phase compressible flow, implementing a third-order upwind Total Variation Diminishing (TVD) scheme. The solver for these equations was Roe’s approximate Riemann scheme, which was modified to take into consideration the wetness level. This was used to compute homogenous nucleation based on the classical Volmer-Frenkel model and droplet growth in transonic flow regimes that comprise complex shock waves. According to the latter corrected classical theory, the effect of the droplet temperature was taken into account for the droplet temperature being higher than the vapour temperature (non-isothermal process) due to released latent heat. Two approaches to modelling the heat transfer controlled droplet growth were taken: (1) a semi-empirical two-layer model (valid over a broad variety of Knudsen number) and (2) a free molecular flow model. Another part of the study mainly focused on a convergentdivergent Laval nozzle. The droplet growth was calculated by deploying the surface averaged radius as the mass and heat fluxes on the surface of droplets can appreciably govern this growth rate. The generated liquid

phase and its growth were modelled by applying conservation equations for the first four moments of the droplet size distribution that were coupled with nucleation and droplet growth expression. Both schemes of steady and unsteady condensing flow were included and two types of self-excited flow oscillation approaches (symmetric for lower inlet sub-cooling & asymmetric for the higher) were devised. The study proved that a significant variation in expansion rate led to various droplet sizes. Furthermore, the two-layer model's prediction of droplets diameters, were in good agreement with the experimental data. The pressure distribution and sauter mean droplet diameters were identified and results agreed well with experiments. The study also concluded that the modified solver provided more numerical stability and high accuracy particularly in the transonic region. Thus, more important information on the phase change and the complex interaction can be obtained. The computational results showed that "oblique shock waves can turn the flow direction and increase the local flow area independently of the geometrical cross-section of the nozzle". This local flow area increment resulted in more heat addition to be absorbed and led to unsteady and unstable flow.

Yang and Shengqiang [137] presented a study on a conventional Laval nozzle. This was based on a numerical simulation for the prediction of the non-equilibrium steam flow with spontaneous condensation. The numerical calculation was considered as a conservative 2D compressible model for supersonic non-equilibrium condensing steam flow. The EulerianEulerian approach was adopted based on Navier-Stokes equations with transport equations for the number of liquid droplets per unit volume and the liquid mass fraction. The representation of these conservative equations was based on the classical nucleation theory and the droplet growth model for the liquid phase, and the Virial style equation of state for the gas phase. A conservative finite-volume second-order upwind scheme of integration was selected to discretize the liquid and gas phase conservation equations over a control volume. However, several assumptions were performed: the liquid was mono-dispersed (the droplets are of the same size and the interaction between droplets is negligible); the condensing steam was adiabatic and inviscid; the slip velocity was equal to zero and the influence of the condensed liquid droplets was ignored. In the simulation of the turbulence, the standard k-ε model was considered only for the gas phase whereas the influence of the liquid droplets on turbulence conditions was indirectly modelled through the velocity field instead of the direct effect on the turbulence model. In terms of the framework for the solution of the governing

equations, the above mentioned model was implemented and solved within commercial CFD code FLUENT. With these assumptions, a qualitative and quantitative description for the physical phenomenon of a condensing flow was well presented. Validation was attempted and results showed good agreement between the current numerical calculation and existing experimental data. The study showed that transonic or supersonic flow dynamics can be strongly affected by the release of latent heat resulting from a homogenously nucleating steam. Flow shock waves are also present. The study proved that, there is a difference between the dry isentropic expansion and the supersonic steam flow as the latter can introduce non-equilibrium condensation in the form of "a condensation shock".

Gerber and Mousavi [138] investigated the droplet size distributions existing in low-pressure steam turbine stages. The work was aimed at the development of fluid power machines based on Quadrature Method of Moments (QMOM) and this was to treat poly-dispersed droplet spectrums. The above method was achieved by extending the lower-order moments approach, which was firstly introduced by Hulbert and Katz in 1964 "cited in [138]". During highly expanded transonic flow with adequate super-cooling, primary and secondary nucleation could occur along the flow path for particular droplet distributions. One of the aims of this work was to examine how well QMOM represented droplet size information. The study also categorized the phase transition process in a low-pressure turbine into three phases: (1) heterogeneous nucleation of moisture that appeared via the early stages of the turbine (0.1—1μm) (2) primary homogeneous nucleation occurred in subsequent stages due to significant super-cooling (1 × μm) (3) secondary homogeneous nucleation occurred at the last stages where the high vapour expansion and moisture content was found. It is also shown that inclusion of the QMOM method within a CFD code can play a significant role in describing quantitatively the impact of moisture formation at this level of pressure. The study pointed out that a significant improvement in condensation models would be provided by applying the QMOM method.

A study was carried out by Halama et al [147], who developed a numerical method algorithm to solve Ordinary Differential Equations (ODE's) for condensation/evaporation phase change on transonic flow of a steam/water mixture. This was based on solving a system of PDE's of Navier-Stokes equations for wet-steam flows and transport equation for the integral parameters defining the droplet size ranges. Due to the stiff character of the source terms, the numerical calculations were reliant on a fractional step technique. The Lax-Wendroff

finite volume scheme with conservative artificial dissipation terms and a structured grid was implemented to separately calculate the set of homogenous PDE's. Implicit Euler or explicit Runge-Kutta method were used to solve the remaining set of ODE's. It was shown that the model can also distinguish between evaporation and condensation, and this procedure was mainly dependent on two types of critical radius regimes ($r_c > 0$ for *condensation* and $r_c = 0$ for *evaporation*). The model was found applicable for steady and unsteady two-phase transonic flow in 3D turbine cascades, 2D rotor turbine cascades as well as 2D nozzles. Numerical results were in good agreement with existing experimental data particularly the static pressure distribution along the axial direction of the Barschdorff nozzle.

Cioncolini et al [148] proposed two algebraic turbulence models for liquid film and the droplet laden gas core of adiabatic annular two-phase flow. In fact, this type of flow pattern is classified to be the most common and the most complicated form of fluid motion amongst all the flow regimes. The complexity results from the dynamic forces such as gravity, inertia and viscous that could influence hydrodynamics of the liquid film, concurrently the surface tension and the drag of the gas have direct effects on the morphology of the liquid-gas interface. Inside the gas core, the drag exerted by the gas phase on the entrained droplets together with the inertia of the liquid droplet can lead to a reduction in the droplet velocity. It is worth mentioning that the droplets would be entrained continually from the top of the roll wave moving in the liquid film. Although the proposed models were limited to turbulent momentum transport, they were used to foresee key features such as pressure gradient, average liquid film thickness and velocity profiles of the gas-liquid annular flow. The fraction of liquid droplets entrained in the gas core was empirically predicted. Experimental data were carefully identified to critically assess both turbulence models performance. The latter was in better accuracy than both; the universal velocity profile of the single-phase theory and the two-layer annular film model proposed by Dobran in 1983 "cited in [148]".

Cioncolini and Thome [149] extended their work of 2009 to cover cases where evaporation is present. The study mainly focused on modeling momentum and heat transfer (convective boiling) through adiabatic and diabatic annular two-phase flow. This was predominately based on an algebraic turbulence model. Hence, two turbulent eddy diffusivities for momentum and heat transfer were required to provide the velocity and temperature profiles through the liquid film. The annular liquid films here were assumed to be dominated by shear-driven, which behaved like fluid-bounded flows interacting with the gas-entrained droplets

core flow. Other key parameters such as a void fraction, a convective boiling heat transfer coefficient and an average liquid film thickness were determined by implementing the proposed turbulence model. This model was unified with other existing methods to identify the axial fractional pressure gradient as well as the entrained liquid fraction. The current turbulence model was compared with the single-phase wall bounded flow theory and other design correlations. Results from the new turbulence model showed better accuracy than the others. The study was carried on vertical and horizontal tubes whose diameters were in the range of 1.03-1.44 mm, as well as operating pressures were in the band of 0.1-7.2 MPa. Nine fluids; six refrigerants, two hydrocarbons and water were covered from an available database. It was noted “there appears to be no macro-to-microscale transition when it comes to annular flow. Simply better physical modeling is required to span this range”.

3.5.3 Summary

- After an extensive review of existing two-phase flashing flows (steam-water), no CFD study with application to safety relief valves were found. However, the vast majority of the studies presented have been devoted to either nozzles or turbine cascade.
- In reference to the above-mentioned studies, there is no clear unified EulerianEulerian model being proposed to deal with mechanical and thermal non-equilibrium two-phase flashing flows.
- One of the available attempts has included the effect of shock waves particularly on flashing flow conditions where the mass transfer exists. Thus two issues have been thoroughly tackled based on the work of Young and Guha of 1991. Firstly, at certain inlet conditions of super-saturation when steam expands through a nozzle, the droplets do not appear as soon as the condition line crosses the saturation line and the steam remains dry in a metastable equilibrium until the super-saturation ratio becomes high enough to activate an appropriate nucleation rate. Secondly, due to the high latent heat of water, the growth rate of the droplets in pure steam is limited by the rate of heat conducted away from the droplet.
- The droplets are formed and grow in size by exchanging heat and mass with the surrounding vapour. At this point, if the flow velocity in the nucleation zone is

supersonic, the heat released by the growing droplets results in a gradual increase in pressure known as the condensation shock.

- For high initial superheated steam at nozzle inlet, the condensation shock appears in the diverging section and then causes the flow velocity to decrease but always remains greater than the local sonic speed [140].
- The latent heat release due to droplet growth followed by nucleation (droplet increases in size as water molecules condense on its surface), causes a significant rise in droplet temperature then becomes apparently higher than the steam temperature.
- It was observed by Reocreux [70] and in many other fundamental experiments that during fast evaporation the two-phase mixture does not follow the saturation conditions which results in overheating of the liquid phase. Taking this into account, the relaxation model [72], with developed correlation for the relaxation time [73], has been chosen. Its critical velocity tends to the speed of sound of pure liquid when void fraction goes to zero. The relaxation model (REM) belongs to the family of nonequilibrium models represented also by the delayed equilibrium model [74].
- According to Bakhtar et al [141], for validation of nucleation in convergent-divergent nozzle, measurements of nozzle pressure distributions and mean droplet diameter are inadequate to reveal completely independent checks on the aforementioned trends.
- In order to model the nucleation rate of water droplets from supersaturated steam and its growth rate, the latest modified form of the nucleation rate equation is to be adopted. Unfortunately, the available commercial ANSYS CFD Fluent 14.0 does not include explicitly this nucleation form. However, this could be achieved by implementing a nucleation rate as a source term through the user-defined-function procedure. This procedure should ensure that all the conservation equations of mass, momentum and energy for both scalars of the liquid and vapour have included this source term. Nonetheless, the available Fluent code has some limitations on embedding variable source terms through the transport equations (accept only constant values).
- Alternatively, the nucleation rate and droplet growth rate can be modelled based on an available mixture wet-steam model of the CFD Fluent code, which is applicable for a wide range of liquid mass fractions with restricted assumptions of no-slip between

phases (mechanical equilibrium) and also both phases are in thermal equilibrium conditions. It is also limited to a saturation temperature of $273\mathrm{K}$ to $670\mathrm{K}$.

- According to Zhu [144], “Commercial software such as the CFD Fluent-code can only deal with mono-dispersed droplets (uniformly distributed droplets)”. However, the Quadrature Method of Moments (QMOM) was implemented to model the polydisperse droplet spectrums even though the condensing phenomenon in nozzles is relatively simple and the poly-dispersion is not of importance.

Chapter Four

4 Compressible Single-Phase Flow of Air

4.1 Overview

It is of importance to commence investigating single phase flows through safety relief valves before dealing with two phase flows. The general characteristics of single phase flows may pave the way towards an understanding two phase flows. Thus this chapter investigates

computationally and experimentally a compressible single phase flow of air through a conventional spring loaded safety relief valve (SRV). The flow path through the valve is complex and generally multi-dimensional distinguishing it from previous detailed modelling studies of critical flow where simple nozzles have been examined. In this study the main focus of attention is the flow in the vicinity of the seat and piston since this is where the first occurrence of critical flow occurs and controls the valve's mass flowrate. To achieve this, the flow undergoes a series of contractions and expansions in an annular space and can be modelled using two dimensional axi-symmetric assumptions. The inherent unsteady flow process can be simplified to a series of quasi static processes assuming that pressure waves can be ignored, which is attributable to a relatively slow motion of the piston compared to the time scales of the pressure waves. Hence the flow in the valve at various valve openings is adequately represented by a series of steady state conditions. It is expected that this would be more appropriate for the closing operation of a safety relief valve than the opening phase. The main goal of this chapter is to examine the predictive capability of a computational fluid dynamic approach (CFD) then to clearly establish an experimental methodology to validate the CFD prediction. This is based on knowing particularly flow and force lift characteristics. The existing commercial code of ANSYS FLUENT is mainly deployed. The following sections discuss the valve details, the experimental and computational investigations, the results and scaling of the data for the safety relief valve tested under steady state single phase flow conditions.

4.2 Valve Details

A conventional spring loaded safety relief valve commonly used in refrigeration systems was investigated. It is used mainly for refrigerant vapours but it is operated here with air. Figure 4.1 depicts a cross section of the safety relief valve which comprises a movable piston (2), loaded by a spring (5) to the required relief pressure. The spring load is retained and applied by an adjustable gland (4). The valve establishes a seal through a
sealing disk inserted into the piston which sits on the valve seat (3) machined into the valve body, to maintain the system pressure. Detailed manufacture's CAD drawings are shown in Appendix A.

4.3 Valve Operation

The operation of the valve is mainly a dynamic process therefore exceeding the set pressure leads to the piston lifting-off to allow mass to discharge via the available flow area. The piston lift relies essentially on the increasing system pressure which is expected to be limited due to the greater flow discharged. The valve is designed to be held fully closed until an allowable amount of pressure is reached. This predetermined relieving pressure is set by the initial compression of the spring and could be altered easily whenever required. At the time of discharge when the upstream pressure is greater than the set pressure, the valve should reach the full lift which is normally achieved by building up the pressure that follows the opening of the valve. As soon as normal conditions are obtained in the system, the valve must return to a closing position.

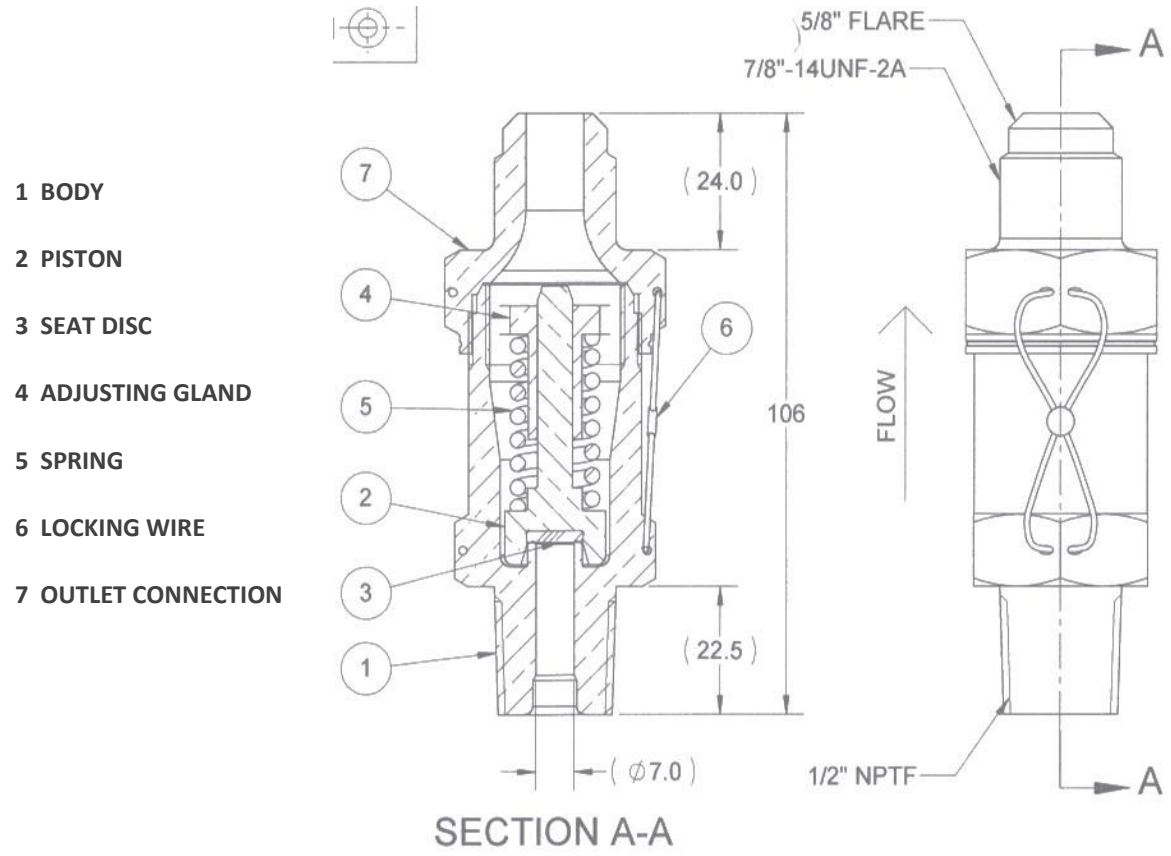

Figure4-1: Valve Construction (Dimensions in mm)

4.4 Single Phase Testing

Experimental work has been carried out to determine the flow-lift and force-lift characteristics which are then used to validate the CFD results. As mentioned, quasi static flow assumptions have been assumed to achieve the characteristics that are associated with single test pressure values. To do so, a test rig was constructed to facilitate the piston displacement (Lift), upstream pressure, back pressure, flowrate and force measurements.

4.4.1 Test rig construction

An experimental flow facility for valve testing under steady state flow conditions based in the Department of Mechanical and Aerospace Engineering at University of Strathclyde has been developed. Figures 4.2 and 4.3 show a schematic diagram and layout of the test rig. This has been developed to allow measurement of the upstream and downstream pressures at various piston displacements, net force acting on the piston and the mass flowrates through the valve.

The tested valve is supplied with compressed air through a 100 mm (4 inch) diameter pipe connected to a compressed air system that can deliver compressed air at a pressure between 1-15 barg. The tested safety valve is connected to the pipe via a brass converging section adapted to the valve entrance. A PVC T junction with a 50 mm diameter side exit is connected to the valve outlet. The T junction could be maintained close to atmospheric pressure. It has a pressure tapping fitted to measure the pressure at the valve outlet. The valve piston is attached to a 250 mm long 6 mm diameter rod which passes through the far end of the PVC tube end and is connected to a lead screw and traverse table allowing the piston position to be adjusted. The valve spring was also removed. The rod was made of steel and selected to have a minimum diameter to resist the aerodynamic forces and prevent buckling. Although the rod results in 14% less flow area at the valve outlet the gland area is modelled consistently where critical flow occurs and leads to conditions upstream of the gland being independent of the valve outlet geometry. Previous studies on similar valves [15][88] indicate no significant effects on the measured and predicted parameters when the spring removed. With regards to the piston force measurement, the end of the rod is attached to a load cell that has a range of (1 to 500 N) (Omega Eng. Limited LC 203-100) with an accuracy of 1 Newton that indicates a measurement uncertainty range of 0.5% to

2% for the measured values. The piston movement via a linear cross slide is in the range of 0-5 mm and was measured by a Mitutoyo digital dial indicator with sensitivity of 0.001 mm. This reports a relative uncertainty of the order of 0.01% to 0.6%. The air flowrate was measured using a Sierra Vortex mass flowmeter (Innova mass 240) and accurate to <1% of reading. The upstream pressure and outlet pressure are measured by Bourdon pressure gauges with an accuracy of 3kpa which gives a relative uncertainty of 0.2-2.5%. The range of upstream pressures (1-15 barg) gives a working air flow rate from 0.004 to 0.12 kg/s. In reference to the back pressure measurements, this was carried out using a modified piston tube. The piston rod was replaced by a steel tube of 6 mm diameter and 245 mm length again attached to the piston back face. The steel tube has an inner diameter of 2 mm and a pressure tapping hole of 1 mm diameter made close to its end near to the piston back face while the other end of the tube is attached to a pressure transducer through a T junction then to a pressure gauge. The tube end is also connected to an extension which is screwed into the load cell. Full details of the steel tube and the fitting used are shown in Appendix B via a CAD drawing.

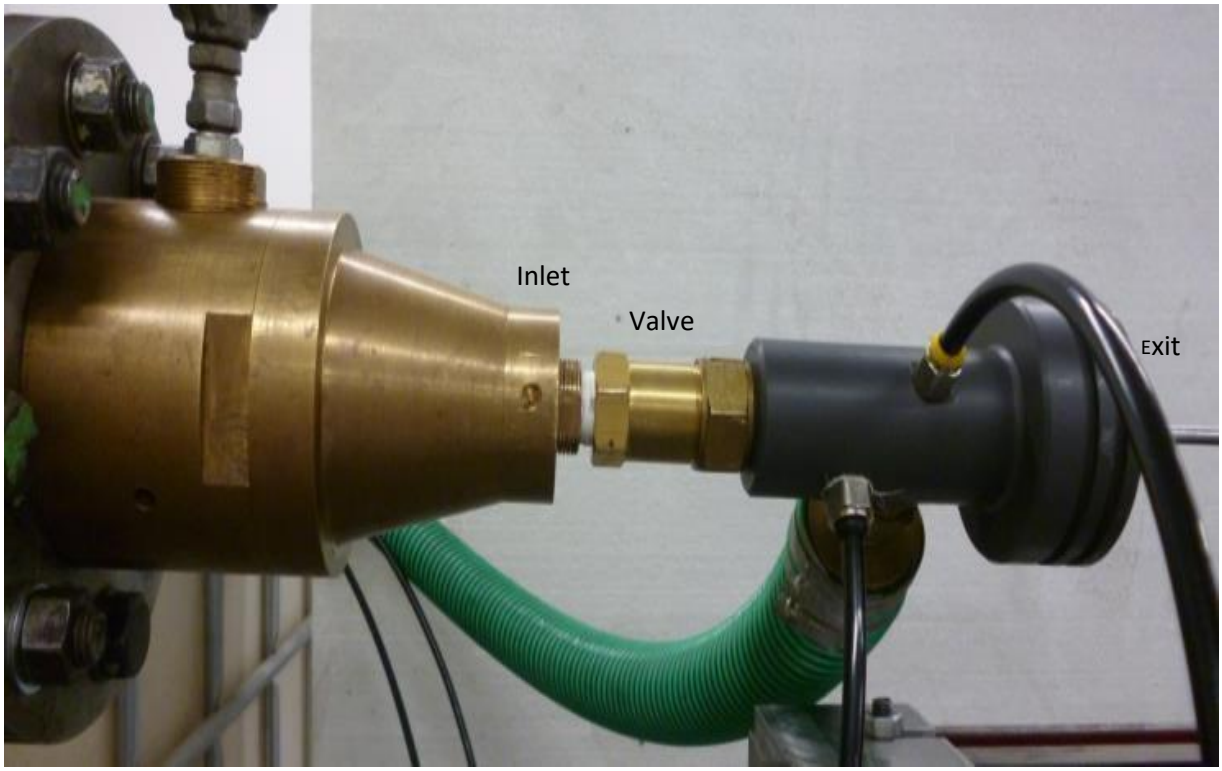

Figure4-2: Construction of the test rig facility for single phase flow

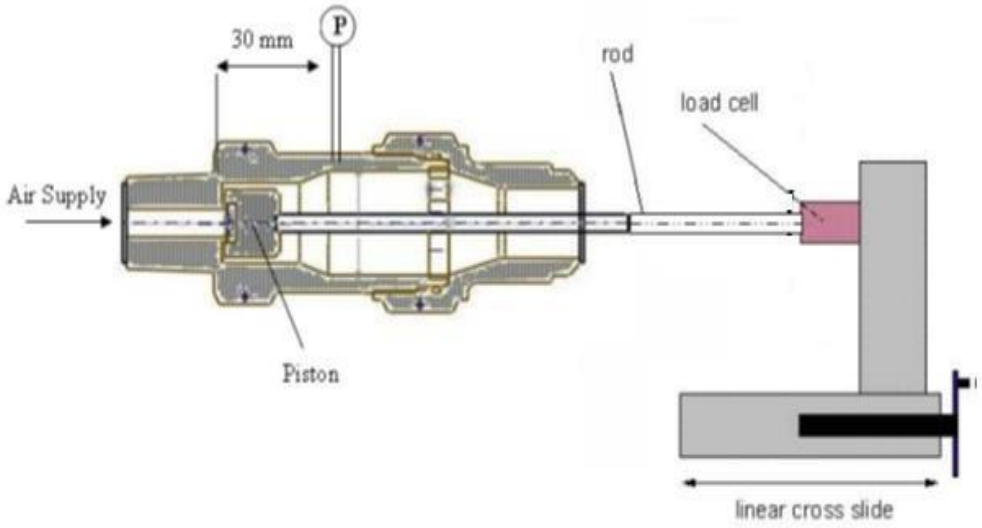

Figure4-3: Schematic drawing of the test rig facility for single phase flow

4.4.2 Experimental Procedure

The rationale was to measure the air flowrates and net piston force at constant upstream pressure for variations in piston displacements. Thus, for each test condition, determined by setting the piston lift and upstream pressure, the air mass flow becomes the uncontrolled quantity (dependant variable) driven by the expansion of the upstream pressure. The net forces acting on the piston result from surface pressures acting on the piston front face and rear face. To achieve this, the piston is set initially at a closed position and air supply isolated using a gate valve (7 in Figure 4.4). The piston is pushed against the seat to ensure that the valve is sealed. As a result of contact between the seat and the piston front face, a reaction force is established. Opening the gate valve (7) leads to air being supplied to the test valve (15) with an additional force on the piston front face being produced. For further opening of the piston at the same test pressure, the reaction force will be reduced. One of the more challenging tasks is capturing the behaviour as the valve is opened from the zero lift position. The initial valve-seat contact, i.e. zero lift can be obtained by noting the piston position when the load cell indicates an increase in force as the piston approaches the seat. However, this is not a fully sealed condition when the system is at pressure. An additional force is required (the sealing force) to compress the piston seal against the seat and close off the valve. This means the initial starting point for any test is effectively a negative lift compared to the first

contact point. It is also noted that when the piston is retracted from the sealed position the piston force reduces, a leakage flow results and a minimum force is reached before increasing again due to flow effects. This minimum force corresponds closely to the first contact position. In this study, this position is taken as the zero lift position. However, it should be noted that an audible but not measureable leakage flow exist at this point.

However, it might not be practical to begin investigating the valve without all of its internal components particularly the spring and the original gland. Fortunately, previous studies based on similar spring loaded safety relief valves were carried out by Elmayyah and Dempster [14] [15], showed clearly that removing the spring of the valve does not affect the mass flowrate, piston forces and back pressure. Accordingly, all the subsequent tests of this study were determined with the spring removed. Furthermore, the original gland of the valve was replaced by a modified one with an equivalent annulus flow area. In fact, this was owing to an obvious difficulty in modelling the original gland in two dimensions. By using an annulus ring as the gland the valve geometry is completely axis-symmetric, which would be taken advantage of time when the computational modelling is considered. The gland of the valve controls the back pressure and plays a predominant role on the piston back face force, and needs to be modelled accurately. The modified gland is presented via a CAD drawing in Appendix E.

As the single phase test aims at covering a range of piston lifts, the piston is moved in small steps of lift (0.2 mm) until a maximum value of 5mm is achieved. The ambient temperature was measured at the start of each test while the back pressure, air mass flowrate and the piston force are recorded at each piston position. The previous steps are repeated for an upstream pressure range of (4 to 13.8 barg) (58 to 200 psig), where critical conditions can be obtained. The following two conditions were investigated:

1. The valve in the standard test arrangement with an annulus modified gland as illustrated in Figure 4.5.
2. The valve in its standard test arrangement but now without the modified gland.

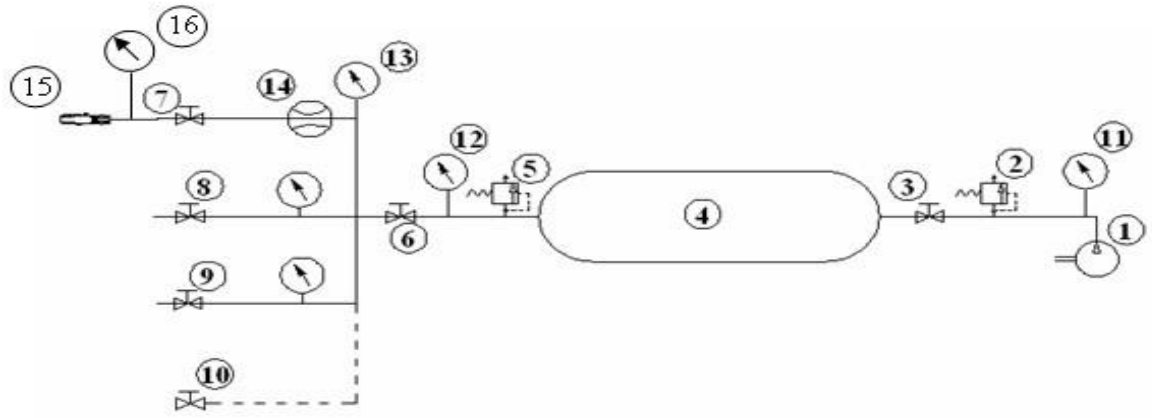

1	Compressor	5	Reservoir	9	Gate Valve	13	P. Gauge
2	PRV	6	PRV	10	Gate Valve	14	Vortex Flow meter
3	Gate Valve	7	Gate Valve	11	P. Gauge	15	Test Valve
4	Reservoir	8	Gate Valve	12	P. Gauge	16	P. Gauge

Figure4-4: Air supply circuit diagram

4.5 Computational Model

The mathematical model, the grid convergence, boundary conditions setup and solution strategy are discussed in this section.

4.5.1 Model Description

Due to the potentially small piston lift values (0.1 mm) investigated in this study the ability to model the flow using continuum modelling assumption was investigated. This was based on identifying the Knudsen number and found to be greater than 2×10^{-6} hence; the model equations are Navier-Stokes based. As the maximum testing pressure used for this study is much less than the 150 bar, the intermolecular forces are ignored and the ideal gas assumption is valid for the working fluid of air [156]. However, the only method of resolving the Navier-Stokes equations is numerical based but still rather challenging to solve the exact equations. Subsequently, the most commonly used approach is the Reynolds Averaged Navier Stokes (RANS). This is essentially based on decomposing the equations into mean (averaging in time) and fluctuating components. As a result, a supplemental term named Reynolds stress appears into the momentum equation to account for the turbulence effects on the mean flow. The most extensively accepted turbulence model is the standard k-ε one.

It consists of two equations (4.5) and (4.6), which account for the turbulent kinetic energy (k) and the turbulent dissipation rate (ε). This standard model was adopted based on previous studies on compressible flow of air through safety relief valves, for instance [39] [40][88] which indicated good predictive capability.

This solution method is based on discretising the governing equations using the Finite Volume Method (FVM). This is a means of dividing the flow domain into a number of small control volumes which contain the properties of interest. For an unsophisticated procedure, these properties are hypothesized to be in the centroid of each volume. The integration of the RANS equations, energy equation and turbulence equations are implemented on each volume individually and the property variation over the volume centroids is described by interpolation profiles.

In this study, the CFD FLUENT code has been deployed to solve the Reynolds Averaged Navier-Stokes equations (RANS) in conjunction with the use of the energy equation and standard $k-\varepsilon$ turbulence model. The numerical calculations were carried out based on steady state conditions and the governing equations utilized are described as following:

4.5.1.1 Continuity equation

$$\frac{\partial}{\partial x_i}(\rho u_i) = 0 \tag{4.1}$$

4.5.1.2 Momentum equation

$$\frac{\partial}{\partial x_i}(\rho u_i u_j) = -\frac{\partial P}{\partial x_i} + \frac{\partial}{\partial x_i}\left[\mu\left(\frac{\partial u_i}{\partial x_j} + \frac{\partial u_j}{\partial x_i} - \frac{2}{3}\delta_{ij}\frac{\partial u_l}{\partial x_l}\right)\right] + \frac{\partial}{\partial x_j}(-\overline{\rho \acute{u_i}\acute{u_j}}) \tag{4.2}$$

Where $\frac{\partial}{\partial x_j}(-\overline{\rho \acute{u_i}\acute{u_j}})$ denotes the Reynolds stress and derived from the following equation:

$$\frac{\partial}{\partial x_j}\left(-\overline{\rho \acute{u_i}\acute{u_j}}\right) = \mu_t\left(\frac{\partial u_i}{\partial x_j} + \frac{\partial u_j}{\partial x_i}\right) - \frac{2}{3}(\rho\kappa + \mu_t\frac{\partial u_l}{\partial x_l})\delta_{ij} \tag{4.3}$$

And

$$\mu_t = \rho C_\mu \frac{k^2}{\varepsilon} \tag{4.4}$$

Where C_μ=0.09

4.5.1.3 The standard k-ε turbulence model

$$\frac{\partial}{\partial x_i}(\rho \kappa u_i) = \frac{\partial}{\partial x_j}\left[(\mu + \frac{\mu_t}{\sigma_k})\frac{\partial k}{\partial x_j}\right] + G_k + G_b - \rho\varepsilon - Y_M + S_k \tag{4.5}$$

$$\frac{\partial}{\partial x_i}(\rho \varepsilon u_i) = \frac{\partial}{\partial x_j}\left[(\mu + \frac{\mu_t}{\sigma_\varepsilon})\frac{\partial \varepsilon}{\partial x_j}\right] + C_{1\varepsilon}\frac{\varepsilon}{k}(G_k + C_{3\varepsilon}G_b) - C_{2\varepsilon}\rho\frac{\varepsilon^2}{k} + S_\varepsilon \tag{4.6}$$

Where

$$G_k = \mu_t S^2 \tag{4.7}$$

And

$$\sqrt{\qquad} \tag{4.8}$$

$$G_b = -g_i \frac{\mu_t}{\rho Pr_t}\frac{\partial \rho}{\partial x_i} \tag{4.9}$$

$$Y_M = 2\rho\varepsilon M_t^2 \tag{4.10}$$

$$\sqrt{\quad} \tag{4.11}$$

And

The above turbulence model has the following constants:

$C_{1\varepsilon} = 1.44$, $C_{2\varepsilon} = 1.92$, $C_{3\varepsilon} = 0.09$, $\sigma_k = 1.0$, $\sigma_\varepsilon = 1.3$,

$Dispersion\ Prandtl\ Number = 0.75$

,

$Turbulent\ Prandtl\ Number = 0.85$, and $Energy\ Prandtl\ Number = 0.85.$

In these equations,G_κ represents the production of turbulent kinetic energy due to the mean velocity gradients, G_b is the generation of the turbulent kinetic energy due to buoyancy, Y_M represents the contribution of the fluctuating dilatation in compressible turbulence to the overall dissipation rate, the quantities σ_κ and σ_ε are the effective prandtl numbers for both κ and ε,respectively, and S_κ and S_ε are user-defined source terms to account for other influences that might affect the turbulence behaviour of the flow.

4.5.1.4 Energy Equation

$$\frac{\partial}{\partial x_i}\left[(u_i(\rho E + p)\right] = \frac{\partial}{\partial x_j}\left[K_{eff}\frac{\partial T}{\partial x_i} + u_i(\tau ij)_{eff}\right] \quad (4.12)$$

Where

$$K_{eff} = K + \frac{C_p \mu_t}{Pr_t} \quad (4.13)$$

And

$$(\tau ij)_{eff} = \mu_{eff}[(\frac{\partial u_j}{\partial x_i} + \frac{\partial u_i}{\partial x_j}) - (\frac{2}{3}\delta_{ij}\frac{\partial u_k}{\partial x_k})] \quad (4.14)$$

Where

$$\mu_{eff} = \mu + \frac{\mu_t}{\sigma} \quad (4.15)$$

However, the effective viscosity μ_{eff} can be added to achieve an accurate description of how the effective turbulent transport varies with the effective Reynolds number (eddy scale), allowing the model to better treat regions which include low-Reynolds number and near-wall flows. This is optional and can be modelled by choosing a differential viscosity model option via the numerical code.

The air is also treated as an ideal gas:

$$\rho = \frac{P_{(abs)}}{\left(\frac{R}{M_\omega}\right)T} \quad (4.16)$$

4.5.2 Computational Grid

The current safety relief valve geometry has been represented as a two dimensional axisymmetric model with an unstructured mesh as shown in Figure 4.5. As mentioned, the original gland is replaced by a modified gland with an equivalent annulus area. This is attributed to the clear difficulty in representing the original adjusting gland of the valve in two dimensions. From previous studies [14] [15] [88], the 2D-axisymmetric model was developed and found to provide adequate predictions for the mass flowrate and piston force, however this modelling uncertainty was removed in this study by using the modified gland.

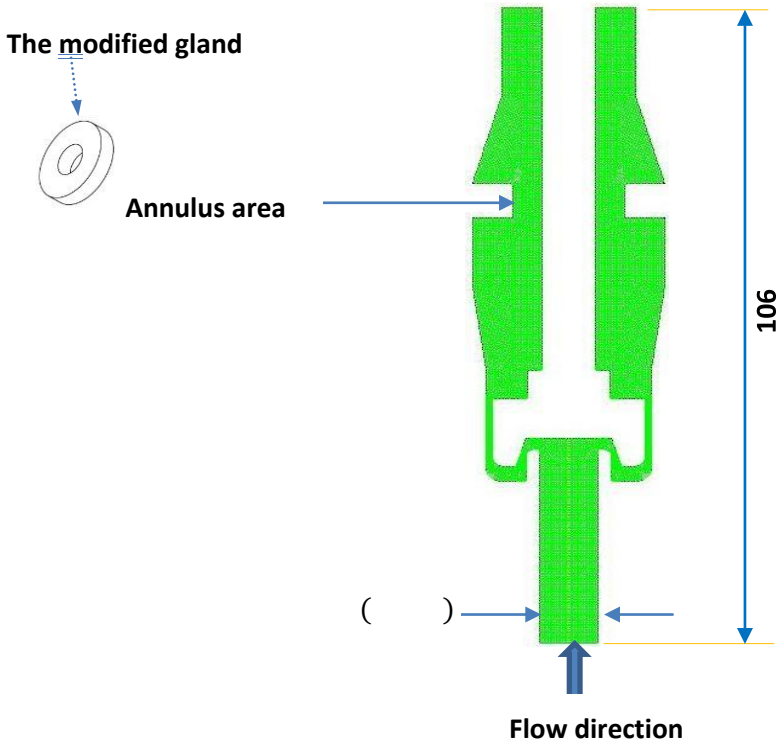

Figure4-5: Computational grid of the valve (Dim. in mm)

In terms of mesh quality, clear attention is paid to the narrow annulus area that appears between the piston and the valve body particularly at high piston lifts. At lower lifts, the attention is made to the area between the piston and its seat. These two regions control the mass flowrate in the valve for critical flow conditions. However, the standard mesh contains approximately 13328 elements, based on a quadrilateral and triangular cell type. On average the mesh density is 7 cell /mm^2 and has been found from previous studies [15] [88] to be sufficiently accurate. The mesh is generated based on the curvature advanced size function

with a fine relevance centre as well as a fine span angle centre. It is well-known that a finer mesh can lead to greater stability in a calculation but does not mean accurate results. The generated grid is also examined using the mesh metric methodology of skewness and found to be 0.69 as a maximum value in only 157 elements all over the flow domain.

An investigation into grid independence was carried out where the results from the standard mesh (13328 cells) were compared with those of a mesh 5 times more dense with 66424 cells, as well as a mesh of 16520 cells; and also compared with different types of proximity and curvature advanced size functions (ASFs). These ASFs are integrated into ANSYS Meshing tools hence used to automatically refine the mesh with little user input required. In other words, the proximity and curvature are functions based on local proximity (between two or more surfaces) and local curvature of the original geometry (curved regions). Therefore it controls the meshing of the domain and gives users the ability to set maximum and minimum size controls at a global level and growth rates, as well as extra elements across gaps where physics are of importance. The results are shown in Table 4.1 and indicate that the 13328 cell mesh is grid independent as far as the mass flowrate and piston force predictions are concerned. Therefore, adopting the curvature mesh type with the 13328 elements can easily make the computational solution more efficient with less time for convergence.

Table 4-1: Predicted air mass flowrate and piston force for a valve at piston lift of 5 mm and upstream pressure of 8.3 barg [Note: experimental mass flowrate is 0.058 (kg/s) and measured force is 151 (N)]

Number of elements	Mesh Type	Predicted air mass flowrate (kg/s)	Predicted piston force (N)	Convergence Time (mins)
13328	Curvature	0.0581	157	35

16520	**Proximity and Curvature**	**0.0583**	**157**	**55**
66424	**Curvature**	**0.0579**	**158**	**70**

4.5.3 Boundary Conditions and Solution Strategy

There are three main zones; the inlet, specified as a pressure-inlet, the outlet defined as a pressure-outlet and the interior-fluid, representing the whole domain as the fluid air. Other zones are considered as walls. At the inlet-pressure boundary condition, the stagnation pressure is specified as the desired values (4-13.8barg) (58– 200 psig), and is restricted to the pressure limits of the facility, delivering a maximum pressure of 15.8 barg (230 psig). The gas temperature is set at the corresponding experimental values and is generally close to 288.15K. The standard $\kappa - \varepsilon$turbulence model is employed with initial guess values of κ andε , which are set to be 0.1 (m^2/s^2) and 0.2 (m^2/s^3), respectively. The pressure-outlet boundary is set at atmospheric pressure and a stagnation temperature is applied. As the critical flow conditions are mainly targeted by this study, the flow should be independent of the outlet boundary conditions. This ensures that the flow is choked at all test pressures.
Also, the initial values of κ and ε are set as the inlet boundary conditions at the pressureinlet zone. The zones representing the walls are considered as stationary valve walls. Each inlet cell is set to the experimental inlet pressure corresponding to a test condition. This adequately sets the phase inlet boundary conditions to those in practice.

With regards to the solution strategy, the solution method used was steady-state and two possible solvers, Density-Based and Pressure-Based were investigated. The two different solvers were examined as shown in Figure 4.6. Figure 4.6 illustrates the predicted air mass flowrate in a 9mm inlet bore size of a similar safety relief valve for an upstream pressure of

13.8 barg and clearly depicts that both solvers results are in good agreement. The predicted air mass flowrates by the pressure-based solver have higher magnitudes compared to these computed by density-based solver. The maximum discrepancy of air mass flowrate prediction is 2-4% and this might be attributed to the number of equations being solved via each solver. It is worth mentioning here that the density-based solver is highly recommended for compressible flow calculations, although it does not use the full NavierStokes equations [126]. As will be found later, however, the pressure-based solver leads to accurate prediction of the experimental results. Furthermore, it is noted that most of the cases converge faster using the density-based solver with approximately 360 seconds (6 mins) difference.

However, as the main goal of this study is the two-phase flow through a safety relief valve the pressure-based solver is the only applicable discretization scheme. This solver is implemented for solving all subsequent single-phase cases. This subsequently required the volume fraction of the second phase to be set to zero. Therefore, with the steady-state pressure-based solver and a segregated algorithm where the governing equations are solved sequentially, a Green-Gauss cell based spatial discretization for the gradient was implemented, as well as second order upwind spatial discretization for the density, momentum, turbulent kinetic energy, and turbulent dissipation rate and energy gradient terms. In addition, the solution is initialized by a hybrid initialization method to obtain accurate results, then being controlled by lowering the under-relaxation factors. The energy equation was not solved for the first 100 iterations, to ensure initial stability of the model. The convergence criterion was based on the residual magnitudes of presented variables,
i.e., mass, velocity components, energy, κ andε for turbulence. The threshold values were absolute with magnitudes of 1×10^{-6} for the energy equation and 1×10^{-3} for the other variables. The convergence time for all cases was about 35 mins on an 8.00 GB desktop PC consisting of 4 parallel processors with the 13328 cell curvature mesh adopted.

A first order upwind spatial discretization scheme was examined prior to implementing the second order scheme. Figure 4.7 presents a comparison between the air mass flowrate that is predicted by using the two different discretization schemes at an upstream stagnation pressure of 13.9 barg (202 psig). The figure shows an obvious consistency between the two schemes used to predict the air mass flow discharged, with a maximum discrepancy of around

3%, particularly at low lifts. It is believed that this scheme of spatial discretization may not affect integrated values; however it is more likely to have an impact on local physical parameters of the fluid domain. Therefore contours of Mach number based on both discretization schemes were investigated, as shown in Figure 4.8. The figure shows contours of Mach number, which are calculated according to the first order upwind scheme (A) and the second order upwind scheme (B), at an upstream stagnation pressure of 13.8 barg (200 psig) and a piston lift of 0.2 mm. As can be noticed, the first order upwind scheme does not fundamentally capture the discontinuity at the shock wave and is smeared over its location, as shown in figure 4.8 (A). Furthermore, it is noted that the 1st order upwind discretisation scheme predicts higher net piston force for the range of piston lifts studied with approximately 7-11 N difference. Therefore the 2nd order upwind discretisation scheme was chosen for the subsequent computational modeling.

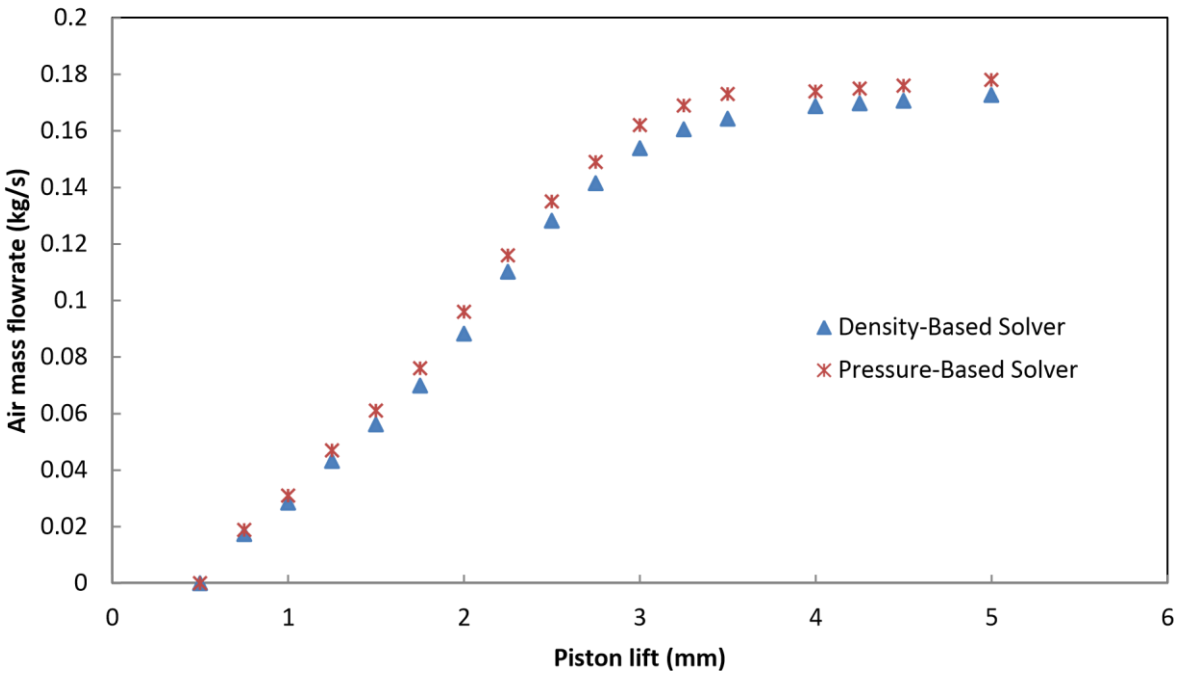

Figure4-6: A comparison between existing solvers for predictions of air mass flowrate at an upstream stagnation pressure of 13.8 barg (200 psig), for 9 mm inlet bore size of similar safety relief valve

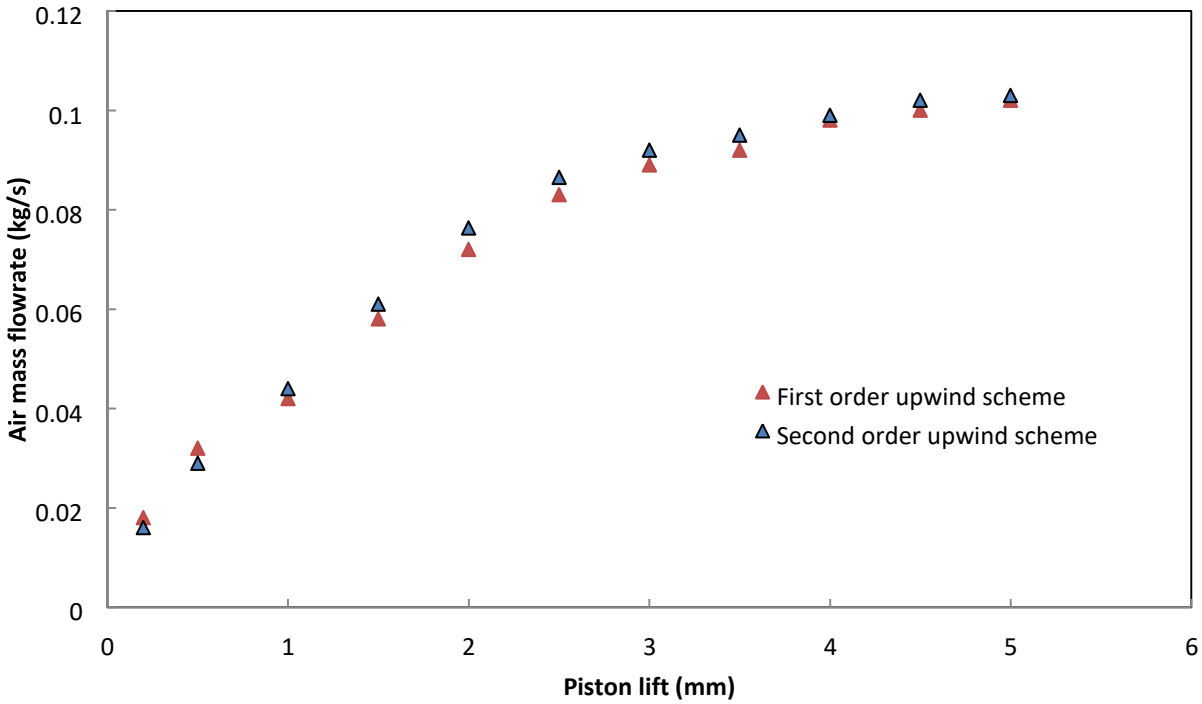

Figure4-7: A CFD comparison between 1st and 2nd order upwind spatial discretization schemes used for predictions of air mass flowrate at an upstream stagnation pressure of 13.9 barg (202 psig), for the valve with the adjusting gland

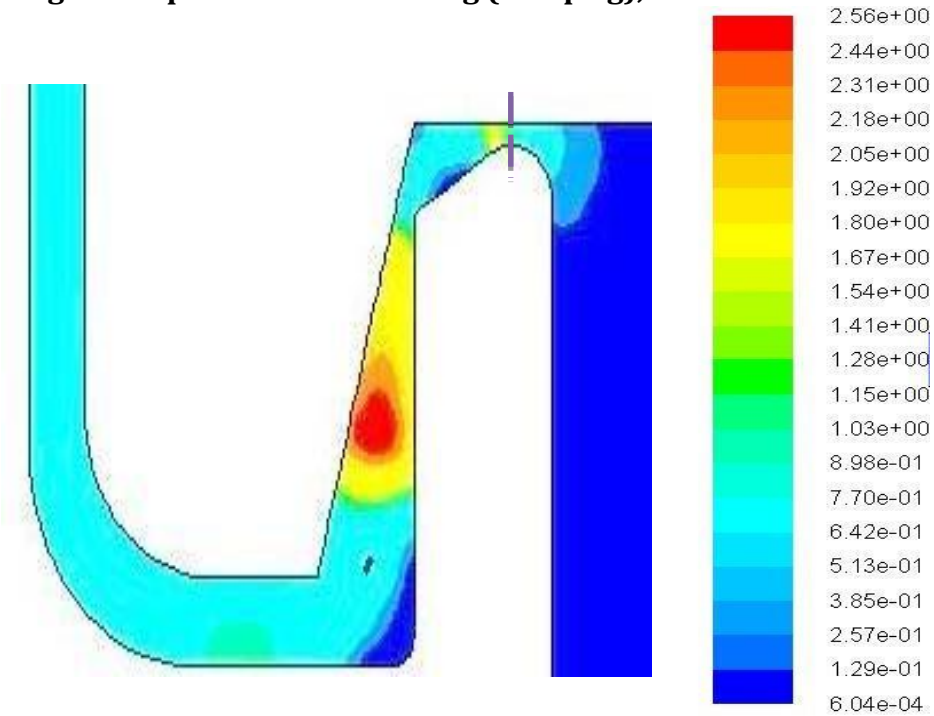

(A) Contours of Mach number based on the 1st order scheme

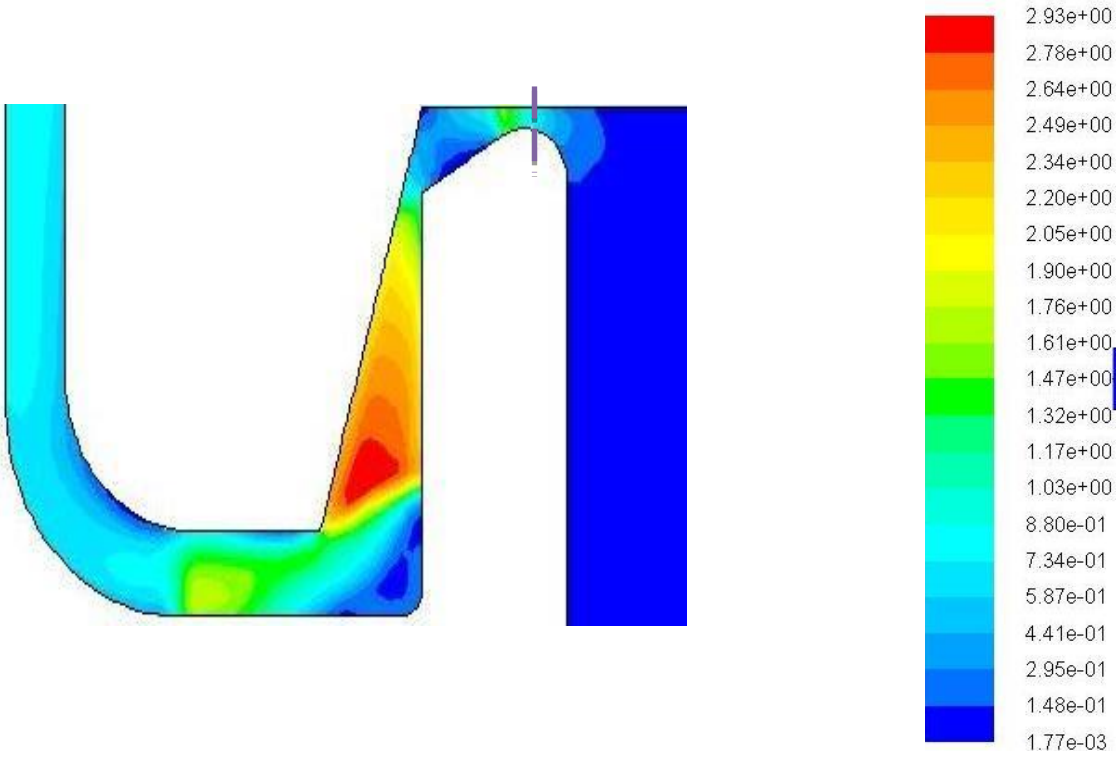

(B) Contours of Mach number based on the 2nd order scheme

Figure4-8: Contours of Mach number at an upstream stagnation pressure of 13.8 barg (200 psig) and 0.2 mm piston lift

4.6 Results

4.6.1 Experimental Results

Figures 4.9 and 4.10 show the variation in the air mass flowrate and piston force with various piston displacements. The data were obtained experimentally for the valve with and without its adjusting gland. The results of air mass flowrate through the valve prove that the adjusting gland principally has no influence on the resulting mass flowrate as shown in Figure 4.9. Under these flow conditions, all the flow cases are choked for all piston lifts at various locations. As can be seen later from Figures 4.19 and 4.20, the first choking occurrence depends mainly upon the piston lift. It varies from the piston front face where the piston has lower lifts to the piston side face at higher piston displacements. The resulting mass flowrate here is denoted as a critical mass flowrate. This critical mass flowrate is essentially independent of downstream flow conditions. The aforementioned main finding ensures that adequate prediction for the critical mass flowrate could be easily achieved by a simplified model of the

valve with no complex exit geometry. Flow-Lift characteristics are discussed further in Section 4.7.1.

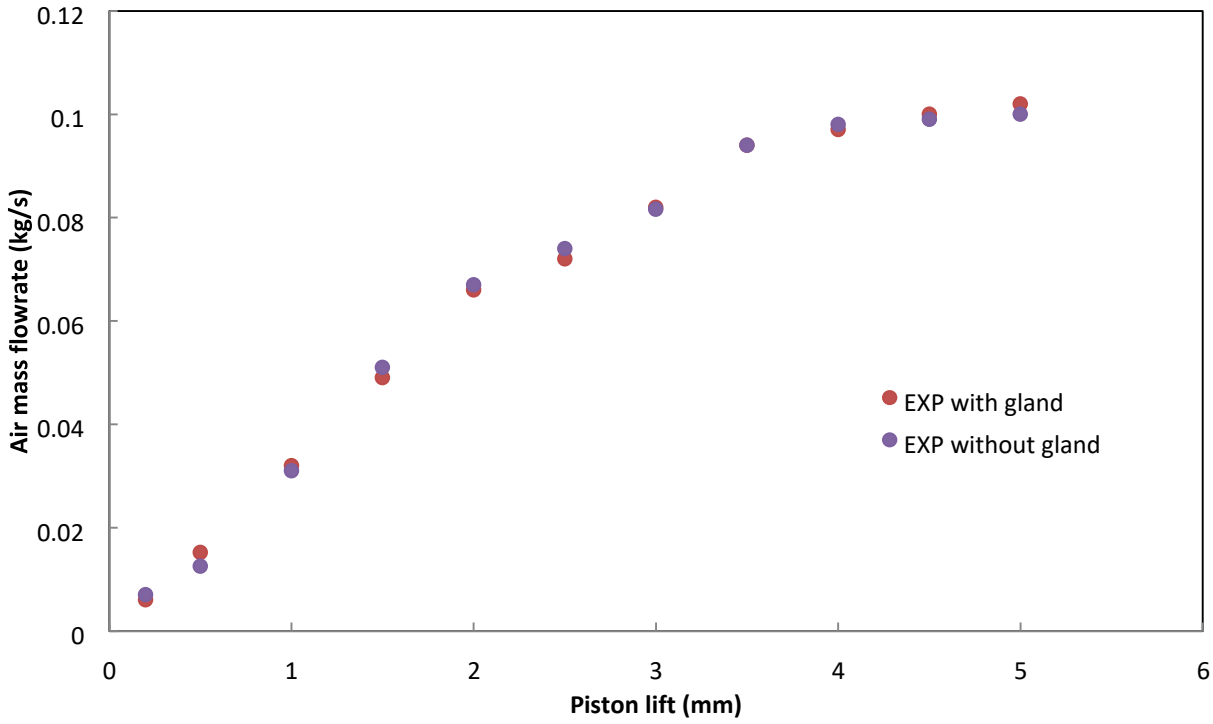

Figure4-9: The influence of the gland on the air mass flowrate at an upstream stagnation pressure of 13.8 barg (200 psig)

Figure 4.10 depicts that there is a noticeable difference on the net piston force of the valve when an adjusting gland is in place. The gland results in lowering the net piston force as it causes higher back pressure on the piston rear face. Figure 4.11 presents the back pressure that is measured at an upstream stagnation pressure of 10.3 barg (150 psig) at the piston rear face using the rod mounted pressure tapping, as is explained in Section 4.4.1. The figure also shows the significant influence of the adjusting gland on the resulting back pressure. Accordingly, higher back pressure values can be seen when the adjusting gland is in place. It is worth mentioning that the back pressure increases also with an increase in piston lift and reaches the highest magnitude at a full lift. Figure 4.10 and 4.11 indicate that, a higher back pressure on the piston back face results in reduction in net piston force.

Force-Lift characteristics are discussed in Section 4.7.2.

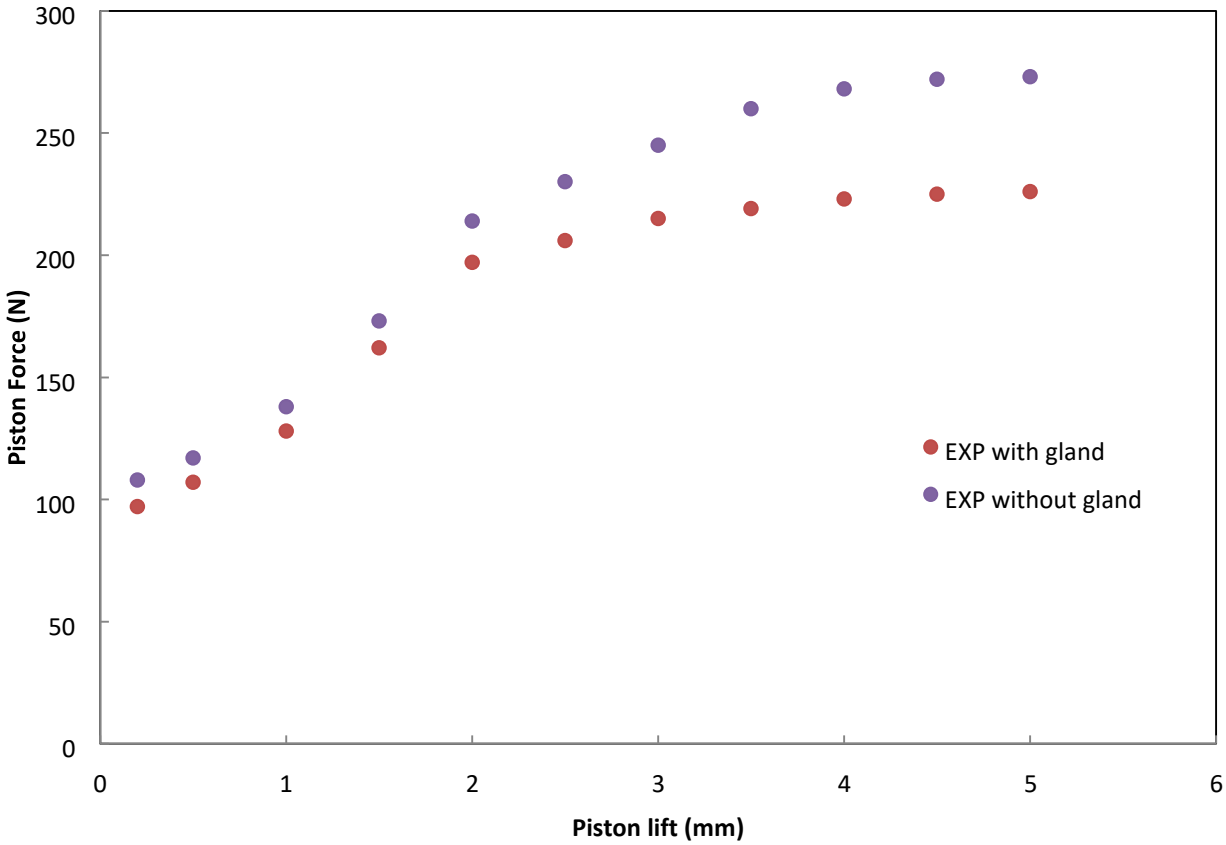

Figure4-10: The influence of the modified gland on the piston force at an upstream stagnation pressure of 13.8 barg (200 psig)

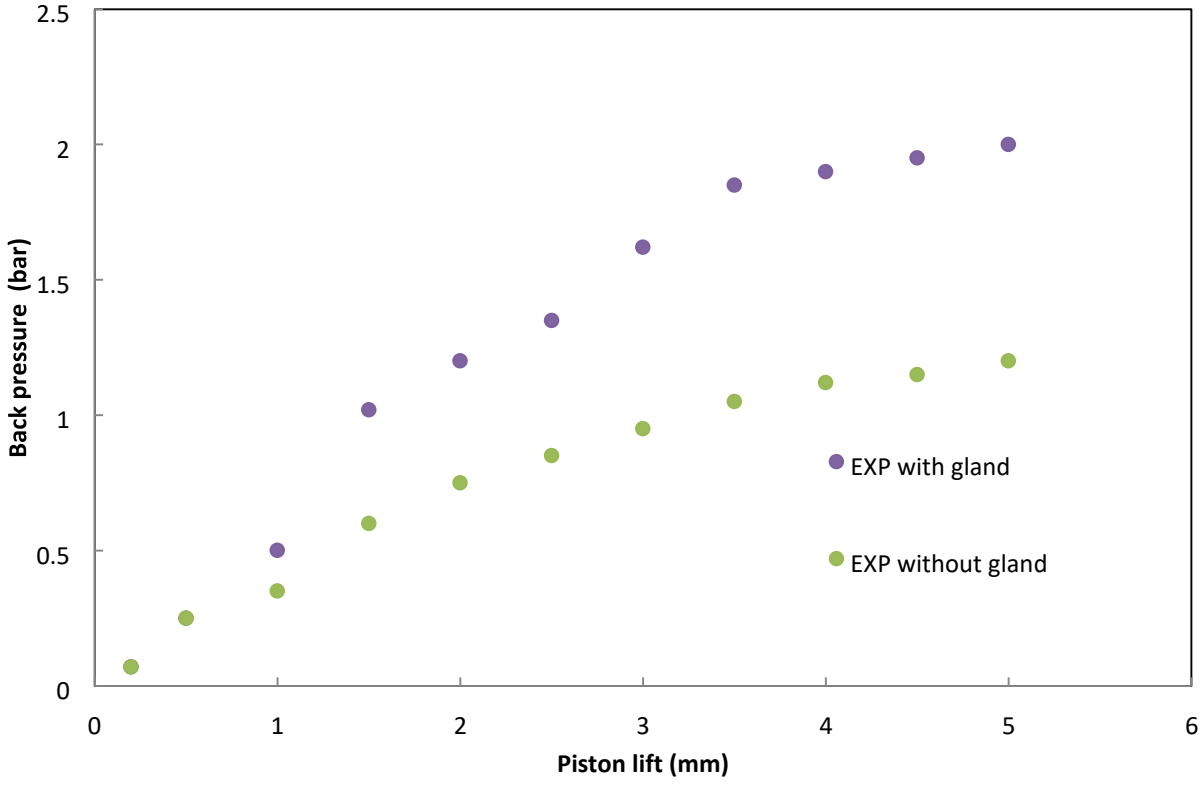

Figure4-11: Experimental back pressure at an upstream stagnation pressure of

10.3 barg (150 psig) for the valve with and without the adjusting gland

4.6.2 CFD Results

The flow behaviour and essential variations of its properties throughout the valve can be presented via contours plots. Hence contours of static pressure, static temperature, velocity and Mach number have been presented for the flow in the valve at different piston displacements. Figures 4.12 and 4.13 illustrate the static pressure, static temperature, velocity and Mach number for an upstream inlet stagnation pressure of 13.8 barg (200 psig) at piston lift of 1.5 mm. For this piston lift, air velocity varies from 0 m/s to 400 m/s, temperature variation is from -104°C to 17°C and Mach number is from 0 to 1.89. Figure 4.12 shows the change of the static temperature and pressure over the whole flow domain. With regards to velocity profiles, contours of velocity have been obtained at different piston lifts. These velocity contours indicate that the flow accelerates from the valve inlet from a low subsonic Mach number to reach the first occurrence of the speed of sound somewhere around the piston. The location of the first incidence of the speed of sound is called the critical plane (choking plane) and is always piston lift dependent. The critical plane can be identified by contours of Mach number at which the Mach number is unity as can be seen later from Figures 4.19 and 4.20. Here for example in Figure 4.13, the first critical plane occurs in an area between the piston front face and the piston seat. Downstream of the choking plane and for a short distance, the flow is exposed to further expansion then shock induced compression downstream the piston end due to the existence of the adjusting gland. The flow performs its final expansion at the valve outlet once passing the adjusting gland.

However, Figures 4.14 and 4.15 exhibit the variation in air mass flowrate and net piston force at different piston positions based on CFD calculations. These theoretical results ascertain again that the adjusting gland has only a significant effect on the piston force while the air mass flowrate is not affected.

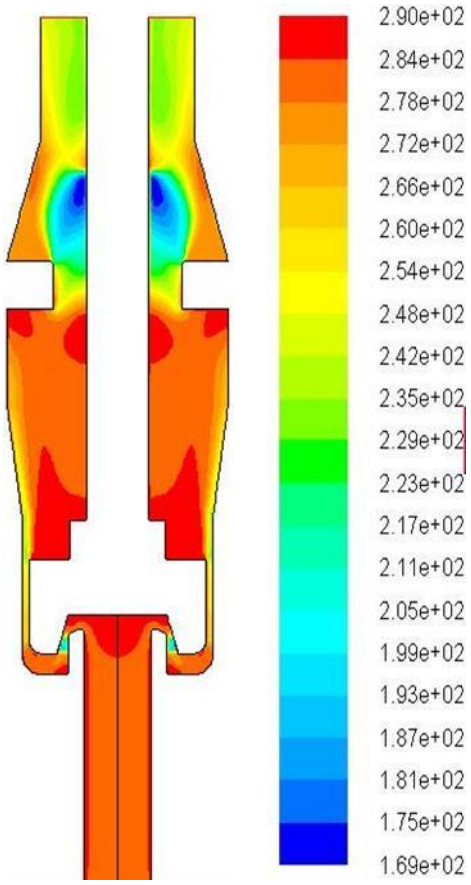

(a) Static Temperature ( )

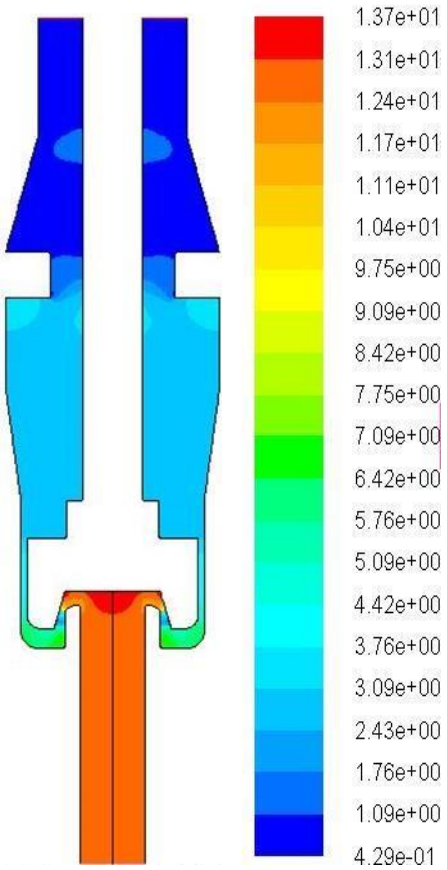

(b) Static Pressure (bar)

Figure4-12: Contours of static temperature and static pressure at an upstream stagnation pressure of 13.8 barg (200 psig) and 1.5 mm piston lift

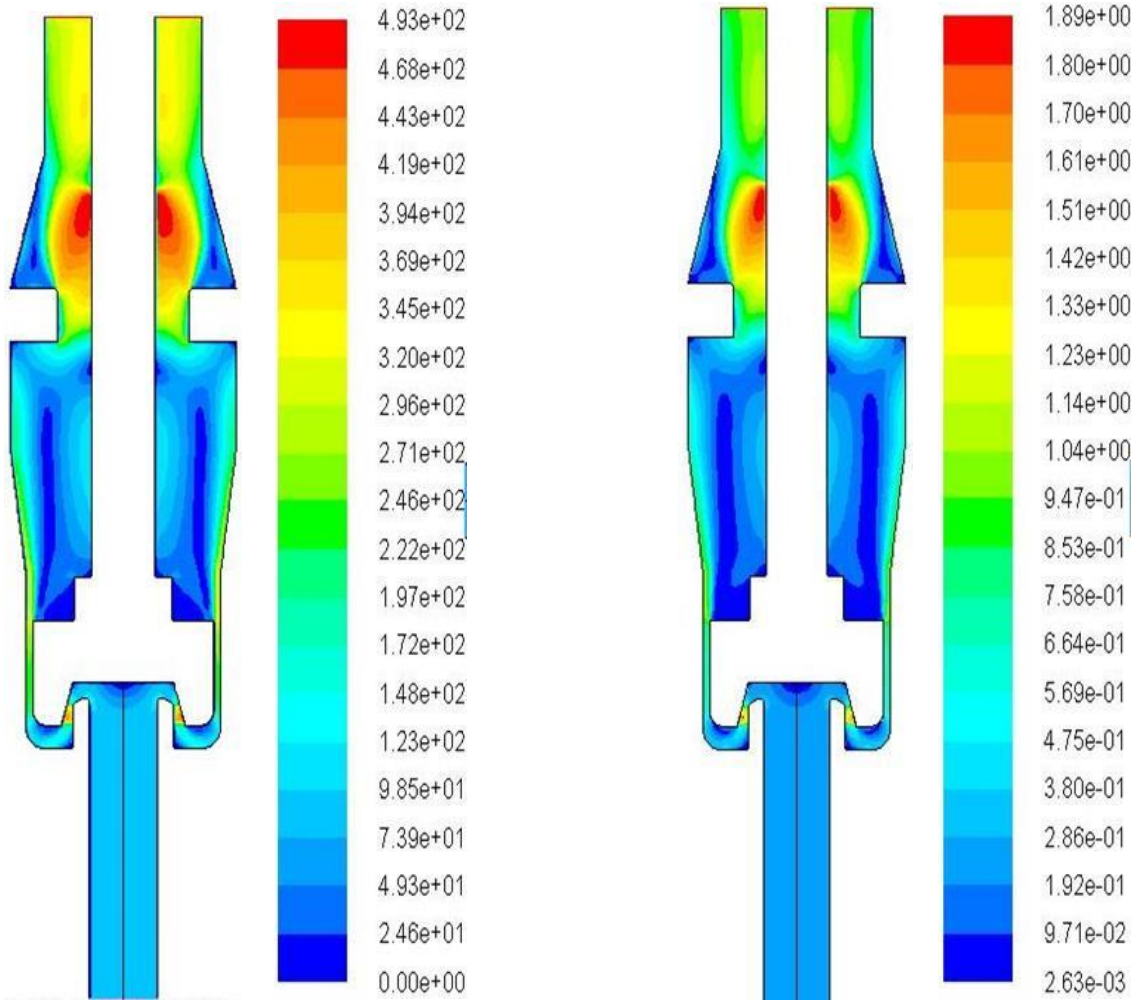

(a)Velocity Magnitude (m/s) (b) Mach Number (-)

Figure4-13:Contours of Air velocity and Mach number at an upstream stagnation pressure of 13.8 barg (200 psig) and 1.5 mm piston lift

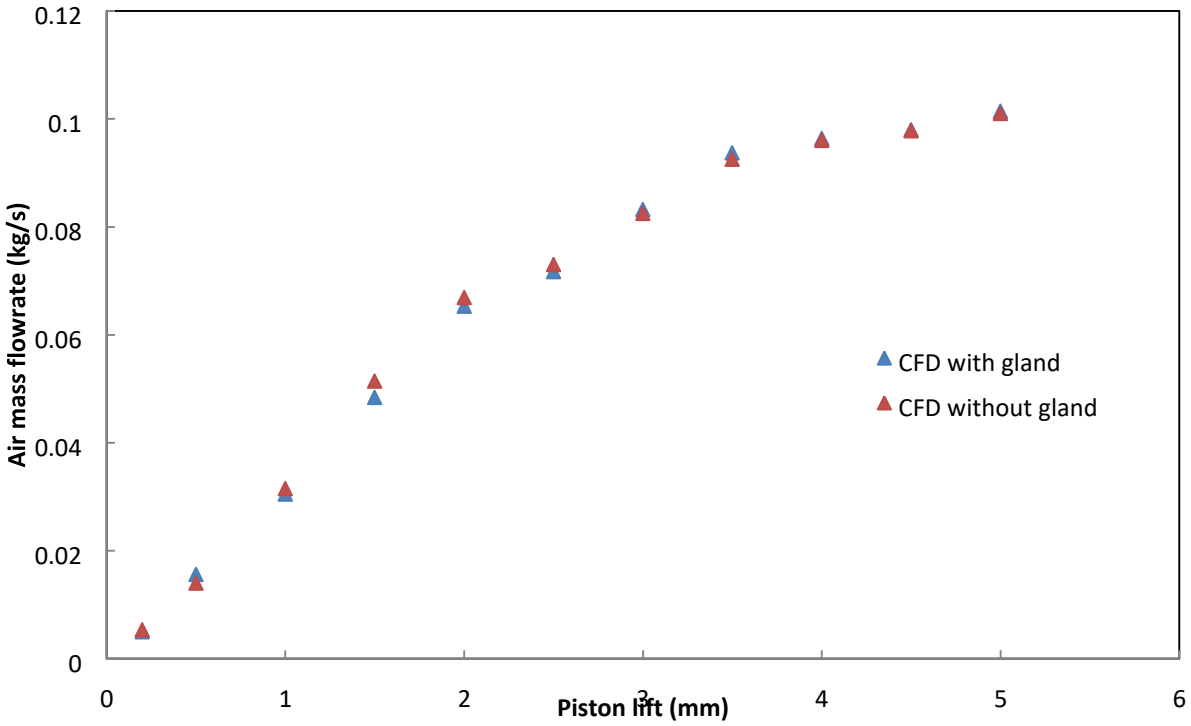

Figure4-14: The effect of the gland on the air mass flowrate at an upstream stagnation pressure of 13.8 barg (200 psig) from CFD calculations based

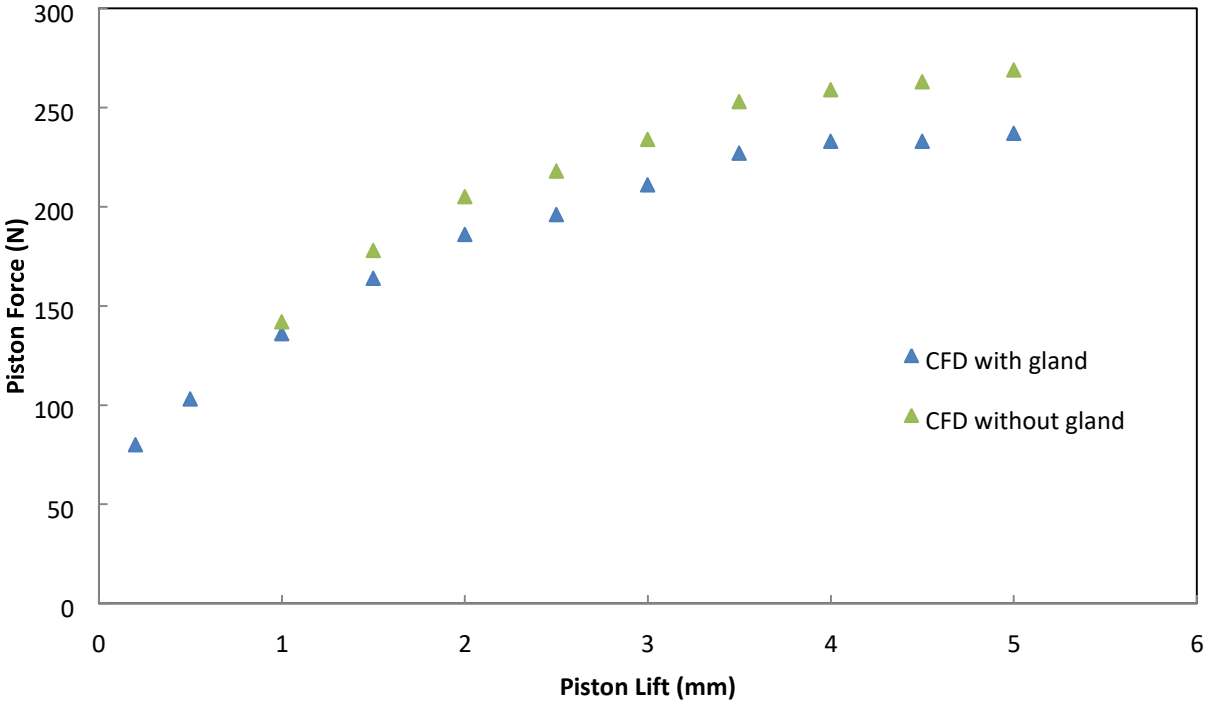

Figure4-15: The effect of the gland on the piston force at an upstream stagnation pressure of 13.8 barg (200 psig) from CFD calculations based

Figure 4.16 indicates that the adjusting gland has a significant effect on the back pressure. Predicted flow-lift characteristics presented via Figures 4.17 and 4.18 compare well with the experimental results at all lifts. The figures show that the gland has no influence on the mass flowrate. However, the predicted force-lift characteristics shown on Figures 4.21 and 4.22 are in good agreement with the measured ones and will be further discussed in more detail in Section 4.7.2. Apparently, there is a slight discrepancy of around 4-6% between the CFD forces and measurements particularly at higher piston displacements, which are possibly attributed to an improper modelling of the geometrical edges of the inner valve body and the adjusting gland as well as the outlet connection. As a consequence, the predicted back pressure could be slightly in error resulting in lower piston rear forces.

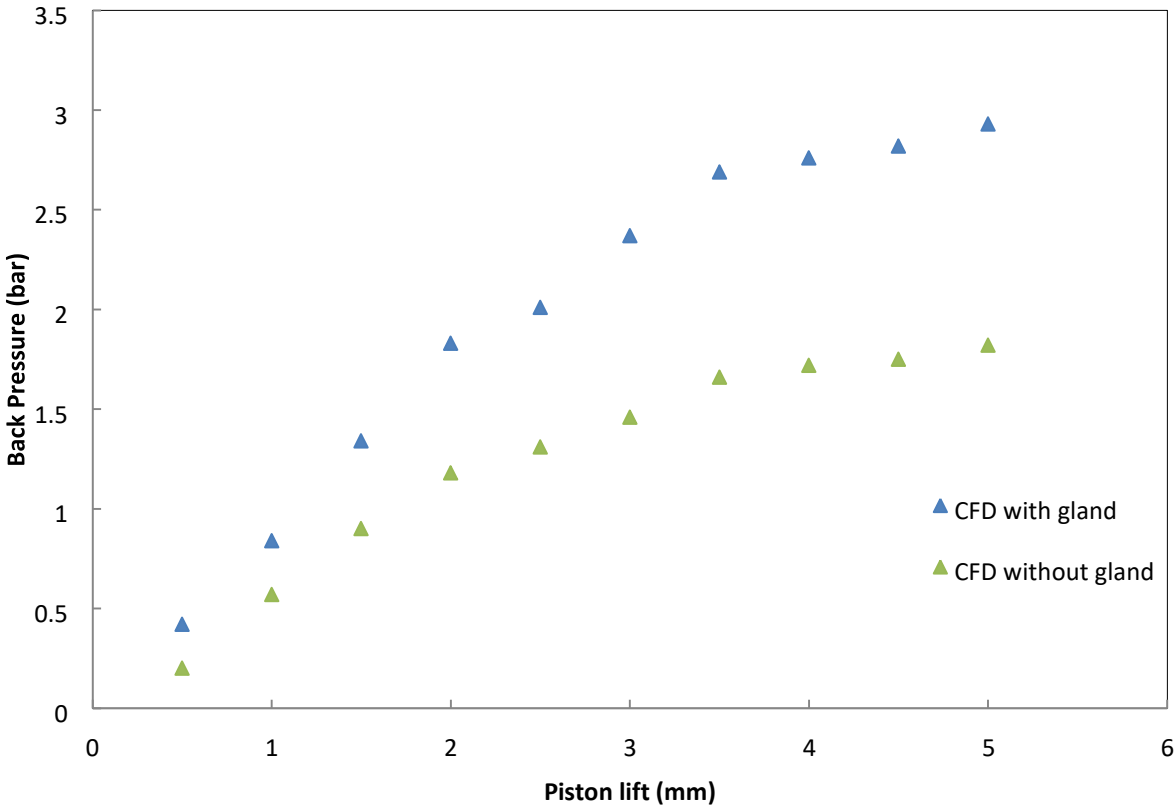

Figure4-16: The effect of the gland on the back pressure at an upstream stagnation pressure of 13.8 barg (200 Psig) from CFD calculations based

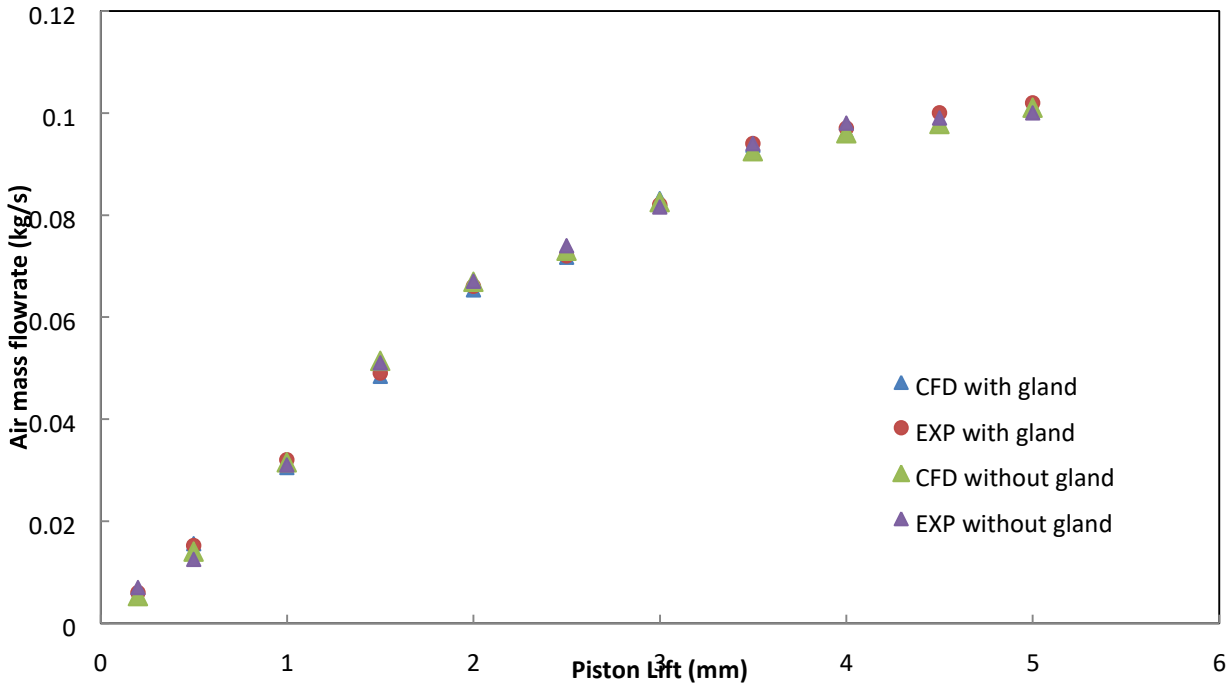

Figure4-17: CFD and experimental flow-lift characteristics at an upstream stagnation pressure of 13.8 barg (200psig)

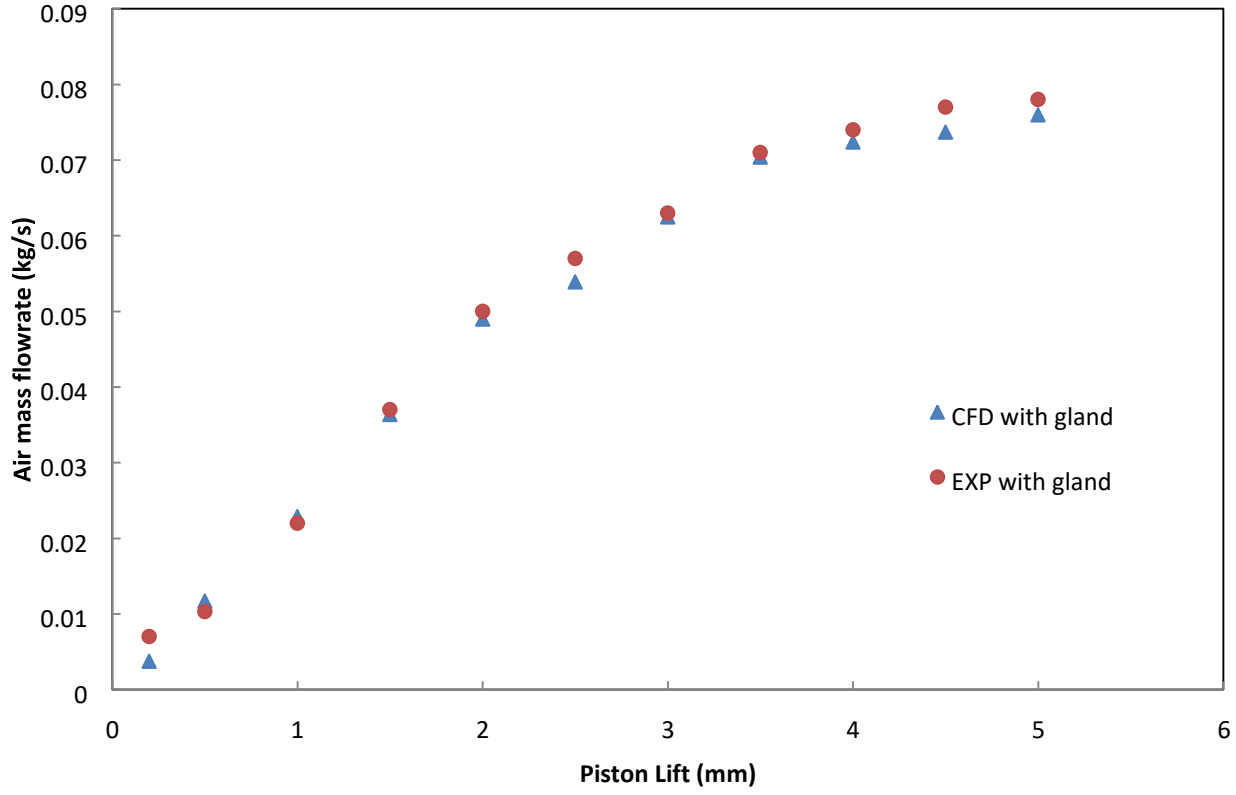

Figure4-18: CFD and experimental flow-lift characteristics at an upstream stagnation pressure of 10.3 barg (150psig)

4.7 Discussion

4.7.1 Flow-Lift Characteristics under Single Phase Flow Conditions

By investigating the predicted air mass flowrate results for a number of piston positions, the flow-lift characteristics could be methodically formed. All figures presenting the flow-lift characteristics can be divided into two stages. Stage 1 starts from 0 mm lift where the valve is postulated to be fully closed to 2 mm lift. Stage 2 begins from the end of stage 1 until where the valve is fully opened at 5 mm lift. For the first phase, the mass flowrate increases rapidly over a 0-2 mm range of lifts. For the second phase, the air mass flowrate has a slight increase till almost reaching a constant magnitude where the valve is fully opened. In fact, the Mach number and pressure distributions around the piston and its seat play the major roles in controlling the air mass flowrate for all lifts. Figures 4.19, 4.20 and 4.24 illustrate in detail these parameters for a number of piston displacements. Figure 4.19 depicts the Mach number contours for the first specified region of the air mass flowrate where the lift is in the range of 0-2 mm. The results of the Mach number contours clarify the location of the choking plane (indicated by a dash line) at lower lifts, this occurs between the piston front face and the piston seat. Accordingly, the mass flowrate is critical and controlled by the area of the geometry for that specific location while the upstream stagnation pressure and temperature are upheld for each piston lift. Since the mass flowrate is area and hence lift dependant, a linear function can be seen to represent the change of mass flowrate.

For the higher lifts stage where lifts are greater than 2 mm, it can be seen that the critical plane travels to a position at the exit from the annular channel between the piston and the inner valve body, as shown on Figure 4.20. At these higher lifts, the choking plane remains at this location irrespective of any further increase in the piston displacement. The increase of mass flowrate with lift is now comparatively slower due to the fixed choking location (steady non-linear function based). The reason behind the increase in the mass flowrate for further lifts greater than 2.5mm is due to an increase in the pressure at the inlet of the annular passageway. As long as the piston moves away from the valve seat while opening, the inlet passageway static pressure increases as shown in Figure 4.26. This then results in the mass flowrate to be increased. Thereafter, there will be no further increase in the mass flowrate as the static pressure reaches a slightly smaller pressure value than the total upstream pressure

(Fig.4.26) owing to friction losses between valve entrance and the piston side. This limits the mass flow to a near constant value at higher lifts.

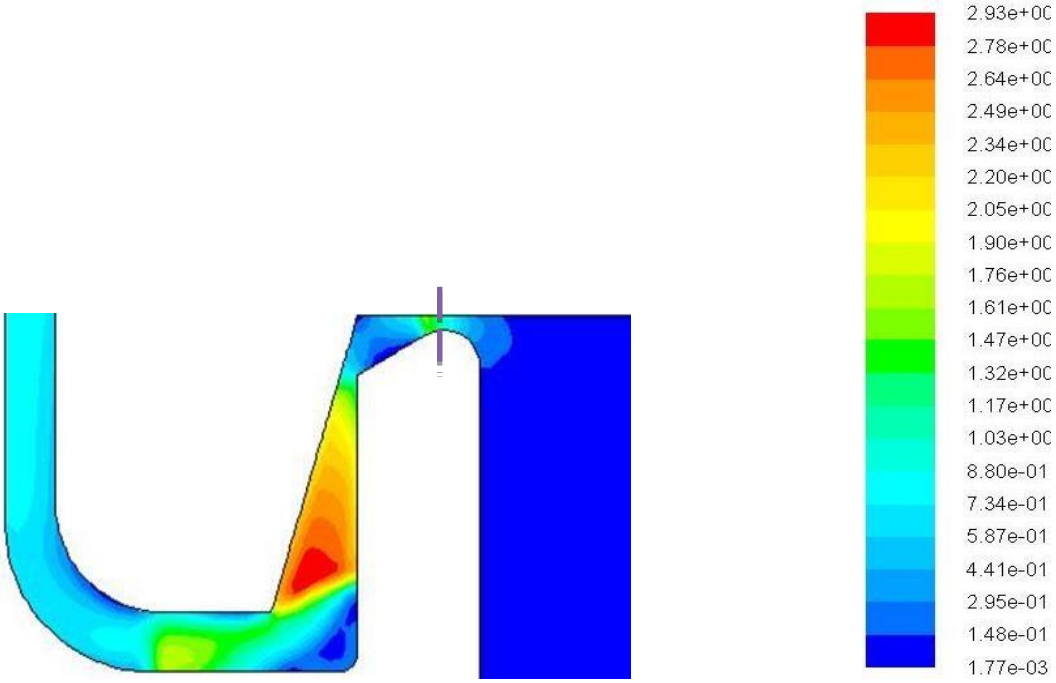

(a) Lift 0.2 mm

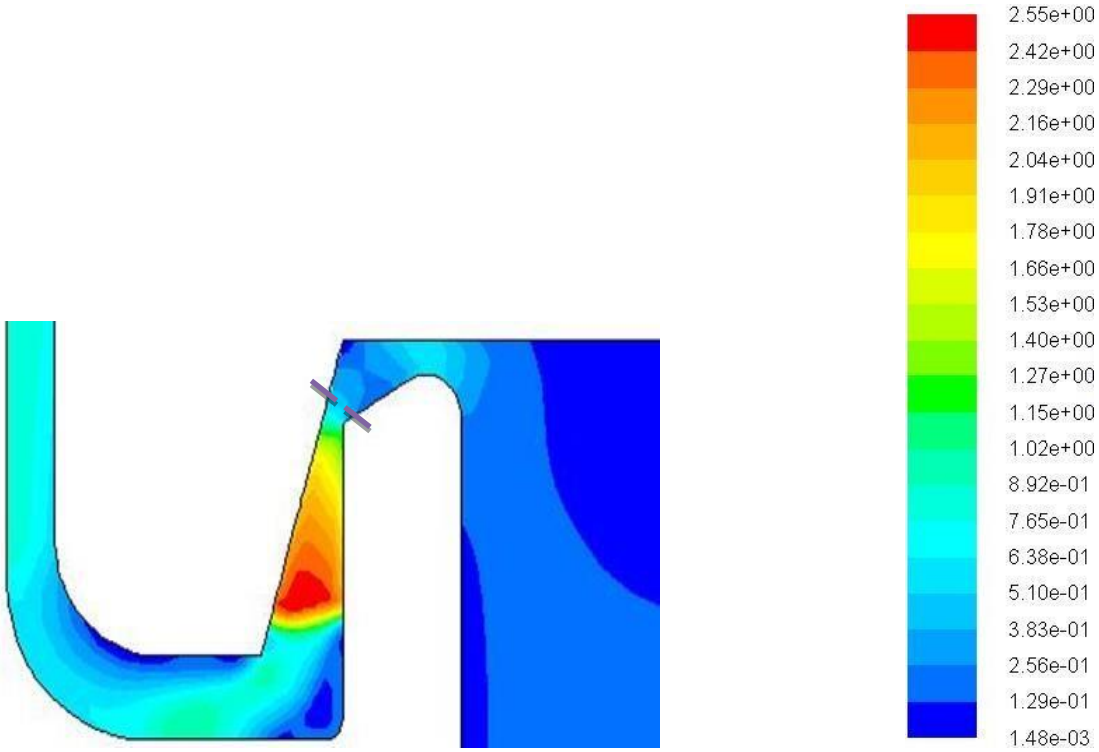

(b) Lift 0.5 mm

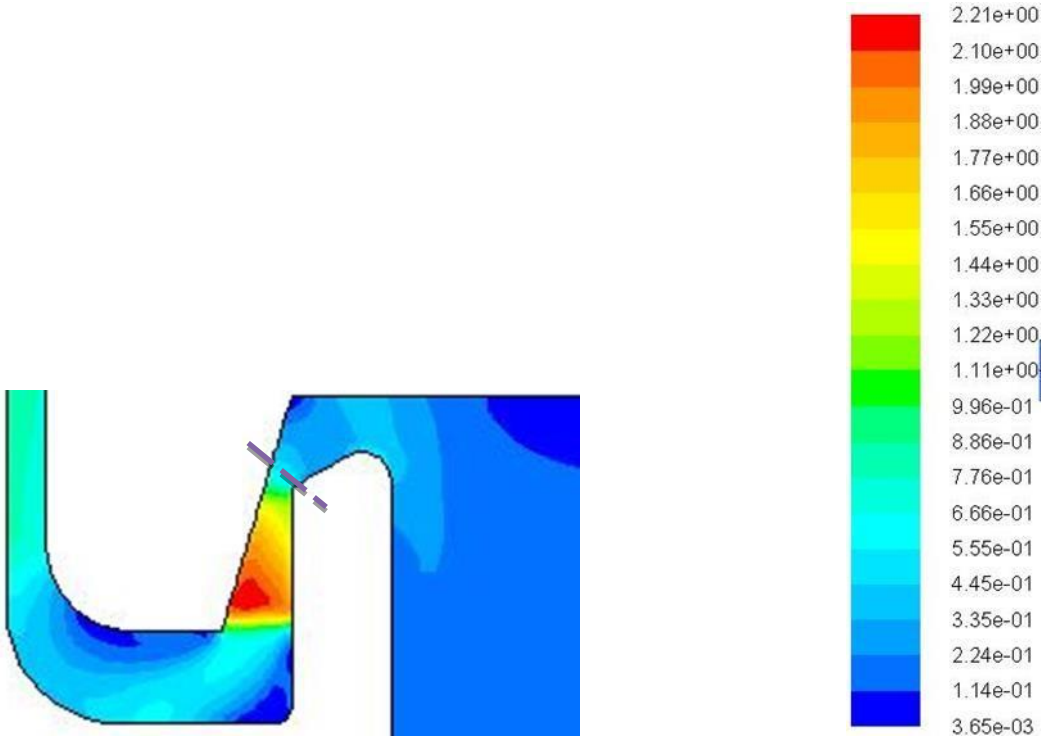

(c) Lift 1 mm

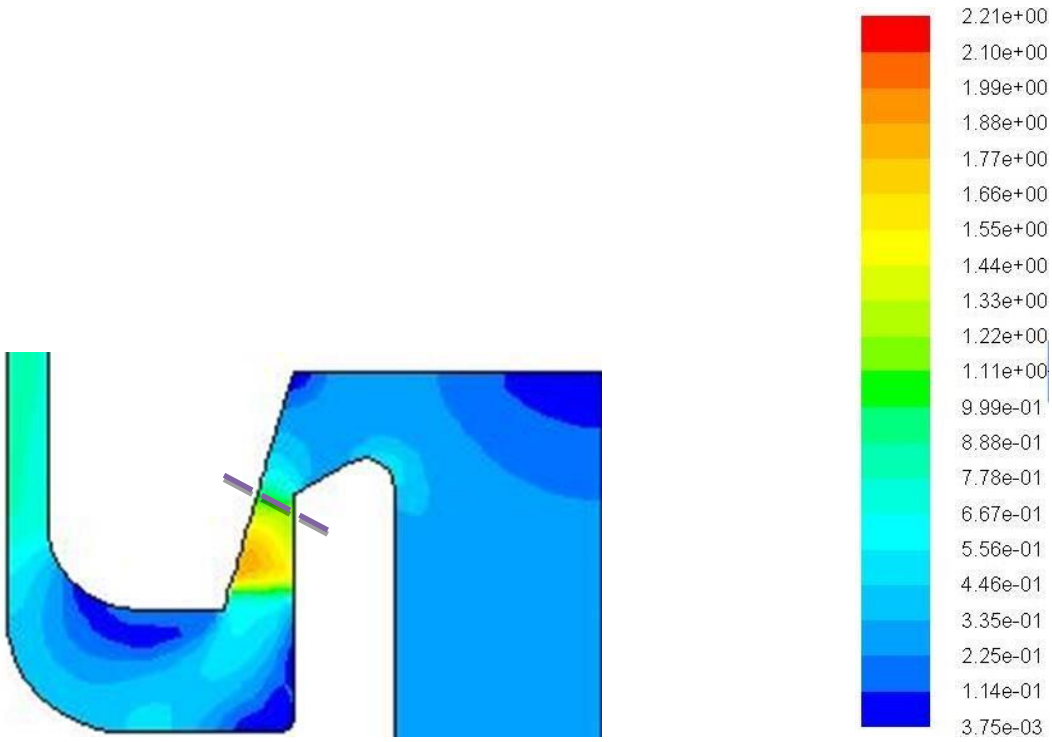

(d) Lift 1.5 mm

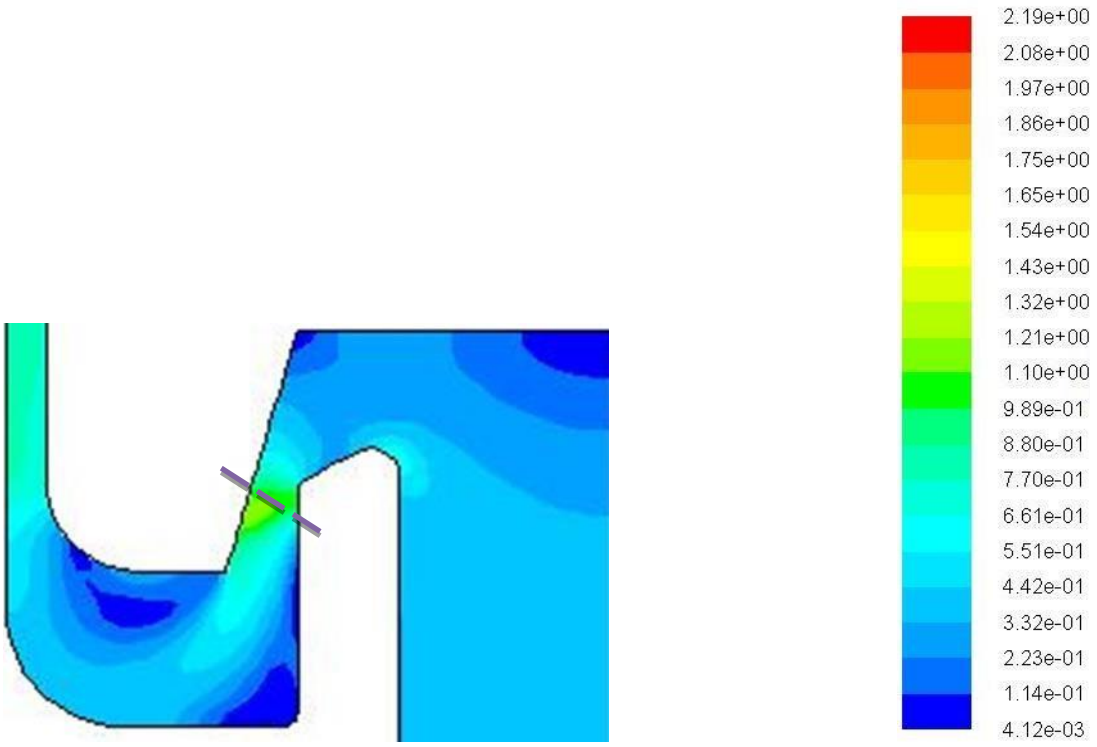
2.19e+00
2.08e+00
1.97e+00
1.86e+00
1.75e+00
1.65e+00
1.54e+00
1.43e+00
1.32e+00
1.21e+00
1.10e+00
9.89e-01
8.80e-01
7.70e-01
6.61e-01
5.51e-01
4.42e-01
3.32e-01
2.23e-01
1.14e-01
4.12e-03

(e) Lift 2 mm

Figure4-19: Contours of Mach numbers and the critical plane at piston front face for lower lifts

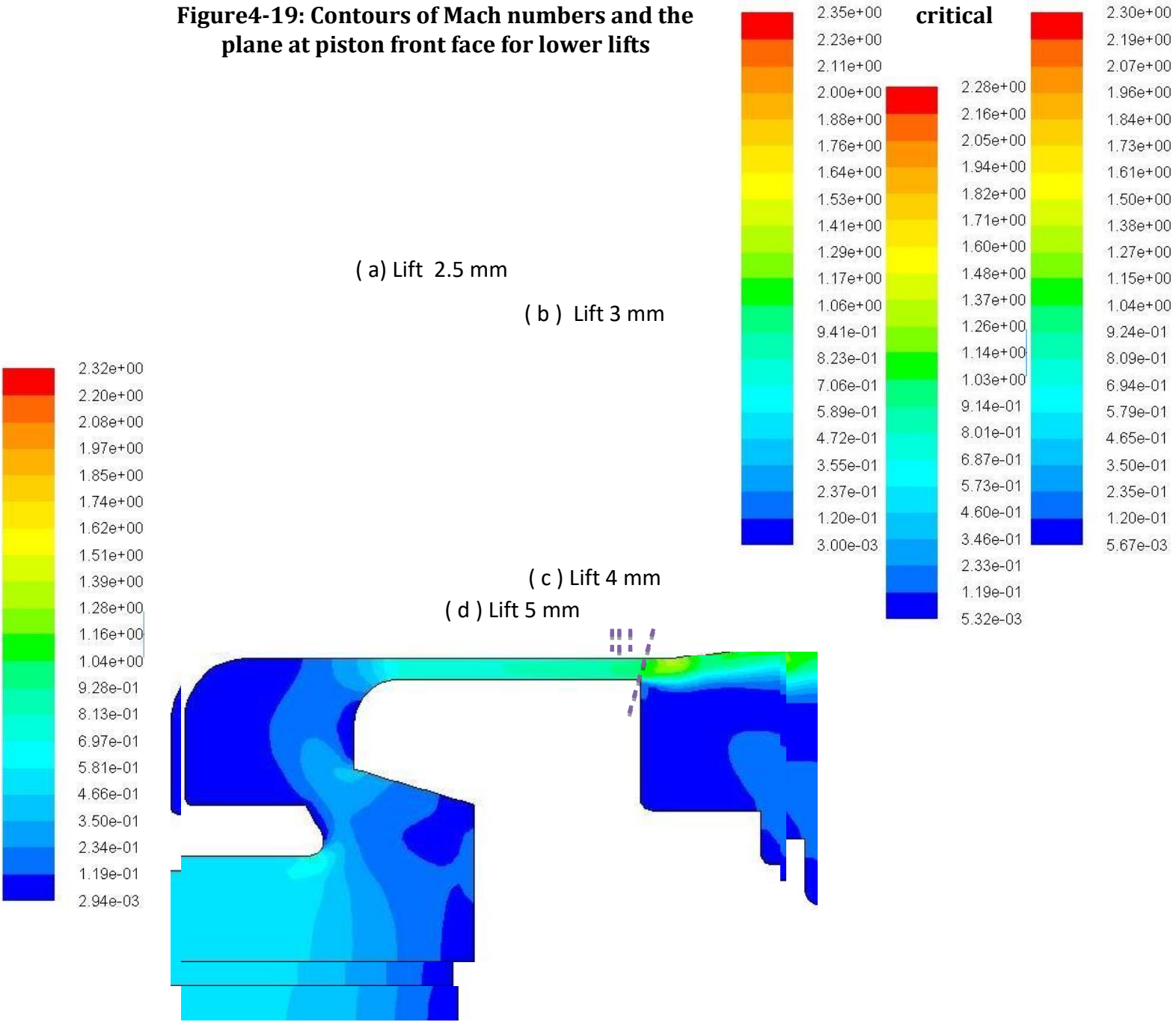

Figure4-20: Contours of Mach numbers and the critical plane at piston side face for higher lifts

4.7.2 Force-Lift Characteristics under Single Phase Flow Conditions

Likewise, the force-lift characteristics can be explained by examining the CFD results. In Figures 4.21 and 4.22, two stages of the force behaviour can be noticed in accordance with the range of piston lifts. Stage 1 starts from 0.2 mm lift until 2mm, where a linear increase in force can be observed. Stage 2 represents the rest of the lifts up to where the valve is fully

opened at 5mm lift. In this latter stage, a steady increase of the net force but reducing in rate until fairly constant value is reached.

Investigating the pressure distributions around the valve for a range of lifts can explain these identified stages. However, it is of interest to begin examining the piston area exposed to the upstream pressure with a particular emphasis given to the front face area as shown in Figure 4.24. This is along with investigating the resulting back pressure and the established choking plane while the piston moves away from its seat. Thus, for the first stage (0.2-2) mm lifts, the net force acting on the piston is mainly front face area dependant as the back pressure recorded is low as shown in Figure 4.25. In stage 2, as the piston lifts further, the flowrate increases before stabilising, and results in an increase in back pressure. The increase in piston back pressure prevents the net force from increasing at the same rate as in stage 1. At higher lifts of stage 2, the piston front face area, A1, A2 and A3 become more exposed to the upstream stagnation pressure. Since the flowrate is now steady so also is the back pressure, resulting in the net force becoming independent of lift.

As far as the modified gland is concerned, the current study shows theoretically and experimentally that the gland has a significant influence on the net piston force particularly at higher lifts. This is due to the strong effect of the gland on the resulting back pressure as depicted in Figure 4.16. Figure 4.21 exhibits experimentally and theoretically the effect of the gland on the resulting net forces. Thus the design of the gland leads to a higher back pressure, gives a greater piston force acting on the piston rear area (A4) and results in a lower net piston force.

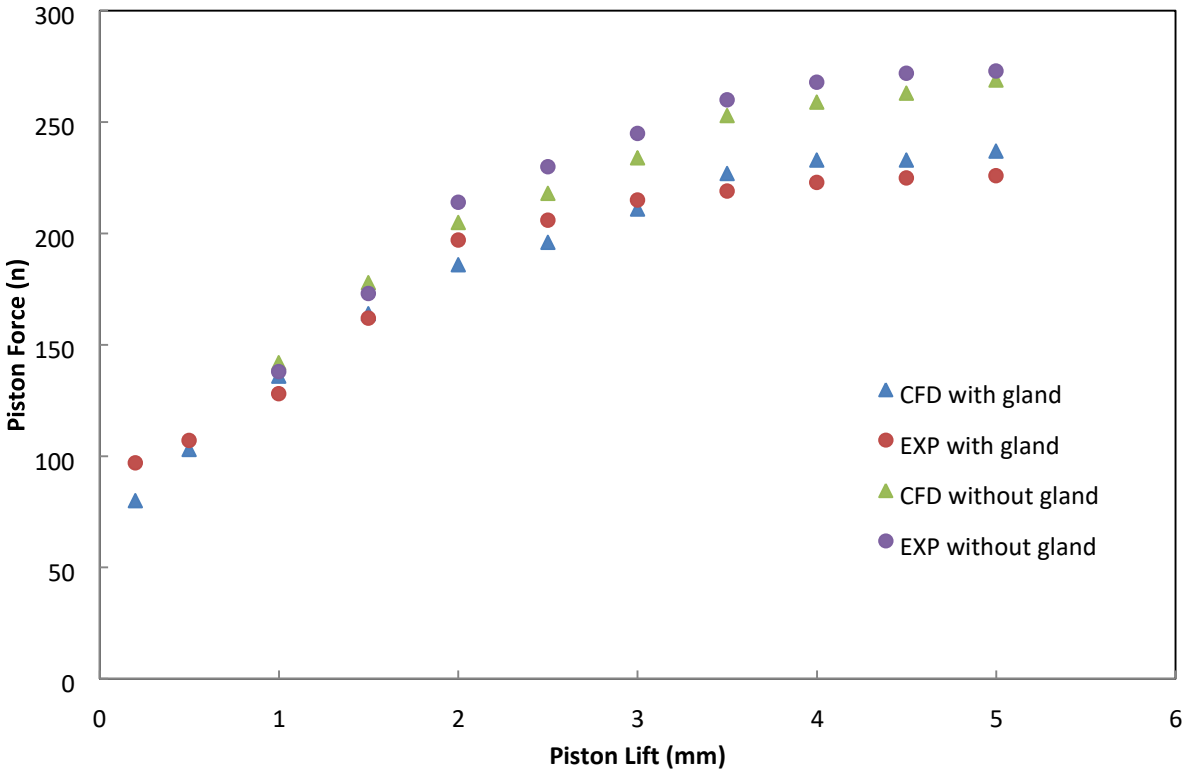

Figure4-21: CFD and experimental force-lift characteristics at an upstream stagnation pressure of 13.8 barg (200 psig)

Figure 4.23 shows a comparison between the measured and predicted back pressure at an upstream stagnation pressure of 10.3 barg (150 psig) for the valve with and without the adjusted gland. The figure proves that the adjusting gland plays a dominant role in the resulting back pressure, which significantly affects the resulting piston force. However there is less agreement between the experimental and CFD predicted back pressure hence the CFD gives higher back pressure magnitudes with a maximum discrepancy of 9% particularly at medium to high lifts of the valve. It is probably attributed to the way of measuring the back pressure, which is associated with buckling issues of the steel tube that are constrained by the nature of the in-house test rig. This is in addition to the proper mesh that is generated on the modified gland and how it is sufficient to capture the physics particularly at the vicinity between the piston rod and the gland. Furthermore, the adjusted gland was found to be eroded particularly the edges of the inner flow area due to the water droplets as the two phase flows experiments were carried out using the same adjusted gland. This would also contribute to the inconsistency in the back pressure predictions.

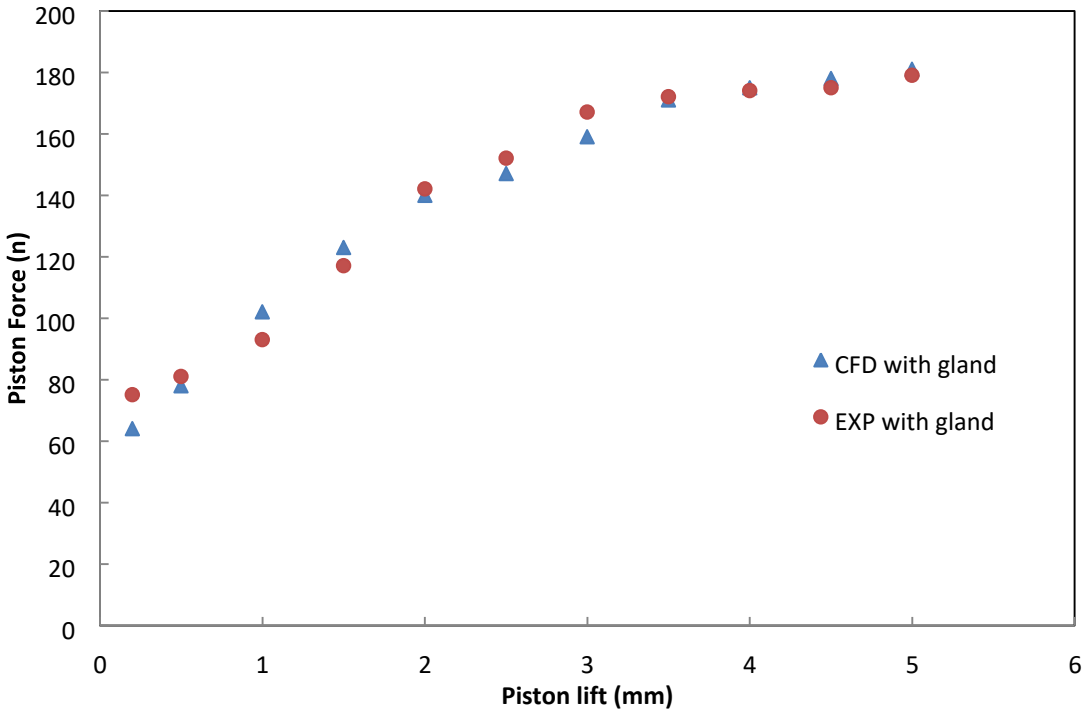

Figure4-22: CFD and experimental force-lift characteristics at an upstream stagnation pressure of 10.3 barg (150 psig)

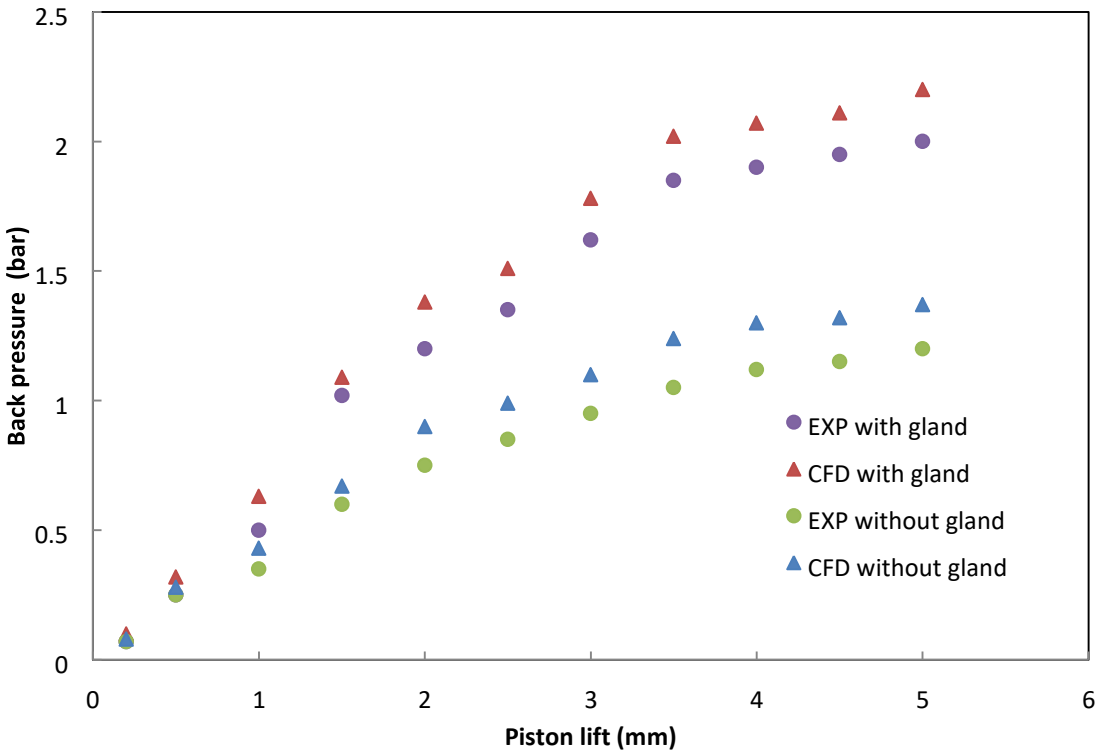

Figure4-23: CFD and experimental back pressure at an upstream stagnation pressure of 10.3 barg (150 psig) for the valve with and without the adjusting gland

A1 piston front face inner area

A2 piston front face outer area “part1”

A3 piston front face outer area “part2”

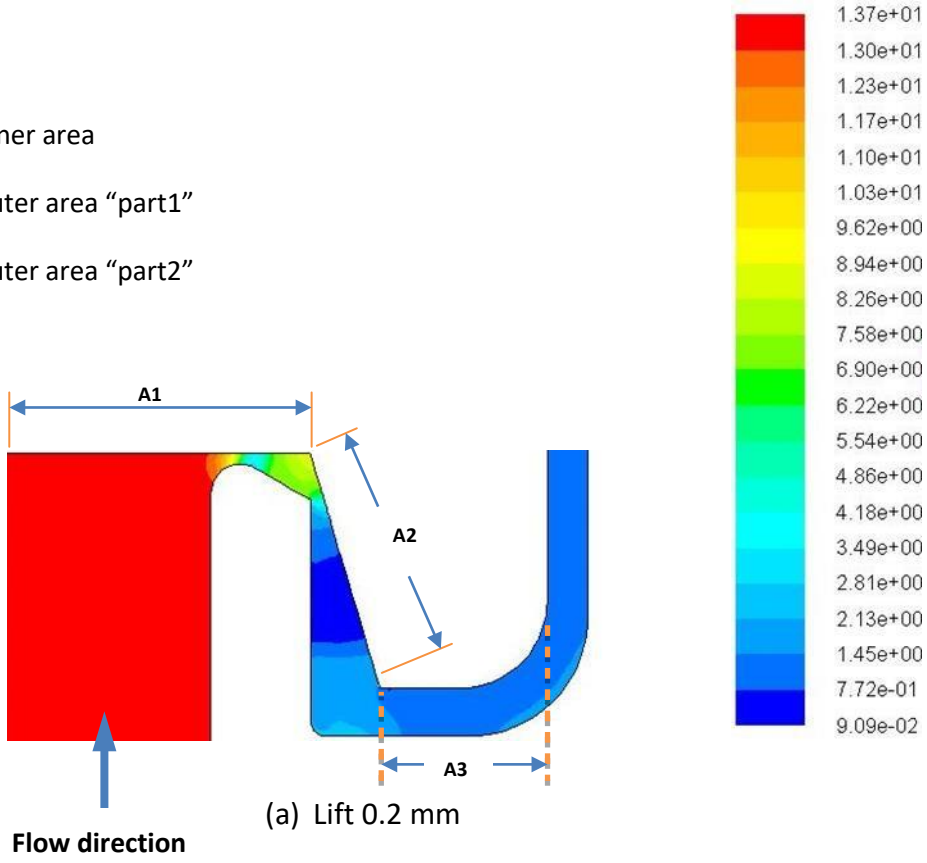

(a) Lift 0.2 mm

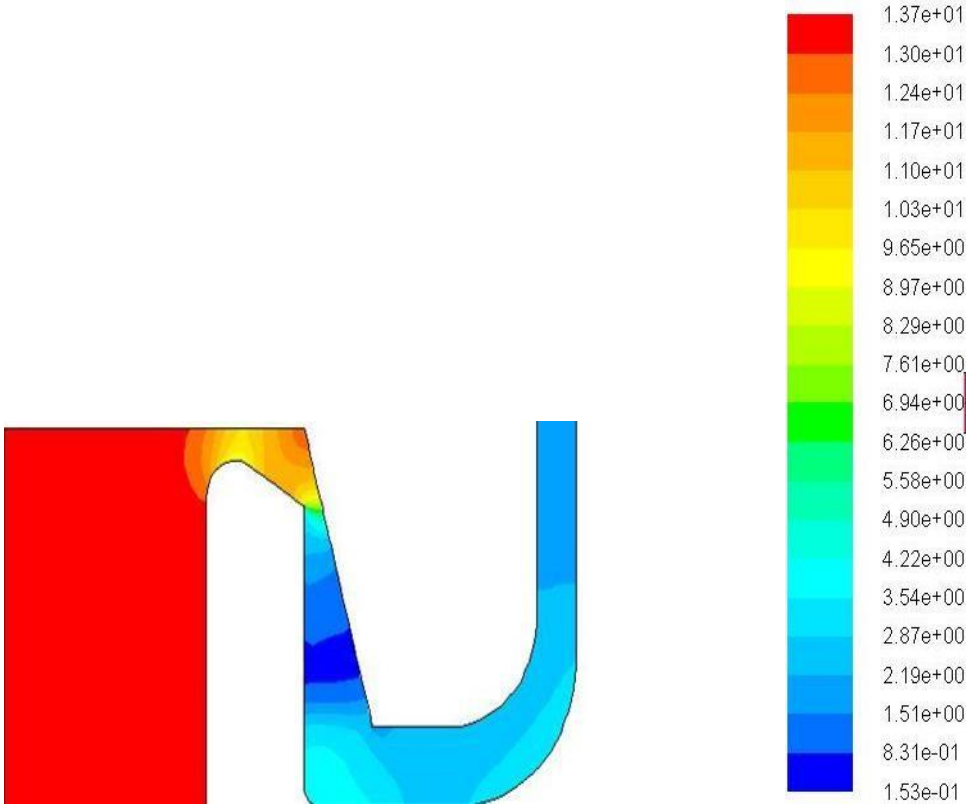

(b) Lift 0.5 mm

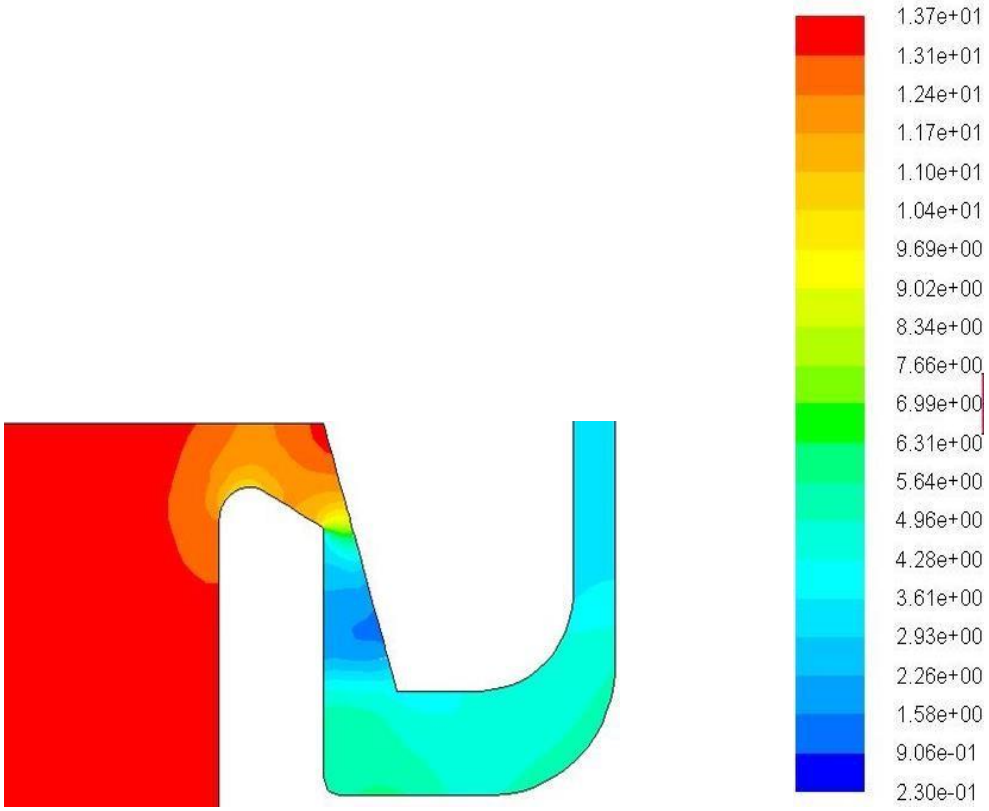

(c) Lift 1 mm

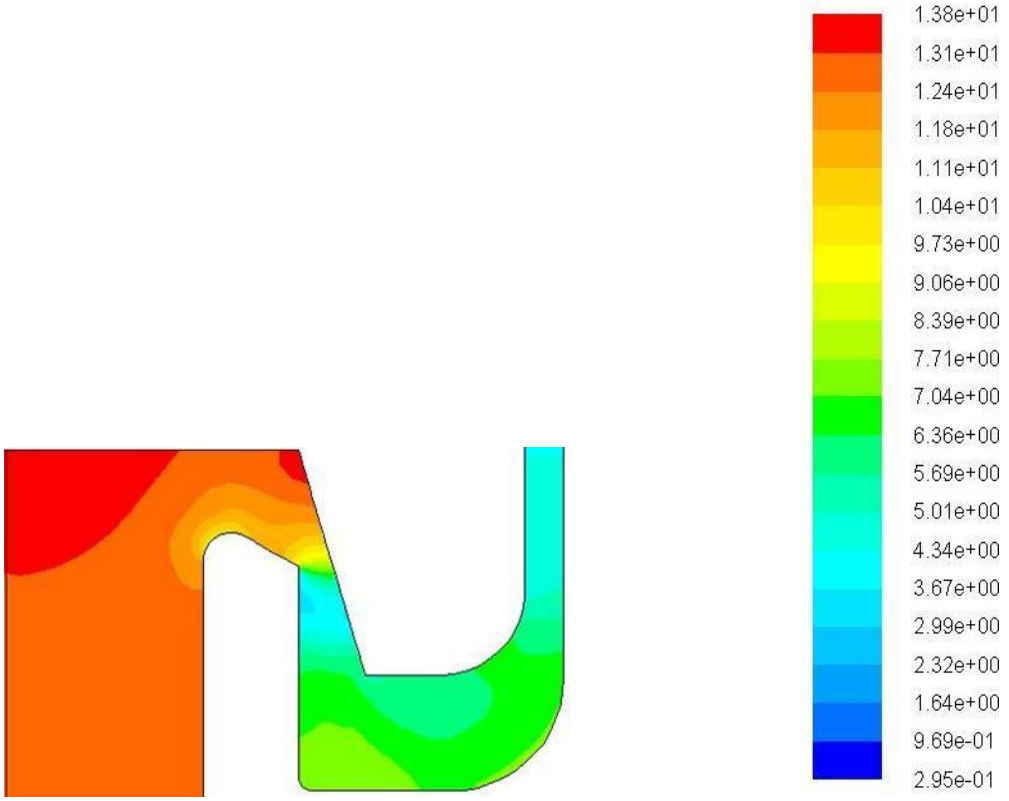

(d) Lift 2 mm

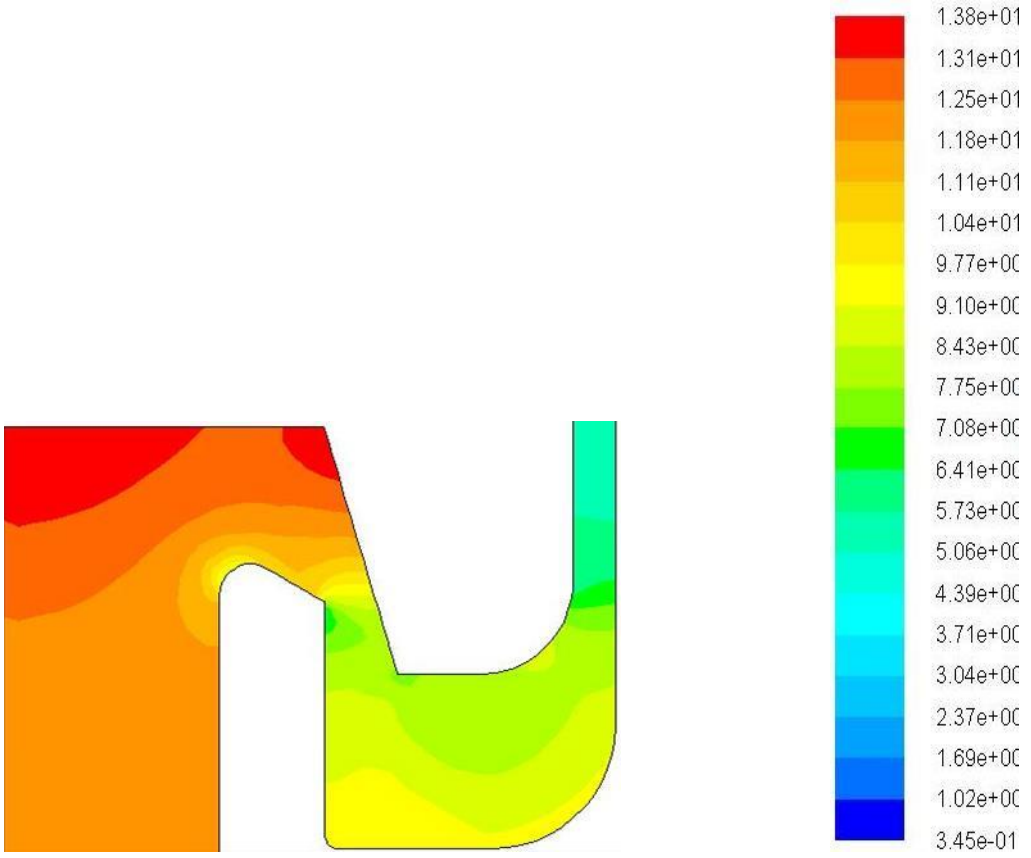

(e) Lift 3 mm

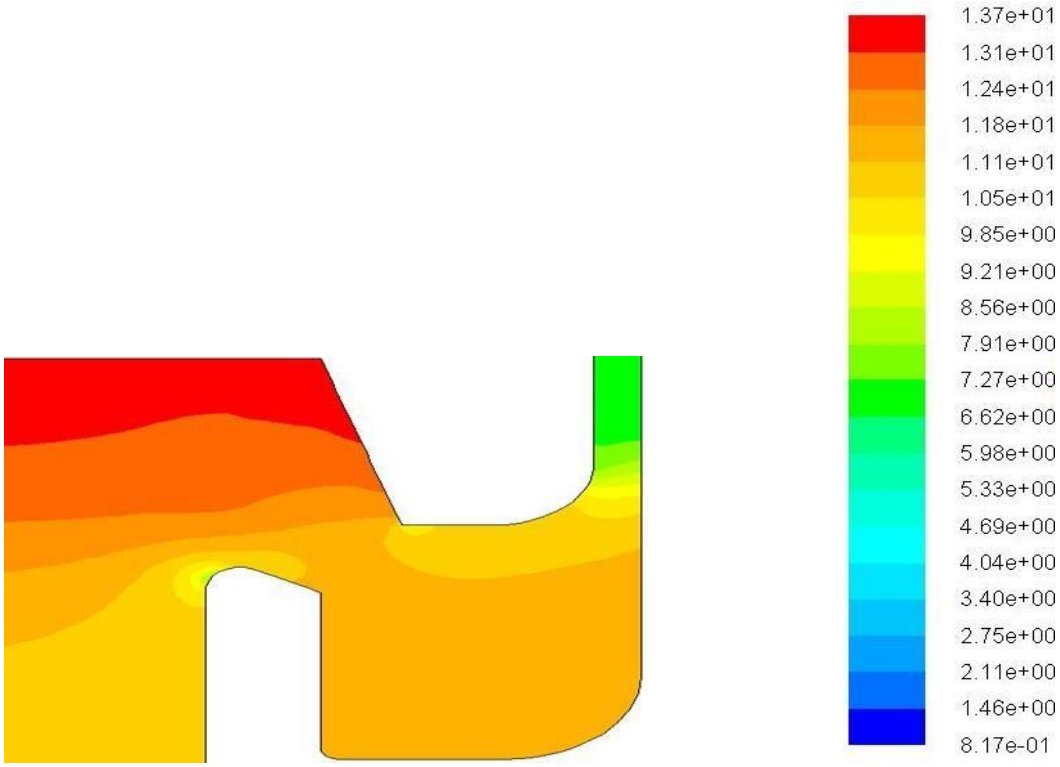

(f) Lift 5 mm

Figure4-24: The pressure contours on piston front face

A4 piston back face “rear area”

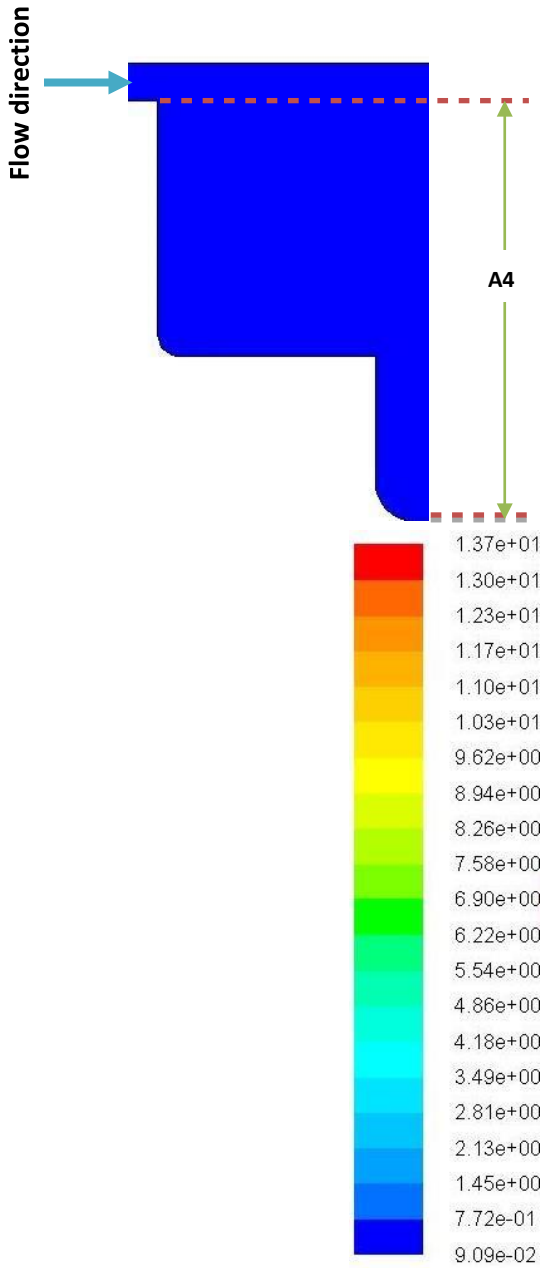

(a) Lift 0.2 mm

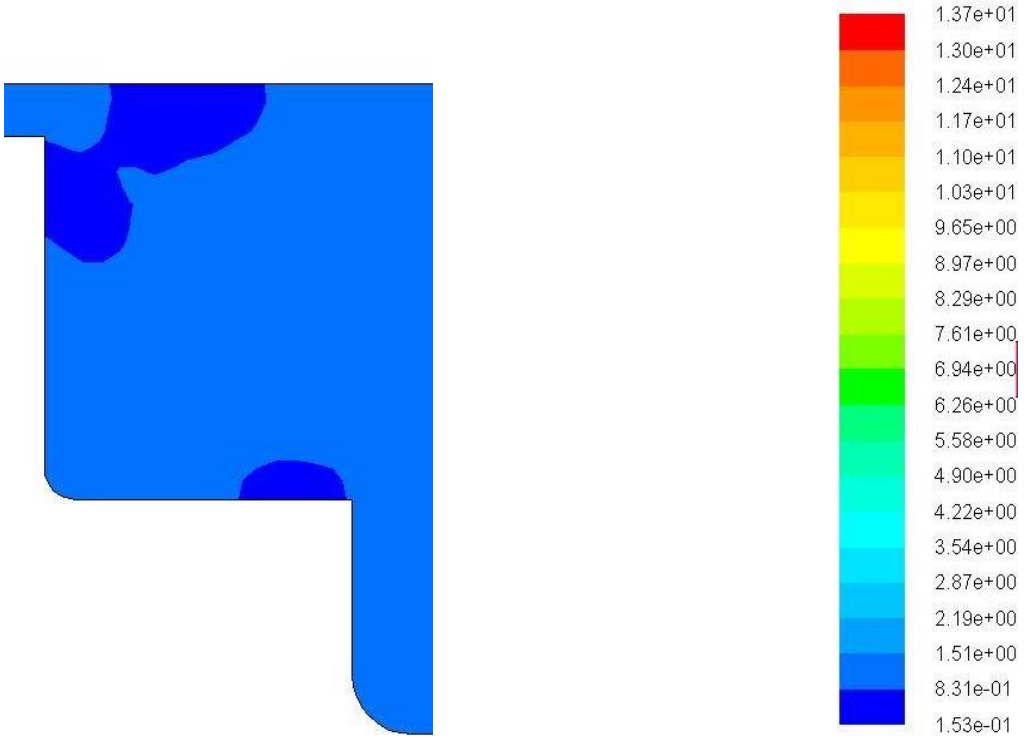

(b) Lift 0.5 mm

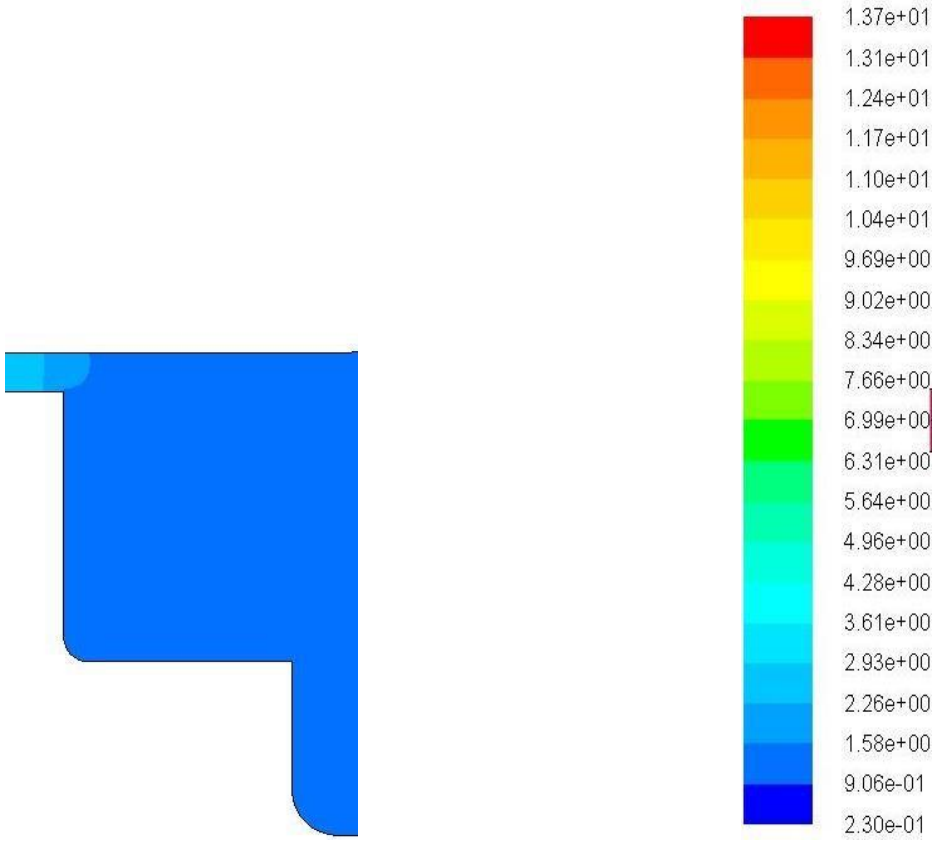

(c) Lift 1 mm

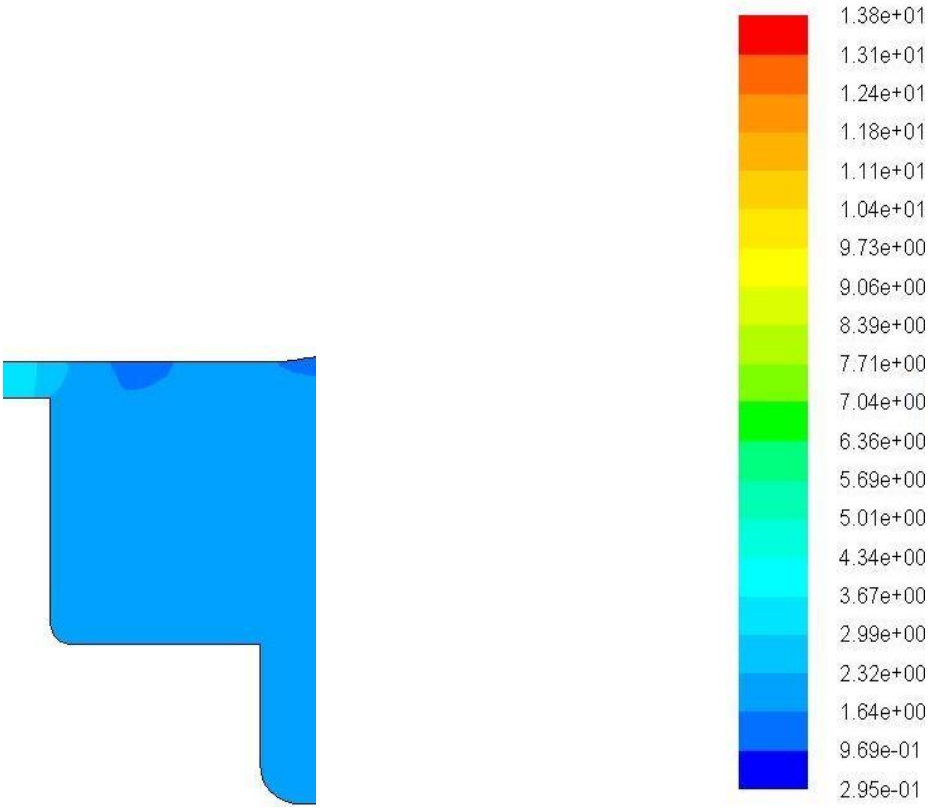

(d) Lift 2 mm

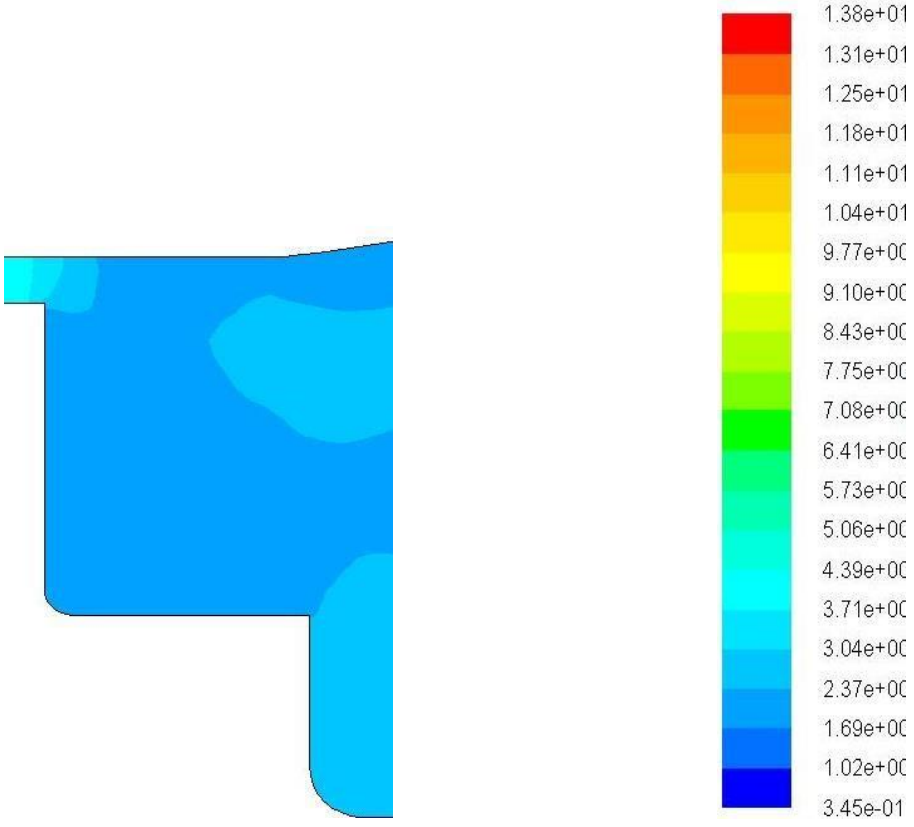

(e) Lift 3 mm

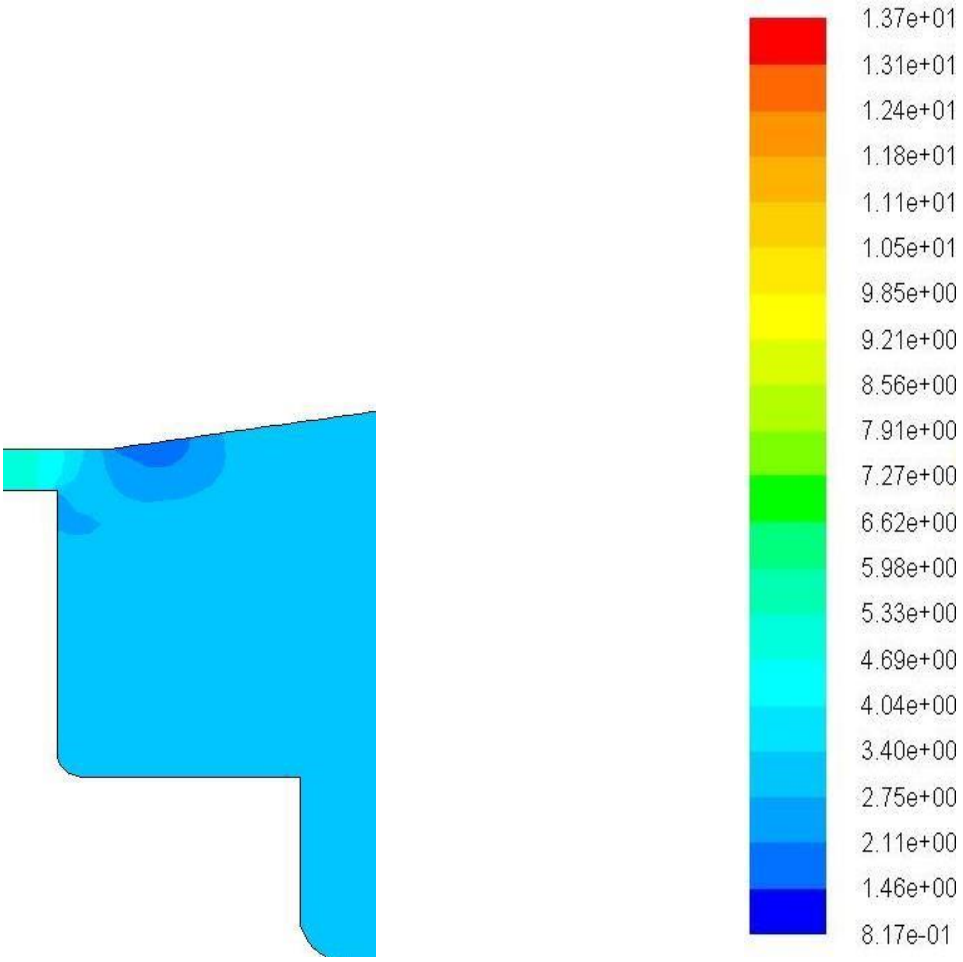

(f) Lift 5 mm

Figure4-25: The pressure contours on piston rear face

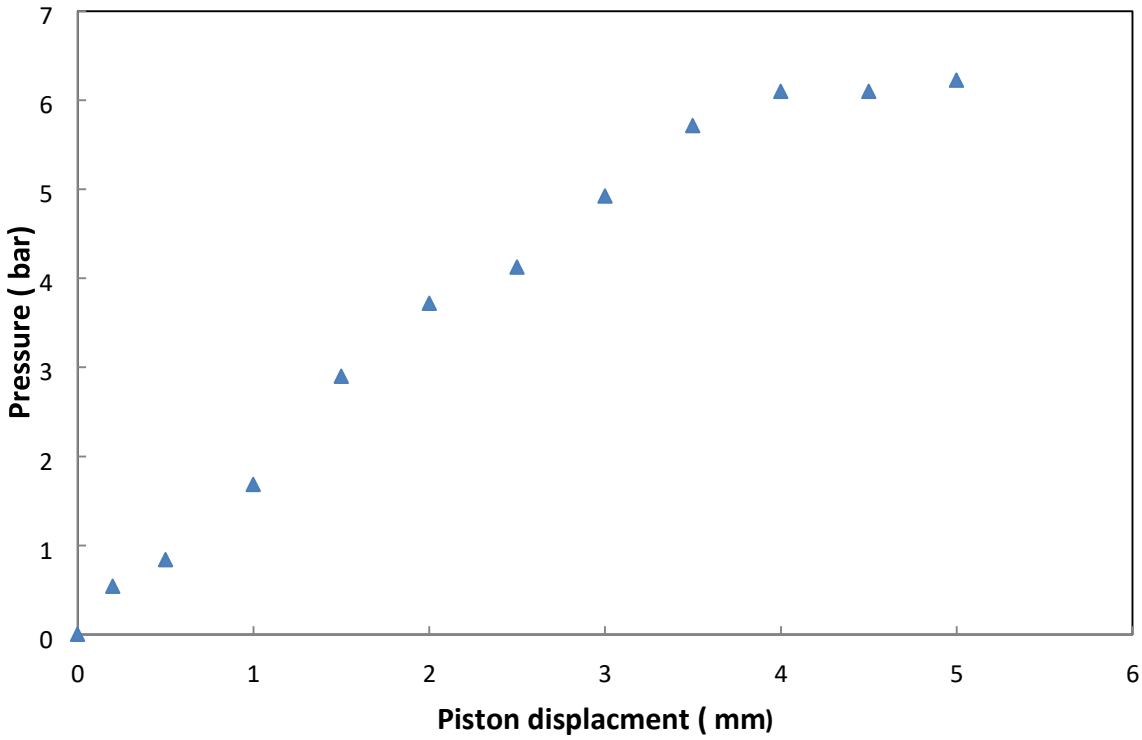

Figure4-26: Static pressure at the inlet of the passageway around the piston for an inlet upstream stagnation pressure of 8.3 barg (120 psig)

4.8 Scaling Approach for the Safety Relief Valve under Steady-State Single Phase Flow Conditions

A general approach relevant to the design of safety relief valves can be achieved as detailed in previous studies of Dempster et al [15] and Elmayyah [88] and allows the flow-lift and force-lift characteristics to be obtained at different working pressures. Two scaling formulas presented in equations 4.17 and 4.18 define the normalised flowrate and normalised piston force, respectively.

For a normalised flowrate when the flow is choked, the following expression can be used:

$$\dot{m}_N = \frac{\dot{m}}{P_0 \, A_{seat}} \sqrt{T_0} \qquad (4.17)$$

F

o

r

a

n

o

r

m

a

l

i

s

e

d

p

i

s

t

o

n

f

o

r

c

e

,

t

h

e

f

o

l

l

o

w

i

n

g

e

x

p

r

e

s

s

i

o

n

c

a

n

b

e

a

p

p

l

i

e

d

:

$$F_N = \frac{F}{(P_0 - P_{atm})\, A_{seat}} \tag{4.18}$$

Figure 4.27 presents the experimentally determined normalised air flowrate-lift characteristics for different working pressures. Since the critical air flowrate at constant lift position is only stagnation pressure dependent, the flow-lift curves based on different upstream inlet pressures collapse into one curve here, with 1.4-2% maximum deviation. Figure 4.28 depicts the normalised piston force-lift characteristics for different working pressures. With approximately maximum uncertainty of 4-6%, the normalised piston forces are also found to collapse into one curve. The net piston force mainly results from the

combination of the front face force and the rear face force. Although the front force is mainly dependent upon the total upstream inlet pressure, the back pressure is associated with the flowrate magnitude and the outlet flow area of the valve plays a dominant role in identifying the back force. Thus attention should be significantly paid to the back pressure of the valve to assist in this type of safety relief valve design for single phase flows. Having the normalised spring force-lift characteristics graphed with the normalised piston force-lift characteristics allow the valve steady state lift to be determined at the intersection point, as shown in Figure 4.29. Also shown in the figure is how the intersection point **A** between the two curves can identify the discharge flowrate from the normalised flow-lift curve.

According to the above mentioned uncertainty particularly in the dimensionless piston forces, the normalised flowrate-lift and force-lift characteristics can be either experimentally or computationally obtained at one of the working pressures. Furthermore, it might be also achieved by identifying the mean force trend line amongst all normalised force curves, hence ensuring less deviation in piston force predictions. Consequently, Figure 4.29 can be used to verify safety relief valve characteristics required for particular working pressures. This will enable the corresponding lifts related to fully open operation conditions as well as the discharge mass flowrate along with the opening pressure to be calculated. In addition, the closing pressure where the spring force is higher than the flow force can be determined by the above mentioned scaling parameters. The spring characteristics can be adjusted to meet specific opening and closing conditions, as shown in Figures 3.1 and 3.2 presented in Section 3.1 of Chapter 3.

However, it is worth mentioning here that the data presented in this section of the valve design are experimental based with the original adjusting gland of the valve in place.

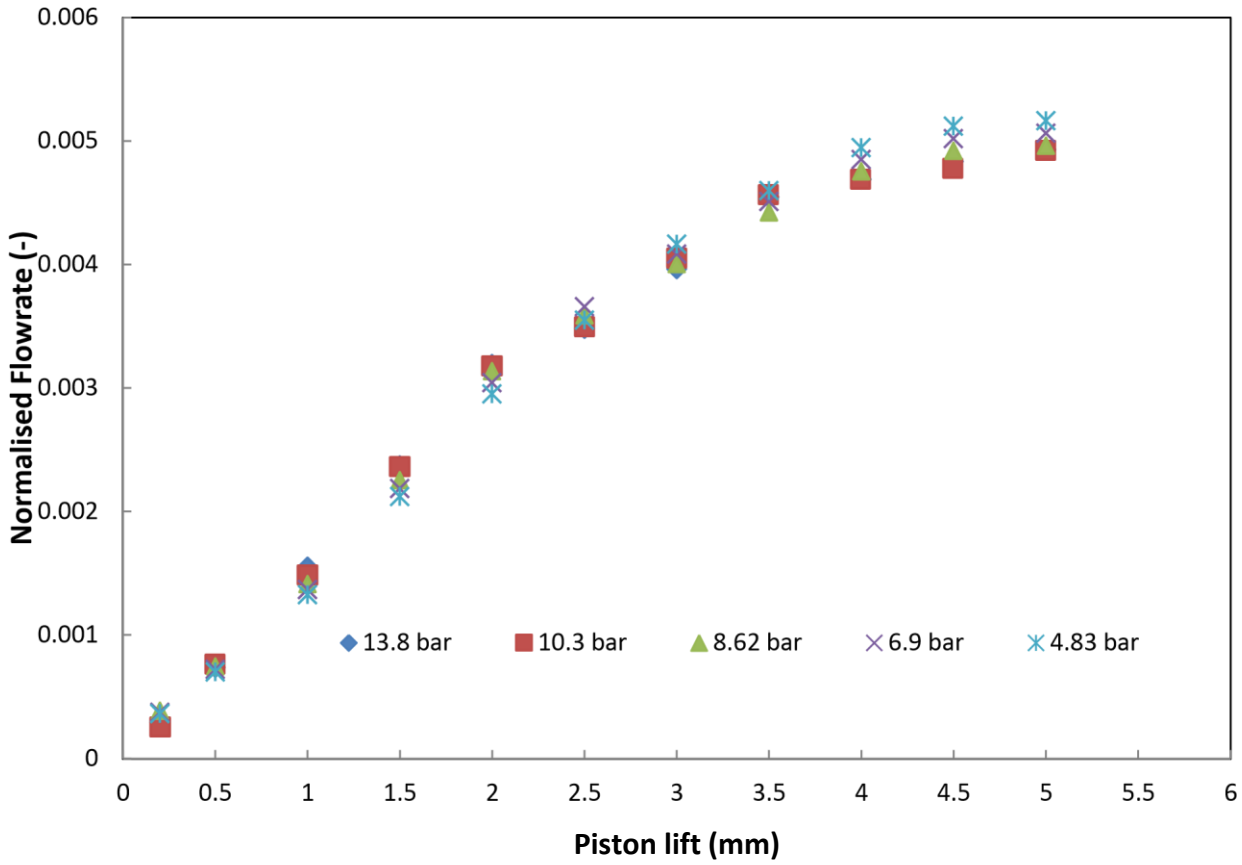

Figure4-27: Normalised flowrate-lift characteristics

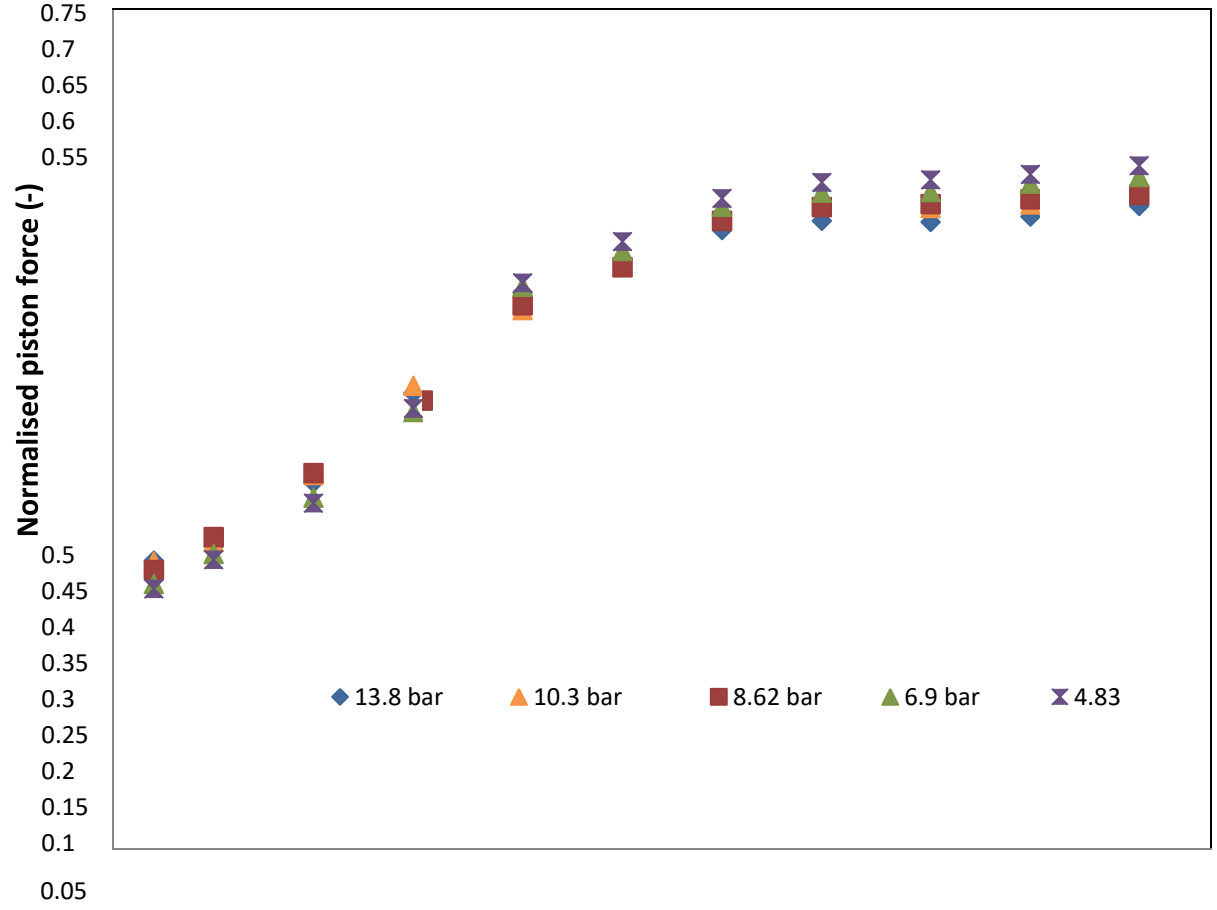

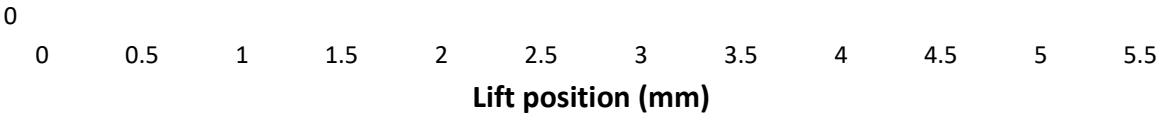

Figure4-28: Normalised piston force-lift characteristics

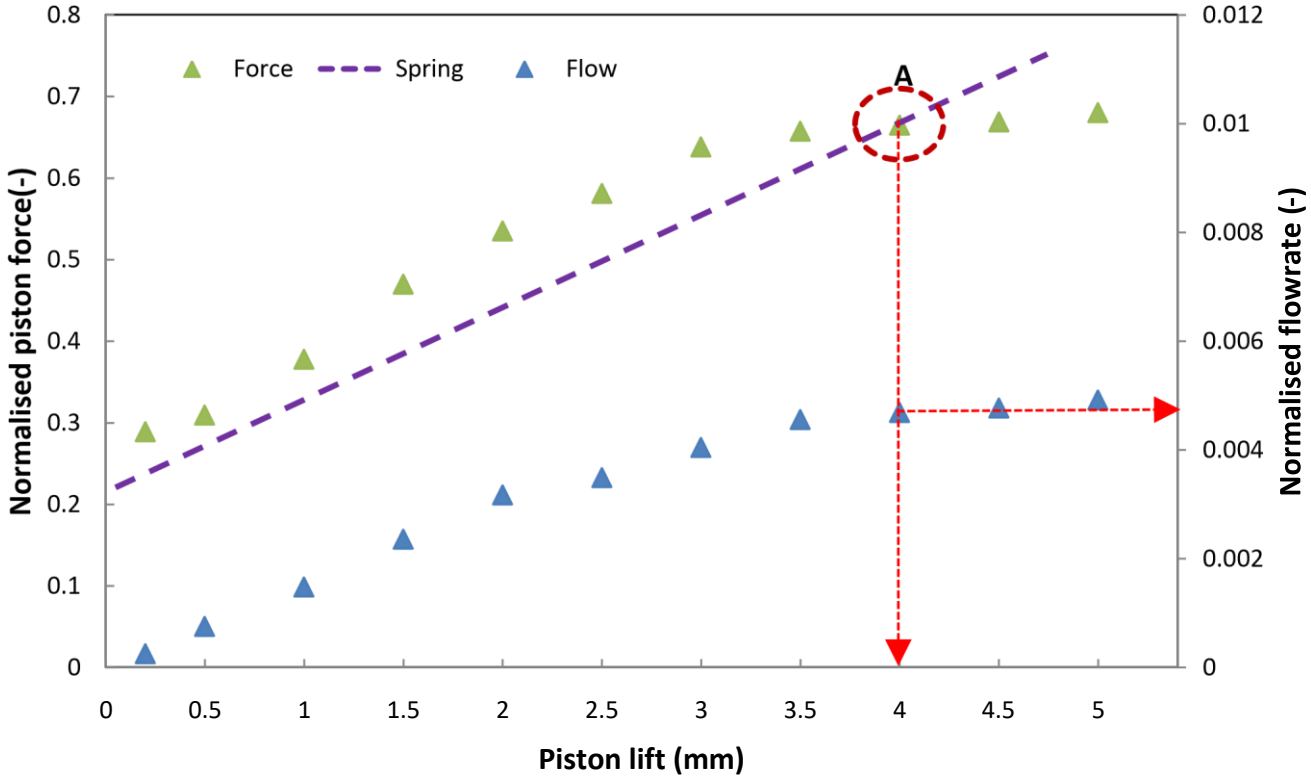

Figure4-29: Normalised force, flow and spring characteristics

Chapter Five

5 Compressible Two-Phase Frozen Flow of Air-Water Mixture

5.1 Overview

The basic characteristics of compressible flow in the studied safety relief valve have been obtained from the previous single phase flow studies. This has provided encouragement to tackle the main objective of this thesis; two phase flow in a safety relief valve. The same safety valve is used to examine computationally and experimentally the air-water two-phase flow characteristics of the safety valve. The aim is to study the two fluid model within the framework of a commercially existing CFD code Fluent. The Fluent code is used to solve the transport and interfacial equations that represent the two phase flow. In addition, an experimental methodology is established for model validation which is fundamentally similar to the one used for single phase studies. An Eulerian-Eulerian model (two-fluid model) with k-Ɛ turbulence model are applied to forecast the two phase flow behaviour under different

flow conditions and determine the flow-lift and force-lift characteristics for the valve with and without its adjusting gland. Test data presented in this study was taken at a pressure range of 6.9 to 13.8 barg (100 – 200 psig) for a liquid flowrate of 0-0.19 kg/s (0-11 $\mathrm{L/min}$) and at a range of piston lift positions of 0 to 5 mm. This allowed a 0-0.87 range of liquid mass fractions- the ratio between the water mass flowrate to the mixture mass flowrate- to be examined which influences the degree of non-equilibrium. Besides the experimental comparison, the predictive capability of the two-fluid model was examined against other well-known simplified computational and algebraic models; namely the CFD mixture model and the Homogenous equilibrium model (HEM) [84], respectively. The rationale is to predict the discharged mass flowrate at various lifts of the valve, pressures and liquid flow conditions. Experimental studies are detailed in Section 5.2. CFD modelling details are presented in Section 5.3. Experimental and CFD results are exhibited in Sections
5.4 and discussed in Section 5.5. Simplified models for validations are discussed in Section 5.6. Scaling of the data for the safety relief valve under steady-state two phase flow conditions is examined in Section 5.7 using the single phase approaches discussed previously in Section 4.8.

5.2 Experimental studies

The purpose of the experimental work is to determine the flow-lift and force-lift characteristics at different upstream air pressures and a wide range of water mass fractions. The rationale was to measure the air flowrates at constant upstream pressure for variations in injected water flowrate. Thus, for each test condition, determined by setting the piston lift, upstream pressure and liquid flowrate, the air mass flow becomes the uncontrolled quantity determined by the circumstances of the two phase interaction with the valve. Upstream of the valve, the water is injected into the flowing air using a spray nozzle allowing the liquid to mix prior to entering the valve producing a two phase flow. The air pressure dominates the magnitude of the air mass flow with the amount of water. Downstream of the valve, the water is collected in a separator/storage tank which also supplies water to the injection pump.

Test data presented in this study allowed a 0-0.87 range of liquid mass fractions to be examined which influences the degree of mechanical and thermal non-equilibrium, i.e.

velocity differences and the sensible temperature changes during the expansion process. The temperature of the gas decreases during the expansion process as the fluid accelerates but will be restricted by the heat transfer from the liquid which changes less due to its larger thermal inertia. Likewise the increasing amount of liquid requires to be accelerated by the air resulting in an interfacial resistance by the liquid. This effect will increase as the liquid mass flow increases. In this study the increased liquid flow acts as a means to introduce greater non equilibrium and takes the form of an independent variable. The effect of the air flow is thus investigated and becomes the dependent variable (the uncontrolled parameter)

A detailed description of the test rig, test setup and procedure are presented in the following subsections.

5.2.1 Experimental setup

An experimental flow facility for valve testing under steady state flow conditions was developed to allow independent control of the valve piston position and upstream water injection at various operating upstream air pressure conditions, Figure 5.1.
The test rig, Figure 5.2, consists of a 100 mm (4 inch) diameter pipe connected to a compressed air system to deliver compressed air at a pressure of 1-15 barg (14.5-217.5 psig) to the valve. The tested safety valve is connected to the pipe via a brass converging section to adapt to the valve entrance. A liquid injection nozzle is fitted into the converging section to inject the water. The injection nozzle located in the centre of the pipe produces a uniform full cone spray with a low spray angle of 30°. A uniformly distributed droplet flow is generated by using a full cone brass spray nozzle. For more details, it is highly recommended to see the entire dimensions which are provided by a diagram located in Appendix C.

Briefly, the later injection contains only one entrance and is connected to a centred inner full cone spray nozzle facing downstream. The outer part of the nozzle is attached to the water supply system. The spray injection device requires only one liquid pipe connection to supply the water flow. The converging section containing the injection system was attached to the air supply pipework via a flanged connection. An additional component (adapter), made of brass, 29.2 mm long, 10 mm diameter, containing a 1 mm pressure tapping was fitted

between the valve and the nozzle. Downstream of the valve, a large tank is used as a separator to separate the water and the air. The water collected in the separator also acts as a water supply for the water injection pump. A PVC T junction with a 50 mm diameter side exit is connected to the valve to direct the two phase mixture to the separator. The T junction could be maintained close to atmospheric pressure. It has a pressure tapping fitted to measure the pressure at the valve outlet. The valve piston is attached to a 250 mm long 6 mm diameter rod which passes through the far end of the PVC tube end and is connected to a lead screw and traverse table allowing the piston position to be adjusted. The piston movement is in the range of 0-5 mm and was measured by a Mitutoyo digital dial indicator with sensitivity of 0.001 mm. The water injection system consists of a positive displacement diaphragm water pump (Hydra Cell D/G-04 series) connected to the injection spray nozzle via a high pressure hose. The pump has a maximum flowrate of 11 $\mathrm{l/min}$ and will deliver the flow independently of the downstream pressure up to 100 bar. The pump is driven by an AC motor controlled by a speed controller, which allows adjustment of the water flow rate. Upstream of the injection nozzle, a turbine flow meter (Omega Engineering FTB 1411) is fitted to facilitate measurement of the water flow rate; it has a flow rate range of 0.4 - 10 $\mathrm{l/min}$ and has an accuracy of +/- 1% of the reading. A compressed gas accumulator (bladder accumulator) (FlowGuard DS-20) is also attached to the pump outlet to ensure pulsations are removed from the pump. The pump is protected against any excessive pressure by using an adjustable relief valve. The air circuit considered here is the one that has been already used for the single phase flow testing and for more details refer to Section 4.4.2 The air flowrate was measured using a Sierra Vortex mass flowmeter (Innova mass 240) and accurate to <1% of reading. The upstream inlet pressure, back pressure and outlet pressure are measured by Bourdon pressure gauges. The range of upstream pressures (1-15 bar) and water flow rates (1-10 L/min) give a working air flow rate from 0.004 to 0.12 kg/s and a water mass fraction range from 0 to 0.87. Consequently, the experimental relative uncertainty of mass fractions (U_X) has been calculated based on experimental uncertainties of both air mass flow measurement ($U_{\dot{m}_a} = \pm 0.01$)and water mass flow measurement ($U_{\dot{m}_w} = \pm 0.0075$), which are already given by the supplier of the flow metres used to measure the air and water mass flowrates. With regards to the force and back pressure measurements, the procedures are similar to those of single phase flow testing, which have been already detailed in Section 4.4.1.

The liquid mass fraction (x) is expressed as:

$$x = \frac{\dot{m}_w}{\dot{m}_a + \dot{m}_w}$$

Where:

$\dot{m}_w$ Liquid mass flowrate (kg/s), $\dot{m}_a$ air mass flowrate (kg/s)

Therefore the relative uncertainty of mass fractions (U_X) has been worked out based on the following statistical expressions:

$$U_X = \pm\sqrt{\left(\frac{\dot{m}_a}{x}\cdot\frac{\partial x}{\partial \dot{m}_a}\cdot U_{\dot{m}_a}\right)^2 + \left(\frac{\dot{m}_w}{x}\cdot\frac{\partial x}{\partial \dot{m}_w}\cdot U_{\dot{m}_w}\right)^2}$$

Hence it has been determined and found to be:

$$U_X = \pm 0.0125 = \pm 1.25\%$$

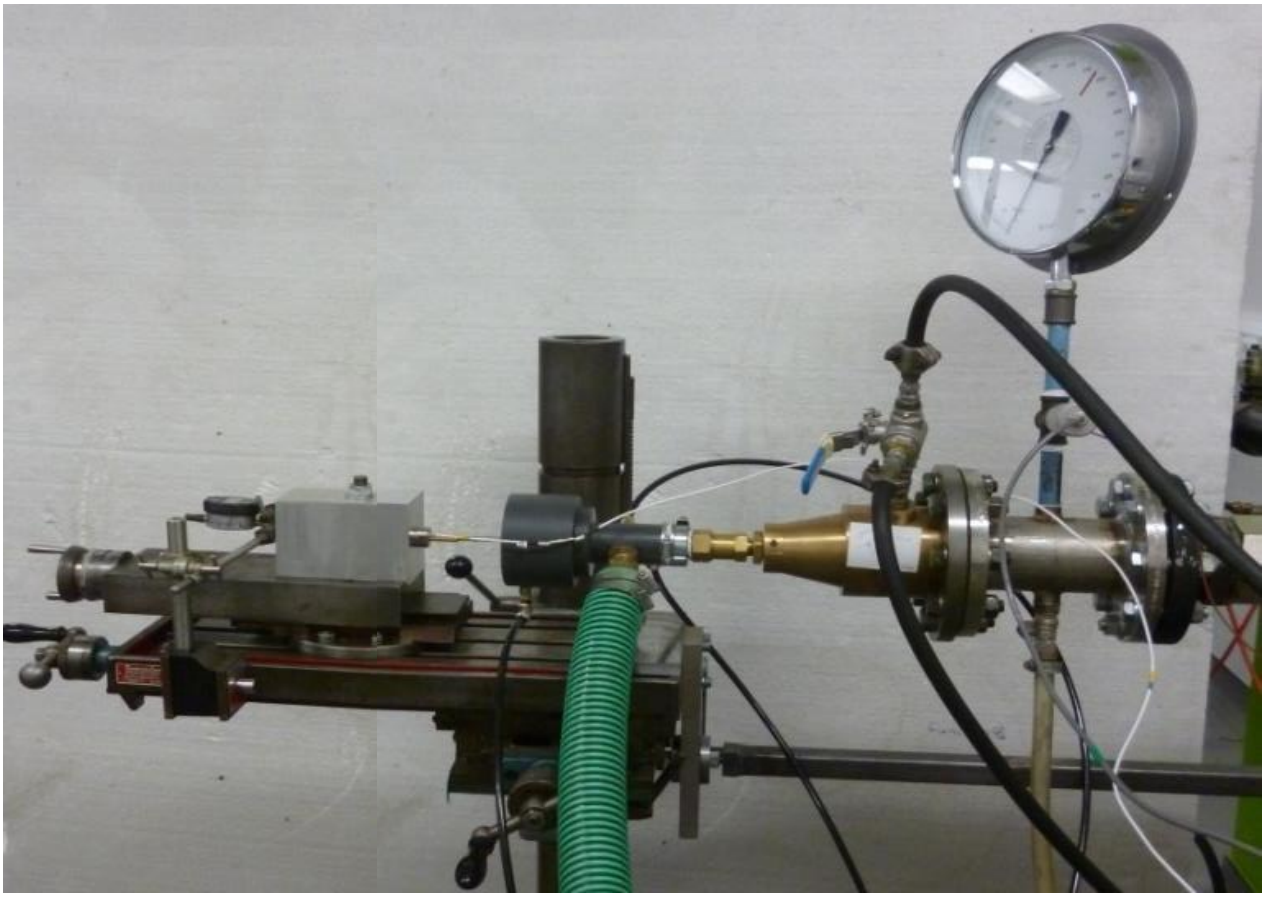

Figure 5-1: Experimental Test Facility

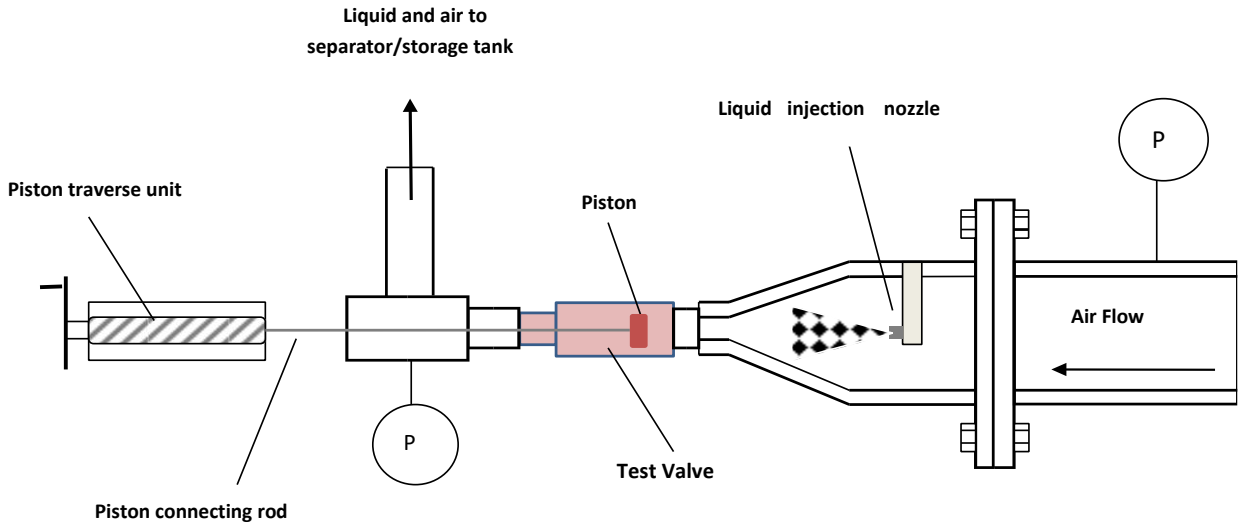

Figure5-2: Schematic drawing of the test rig facility for two phase flow

5.2.2 Experimental procedure

In order to commence the experimental test, the entire system especially the valve internal spaces should be cleared of any residual water. This will be achieved by injecting an amount of air at pressures between 3 to 4 bars by opening the upstream gate valve and setting the piston position (piston lift) to a high value. Opening the gate valve at this stated pressure while the safety valve is fully opened, allows an adequate amount of air to remove the remaining water by carrying it to the separator tank.

After opening the upstream gate valve, the system can be maintained at a working pressure in the range of 6.9 barg to 13.8 barg (100-200 psig), for a liquid flowrate of 0-10 L/min and at a range of piston lift position of 0 to 5 mm. A 5 mm piston displacement corresponds to a fully open position of the valve. At the beginning of the experiment, the piston lift was located at a fixed lift of 5 mm then the pressure gauge was monitored to ensure the pressure required is maintained. The pressure was set at a certain value which was initially fixed at 13.8 barg (200 psig).

The water pump was controlled to achieve a flowrate chosen to match that of the computational calculations. It was observed that the upstream air supply pressure increased as the water flow rate was increased.

This pressure was adjusted back again by using the upstream gate valve after setting the required water flow rate. Once attaining both the desired water flow rate and the operating pressure, the values of the force, air mass flow rate, back pressure, inlet pressure and outlet pressure were recorded in an excel sheet using a PC Laptop. The test proceeded by changing the piston lift in decreasing increments until the 0.0 mm lift was reached. The increments depended on the lift position; a 0.2 mm increment was used in the band between 0.0 mm to 1mm lift and then changed to be 0.5mm in the values between 1 mm and 5 mm. Prior to performing the two phase flow testing, a single phase test is required to determine the zero piston lift position with the same procedure explained in Section 4.4.2. The main reason for this selection is to ensure sufficient data is collected to account for the variations in force and air mass flow. After this the water flow rate would be changed to another mass flow, with the pressure maintained at the previous value. The resulting values of the piston force and air mass flow were again recorded. The previous procedures were repeated to take into account a range of liquid flowrates between 0.4 – 10 L/min which depends upon the computationally calculated water flowrates.

Tests were also conducted to determine the effect of the valve adjusting gland and this was done by either including or excluding the gland during the tests.

5.3 Two-Phase Flow Modelling

There are two generic methods for the numerical simulation of two phase flows: namely, the Eulerian-Eulerian (the two-fluid model) and Eulerian-Lagrangian approaches. The first approach assumes both phases behave like a continuum. The second approach treats one of the phases as a continuum while the second phase is tracked by calculating the particle/droplet equations of motion. In the first approach, the particles/droplets are represented via equations that are developed in the form of volume averaged properties. The Eulerian-Eulerian approach consists of a set of transport equations (continuity, momentum and Energy) for each phase and interfacial equations (drag, lift, slip and heat and mass transfer) to represent the nature of the interactions between phases. Although including the latter concept of interaction between phases makes numerical solutions more complex and difficult to solve, it is not impossible.

The Eulerian-Lagrangian approach has been extended to take into account the interaction between the dispersed phase and the continuous one. In addition, the source term introduced for mass, momentum and energy coupling are evaluated. The EulerianLagrangian method is applicable to both dilute and dense flows, for more details refer to Crowe et al [155]. In this approach, there are two general methods: the *trajectory method* that is suitable for steady/dilute flows while the *discrete element method* is necessary for unsteady/dense flows. It is worth mentioning that, in a dense flow the time between particle-particle collisions is smaller than the response time of particles (or droplets) and vice versa for the dilute flow. Therefore, the applicability of the Eulerian-Lagrangian approach requires a well distributed dispersed phase through the whole flow domain. This is not apparently achievable in many cases particularly dense flows hence this approach is considered to be limited to dilute flows. Thus the Eulerian-Eulerian approach would be a better representation for two phase flows having a wide range of second phase volume fractions.

However, it is believed that for two phase flows existing in the high speed regions of a safety relief valve either dispersed droplets or annular flows with phase distribution, heat transfer and velocity slip modelling will be the dominant conditions. The simplest CFD Eulerian-Eulerian model namely, the mixture model was successfully applied to two phase flows conditions with different applications [21] [126]. As mentioned in the literature, there have been few studies established to examine the multi-dimensional two phase flows in safety relief valves. This mixture model has been applied to a conventional spring loaded safety relief valve and showed good predictive capability of general trends of two-phase critical flow conditions of low liquid mass fractions [53]. In this study, a homogenous thermal and mechanical non-equilibrium two-fluid model was developed to increase the consistency of the multiphase models for a range of two phase flow conditions. The Eulerian approach has been successfully implemented in different applications [110] [11] [137] [138] [139]. This Eulerian-Eulerian model will be discussed via the following subsection. In this study the two phase flow is generated by injecting water into a flow of air.

5.3.1 Euler-Euler Model

An Eulerian-Eulerian multi-phase model for thermal and mechanical non-equilibrium in high-speed supersonic turbulent flow is implemented within a full Navier-Stokes viscous flow solution procedure. The model employs a pressure based finite-volume/finite element discretization of the governing conservation equations of fluid motions with an implicit time-averaged scheme ($\frac{\partial}{\partial t} = 0$) (Steady state) applicable to flow at all speeds. In fact, the latter context of speeds depends obviously upon a progressive reduction on pressure values at the valve exit. The following sections exhibit the computational grid; boundary conditions and solution strategy; and the governing equations of both phases; and eventually the turbulent closures (Turbulence Modelling) and the near-wall treatment.

5.3.1.1 Model Equations

The two phase mixture of air-water comprises gas at pressure P and temperature T_v, and spherical droplets of water with a constant diameterd_p, or film of water; at temperature, T_L. Based on Euler-Euler modelling of two-phase flows, a set of six main equations is to be employed to represent both components as two continuous phases as follows:

5.3.1.1.1 Conservation of mass

There are two continuity equations (one equation per each phase) which are utilized for the calculation of the volume fractions. The solution of this equation for each secondary phase (water), along with the conditions that the volume fractions sum to one, allows for the calculation of the primary –phase volume fraction (vapour).

$$\nabla \cdot \left(\alpha_q \rho_q \ \vec{V}_q\right) = \sum_{P=1}^{n} \left(\dot{m}_{pq} - \dot{m}_{pq}\right) \tag{5.1}$$

The description of multiphase flow as interpreting in term of volume fraction:

$$V_q = \int \alpha_q \, . \, dV \tag{5.2}$$

Hence,

$$\sum_{q=1}^{n} \alpha_q = 1 \tag{5.3}$$

Then the effective density of phase (q) can be defined by:

$$\hat{\rho}_q = \alpha_q \rho_q \tag{5.4}$$

Where: α_q is the volume

fraction of phase q and ρ_q its

d e n s i t y , a n d ρ_{rq} i s t h e p h a s e r

e

f

e

r

e

n

c

e

d

e

n

s

i

t

y

o

r

t

h

e

v

o

l

u

m

e

a

v

e

r

a

g

e

d

d

e

n

s

i

t

y

“

t

h

i

s

i

s

c

l

e

a

r

l

y

b

a

s

e

d

u

p

o

n

t

h

e

s

o

living procedure”, and $\vec{V}_q$ list

h

e

v

e

l

o

c

i

t

y

o

f

p

h

a

s

e

q

a

n

d

$\dot{m}_{pq}$

c

harakteristemassstran

s f e r f r o m t h e p t o q p h a s e , a n

d

$\dot{m}_{qp}$

c

h

a

r

a

c

t

e

r

i

z

e

s

t

h

e

m

a

s

s

t

r

a

n

s

f

e

r

f

r

o

m

p

h

a

s

e

q

t

o

p

h

a

s

e

p

,

a

n

d

w

e

a

r

e

a

b

l

e

t

o

s

p

e

c

i

f

y

t

h

e

s

e

m

e

c

h

a

n

i

s

m

s

s

e

p

a

r

a

t

e l y . T h i s t e r m w a s c o n s i d e r

e

d

a

s

z

e

r

o

a

s

t

h

e

r

e

w

a

s

n

o

m

a

s

s

t

r

a

n

s

f

e

r

b

e

t

w

e

e

n

t

h

e

a

i

r

a

n

d

w

a

t

e

r

p

h

a

s

e

s

b

e

i

n

g

c

o

n

s

i

d

e

r

e

d

.

5.3.1.1.2 Conservation of momentum

Again, there are two momentum equations (one equation per each phase) to be employed for the velocities of both phases. The momentum balance for phase q produces

$$\nabla \cdot \left(\alpha_q \rho_q \, \vec{V}_q \vec{V}_q\right) = -\alpha_q \, \nabla P + \nabla \cdot \bar{\bar{\tau}}_q \, + \alpha_q \rho_q \, \vec{g} + \sum_{P=1}^{n} \left(R_{pq} \, + \dot{m}_{pq} \, \vec{V}_{pq} - \dot{m}_{qp} \vec{V}_{qp}\right) + \left(\vec{F}_q \, + \vec{F}_{lift,q} \, + \vec{F}_{vm,q}\right) \quad (5.5)$$

Where: $\vec{g}$ is the gravitational acceleration, $\bar{\bar{\tau}}_q$ is the q phase stress-strain tensor that could be easily calculated based on the shear and bulk viscosity of the q phase, $\vec{F}_q$ is an external body force, $\vec{F}_{lift,q}$ is a lift force, $\vec{F}_{vm,q}$ is a virtual mass force, R_{pq} is an interaction between phases, P is the pressure shared by all phases, and $\vec{V}_{pq}$ is the interphase velocity that can be defined according to the direction of the mass transferred from one phase to another.

For the present cases, both lift and virtual mass forces are ignored since they are computationally expensive to converge and most likely cause instability in the solution [126]. However, in this study in particular, the lift and virtual mass forces were examined through an initial study under various two phase flow conditions and showed no significant influences on the integrated results of flow and force. Therefore, only the drag force is included during the calculation and is handled based on the *Schiller-Naumann* model for the Drag Coefficient (C_D) for each pair of phases. The aforementioned default model is generally acceptable for use in all fluid-fluid drag coefficients and it is described by the following equation:

$$\sum_{p=1}^{n} R_{pq} = \sum_{p=1}^{n} K_{pq} (\vec{V}_p - \vec{V}_q) \quad (5.6)$$

Where $K_{pq}$is the fluid-fluid exchange coefficient , and can be determined

from :

$$K_{pq} = \frac{\alpha_q \alpha_p \rho_q f}{\tau_p} \quad (5.7)$$

With the assumption that the secondary phase for the fluid-fluid flows forms droplets and this clearly has an impact on how each phase of the fluids is assigned to a particular phase. The present case has unequal amounts of two fluids hence; the predominant fluid must be modelled as the primary fluid. Although the drag function is different from one model of exchange-coefficient to another, the particulate relaxation time (τ_p) of available models has the same equation.

$$\tau_p = \frac{\rho_p d_p^2}{18\mu_q} \quad (5.8)$$

While the drag factor is reflected in the following equation:

$$f = \frac{C_D.Re}{24} \quad (5.9)$$

However, all definitions of the drag factor (f) includes a drag coefficient (C_D) that is calculated based on a relative Reynolds number(Re). The relative Reynolds number for the primary phase$q$ and secondary phase$p$ can be described according to the flowing equation:

$$\mathrm{Re} = \frac{\rho_q |\vec{v}_p - \vec{v}_q| d_p}{\mu_q} \tag{5.10}$$

$$C_D = \begin{cases} \frac{24(1+0.15Re^{0.687})}{Re} & Re \leq 1000 \\ 0.44 & Re > 1000 \end{cases} \tag{5.11}$$

5.3.1.1.3 Conservation of energy

In order for the conservation of energy in Eulerian multiphase applications to be described, a separate enthalpy equation can be written for each phase as follows:

$$\nabla \cdot (\alpha_q \rho_q \vec{u}_q h_q) = \alpha_q \frac{\partial P_q}{\partial t} + \bar{\bar{\tau}}_q : \nabla . \vec{u}_q - \nabla . \vec{q}_q + \sum_{p=1}^{n} (Q_{pq} + \dot{m}_{pq} h_{pq} - \dot{m}_{qp} h_{qp}) \tag{5.13}$$

Where: h_q is the specific enthalpy of the q phase, $\vec{q}_q$ is the wall heat flux, $Q_{pq}$is the intensity of heat exchange between both phases, and h_{pq} is the interphase enthalpy. The heat exchange between phases must comply with the local balance conditions as the sum equals to 1. However, the *Ranz-Marshall* model is applicable for modelling heat transfer between the two phases then the first term of the mass transfer equation is achieved by means of "sensible heat". The Ranz-Marshall model is defined by the following expression of heat transfer.

The internal energy balance for the primary phase q is defined by:

$$H_q = \int C_{P,q} \, dT_q \tag{5.14}$$

Where $C_{P,q}$is the specific heat at constant pressure and all the thermal boundary conditions are specified automatically as soon as the multiphase materials are chosen. The heat exchange coefficient is based upon the volumetric rate of energy transfer between phases is assumed to be a function of the temperature difference:

$$Q_{pq} = \lambda_{pq} (T_p - T_q) \tag{5.15}$$

The volumetric heat transfer coefficient between the two phases is related to the primary phase *Nusselt number*, Nu_p, by the following equation:

$$\lambda_{pq} = \frac{6.\mathrm{K}_q \alpha_p \alpha_q \, Nu_p}{d_p^2} \tag{5.16}$$

Where : K_q is the thermal conductivity of the phase q.

The Nusselt number is a function of both relative Reynolds number and the Prandtl number. It can be typically determined by one of the many correlations reported in the literature. One of these correlations is the *Ranz-Marshall* correlation that has been employed specifically for fluid-fluid multiphase flows. The following correlation of Nusselt number is only appropriate when the Reynolds's number lies in the range of 0.1 to 4000. Exceeding the Reynolds's number of 4000, however, would require the correlation of Whitaker.

$$Nu_p = [\ 2.0\ + 0.6\, Re^{1/2} Pr^{1/3}\ ]$$

[Ranz-Marshall's correlation] (5.17)

$$Nu_p = \left[\ 2.0\ + \left(\ 0.4\, Re^{\frac{1}{3}}\ + 0.06\, Re^{\frac{2}{3}}\right) Pr^{0.4} \left(\frac{\mu_\infty}{\mu_s}\right)^{\frac{1}{4}}\right]$$

[Whitaker's correlation] (5.18)

The Prandtl number is defined by the following equation:

$$Pr = \frac{C_{p,q}\mu_q}{\mathrm{K}_q} \tag{5.19}$$

5.3.1.1.4 Turbulent closures and near-wall treatment

In the present work, the type of turbulence model is significant so the well-established high –Reynolds number $\kappa - \varepsilon$ turbulent model is applied. In general, most of the cases require a turbulence model to represent the turbulent Reynolds stress terms and this could be introduced via an eddy viscosity that is normally added to the molecular viscosity to acquire the so-called effective viscosity. Three $\kappa - \varepsilon$ type turbulence multiphase model options are

available in the context of the standard, the RNG and the realizable$\kappa - \varepsilon$ model. These turbulence multiphase models represent the extension of the single-phase$\kappa - \varepsilon$ model. However, in this study, there are two different possible scenarios, which are fundamentally dependent upon the second phase quantity (liquid droplets content). Firstly, for the case where liquid mass fraction is low, it is assumed that the droplets have no direct influence on the turbulence even though there will be an indirect influence through the so-called velocity field. Secondly, in the case of high liquid mass fraction, there might be a more direct effect on the turbulence. In addition, the turbulence in the gas phase must be taken into consideration as it does have a clear influence on the dispersion of the liquid droplets. This was deployed through the two fluid model based on the so-called turbulent drift force (dispersion force). According to a pilot study, it was found to predict significantly higher piston forces and less flowrates therefore it was disabled for all the subsequent cases of this study.

However, the latest code version of CFD fluent has the three options of turbulence multiphase eulerian model; Mixture, Dispersed and the Per-phase. According to the current numerical calculations, the dispersed turbulence multiphase model has led to stability across the variety of conditions studied particularly for low liquid volume fraction modeling up to approximately 1% (maximum 38% liquid mass fraction).Above this water quantity as the second phase may not be considered as dilute, the two fluid models were found not to work (rapid divergence after the first 300 iteration). Despite the fact that the mixture turbulence multiphase model is only applicable when the density ratio between the two phases is nearly unity, it was found to provide similar force and mass flow results for two phase modelling of low liquid volume fractions. Therefore the mixture turbulence multiphase model was chosen for all subsequent two phase flow model calculations using mixture velocities and mixture properties might be sufficient to capture important features of the turbulent flow. In this study, this mixture turbulence model derived from the instantaneous Navier-Stokes equations was employed based on the standard$\kappa - \varepsilon$ model. Furthermore, this mixture turbulence multiphase model with the three different contexts of the$\kappa - \varepsilon$ model has been applied and lead to no major influence on the predicted results.

This $\kappa - \varepsilon$ mixture turbulence model has the following transport equations:

$$\nabla.(\rho_m \vec{v}_m \kappa) = \nabla.\left\{\left(\frac{\mu_{t,m}}{\sigma_k}\nabla\kappa\right)\right\} + G_{\kappa,m} - \rho_m \varepsilon \tag{5.20}$$

And

$$\nabla.(\rho_m \vec{v}_m \varepsilon) = \nabla.\left\{(\frac{\mu_{t,m}}{\sigma_\varepsilon}\nabla\varepsilon\right\} + \frac{\varepsilon}{\kappa}(C_{1\varepsilon}G_{\kappa,m} - C_{2\varepsilon}\rho_m\varepsilon) \quad (5.21)$$

Where the mixture density$\rho_m$and velocity$\vec{v}_m$, are calculated from

$$\rho_m = \sum_{i=1}^{N} \alpha_i \rho_i \quad (5.22)$$

And

$$\vec{v}_m = \frac{\sum_{i=1}^{N} \alpha_i \rho_i \vec{v}_i}{\sum_{i=1}^{N} \alpha_i \rho_i} \quad (5.23)$$

The turbulent viscosity $\mu_{t,m}$, is calculated from

$$\mu_{t,m} = \rho_m \,.\, C_\mu \,.\, \frac{\kappa^2}{\varepsilon} \quad (5.24)$$

And the production of turbulent kinetic energy

$$G_{\kappa,m} = \mu_{t,m}(\nabla\vec{v}_m + (\nabla\vec{v}_m)^T : \nabla\vec{v}_m \quad (5.25)$$

And,

$$C_\mu = 0.09$$

Using the mixture turbulence model in the context of the Realizable$\kappa - \epsilon$ model, however, the$C_\mu$becomesa function of the mean strain and rotation rates, the angular velocity of the system rotation, and the turbulence field ($\kappa \; and \; \varepsilon$). Hence, it is no longer constant and can be computed from:

$$\overline{\qquad\qquad}\qquad\qquad(5.26)$$

$$U^* = \sqrt{s_{ij}.s_{ij} + \Omega_{ij}\Omega_{ij}} \qquad (5.27)$$

Where Ω_{ij} denotes the mean rate-of-rotation tensor.

$$A_0 = 4.04\,, \quad A_s = \sqrt{6}\cos\phi \qquad (5.28)$$

Where:

$$\phi = \frac{1}{3}\cos^{-1}(\sqrt{6W}) \qquad (5.29)$$

And,

$$W = \frac{S_{ij}S_{jk}S_{ki}}{\check{S}^3} \qquad (5.30)$$

$$\sqrt{\qquad\qquad} \qquad (5.31)$$

$$s_{ij} = \frac{1}{2}\left(\frac{\partial u_j}{\partial x_i} + \frac{\partial u_i}{\partial x_j}\right) \qquad (5.32)$$

With regards to the near-wall treatment, the standard wall functions are implemented based on the law-of-the-wall for *flow mean velocity* in terms of momentum transport and the *flow mean temperature* for energy transport. It can be considered as Reynolds' analogy between energy and momentum due to similarity. However, the Y^+ value has been calculated along the piston side passage way and found to be in most of the cases greater than 11, hence applying the standard wall functions would be appropriate and follows the recommendations of the Fluent User's Guide. In addition, the scalable wall functions were also examined and showed no significant difference in results predicted using the standard wall functions. However, other wall functions such as the non-equilibrium wall functions were found to give divergence on simulations within 200-500 iterations.

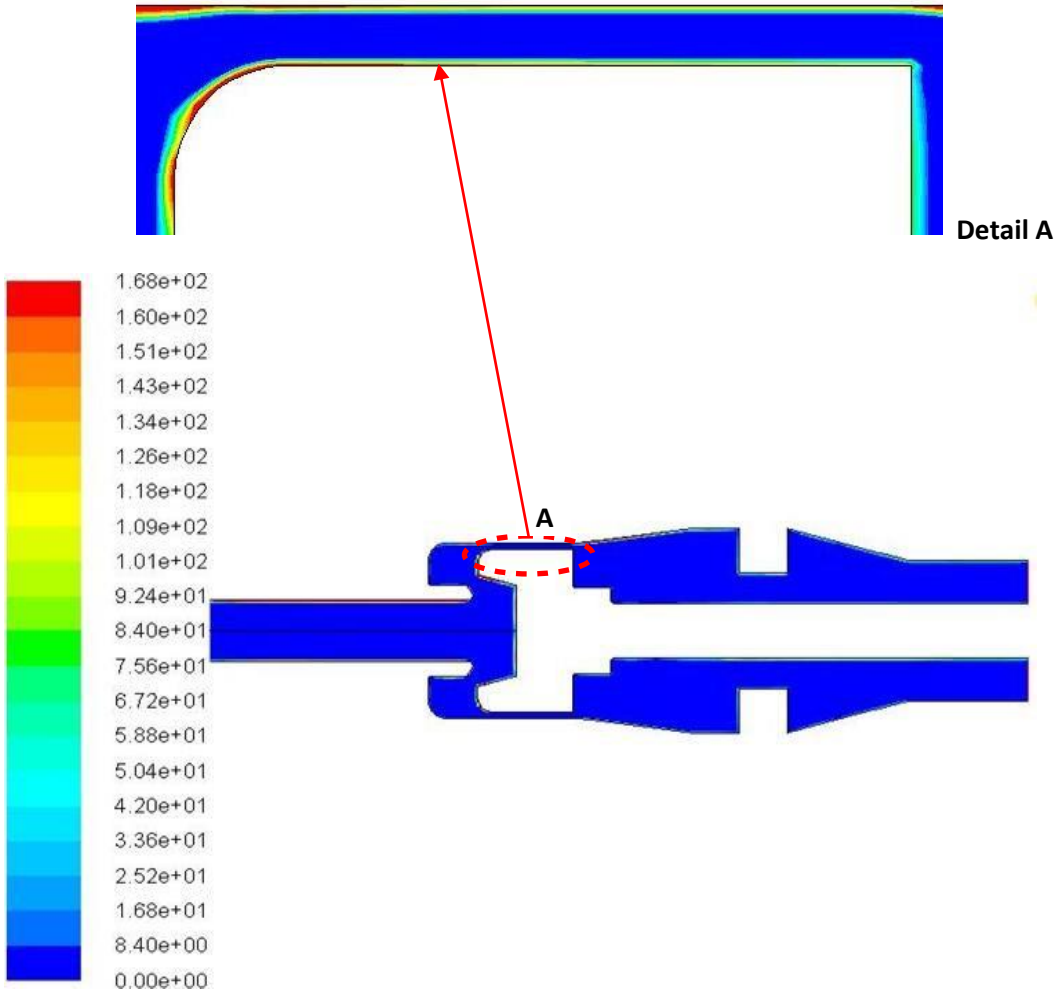

Figure 5-2a: Y^+ value along the piston side passage way for the above mentioned flow conditions

In industrial flows, the standard wall functions are widely utilized based on the work of Spalding and Launder and they are the default option in ANSYS fluent. The temperature distribution in the near-wall is of importance especially in highly compressible flows owing to the heating by viscous dissipation. Hence, the contribution from the viscous heating should be included to ensure rightly the model of the temperature wall functions. As far as the turbulence at the wall-adjacent cells is concerned, the κ equation would be solved normally in the whole domain including the wall-adjacent cells with the boundary condition assumption that $\frac{\partial \kappa}{\partial n} = 0$ at the wall (where: n is the local coordinate normal to wall).

Meanwhile, the production $G_{\kappa,M}$ and its dissipation rate are both computed at the walladjacent cells based on the local equilibrium hypothesis. With this assumption, the production of κ and its dissipation rate ε are equal in the wall-adjacent control volume. The ε equation will not be solved at the wall-adjacent cells as for the whole domain but instead

will be computed at this region according to its empirical equation.

The above turbulence model has the following constants, which are established to perform well under certain flow constrains.

$$C_{1\varepsilon} = 1.44\ ,\ C_{2\varepsilon} = 1.92, \sigma_k = 1.0\ , \sigma_\varepsilon = 1.3\ ,$$

5.3.2 Computational Grid

The safety relief valve geometry is rotationally symmetric along the axis and can be represented using a 2d-axisymmetric model with an unstructured mesh type, Fig 5.3. It contains of around 13228 elements with an approximate mean dimension of 0.25 mm, based on a triangular and quadratic cell type. The mesh is generated using proximity and curvature advanced sized functions with a fine relevance centre as well as a fine span angle centre. It is well-known that a finer mesh can lead to more stability in a calculation but does not mean accurate results. The generated mesh is also examined based on a mesh metric methodology of skewness and found to be 0.69 as a maximum value in only 157 elements all over the flow domain. An investigation into grid independence was carried out where the results from the standard mesh (13328 cells) were compared with those of a mesh 5 times more dense with 66424 cells. The results are shown in Figures 5.4 and 5.5 and indicate that the 13328 cell mesh is grid independent as far as the mass flowrate and piston force predictions are concerned. However, the less dense mesh with approximately 7200 cells was found to predict less mass flowrates and forces.

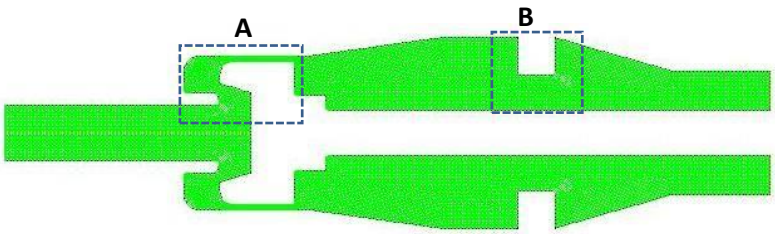

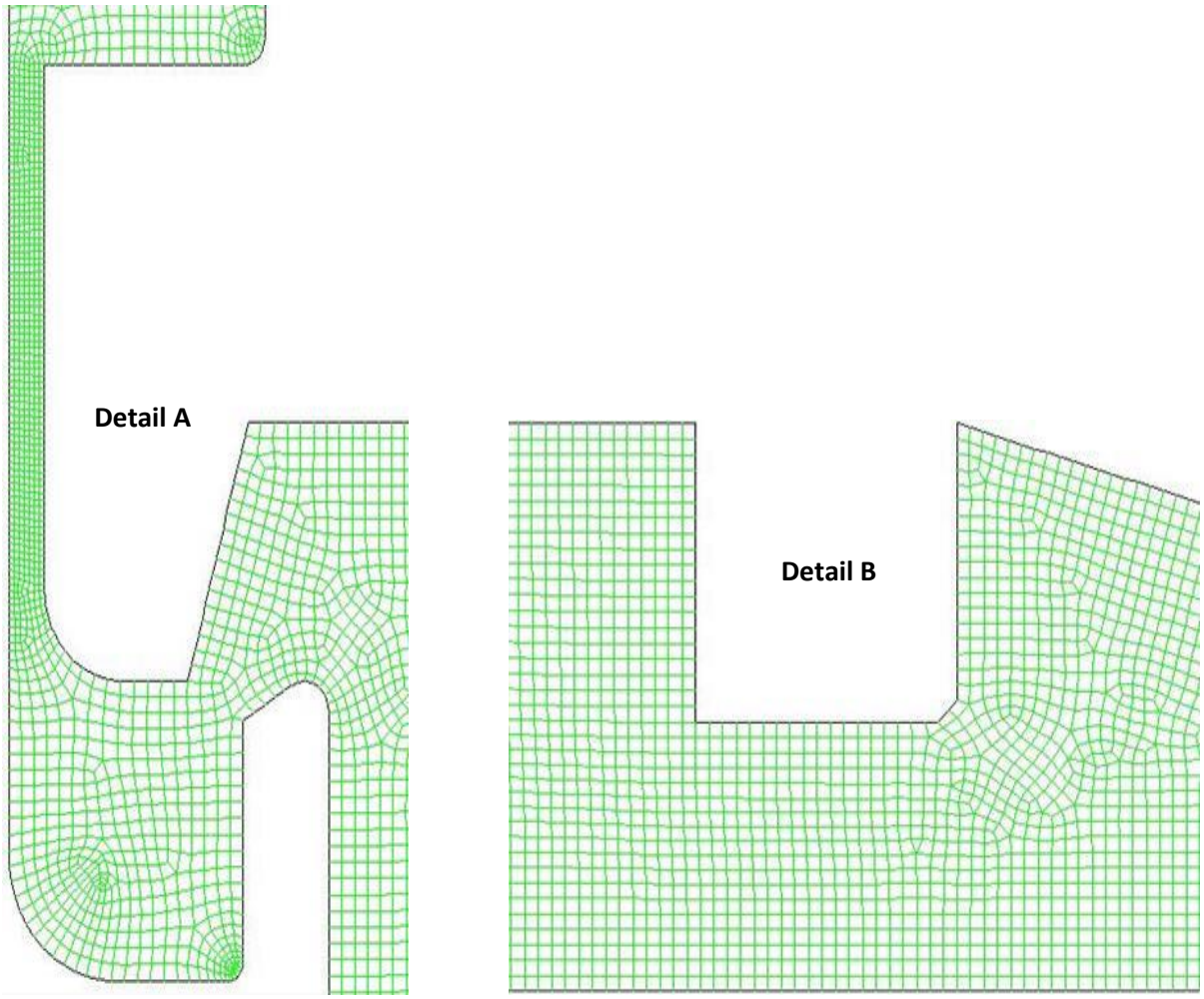

Figure5-3: The Computational Grid

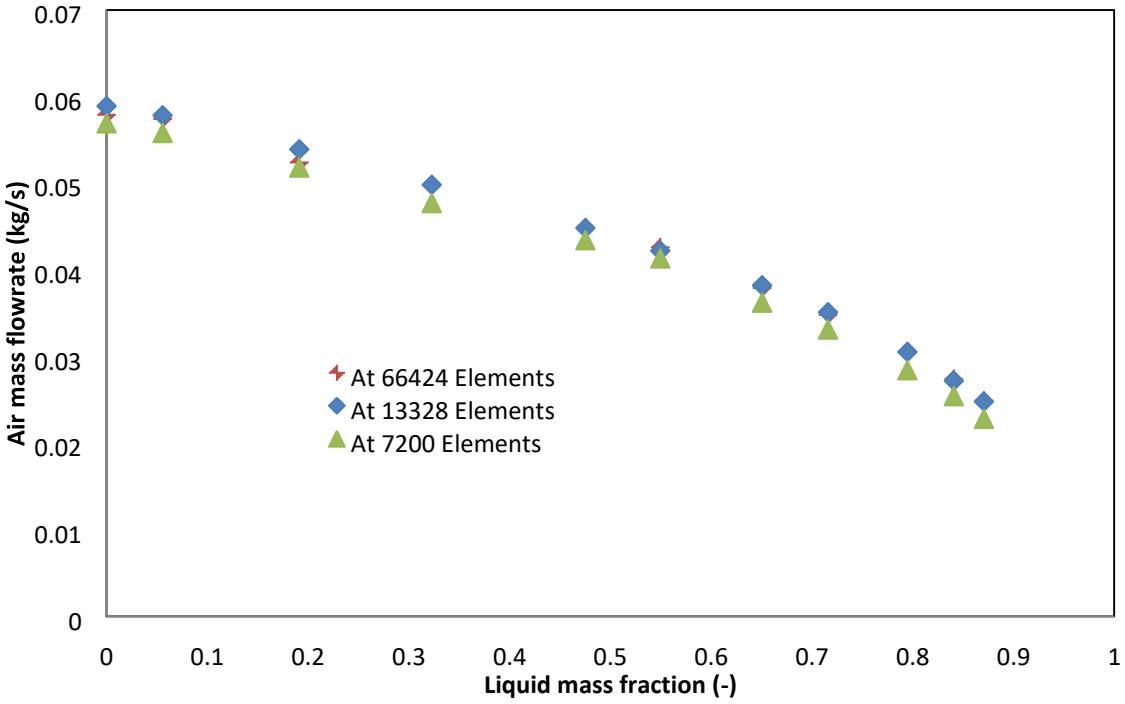

Figure5-4: The grid independency, predicted mass flowrate based

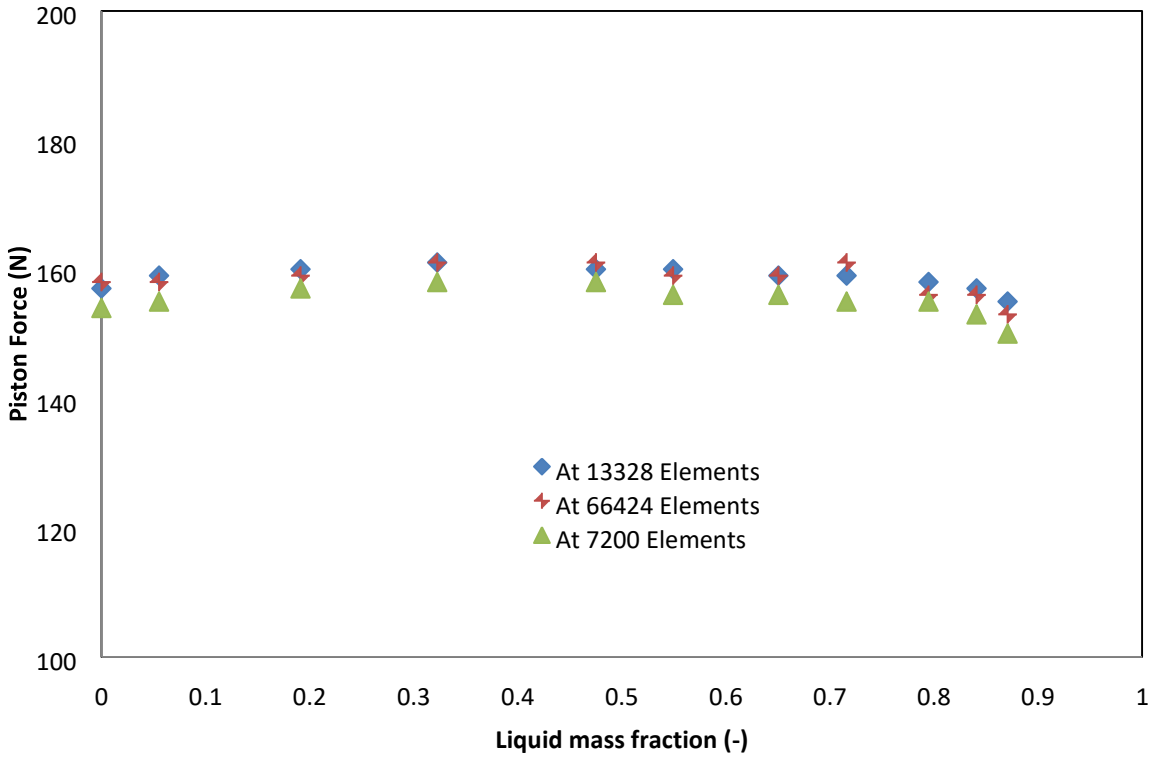

Figure5-5: The grid independency, predicted force based

5.3.3 Boundary Conditions and Solution Strategies

There are three main zones in the computational domain; the inlet, specified as a pressureinlet, the outlet specified as a pressure-outlet and the interior-fluid represented by the whole domain as an air/water mixture. Other zones are considered as walls. At the inletpressure boundary condition, the total pressure of the mixture is specified. The gas and liquid temperatures are set at the corresponding experimental values and are generally close to 288.15K. The liquid mass fraction has different values (from 0 to 0.87). As the mixture turbulence multiphase model is employed an estimate values of κ and ϵ are set at 0.1 (m^2/s^2) and 0.2 (m^2/s^3), respectively. The pressure-outlet boundary is set at atmospheric pressure. Also, initial values of κ and ϵ and the volume fraction of the water are to be equal to those of the pressure-inlet zone. The zones representing the walls are considered as stationary walls. The inlet pressure boundary has been used to apply both the inlet air and water conditions. A uniformly distributed two phase flow has been assumed to represent the experimental use of a full cone nozzle droplet spray. Each inlet cell is set to the experimental inlet pressure and a volume fraction established to inject an appropriate amount of liquid corresponding to a

test condition. This adequately sets the phase inlet boundary conditions to those in practice but does not directly correspond to the test conditions where a liquid inlet mass flow combined with an air pressure inlet would have intuitively been more representative. Unfortunately, this was found not to give physically correct results and is believed to be a code related issue. In other words, the actual effect of the real injector is not examined due to a difficulty in representing the second phase (the liquid phase) on the Euler-Euler two phase flow approach based on separate inlet boundary conditions. However, it is worth mentioning here that checking such an issue as well as the justification for using no nozzle through the simulation was of importance. Therefore, some CFD modelling by including the effect of the injection nozzle rather than starting the modelling from the valve inlet were carried out and found that the predictions are actually better by approximately 1-2% but increases computational time to achieve convergence. One of the major concerns which was posed to perform such investigations is the magnitude of the total pressure drop and is found to be still pretty low so the effect may be due to mixing and slip effects at the inlet, hence all the subsequent CFD modelling have been started from the valve inlet. For more detailed calculations, refer to appendix F. With regards to the solution strategy, the solution method used was the steady-state pressurebased solver for segregated iterative procedure of the popular phase coupled SIMPLE method to resolve the pressure-velocity coupling in the flow. A Green-Gauss cell based spatial discretization for the gradient was implemented and a second order upwind spatial discretization for the density, momentum, turbulent kinetic energy, turbulent dissipation rate and energy gradient terms, whereas the volume fraction was discretized based on a first order upwind scheme to ensure a more stable convergence. In addition, the solution is initialized with a hybrid initialization method to obtain accurate results, then being controlled by lowering the under-relaxation factors. The energy equation was not solved for the first 100 iterations, to ensure initial stability. In terms of convergence criteria, all cases have converged with threshold values in the order of 10^{-5} for all variables except for mass continuity and energy which were in the order of 10^{-3} and 10^{-6}, respectively. In addition, the convergence time for all cases was around 75 mins on 8GB desktop PC consisting of 4 parallel processors with a 13228 element mesh adopted.

5.3.4 Droplet size modelling

The droplets are injected via a spray nozzle that produced a full cone spray at a 30^{0} spray angle and droplet diameters of the order of 400µm. The spray was injected into the air flow at the entrance of a converging nozzle with an area contraction ratio of 70, as shown schematically in Figure 5.2, and under typical operating conditions would lead to the acceleration of the air flow from a negligible Mach number to one of 0.6, with velocities reaching 200 m/s. In doing so, we have assumed that injected droplets undergo a series of aerodynamic break up processes which result in a critical Weber number being reached. In this study the breakup of droplets following contact with a gas is governed primarily by the balance between pressure distorting forces across the drop and surface tension forces. This balance was considered by Hinze in 1949, who suggested that the breakup could be expressed in terms of a Weber number (We) defined as:

$$\mathrm{We} = \frac{\rho_g V^2 d_P}{\sigma}$$

Where: V is the velocity difference (slip velocity) between the droplet and the gas (m/s); $\rho_g$is the gas density ($\mathrm{kg/m^3}$); $d_P$is the droplet diameter (m); $\sigma$is liquid surface tension (N/m).

Figure 5.6 shows a typical dispersed flow at the exit of the nozzle, inlet to valve. Kolev [116] reviews much of the current work in this topic and indicates that the critical Weber number determined from experiments generally fall in the range 5-20. The liquid is injected into the converging section could produce relative velocities in the range 50-150 m/s resulting in predicted droplet diameters of the order of 5-40 µm. There is some evidence that this range is consistent with the limited experimental evidence of droplet sizes in sonic nozzles. Lemonnier et al [117] measured droplet sizes at the exit of a converging nozzle for air-water flow conditions and showed that sauter mean droplet diameters were in the range of 20-40 µm. Similar studies with steam flow [118] have measured droplet sizes in the range 1-10 µm but these sizes may have resulted from thermal break up processes in addition to aerodynamic. To account for this uncertainty we have assumed a single diameter droplet size (i.e. mono dispersed) at the inlet of the valve and obtained multiple solutions for a range of droplet diameters. For the reference case we have assumed a 10 µm diameter and investigated the effect of droplet sizes between 5 and 35 µm. It was found that 1 µm would match homogenous conditions. In the absence of breakup and/or coalescence of the droplet,

however, the number of droplets that are generated by the spray nozzle will be in the order of 10^{11}, as shown in Figure 5.7. The figure presents, for the valve at full lift, the total number of droplet flowrate at an upstream pressure of 10.3 barg (150 psig) and various liquid mass fractions for the reference spherical droplet diameter of 10 µm.

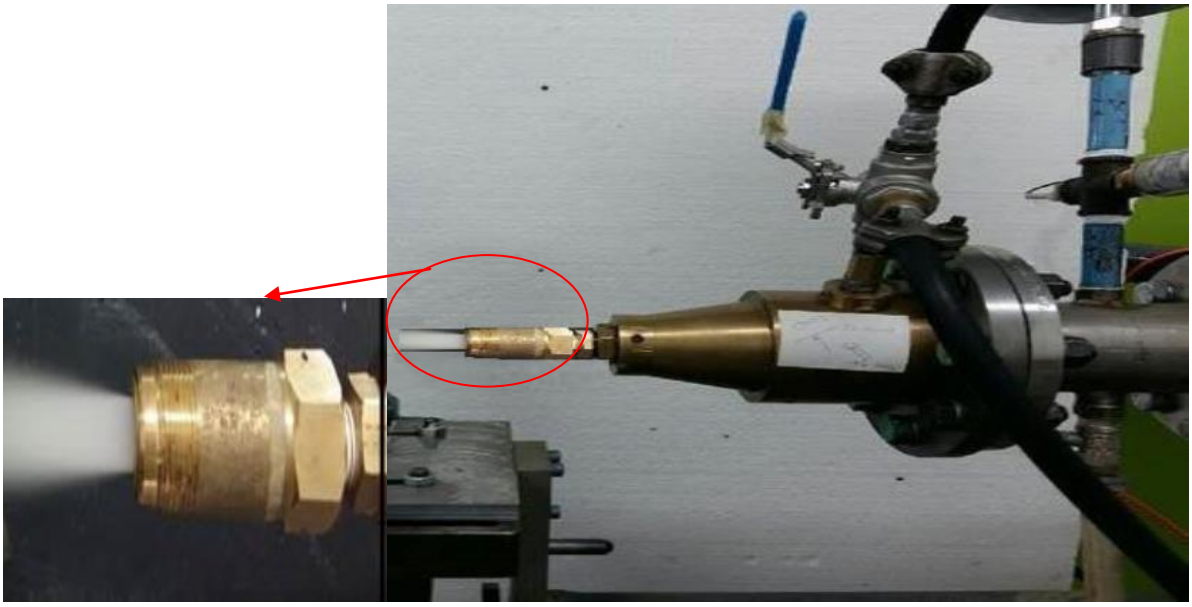

Figure5-6: The water injector system

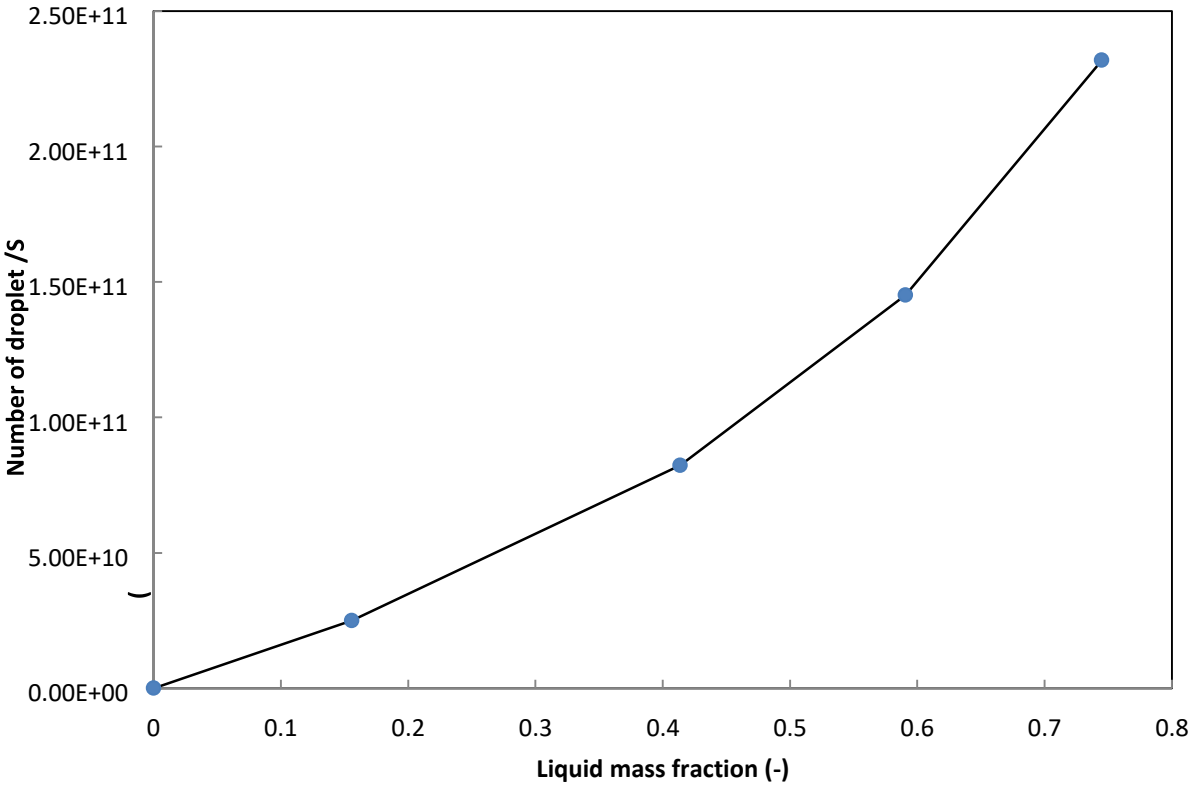

Figure5-7: The resulting droplets (#/s) at an upstream stagnation pressure of 10.3 barg (150psig) and 5 mm lift for various liquid mass flows

5.4 Results

The following sections of 5.5.1 and 5.5.2 will present the experimental and CFD results of the Flow-Lift and Force-Lift characteristics of the relief valve under various two phase flow conditions. However, all subsequent results of mass flowrate, force and backpressure will be plotted using fixed inlet liquid mass fractions rather than fixed inlet liquid mass flowrates. As mentioned, the water mass flowrate value was experimentally controlled to match that of the CFD calculation. However, this could not be maintained constant for all piston lifts. This was due to the computational calculation being based on fixed inlet liquid volume fractions in the range of 0 to 0.05. This inlet liquid volume fraction range is homogenous based and the water droplets were uniformly distributed through the inlet of the valve; therefore a constant liquid mass fraction was achieved for the range of piston lifts examined here.

5.4.1 Experimental Results

5.4.1.1 Flow-Lift Characteristics

As mentioned in Chapter 4, a comprehensive description of the valve discharge with respect to piston displacement has been achieved through the so-called flow-lift characteristics. Figures 5.8 and 5.10 present the air mass flowrates at upstream inlet pressures of 13.8 barg (200 psig) and 8.28 barg (120 psig) respectively. These figures show clearly that the air mass flowrate decreases with an increase in water mass flowrate. This reduction in air mass flowrate will not be equal to the amount of water added. In other words, the air mass flowrate decreases by an amount less than the water mass flowrate is increased. Figures 5.9 and 5.11 point out that, the total mixture discharged through the valve increases when the water mass flowrate is increased. In spite of the flow-lift characteristics for two phase flow conditions matching the single phase flow behaviour; there is an obvious difference in the slope of the air flowrate-lift relation particularly at high lifts (2 – 4 mm). This difference in slope is significant particularly at high liquid mass fractions. It is noted that this slope is almost flat with an increase in water flowrate. A more informative study on two phase flow conducted by Elmayyah [88] proved that a lower pressure-lift slope upstream of the inlet of the passageway encircled the piston-due to water flow- results in these changes in the slope. The critical planes, however, have been found to be at the same locations pronounced in single phase flow studies. Flow-lift characteristics will be further detailed in Section 5.6.1.

Two sets of experiments have been performed; the first is when the modified gland is in place and the other with no gland. Figure 5.12 presents the air mass flowrate at an upstream inlet pressure of 10.3 barg (150 psig) with various inlet water quantities of 26% and 84%. Similarly, the gland has no significant impact on the discharged air mass flowrate, as shown in Figure 5.12.

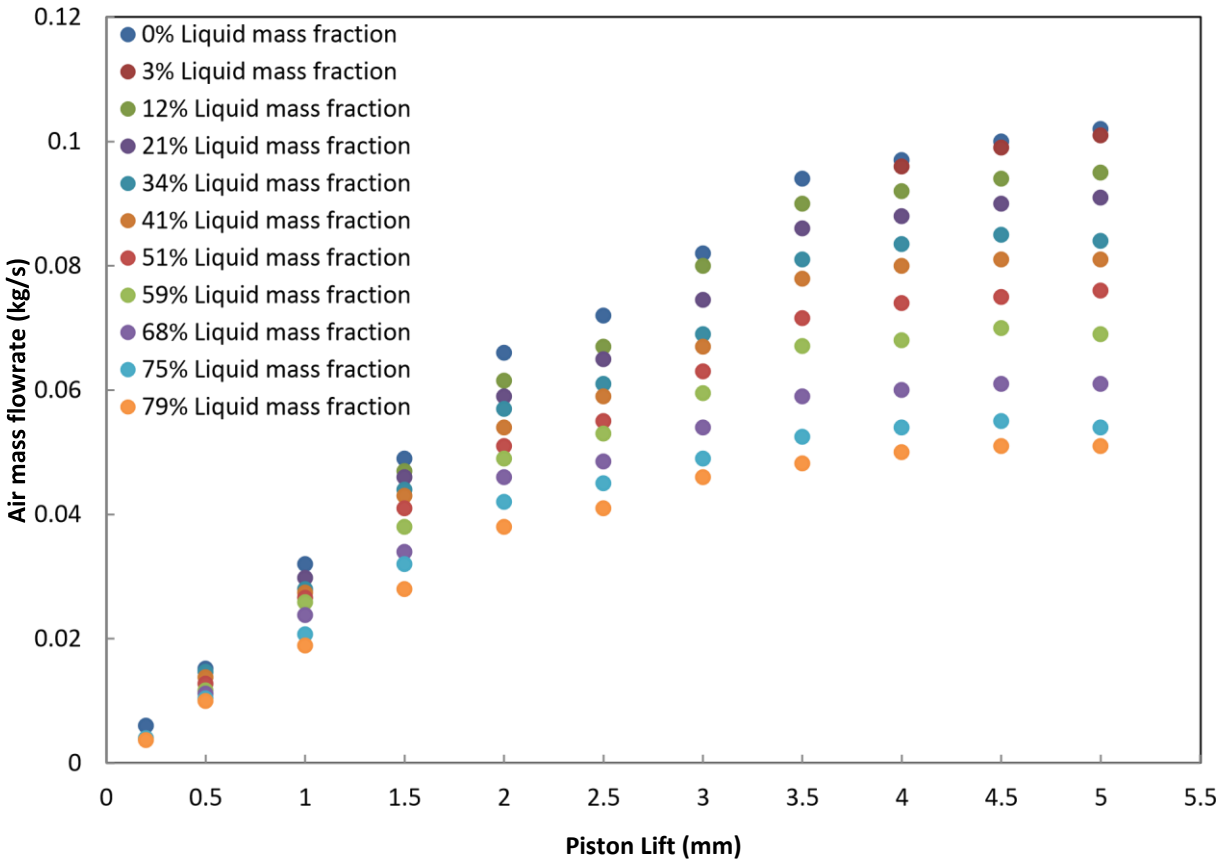

Figure5-8: Air flow-Lift at an upstream stagnation pressure of 13.8 barg (200 psig)

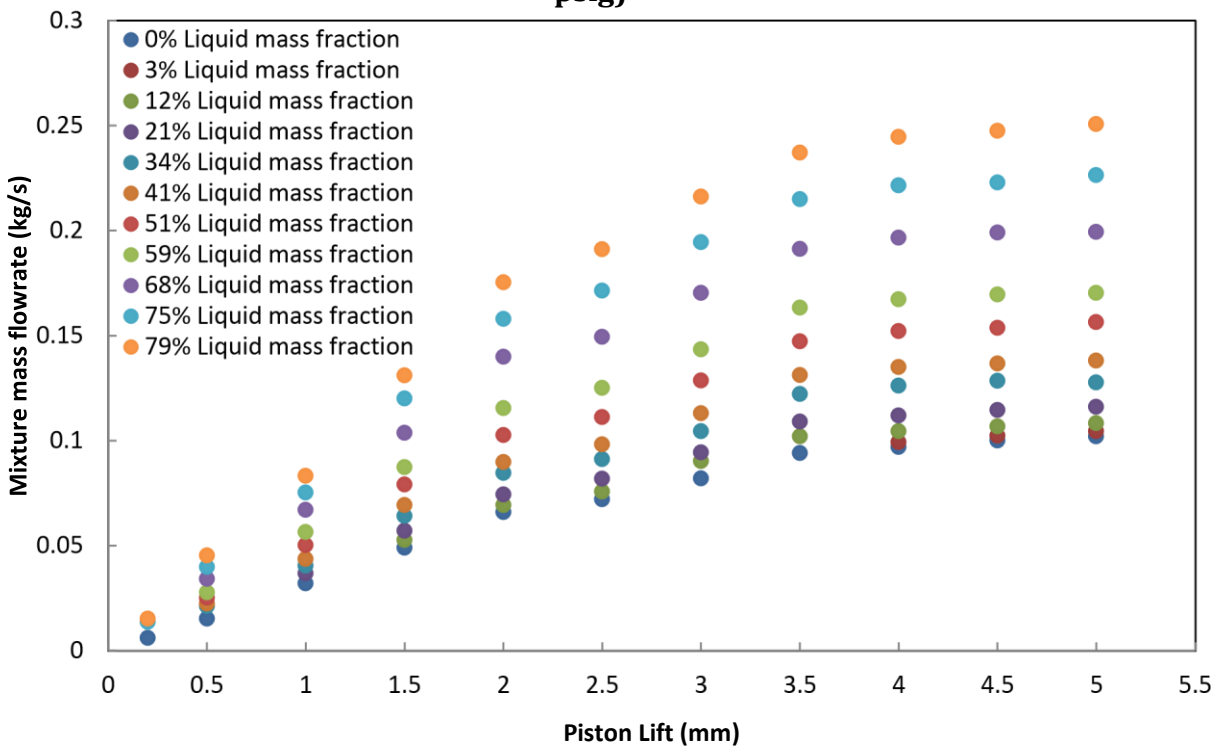

Figure5-9: Mixture flow-Lift at an upstream stagnation pressure of 13.8 barg (200 psig)

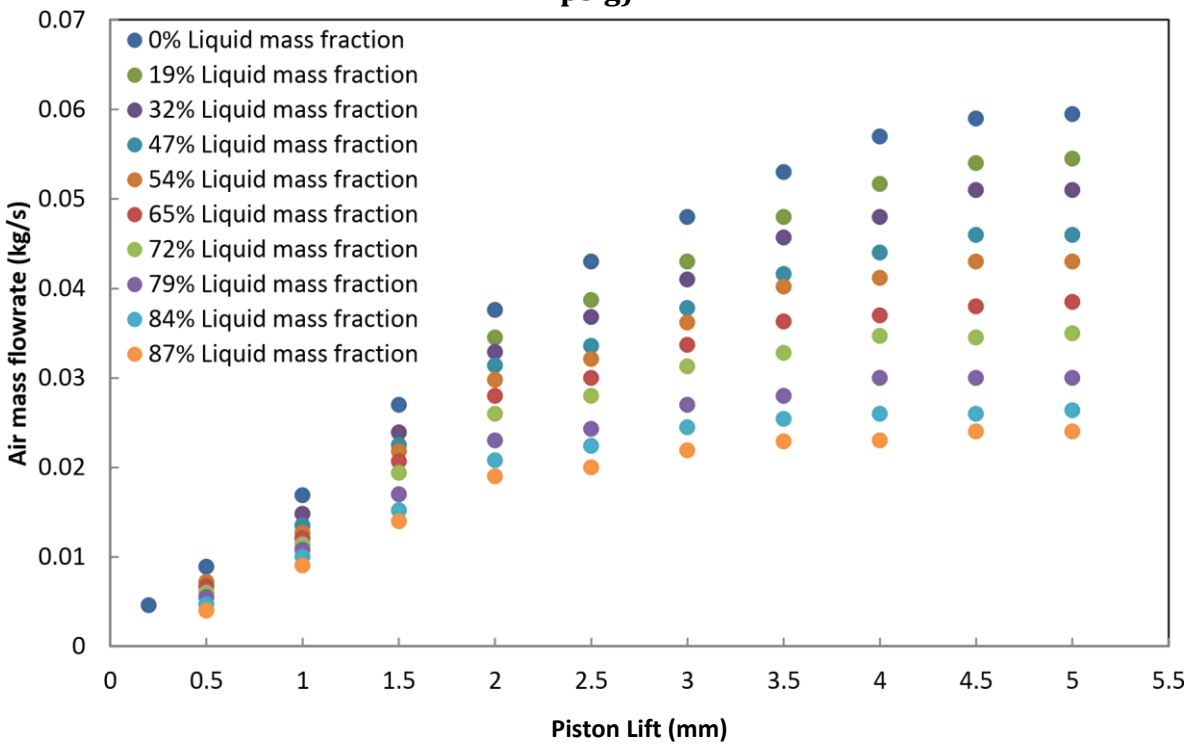

Figure5-10: Air flow-Lift at an upstream stagnation pressure of 8.28 barg (120 psig)

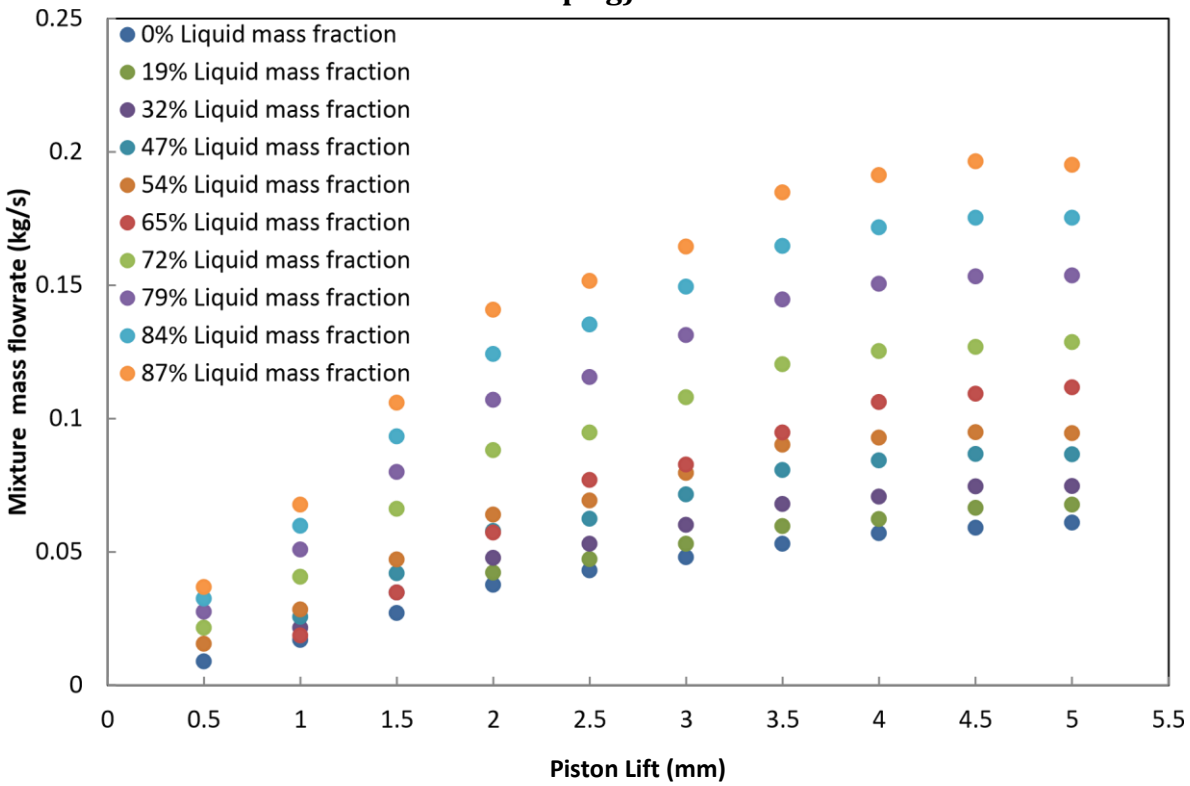

Figure5-11: Mixture flow-Lift at an upstream stagnation pressure of 8.28 barg (120 psig)

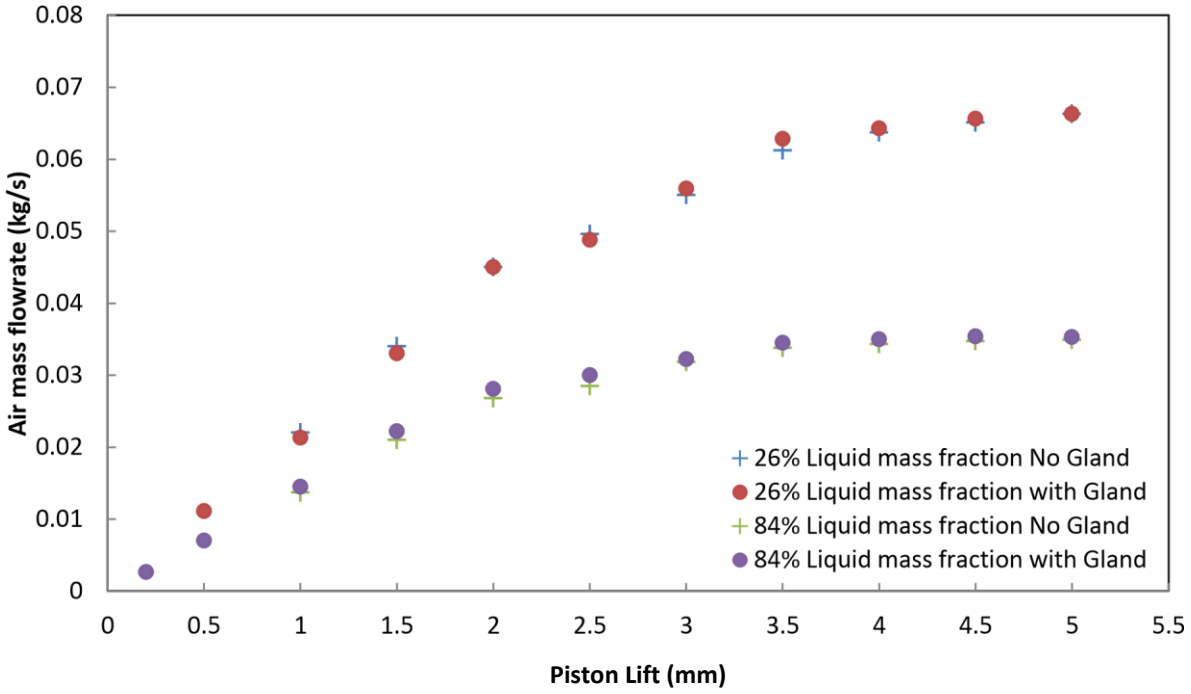

Figure5-12: The influence of the modified gland on air mass flowrate at an upstream stagnation pressure of 10.3 barg (150 psig) for various water quantities

5.4.1.2 Force-Lift Characteristics

Force-lift characteristics exhibit the fluid dynamic force exerted on the piston at known lifts (0 - 5 mm). Figure 5.13 presents the piston forces at an upstream inlet pressure of 13.8 barg (200 psig) for different water mass fractions at a 5mm piston lift. Figure 5.14 shows the piston forces at an upstream inlet pressure of 10.3 barg (150 psig) for different water quantities at a 5mm lift. The figures demonstrate that the effect of the modified gland on piston force is highly significant. A lower piston force can be observed for the modified gland in place whereas higher forces appear when there is no gland. This is attributed to the resulting back pressure which is increased due to the reduction in the outlet area caused by the existence of the gland, as shown in Figure 5.15. In reference to the magnitude of the back pressure, Figure 5.15 shows the pressure on the rear side of the piston measured by the tapping in the piston rod, at an upstream pressure of 13.8 barg (200 psig) and a water liquid mass fraction of 0.34 for the valve with and without the gland in place. According to the figures which are relevant to forces, the piston force increases slightly when more water is added, however, this is approximately up to a 0.15-0.20 liquid mass fraction. This is believed to be due to water

inertia, which continuously acts upon the front face of the piston. It is worth mentioning here that the back pressure acting on the piston rear face is also increased whenever water mass flowrate is increased. For a two phase flow having a liquid mass faction greater than 0.25, the latter concept of back pressure reducing the influence of the pressure on the piston front face leads to a reduction in piston forces is observed, as shown in Figures 5.13 and 5.14. In fact, this reduction is relatively significant when the modified gland is in place, as shown in Figure 5.16 and 5.17. The influence of the gland will be discussed in detail in Section 5.6.3.

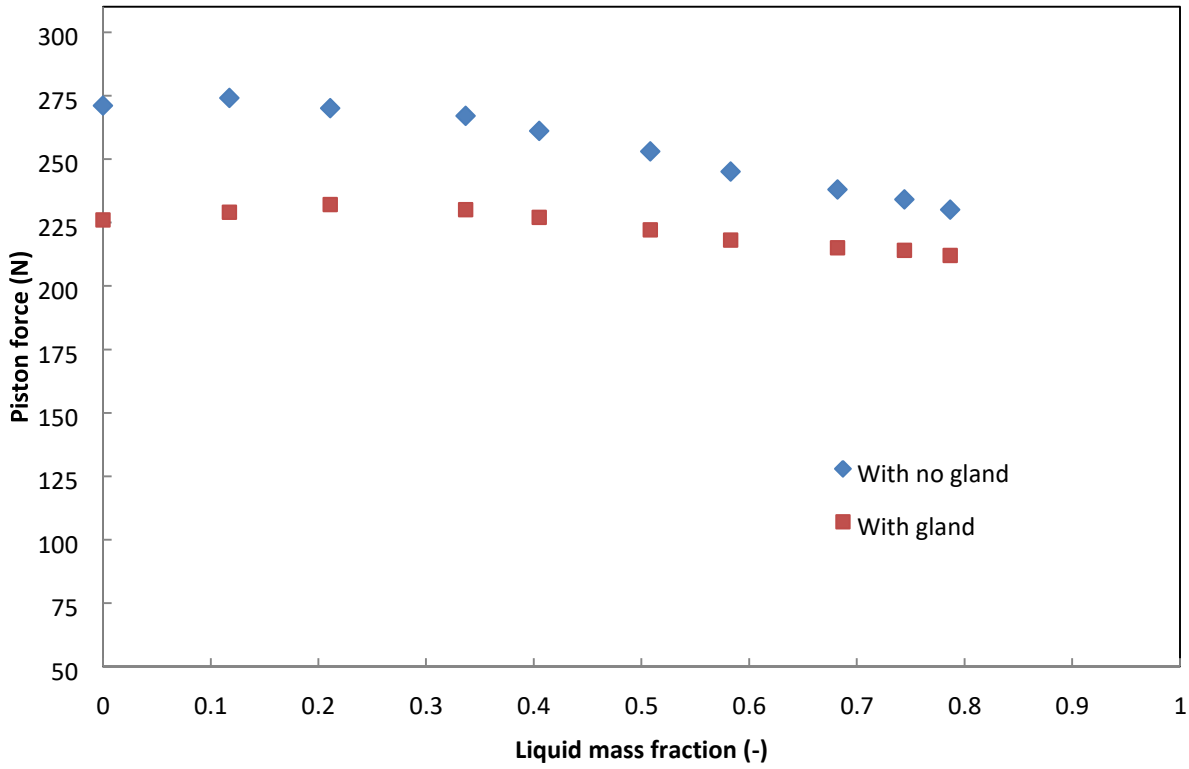

Figure5-13: The influence of the modified gland on piston force at a piston lift of 5 mm for an upstream stagnation pressure of 13.8 barg (200 psig) and various water quantities

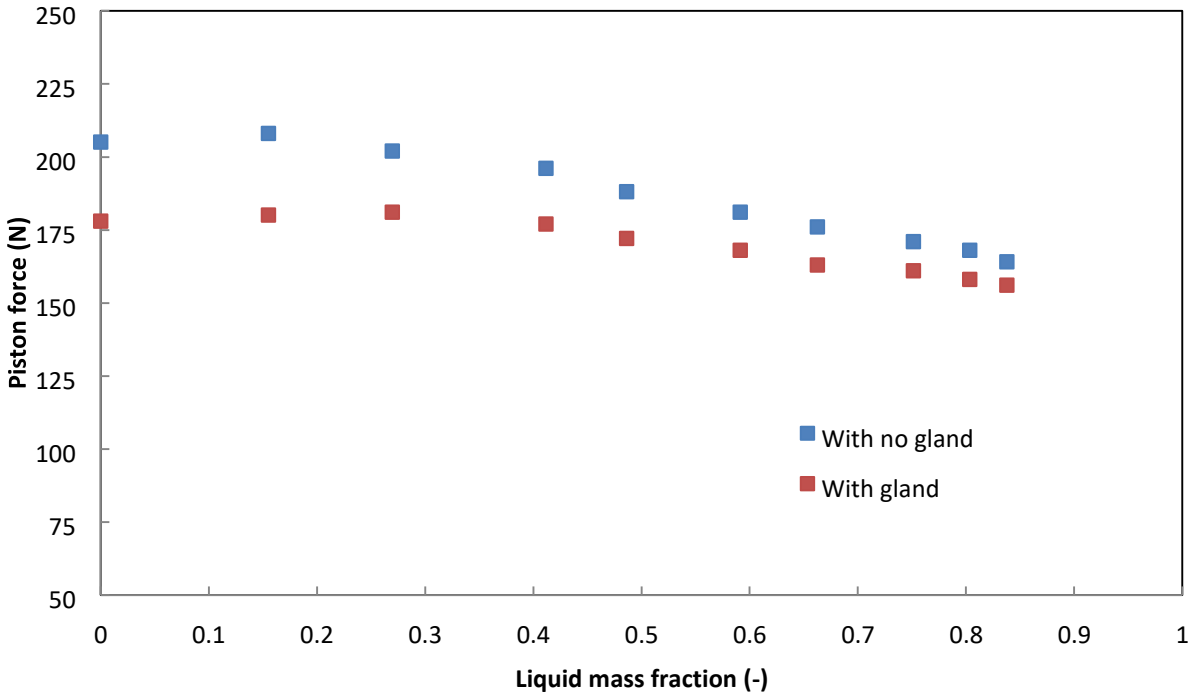

Figure5-14: The influence of the modified gland on piston force at a piston lift of 5mm for an upstream stagnation pressure of 10.3 barg (150 psig) and various water quantities

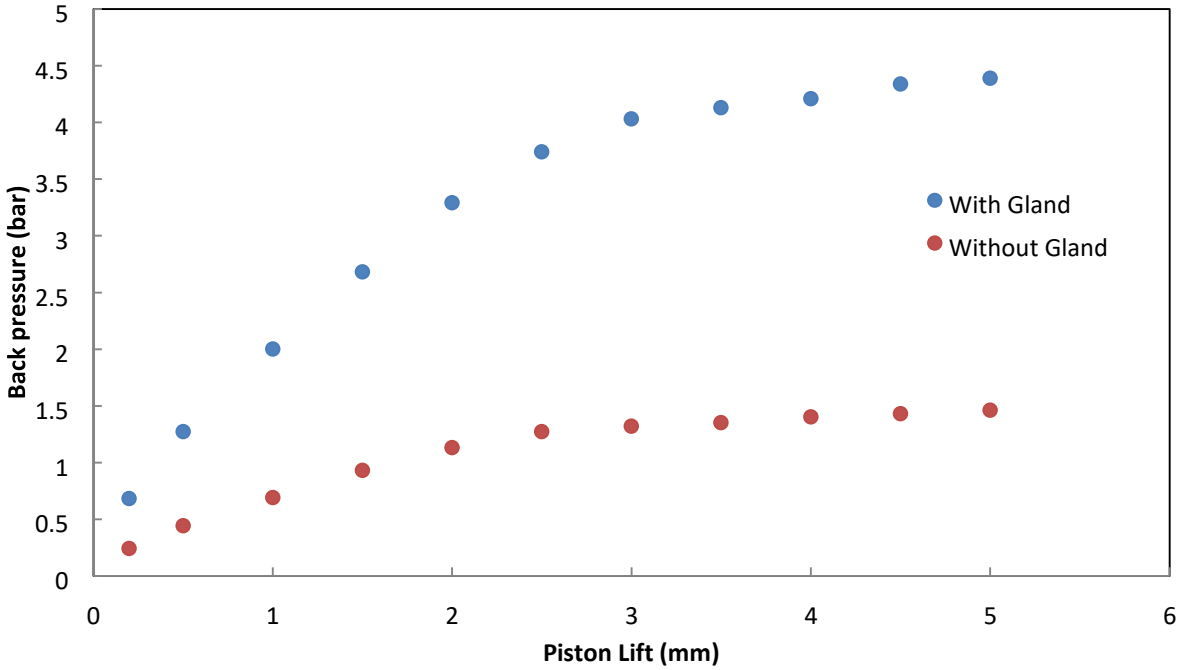

Figure5-15: The influence of the modified gland on measured piston back pressure at an upstream stagnation pressure of 13.8 barg (200 psig) and a liquid mass fraction of 0.34 for a full range of piston position

Figure 5.16 and 5.17 show the force-lift characteristics at an upstream inlet pressure of 13.8 barg (200 psig) and 10.3 barg (150 psig) respectively with the modified gland. In terms of the trends, the figures show that all curves are similar to each other for this range of liquid mass fraction. Water quantity has no significant influence on the piston force at lower piston displacements up to 2-2.5 mm lifts. On the other hand, a minor difference in piston force can be observed at higher lifts that lie in the range of 2.5 to 5 mm lifts. Figure 5.18 and 5.19 explain the force-lift characteristics at an upstream inlet pressure of 13.8 barg (200 psig) and 10.3 barg (150 psig) respectively without the modified gland.

It is noted that, the force-lift characteristics of the two phase flow are similar to the single phase behaviour. Principally, the higher the inlet upstream pressure the greater are the forces exerted on the valve piston. However, the single phase characteristics have lower force magnitude at lower lifts up to approximately 1 mm piston lift while the two-phase flow produces the lowest forces at the highest liquid mass fraction for the piston higher lifts of 1.5-5mm, as shown in Figures 5.16, 5.17, 5.18 and 5.19. This will be discussed in Section 5.6.2.

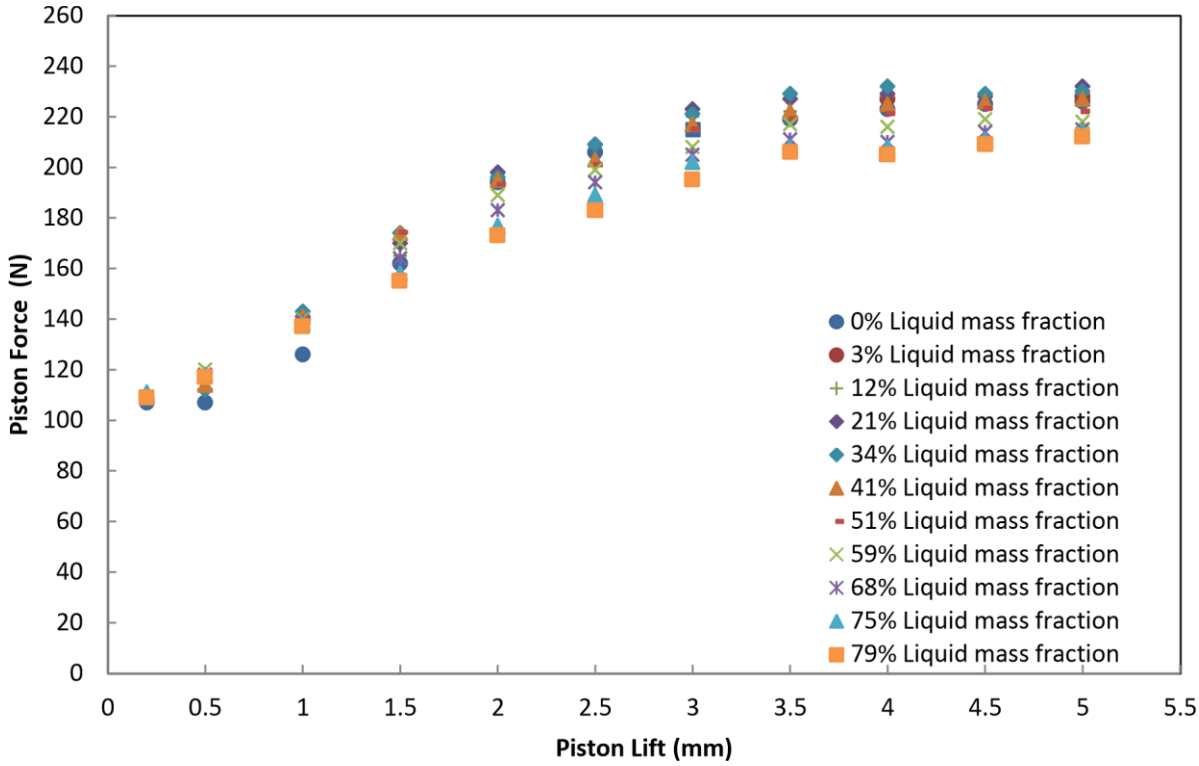

Figure5-16: Force-Lift at an upstream stagnation pressure of 13.8 barg (200 psig) with modified gland

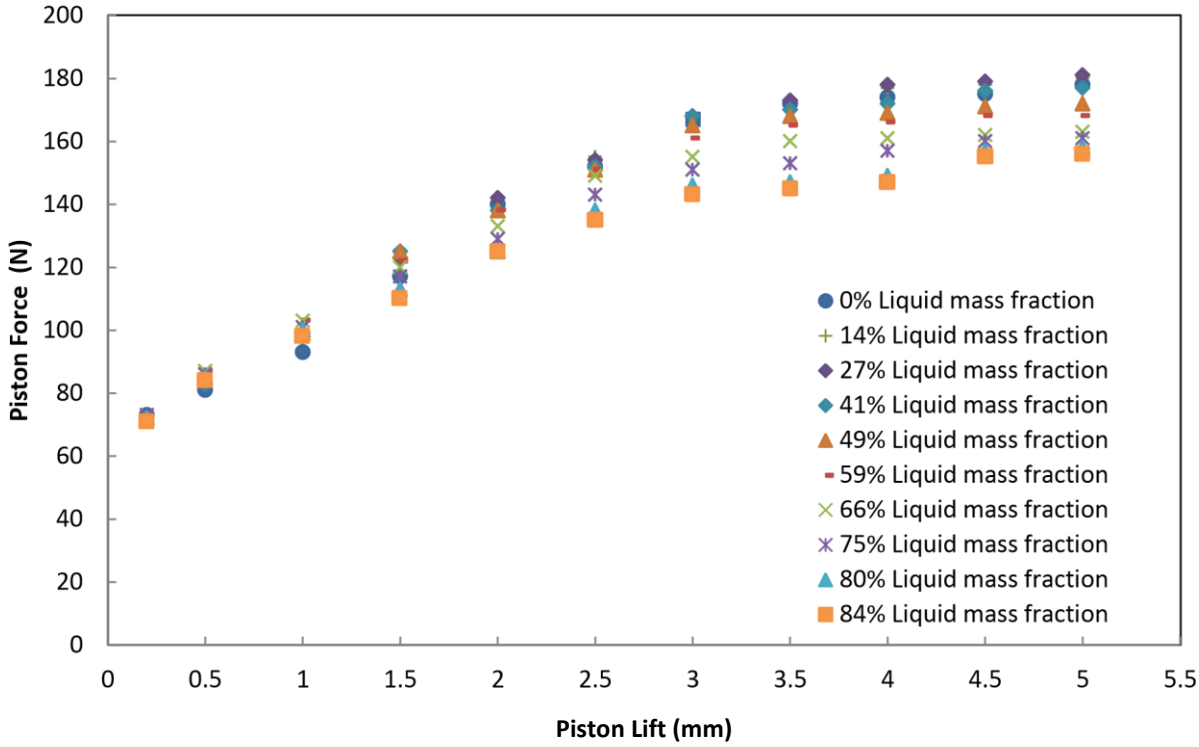

Figure5-17: Force-Lift at an upstream stagnation pressure of 10.3 barg (150 psig) with modified gland

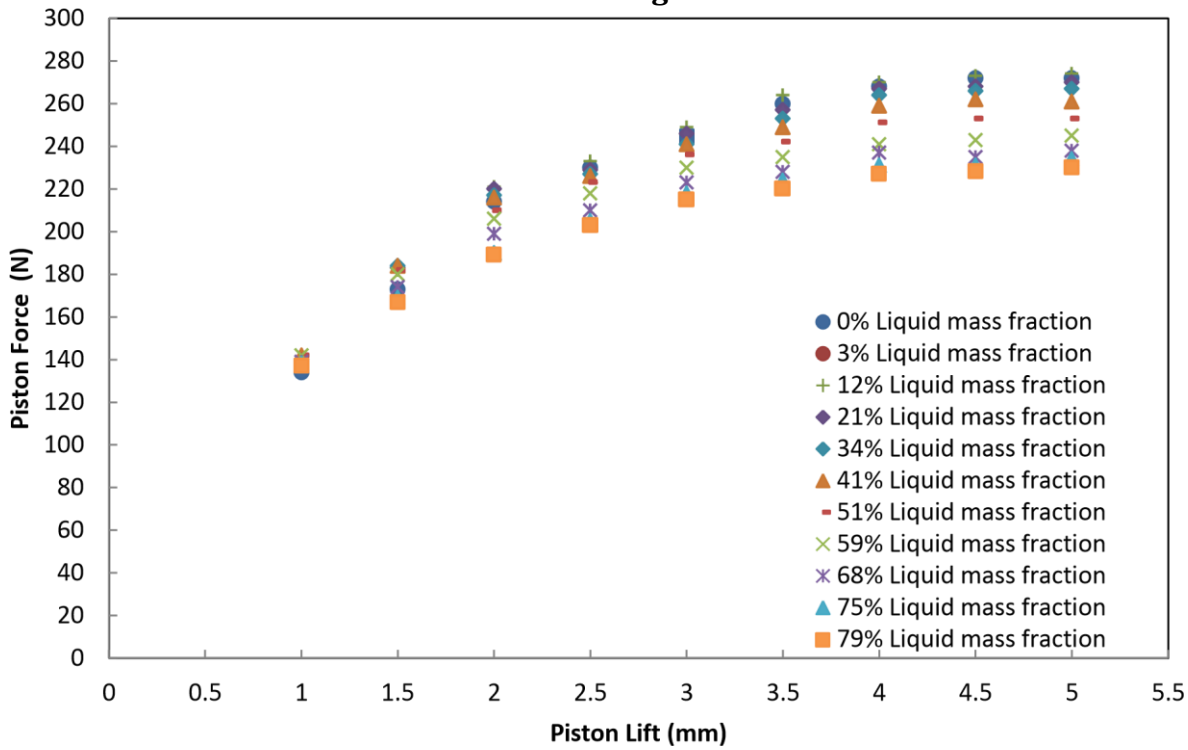

Figure5-18: Force-Lift at an upstream pressure of 13.8 barg (200 psig) without modified gland

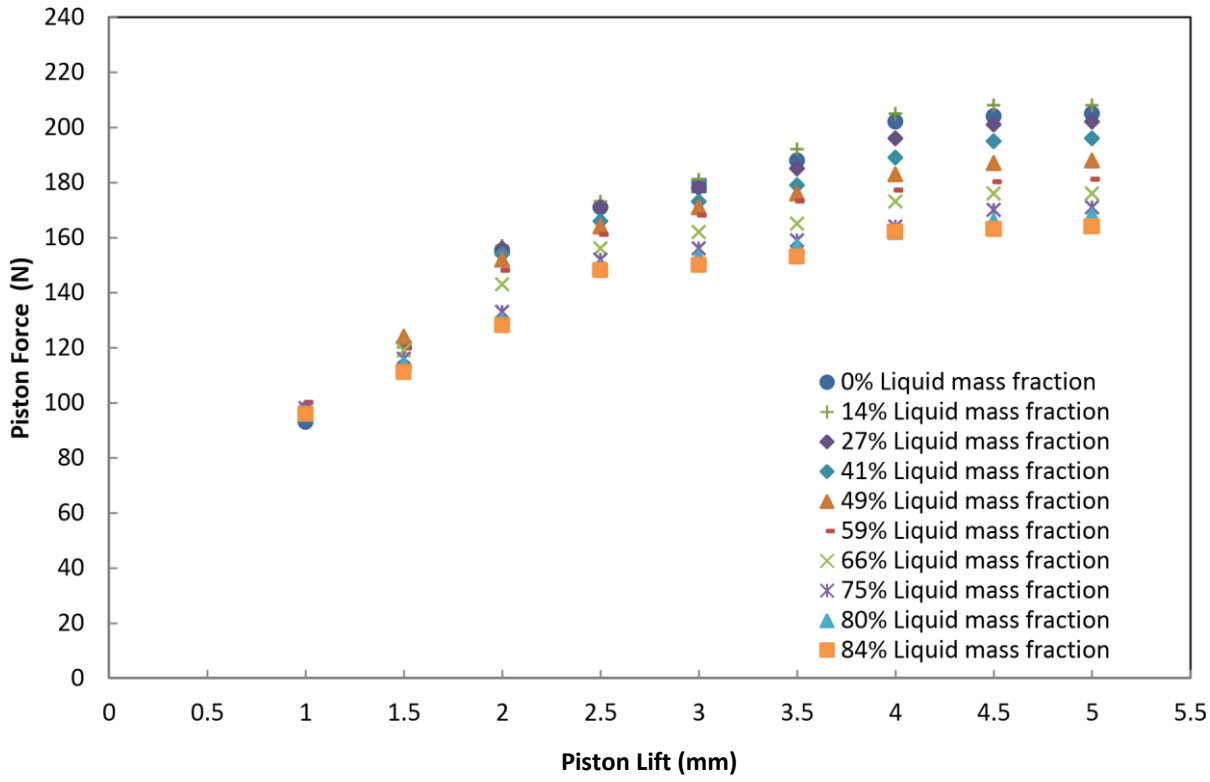

Figure5-19: Force-Lift at an upstream stagnation pressure of 10.3 barg (150 psig) without modified gland

5.4.2 Euler-Euler model CFD Results

In brief, using the Euler-Euler model to predict the two phase flows characteristics is numerical based calculations, which presents the physical properties of the flows insight the valve. The Euler-Euler model results are presented as following.

Figure 5.20 exhibits contours of Mach number for single phase (a) and two phase flow at 58% water mass fraction (b); at an upstream pressure of 13.8 barg (200psig) and a 2.5 mm piston lift. Although the existing Euler-Euler model of the ANSYS Fluent code does not sufficiently detail the determination of predicted speed of sound for a two phase flow, it uses air Mach number and never references the mixture Mach number. However, there is evidence which indicates that presented Mach number is referred to the air phase velocity rather than the mixture velocity of the air-water flow. This evidence, however, is shown by the magnitudes of the Mach number that are presented in Figure 5.20 (a) and (b).It is obvious that having only the single phase flows into the valve can produce a higher magnitude of Mach number, as shown in Figure 5.20(a). On the other hand, significantly lower Mach numbers are observed for two phase flow conditions particularly when more liquid mass flowrate is encountered;

which drags the air phase then results significantly in less expansion of the air, as shown in Figure 5.20(b).According to the two fluid model studies of Städtke [107], the nonhomogeneous mixture acoustic speed based on Wallis model where the air phase velocity is not equal to the water phase velocity, is considered in this study for the calculation of the Mach number presented as the air volume fraction is in the range 0.95-1. The Mach number is defined as follows:

$$Mach\ Number = \frac{gas\ velocity\ (v_g)}{nonhomogeneous\ mixture\ sound\ velocity\ (a_{mixture})} \tag{5.33}$$

$$\sqrt{\quad\quad} \tag{5.34}$$

Where:

$\rho_l$the liquid phase density,α_g the gas phase volume fraction,

$\rho_g$the gas phase density, α_l the liquid phase volume fraction.

$a_g$the sound velocity in air and a_l the sound velocity in water.

The above definition of Mach number was checked against the data presented by the fluent code, by using the so-called custom field functions (CFFs) provided in the fluent code. The Mach number values were found to give similar results presented by the fluent code.

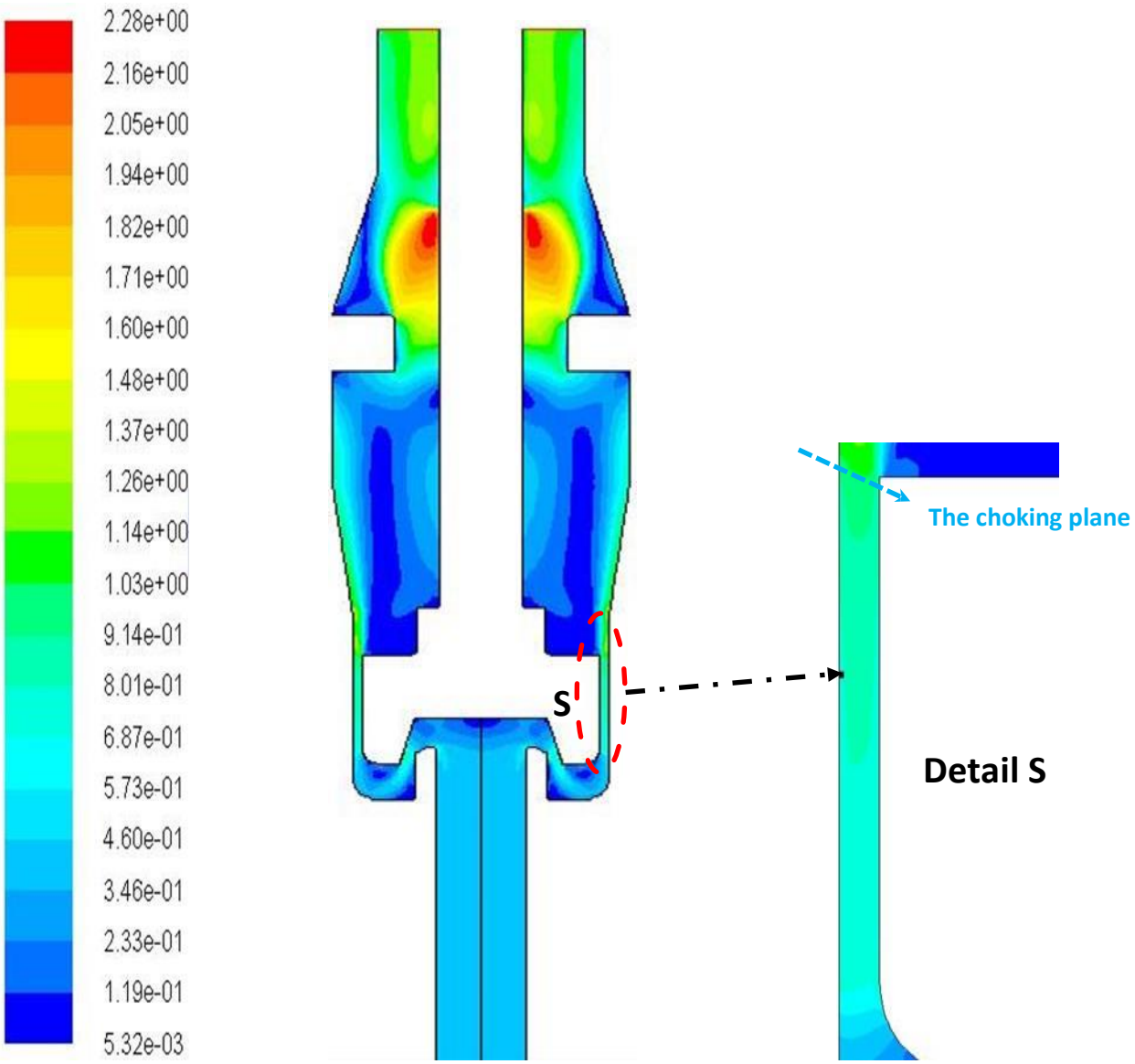

(a) single phase flow

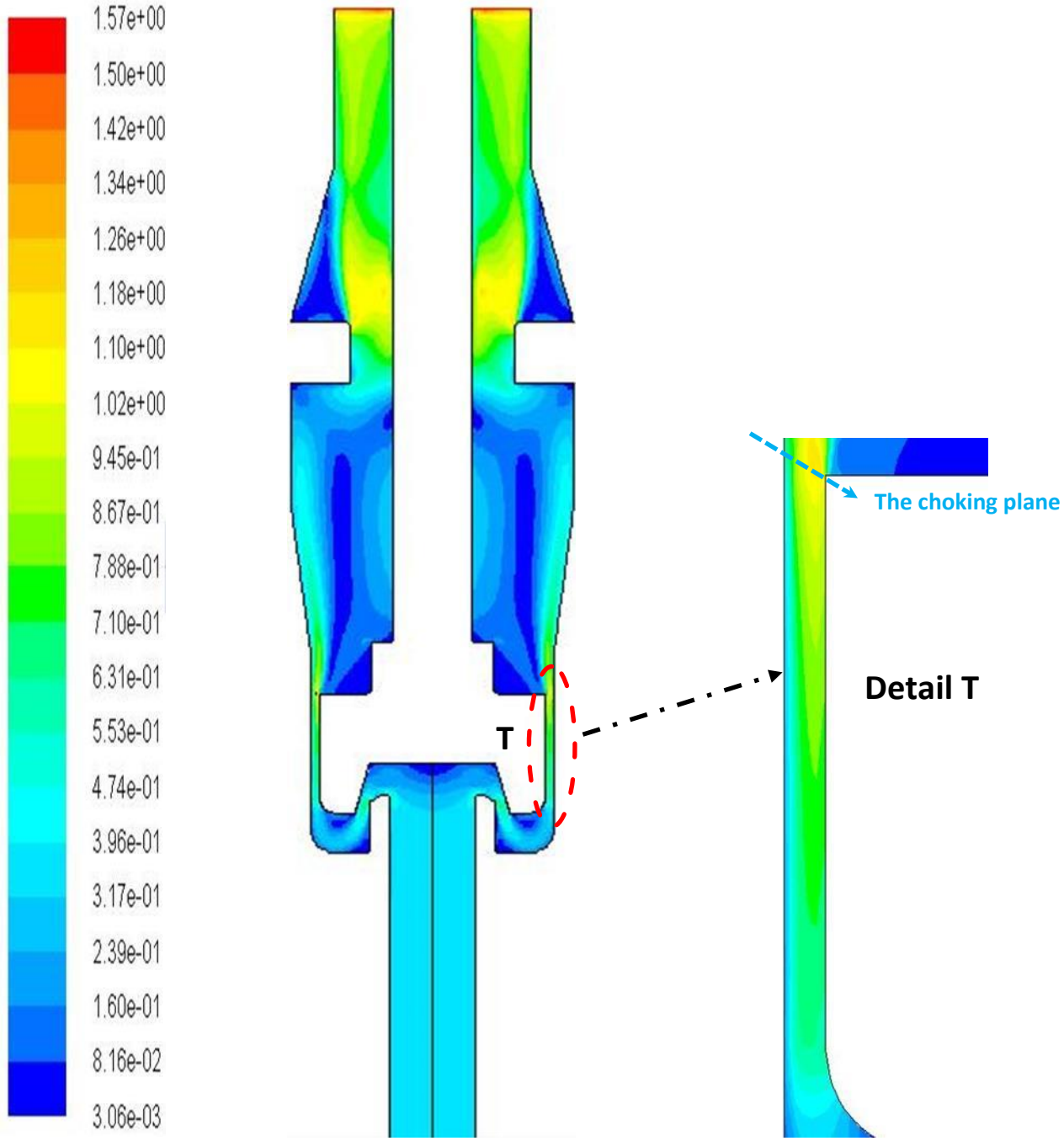

(b) Two Phase flow

Figure5-20: Contours of Mach number (-) at 0% water mass fraction (a) and 58% water mass fraction at an upstream stagnation pressure of 13.8 barg (200 psig) and 2.5 mm lift, with gland

However, it is apparent that the position of the critical plane (choking plane) (Mach number of unity) is similar in the two mentioned cases of single and two phase flow of Figure 5.20, which gives similar flow-lift characteristics. This choking plane for both cases appears near

the end of the passageway around the piston side faces but not exactly at the same locations. Furthermore, the choking plane position in the two phase flow appears further away towards the end of the passageway, which obeys the "internal *Raleigh flow"* phenomenon" as the heat transfer between the two phases flowing into the valve is taken into account. It also obeys the "*Fanno flow"* phenomenon" as the flow friction is considered. Owing to a significantly higher air volume fraction of up to 95%, the flow in both cases accelerates from a very low Mach number at valve entrance until the flow is choked at the piston side faces then undergoes an expansion downstream of the critical plane for a short length followed by a compression owing to the existence of the modified gland. Even though the flow remains subsonic upstream of the modified gland, the flow reaches the supersonic speed downstream of the modified gland when passing through the gland. Figure 5.21 presents contours of static pressure of the mixture (a) and the water volume fraction (b) at a piston lift of 5 mm for an upstream pressure of 13.8 barg (200 psig) and inlet water mass fraction of 79%, with the modified gland in place. According to the mixture static pressure contours, the flow undergoes a series of expansions and compressions while flowing through the valve. In terms of water volume fraction, the figure shows that the majority of the water phase is evenly distributed over the majority of the flow domain and assumed to be characterised by a mono-dispersed flow regime with a single droplet diameter. However, a higher concentration of water exists on the piston front face wall, the upstream face wall of the modified gland and part of the piston seat, as shown in Figure 5.21 (b). The degree of this water concentration is mainly associated with the inlet water volume fraction; however, a lower concentration might be observed when less water is injected into the system.

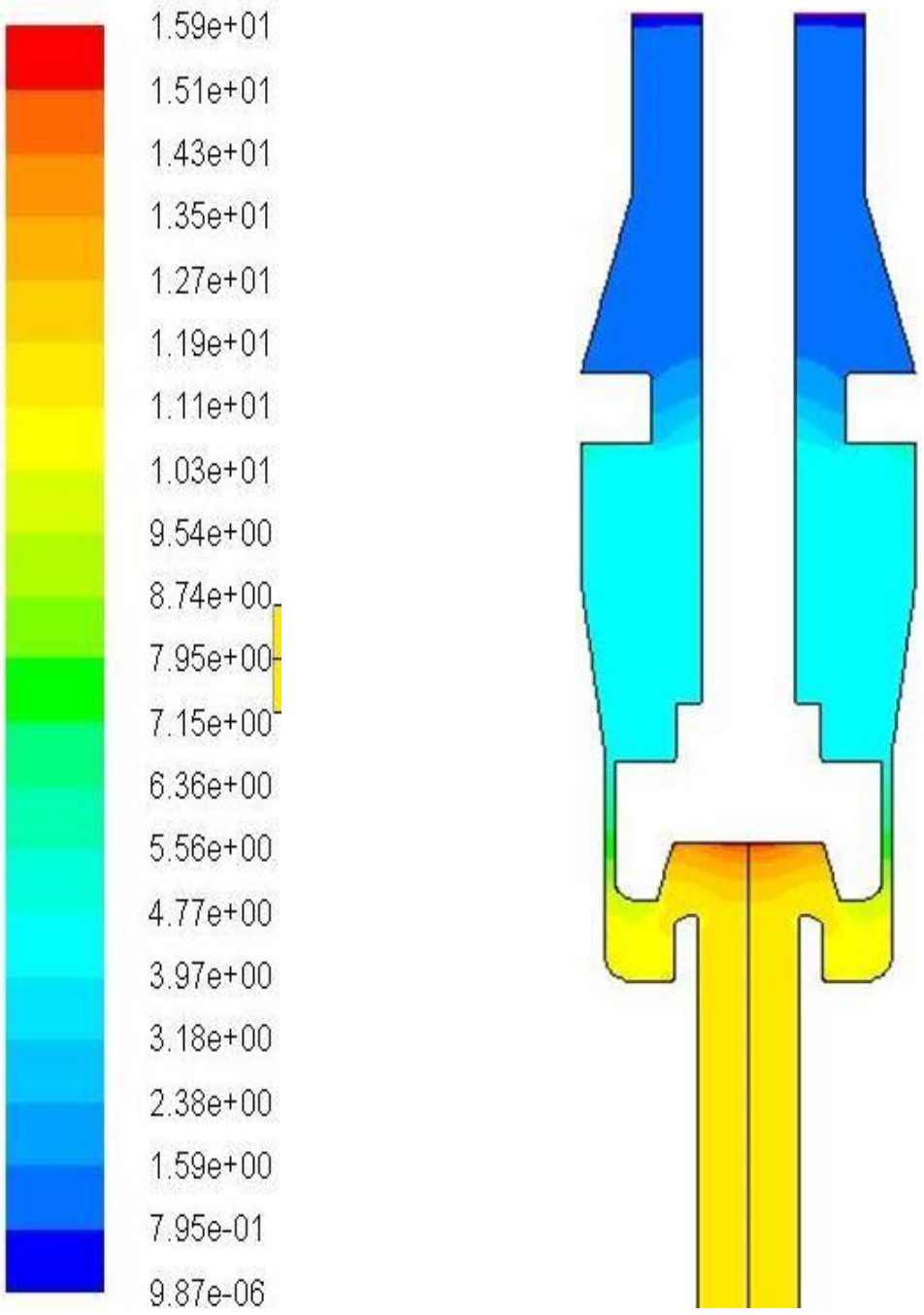

(a) Static pressure (bar)

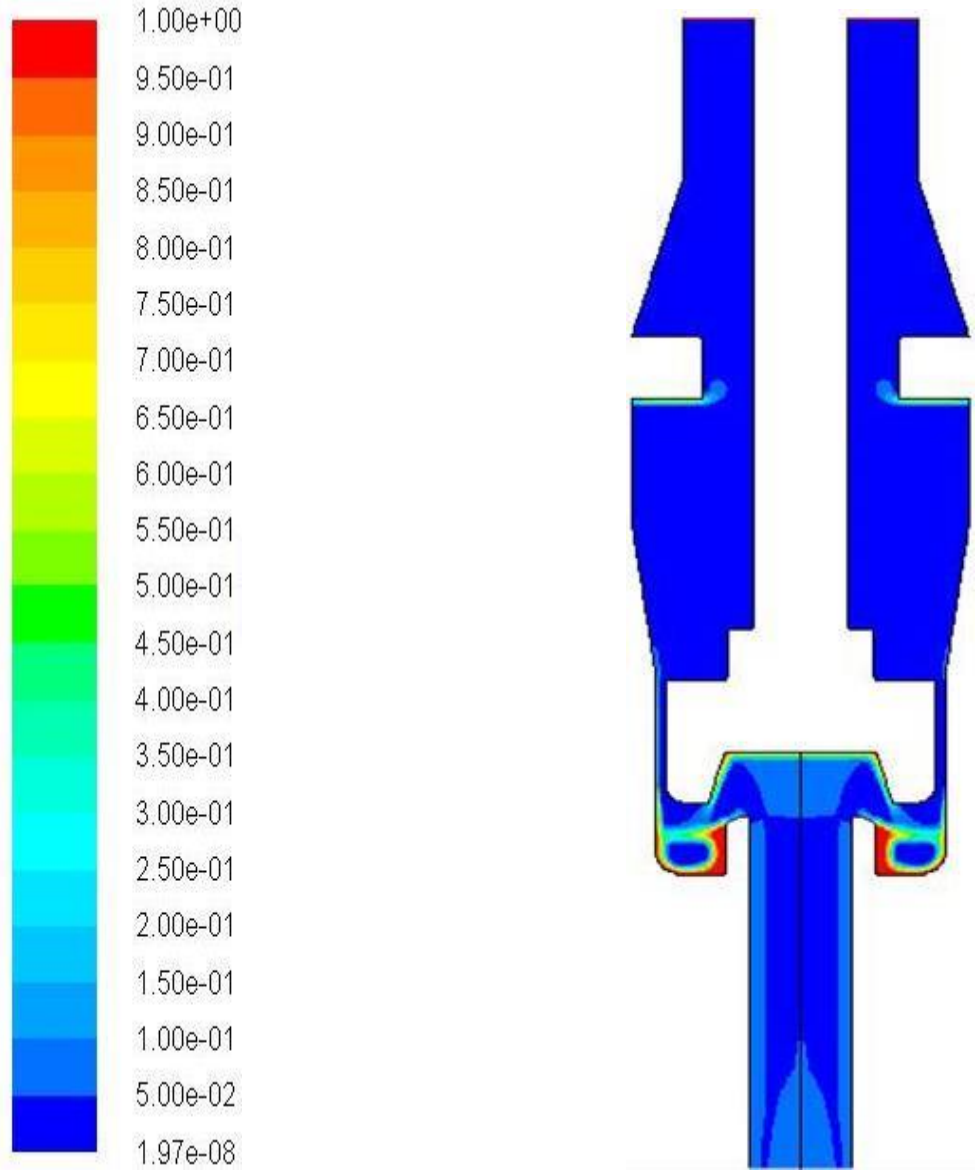

(b) Water volume fraction (-)

Figure5-21: Contours of static pressure of the mixture (bar) (a) and water volume fraction(-) (b) at an upstream stagnation pressure of 13.8 barg (200 psig) and liquid mass fraction of 79% (5% water volume fraction) and 5 mm lift, (with the modified gland)

The water volume fraction is in the range of 0 to 1 therefore there is a possibility of having an annular flow regime (wall film) particularly at these locations where the water volume fraction is highly concentrated on the wall. Modelling the wall film flow is beyond the scope of this study and was assumed to have a secondary effect due to the close correspondence of the current modelling approach and the experimental data.

Figure 5.22 presents the contours of the relative velocity (the slip velocity) between the two phases at 2 mm lift, an upstream pressure of 10.3 barg (150 psig) and 15% water mass fraction, with the modified gland in place. From the figure, the slip velocity varies through the flow domain from -175 $(\mathrm{m/s})$, where the water velocity is greater than air velocity, to 391 $(\mathrm{m/s})$ where the air velocity is greater than the water velocity. Consequently, the high air flowrate associated with low water flowrates results in greater slip between the two phases. It is noted that the two phases of air and water become even more homogenous at the entrance of the valve due to the method of water injection but for only a short distance. It is a volume fraction based boundary condition that allows the second phase (water) to be uniformly injected at the cells representing inlet boundary conditions of the valve. On the other hand, higher slip magnitudes can be seen downstream of the modified gland owing to the occurrence of more expansion.

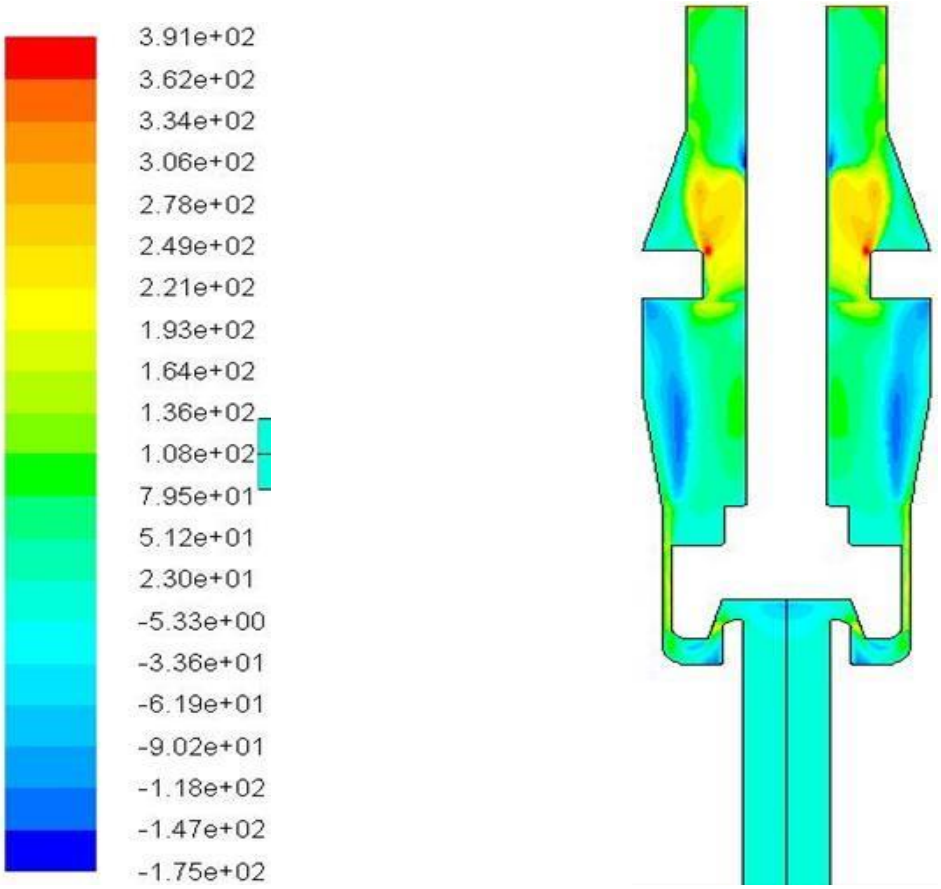

Figure5-22: Contours of slip (m/s) at 2 mm piston lift and an upstream stagnation pressure of 10.3 barg (150 psig) and a liquid mass fraction of 15% (0.2% water volume fraction) (with the modified gland)

Likewise, Figure 5.23 presents the contours of the relative velocity (the slip velocity) between the two phases at 2 mm lift, an upstream pressure of 10.3 barg (150 psig) and a liquid mass fraction of 84%, with the gland in place. According to the flow domain shown in the figure, the slip velocity varies between -65 $(\mathrm{m/s})$ and 320 $(\mathrm{m/s})$. A negative value of slip denotes that the water phase in a certain region has a higher velocity magnitude than the air phase and vice versa for the positive value of slip.

For this case while more water is encountered, a relatively lower slip would be incurred resulting from lower air mass flowrates. Despite the slip velocity shown by Figure 5.22 being comparatively higher than the slip velocity presented by Figure 5.23, the latter figure still provides a high slip velocity downstream of the modified gland with the greatest slip velocity experienced at the valve outlet. However, having another choking point at the outlet of the valve is practically unacceptable and may damage the pipe line fitted to the outlet of the valve plus generating more noise from the valve [88]. To remedy this issue, a sudden expansion fitting should be attached to the valve outlet.

To conclude, for large liquid fractions, assumptions of having homogenous two phase flows are not applicable due to mechanical non-equilibrium effects. Subsequently, the slip will not equal zero so the relative Reynolds number as well as the drag coefficient will not equal zero. Therefore the drag that represents the mechanical interaction between the two phases should not be disabled by the fluent facility. The Influence of the slip will be discussed in Section 5.5.1 based on computational modelling.

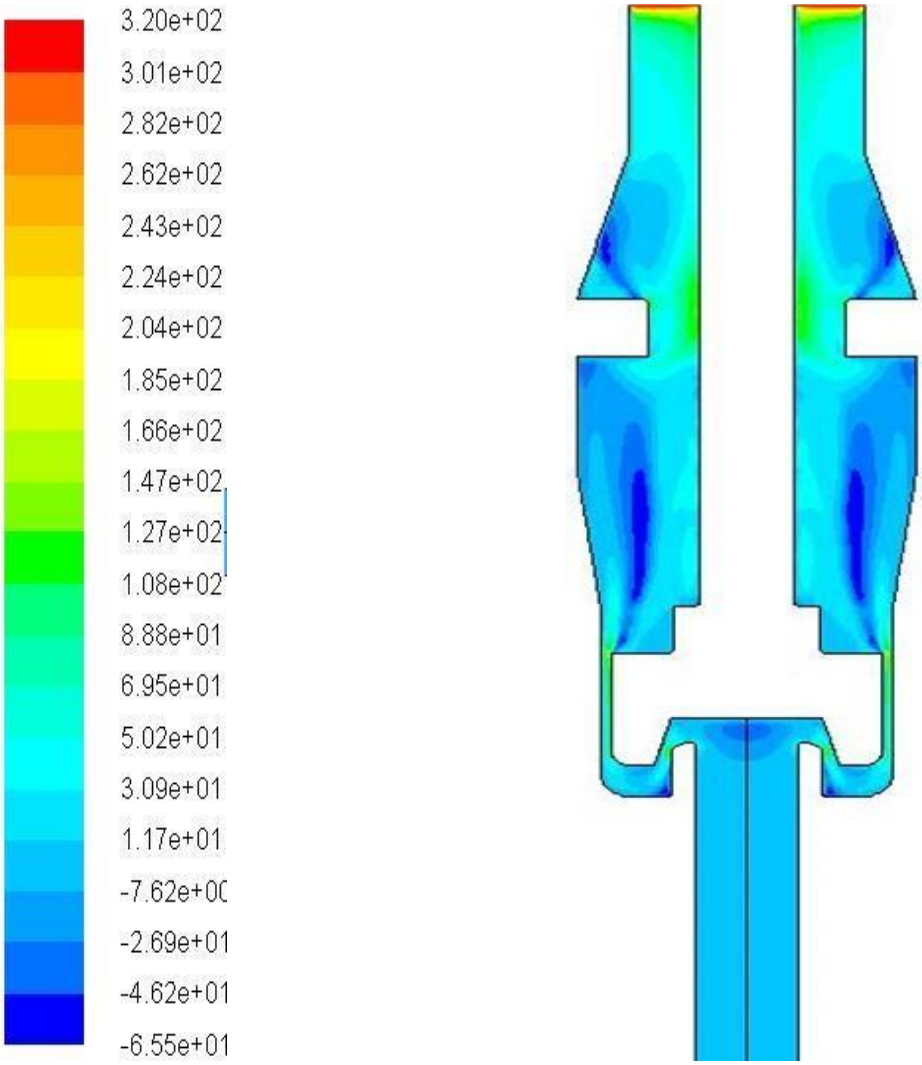

Figure5-23: Contours of slip (m/s) at 2 mm piston lift and an upstream stagnation pressure of 10.3 barg (150 psig) and a liquid mass fraction of 84% (5% water volume fraction) (with the modified gland)

Figures 5.24 and 5.25 show the contours of static temperature of air and water, respectively, at 4 mm piston displacement and an upstream pressure of 10.3 barg (150 psig) and water mass fraction of 26%, with no gland in place. From Figure 5.24, the static temperature of the air is in the range of 145K to 309K (-128^{0}C to +35^{0}C). As shown, there is a region where the air static temperature is relatively high downstream of the piston due to a viscous heating near the valve walls and follows a compression which is geometry dependant. Although removal of the gland is not practical, the flow experiences more expansions downstream of the piston in particular and results in much colder air. However, the heat transfer associated with the expansion of the air will be restricted by the thermal inertia of the water phase. In

fact, encountering more water in the valve will result in limiting the air expansion all over the flow domain and leads to higher air temperatures.

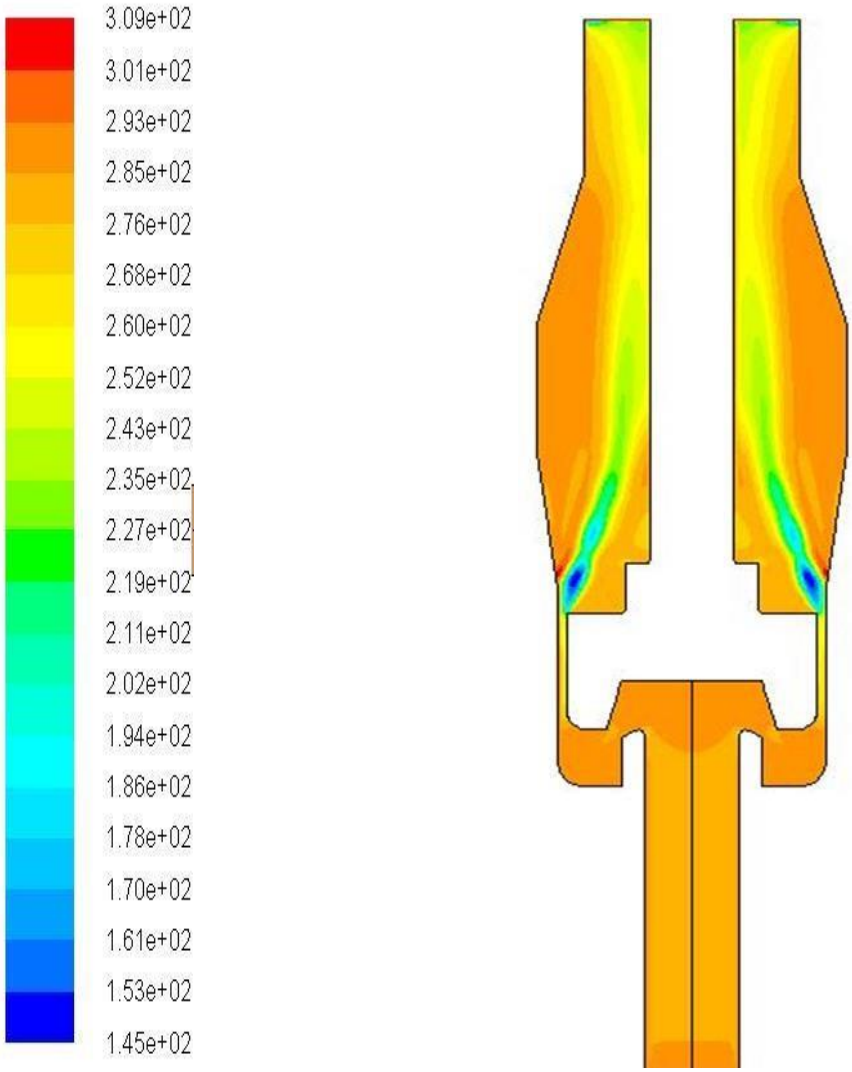

Figure5-24: Contours of static temperature of air (K) at 4 mm piston lift and upstream stagnation pressure of 10.3 barg (150 psig) and water mass fraction of 26% (with no modified gland)

In Figure 5.25, the range of water static temperature is between 256K and 296K (-17^{0}C and +23^{0}C). There is a significant reduction in the water temperature particularly downsteam of the piston while it is kept slightly below the water inlet temperature of 288Kfor the remaining regions of the fluid domain. It is of interest to disclose that there is a possibility of water solidification which might affect the integrated parameters as well as physics of the two phase flow. Furthermore, a simple calculation was carried out to determine the possible amount of ice in the flow domain as a third phase, and found to be a maximum of 1.3% of the inlet water

mass flowrate. Moreover, this amount of ice was determined for the worst scenarios of having less liquid mass flowrates in the valve as well as by assuming that all the heat transfer is all latent (total heat = latent heat). As it is noted, this amount of ice occurs downstream of the piston (away from the choking plane) hence the critical conditions of the two phase flow fundamentally will not be affected. However, Figure 5.26 presents contours of water static temperature at an upstream stagnation pressure of 10.3 barg (150 psig) and a liquid mass fraction of 58%, at a piston lift of 4 mm for the valve with the adjusted gland. In addition, the range of water static temperature is between $277\text{K and } 300\text{K}$ ($+4^0\text{C and } +27^0\text{C}$), hence ice formation is now no longer possible owing to the higher temperature. Accordingly, the thermal non-equilibrium hypothesis becomes more evident. The influence of the temperature difference between the two phases and the associated heat transfer will be discussed in Section 5.5.1 based on computational simulations.

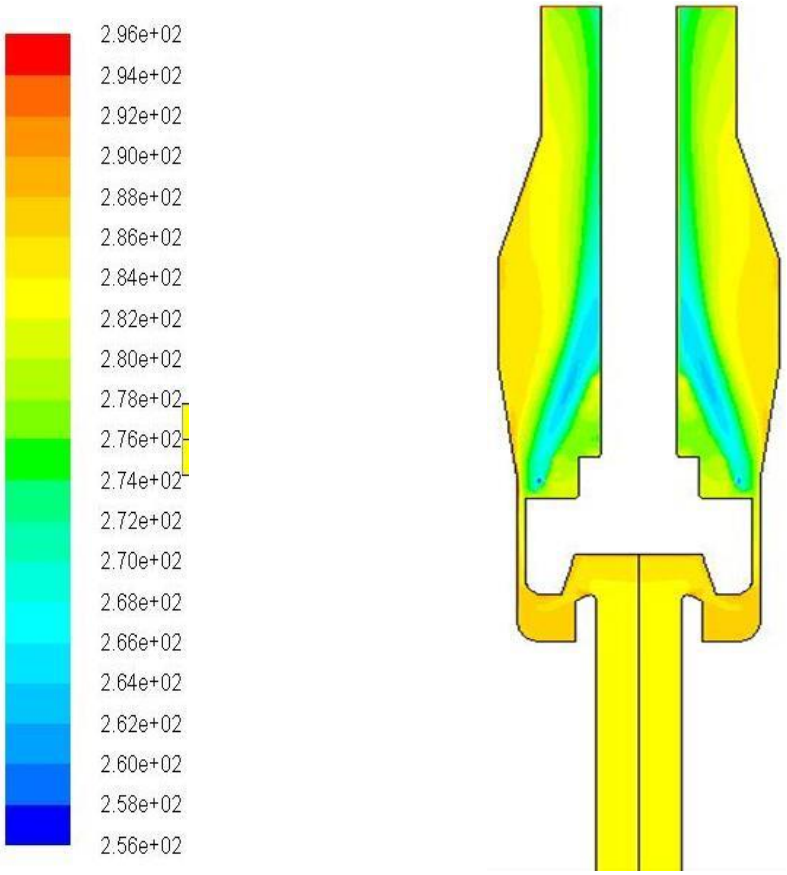

Figure5-25: contours of static temperature of water (K) at 4 mm piston lift and an upstream stagnation pressure of 10.3 barg (150 psig) and water mass fraction of 26% (with no modified gland)

Figure 5.27 shows the air flow-lift characteristics predicted by the Euler-Euler model and the experimental air flow-lift characteristics at 10.3 barg (150 psig) and various water quantities

of 14%, 48% and 84% liquid mass fractions. Figure 5.28 exhibits a comparison between the mixture flow-lift characteristics predicted by the CFD model and the experimental mixture flow-lift characteristics at 8.28 barg (120 psig) and liquid mass fractions of 19%, 54% and 87%. In general, these Figures present very good agreement between the predictions and the experiments with a maximum discrepancy of 8% appearing at very low lifts (0.2 – 1 mm). Flow-lift characteristics will be discussed in Section 5.6.1.

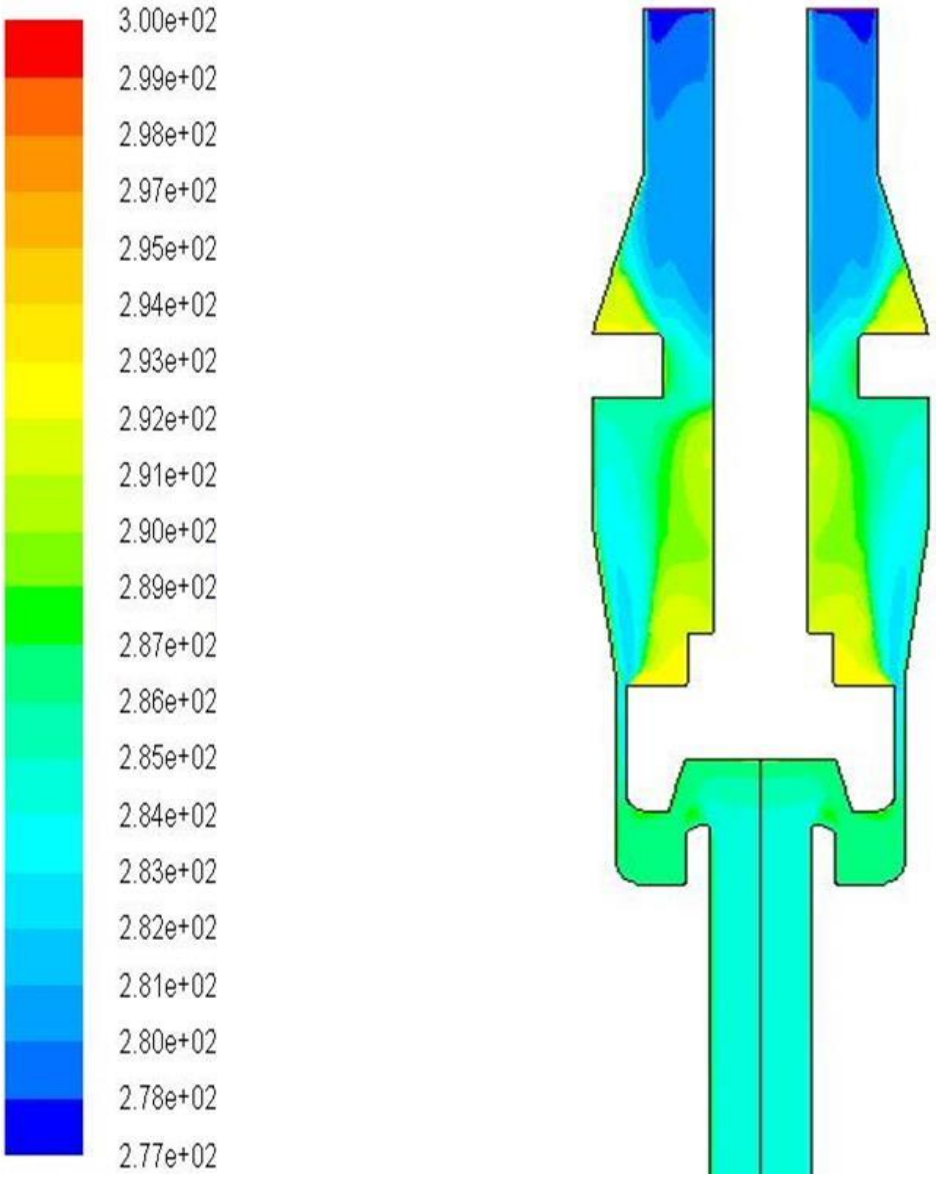

Figure5-26: contours of static temperature of water (K) at 4 mm piston lift and an upstream stagnation pressure of 10.3 barg (150 psig) and water mass fraction of 58% (with the modified gland)

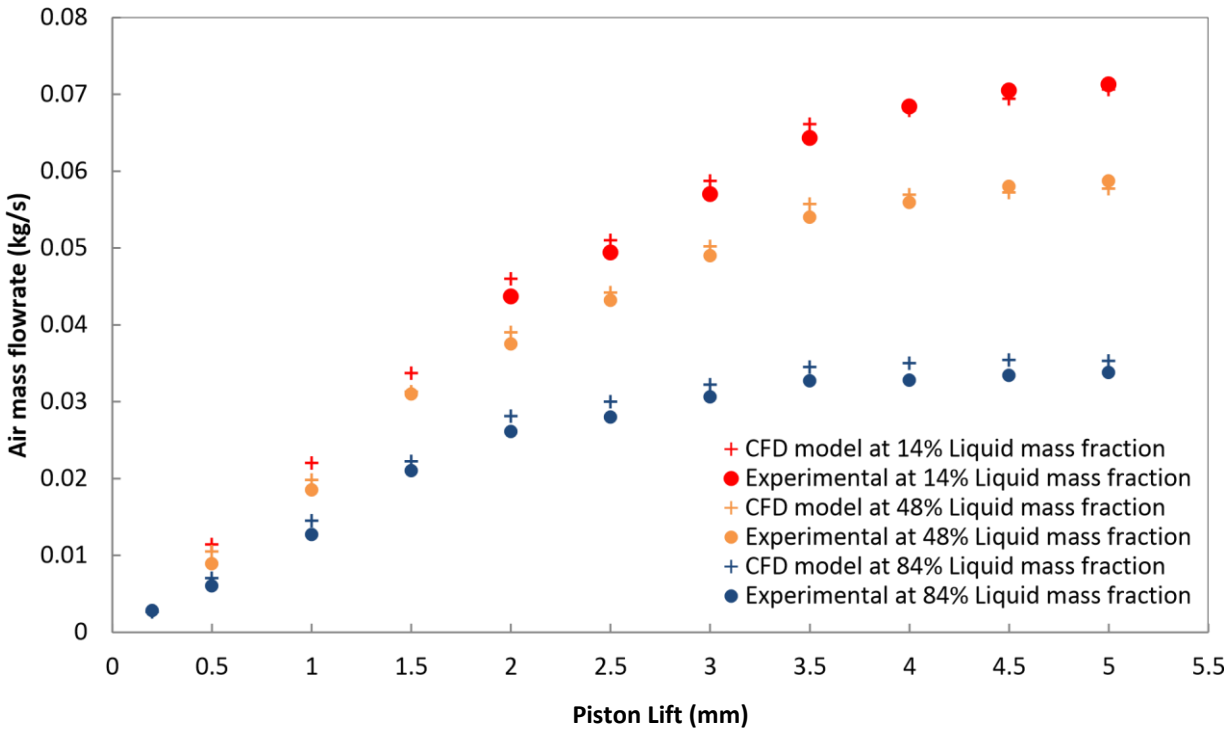

Figure5-27: Air flowrate at an upstream stagnation pressure of 10.3 barg (150 psig)

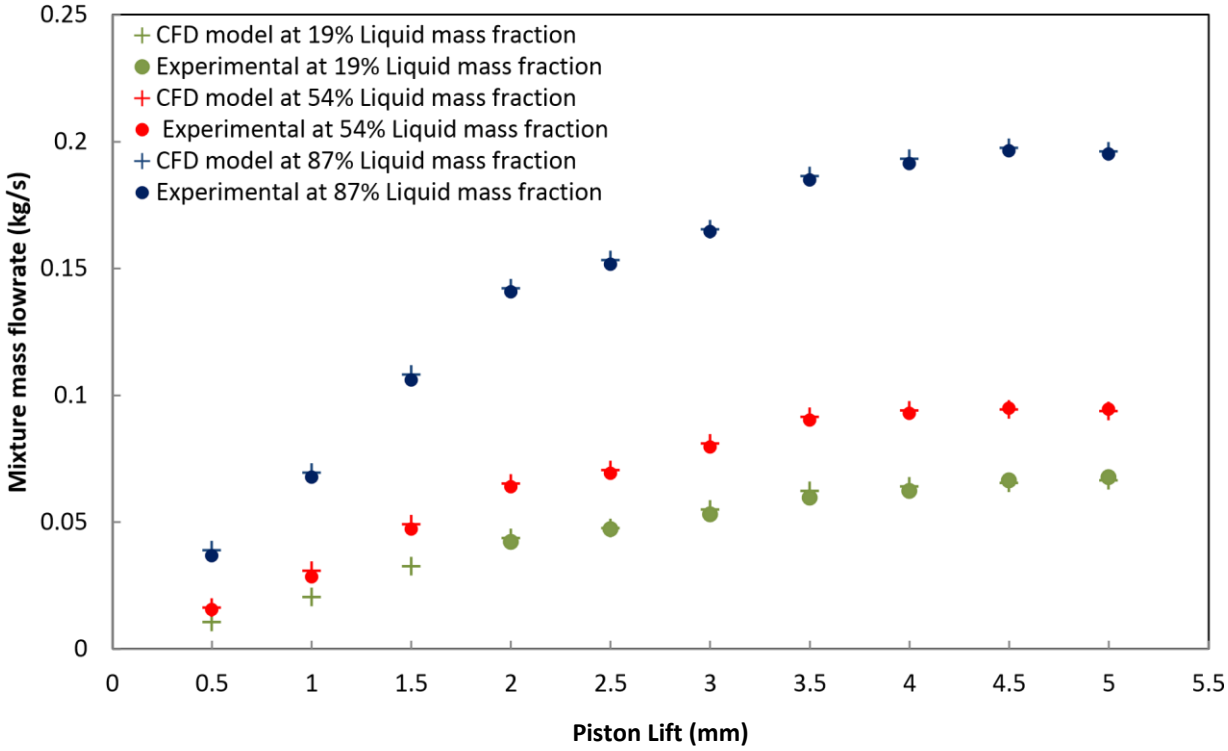

Figure5-28: Mixture flowrate at an upstream stagnation pressure of 8.28 barg (120 psig)

Figures 5.29 and 5.30 present the force-lift characteristics predicted by the Euler-Euler model at 13.8 barg (200 psig) and 10.3 barg (150 psig) respectively, with different water quantities and the modified gland in place. It is apparent that the pattern of the force-lift curves is relatively similar to those in experiments. Again, the figures fundamentally show that, having more inlet upstream pressure leads to higher forces exerted on the piston and to increase while the piston is lifting.

However, Figure 5.31 shows a comparison between the force-lift characteristics predicted by the CFD Euler-Euler model and the experimental force-lift characteristics at 13.8 barg (200 psig) and low liquid mass fraction of 21% (volume fraction of 0.4%) with the modified gland included. Figure 5.32 exhibits a comparison between the predicted force-lift curve and the experimental one based on an upstream inlet pressure of 13.8 barg (200 psig) but now with higher liquid mass fraction of 79% (volume fraction of 5%) and the modified gland applied to the valve. According to these figures, the CFD model tends to overpredict the piston forces particularly at high lifts and high liquid mass fractions. In other words, it can be seen that there is good agreement between the data and the experiments with a maximum discrepancy of around 4-6% at low piston displacements for both cases of different water volume fractions. On the other hand, there is less agreement between the predicted results and the experimental data at high piston lifts, high liquid mass fraction for both cases presented, with slightly higher discrepancy of around7-9% for the case with the higher liquid mass fraction. Force-lift characteristics and the influence of the back pressure associated with the modified gland will be discussed in Section 5.6.2 and 5.6.3, respectively.

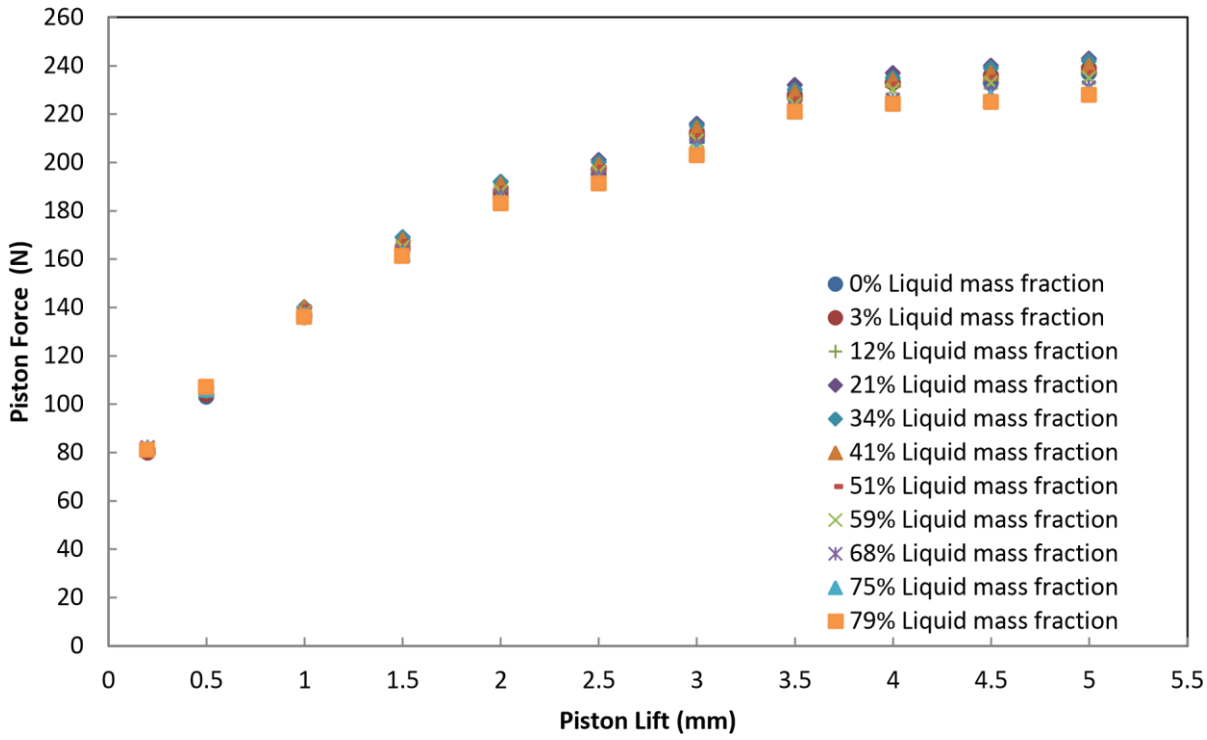

Figure5-29: Force-Lift at an upstream stagnation pressure of 13.8 barg (200 psig) with modified gland (CFD based)

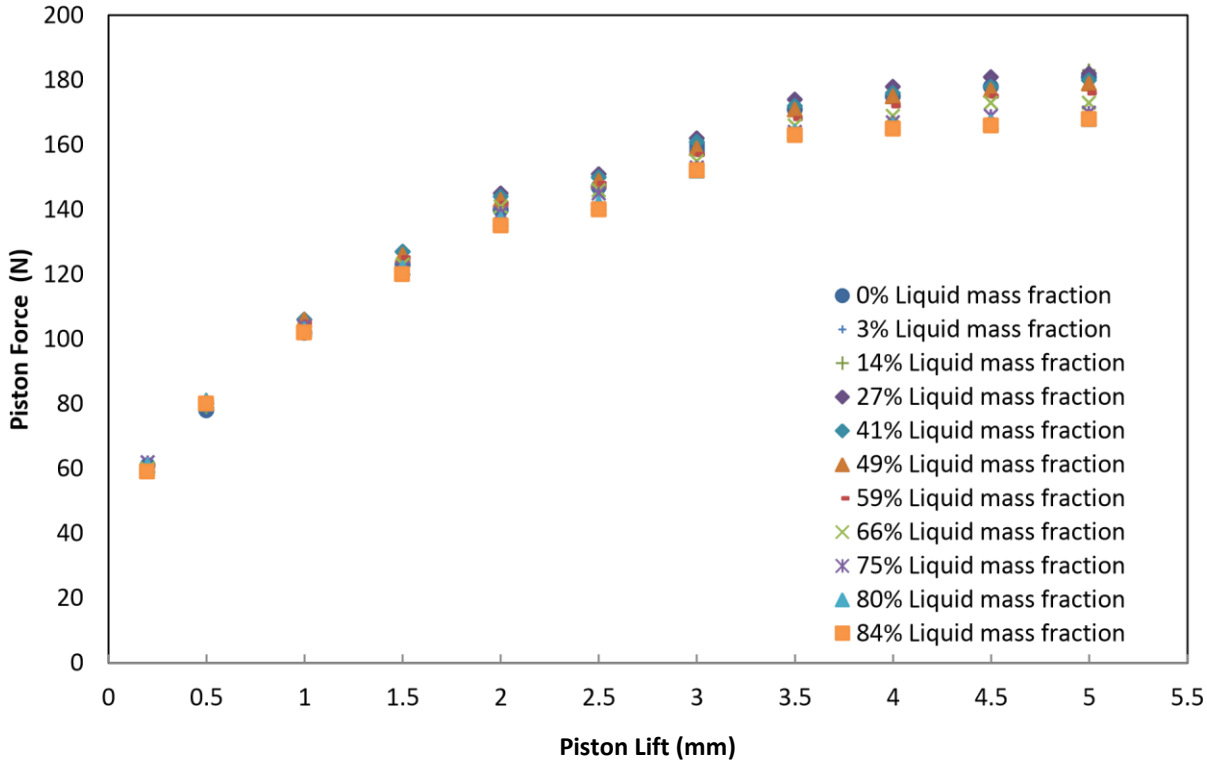

Figure5-30: Force-Lift at an upstream stagnation pressure of 10.3 barg (150 psig) with modified gland (CFDs based)

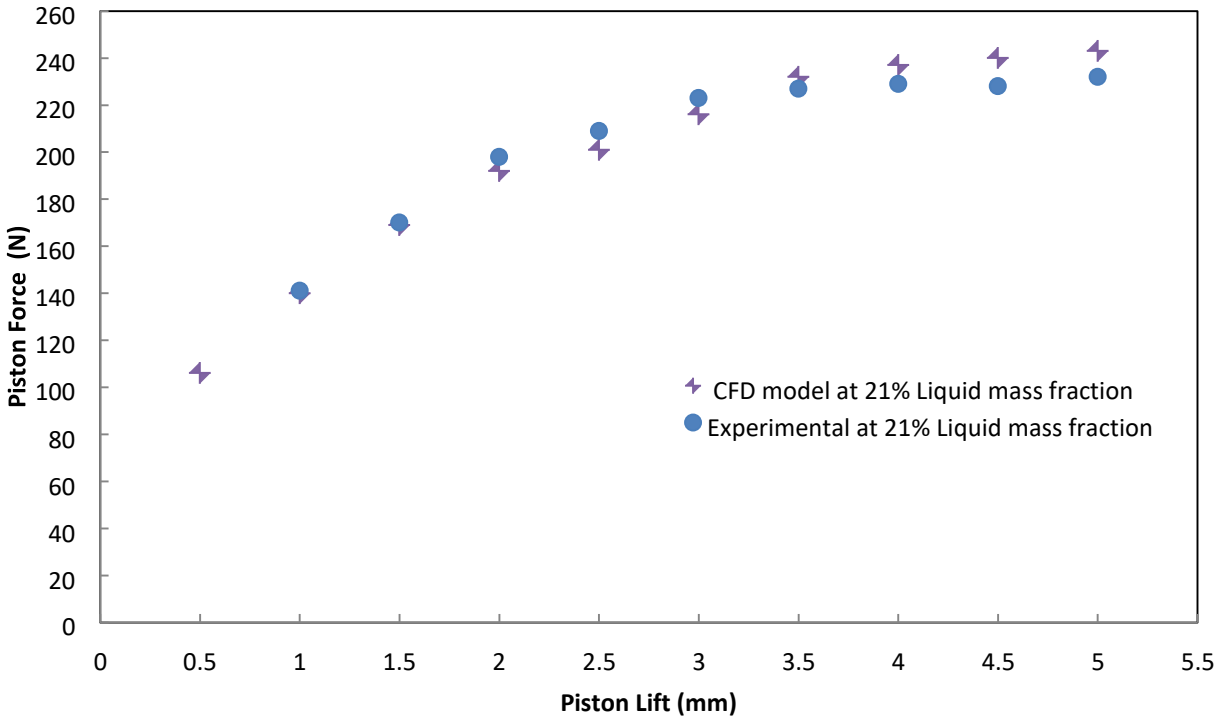

Figure5-31: Force-Lift at an upstream stagnation pressure of 13.8 barg (200 psig) and a lower water volume fraction of 0.4% with modified gland

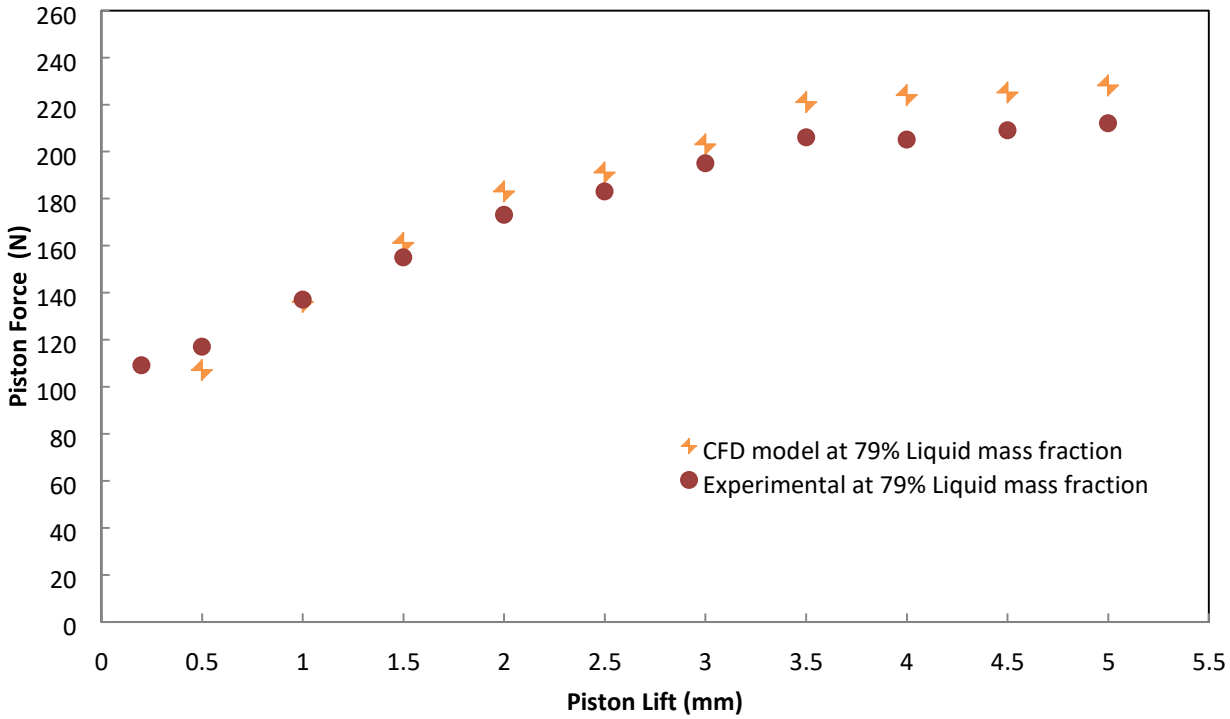

Figure5-32: Force-Lift at an upstream stagnation pressure of 13.8 barg (200 psig) and a higher water volume fraction of 5% with modified gland

In addition, Figures 5.33 and 5.34 present a comparison between the predicted forces and the experimental forces at an upstream pressure of 8.28 barg (120 psig) and various liquid mass fractions at piston lifts of 1mm and 5mm, respectively, with the modified gland in place. The figures show good agreement between the results predicted by the Euler-Euler model and the experimental data with significantly higher discrepancy of up to 12% at higher lift when more liquid is injected to the system.

Figures 5.35 and 5.36 present a comparison between the force results predicted by the CFD model and the experimental forces at an upstream pressure of 13.8barg (200 psig) and various water mass fractions at piston lifts of 1 mm and 4.5 mm, respectively, with no gland added to the valve. The figures prove once more that there is good agreement between the predictions and the experiments with up to 7% discrepancy at low lifts. At higher lifts with higher liquid mass fraction and without the modified gland, the CFD model overpredicts the piston forces with around 16%. Force –lift characteristics are discussed in section 5.6.2.

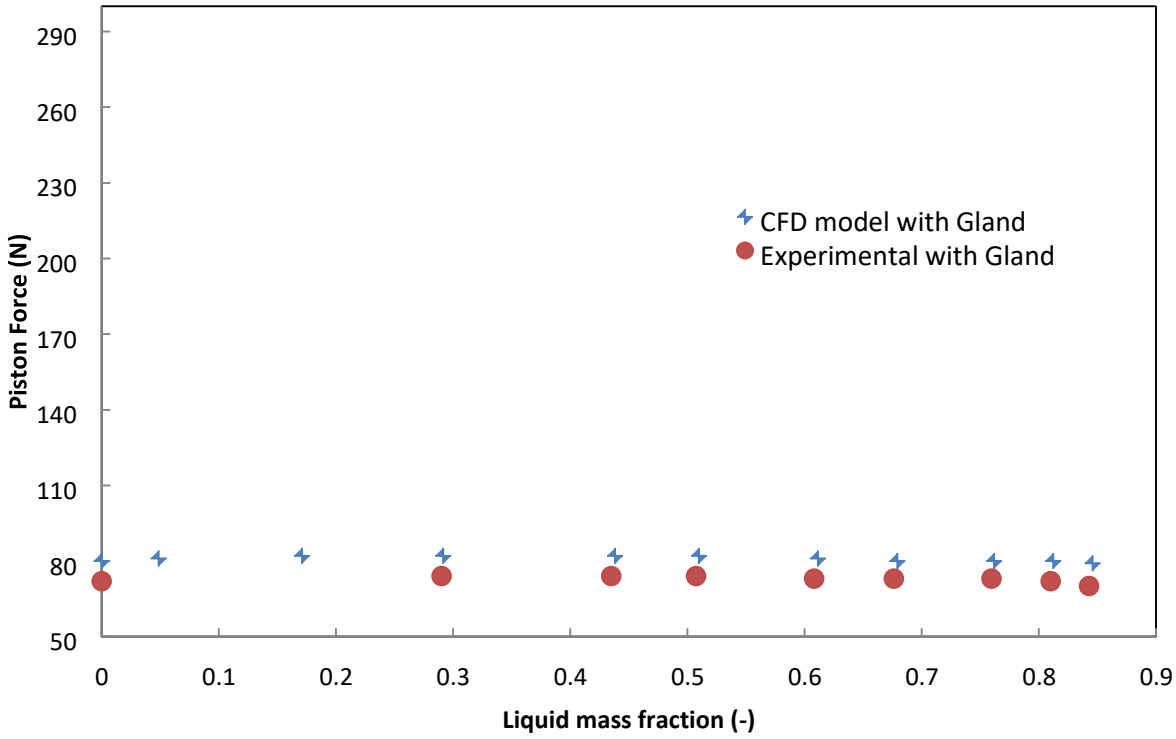

Figure5-33: The effect of water quantity on piston force at 1 mm piston lift for an upstream stagnation pressure of 8.28 barg (120 psig)

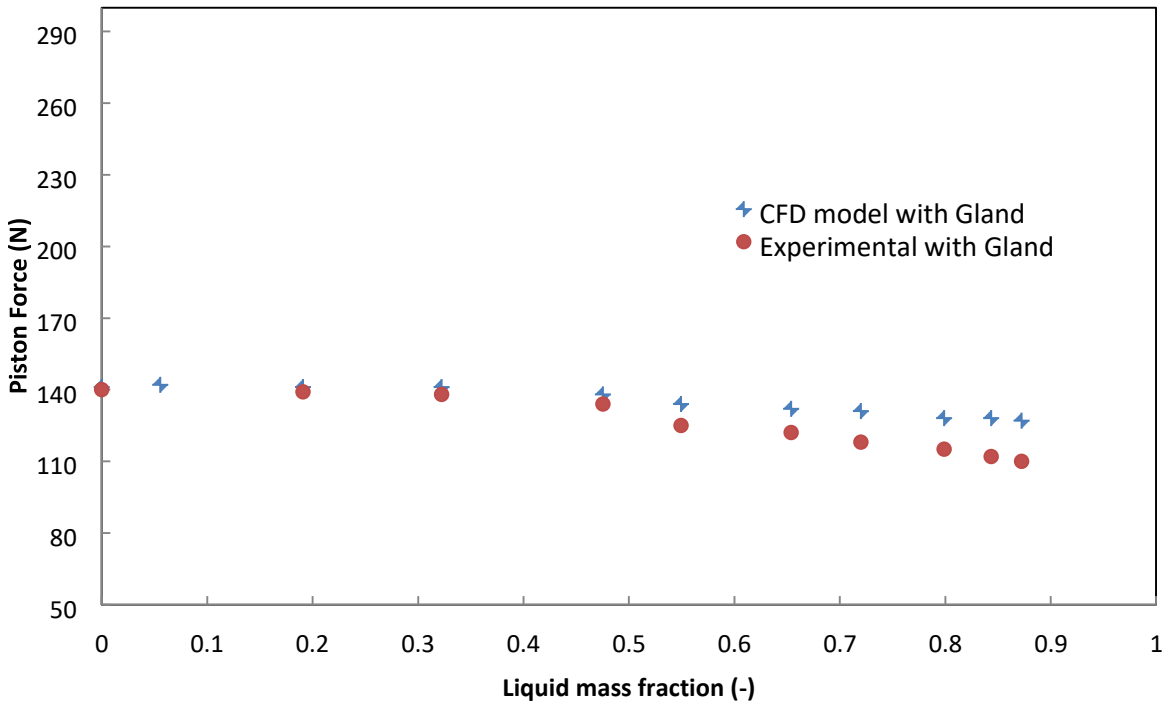

Figure5-34: The effect of water quantity on piston force at 5 mm piston lift for an upstream stagnation pressure of 8.28 barg (120 psig)

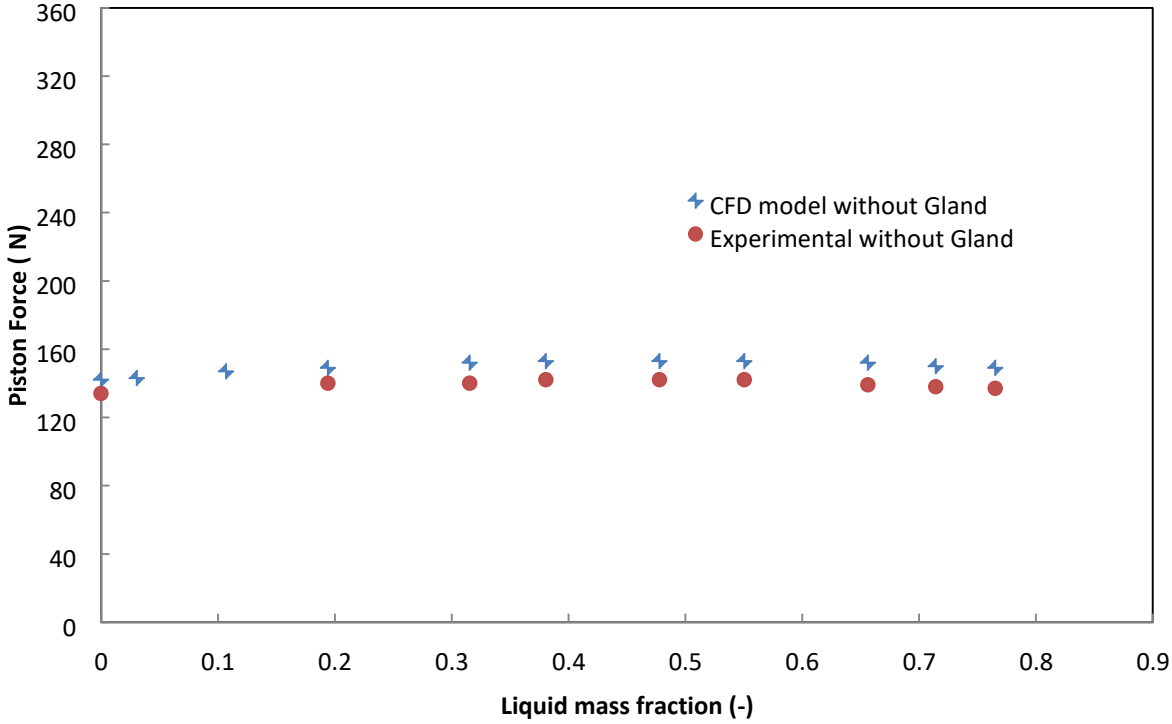

Figure5-35: The effect of water quantity on piston force at 1 mm piston lift for an upstream stagnation pressure of 13.8 barg (200 psig)

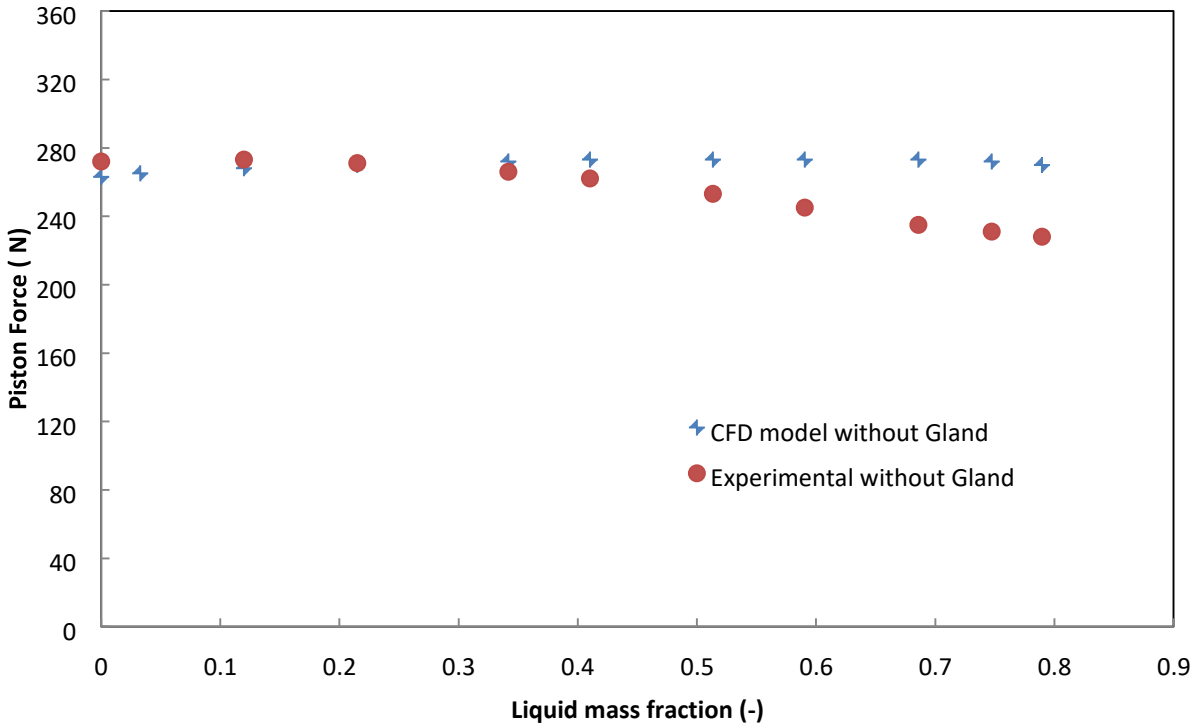

Figure5-36: The effect of water quantity on piston force at 4.5 mm piston lift for an upstream stagnation pressure of 13.8 barg (200 psig)

5.5 Further assessment of the Euler-Euler Model

5.5.1 Comparison with Mixture Model

The mixture model is a simplified model of the full Eulerian-Eulerian multiphase model. This model is essentially associated with simulating dilute flows of liquid droplets in a gas, small bubbles in a liquid or suspensions of solid particles in a gas. One of the assumptions considers the flow phenomena are dominated by one phase while the influence of the other phases is ignored. As a result, the multiphase flow could be treated as a pseudo single phase flow where a considerably smaller number of variables are solved resulting in a computationally more efficient calculation. However, the strength of coupling between the phases plays a predominate role in classifying a multiphase model as a homogenous mixture or a multi-fluid model. The mixture model proposes strongly coupled phases when their velocities equalise over short spatial length scales, hence all phases move at the same velocity (namely homogenous flow). A recent study conducted by Elmayyah [88], who reviewed most of the

models that have been developed on the basis of an assumption of local equilibrium. The study also showed other cases in which the gravity and centrifugal forces could easily result in velocity slip. The mixture model was formed based on the continuity and energy equation for the mixture in addition to one equation representing the momentum but includes an additional term to account for the influence of velocity differences. A force balance model was required for the dispersed phase to determine the relative velocity. An equation for the volume fraction of the dispersed phase was introduced. However, the interface between phases and the associated discontinuities considered to be major issues which represent the main difficulties in all multiphase models. These issues may make the multiphase models less reliable compared to the simplified mixture model even though their equations are theoretically more advanced [88]. Full details of the simplified mixture model and the associated governing equations for continuity, momentum, energy, volume fraction and an algebraic expression for slip velocity are presented in the Fluent user guide [126].

In this study, however, a mixture model was also implemented to the two phase frozen flow of air-water to address the limiting homogenous flow conditions then to assess the predictive capability of the two fluid model developed.

Figure 5.37 compares both the predicted air mass flow by the mixture and the two fluid model predictions against the experimental data at a piston full lift of 5 mm and an upstream inlet pressure of 13.8 barg (200 psig) for a range of water mass fractions. The models assume a droplet size of 10 microns is applicable. The figure shows that both mixture and two fluid approaches predict the general trends correctly. The mixture model correctly predicts the mass flows within 5% discrepancy for liquid mass fractions less than 0.4 but for greater mass fraction errors can be as high as 16% and suggest that the nonequilibrium effects are important and need to be accounted for. The predictions of the two fluid model can be seen to be satisfactory over the range of liquid mass fractions examined and generally predict the air mass flow rate within 4% error.

However, it is of interest to identify the reasons of the obvious disagreement between the Euler-Euler model and the homogenous mixture model. One can declare that this should be expected due to the simplification of the homogenous mixture model compared to the two

fluid model. In fact, thermal and mechanical nonequilibrium between the two phases are accounted for by implementing the two fluid model approach as discussed earlier. These can be represented as a slip velocity to account for the difference in velocity between the two phases and the temperature difference to account for the thermal nonequilibrium phenomenon. Figure 5.38 shows the predicted air velocity at the valve outlet for an upstream pressure of 13.8 barg (200 psig) and different liquid mass fractions at a piston lift of 5 mm. The figure indicates that there is a lower air velocity predicted by the homogenous mixture model compared to the Euler-Euler model for medium to high liquid mass fractions, which might account for the lower predicted air mass flowrate, as shown in Figure 5.37. On the other hand, the existing mixture model of the CFD Fluent code consists of a slip velocity model. Although the latter concept of the slip model is optional through the simulation procedure, it has not worked for this study as iterative divergence occurred after no more than 2300 iteration particularly when the calculation of drag between the two phases is included.

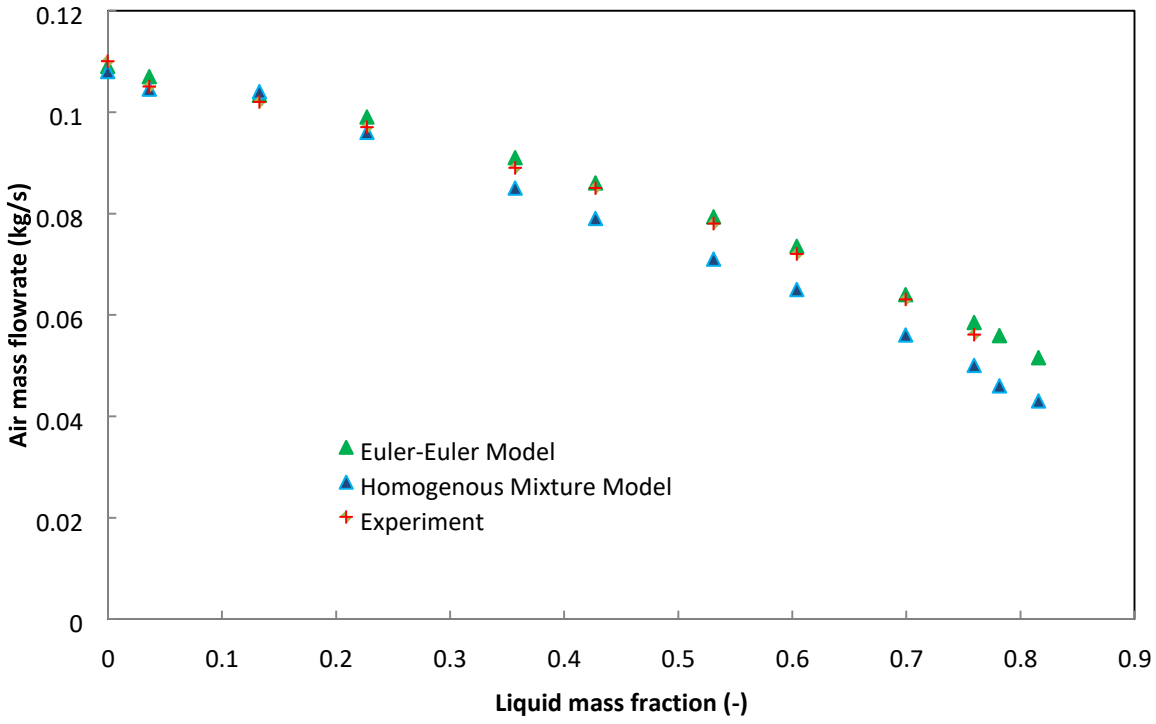

Figure5-37: Comparison between the experimental data and CFD predictions at an inlet upstream stagnation pressure of 13.8 barg (200 psig) with 5 mm piston lift

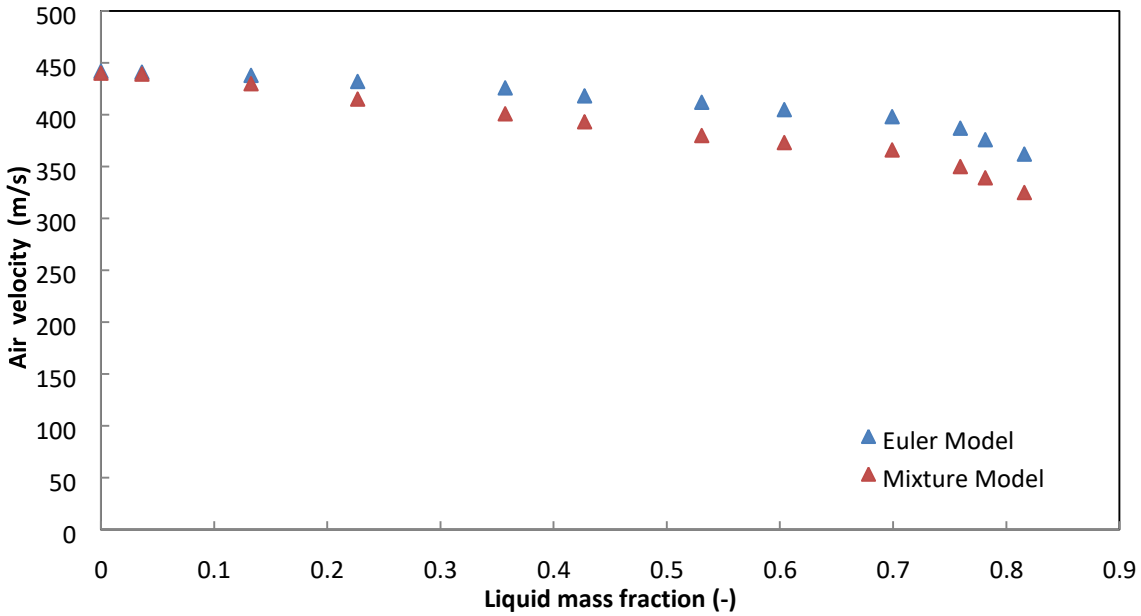

Figure 5-38: Predicted air velocity at outlet of the valve for an upstream stagnation pressure of 13.8 barg (200 psig) at 5 mm piston lift

5.5.2 Effect of Droplet Size

Noting that the assumption here is for a mono dispersed droplet flow, the droplet size is one of the most uncertain parameters in the application of the model. Therefore, predictions for a range of droplet sizes have been carried out and are shown in Figure 5.39.

Figure 5.39 shows the effect of using droplet sizes from 5-35 microns and indicates an increasing influence as the liquid fraction increases, leading to an increase in the air flowrate as the droplet size is increased. However for this range of droplet sizes the predictions of air flowrates vary only by a maximum of 8%. The experimental values for the air flowrates fall within the range of flowrates. Thus for an estimated droplet size based on a critical weber number of We=12 reasonable predictions of mass flow can be achieved. Further verification can be achieved by examining the predicted Weber numbers.

As identified earlier, the predictions of Mach number from the Euler-Euler model for the range of liquid mass fractions examined, indicates that the critical flow location occurs at the end of the channel between the piston and valve body particularly when the piston lift is in the range between 2.5 and 5 mm. This is the choking location for all flow conditions at the aforementioned piston lifts. Figure 5.40 shows the predicted Weber numbers in this location

for the 10 micron diameter case and for liquid fractions of 13% and 70% at a piston lift of 5 mm and an upstream pressure of 13.8 barg (200 psig). The figure shows that Weber numbers generally lie in the 10-20 range confirming the initial assumptions and the droplet diameters investigated.

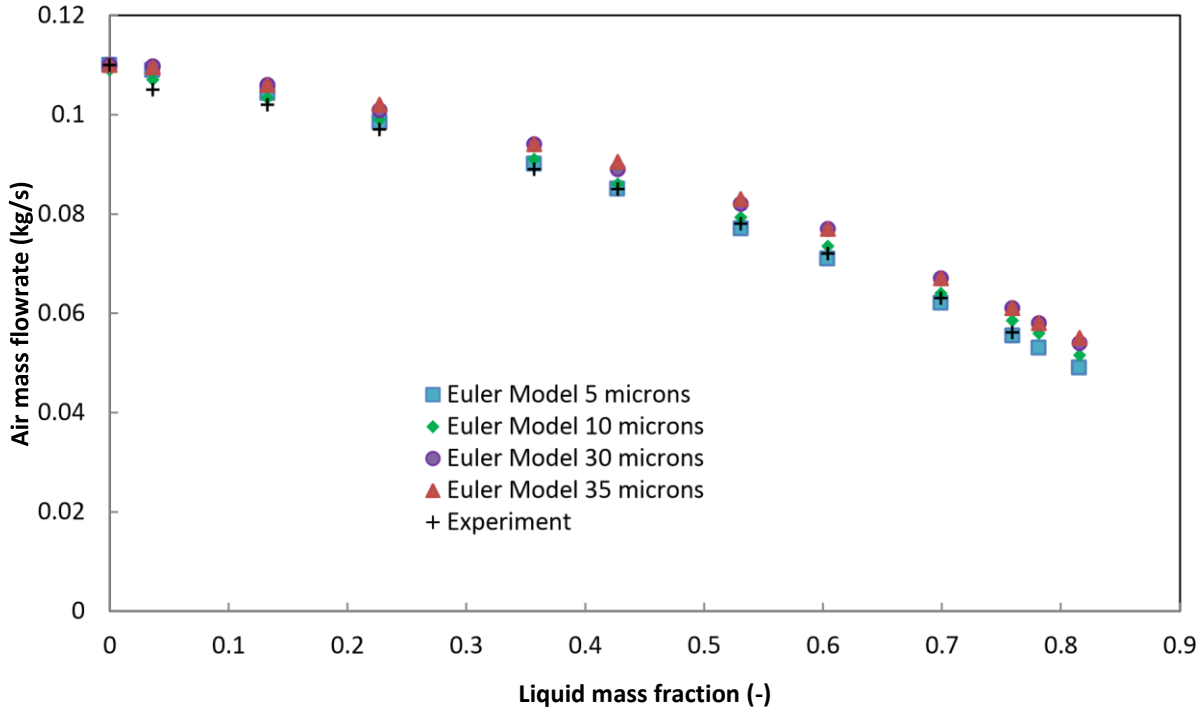

Figure5-39: Comparison between experimental data and Euler-Euler predictions for droplet sizes 5-35 microns at an inlet upstream stagnation pressure of 13.8 barg (200 psig) with 5 mm piston lift

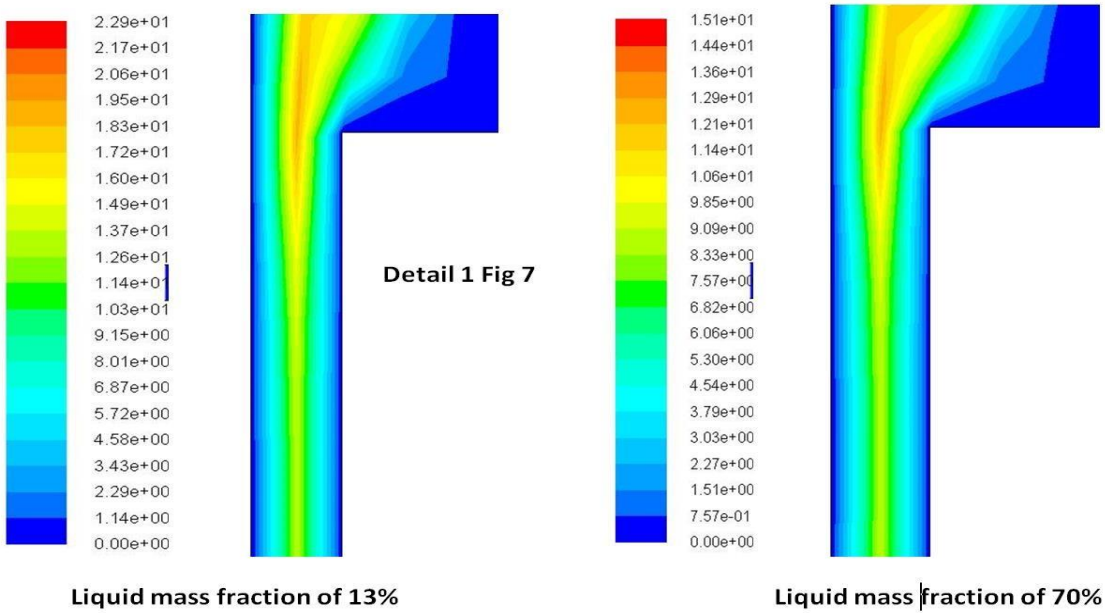

Figure 5-40: Two fluid model (Euler-Euler) Weber number in the choking plane end of the passageway between the piston and valve body at an upstream stagnation pressure of 13.8 barg and piston lift of 5 mm

5.5.3 Effects of Sensible heat transfer

However, an attempt was made computationally to determine the influence of the water temperature in the predicted air mass flowrate. Figure 5.41 presents the predicted air mass flowrate for an upstream pressure of 10.3 barg (150 psig) and different water mass fractions and different inlet water temperatures at a piston lift of 5 mm. The figure indicates no significant difference in the predicted air mass flowrate with an increase in the water temperature up to a water temperature of 323K. A 2-3% maximum reduction in the predicted air mass flowrate can be observed for the higher inlet water temperature of 323k which approaches approximately the saturation temperature of the local pressure. This can be justified in accordance with the ideal gas law as an increase in gas temperature at a constant pressure will lead to a decrease in gas density which ensures a smaller air mass flowrate. Even though this higher water temperature can affect the choking conditions of the flow by increasing the flow speed of sound, decrease of the density has an impact on the discharged air mass flowrate which compensates for the increase in the speed of sound. The influence of inlet water temperature and the associated heat transfer, on the choking conditions particularly the speed of sound and density of air will be further explained later in this section. However, it is worth mentioning here that having a two phase flow at a very significant difference in temperature particularly at the inlet of the valve may not be a practical issue. Thus it is proposed here to examine the effect of heat transfer between the phases and the associated sensible heat in the air mass flowrate. In this study, it is believed that the flow path and residence time through the valve tested are not sufficient for significant heat transfer between the phases. With reference to the heat transfer magnitude, Figure 5.42 presents the heat transfer at different inlet water temperatures and various water mass fractions for the valve at a full lift and an upstream stagnation pressure of 10.3 barg (150 psig). The figure shows the predicted heat transfer between the phases, which is computationally calculated according to Eq. 5.13. The total heat transfer increases with an inlet water temperature increase, and noticeably peaks at approximately 58% liquid mass fraction. Also, the predicted net piston forces were found not to be significantly affected by an increase in inlet water temperature, as shown in Figure 5.43. The figure exhibits predicted net forces that are exerted on the piston at an upstream stagnation pressure 10.3 barg (150 psig) and a piston lift of 5 mm.

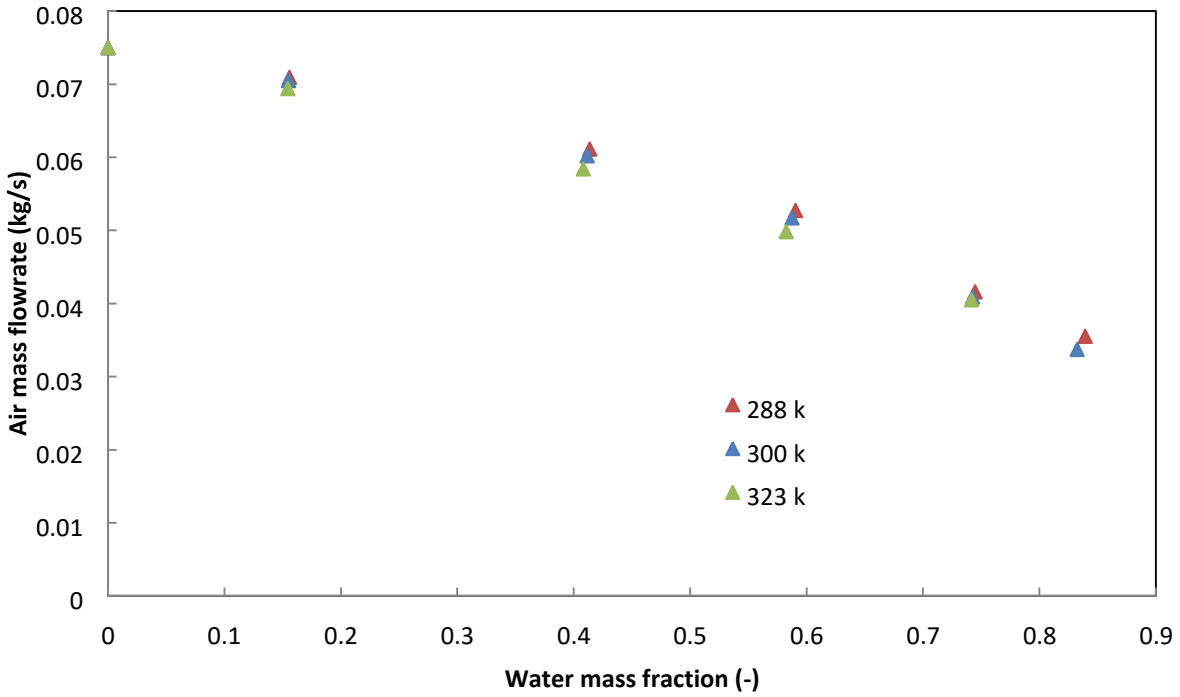

Figure5-41: Predicted air mass flowrate for an upstream stagnation pressure of 10.3 barg (150 psig) at 5 mm piston lift and different inlet water temperature

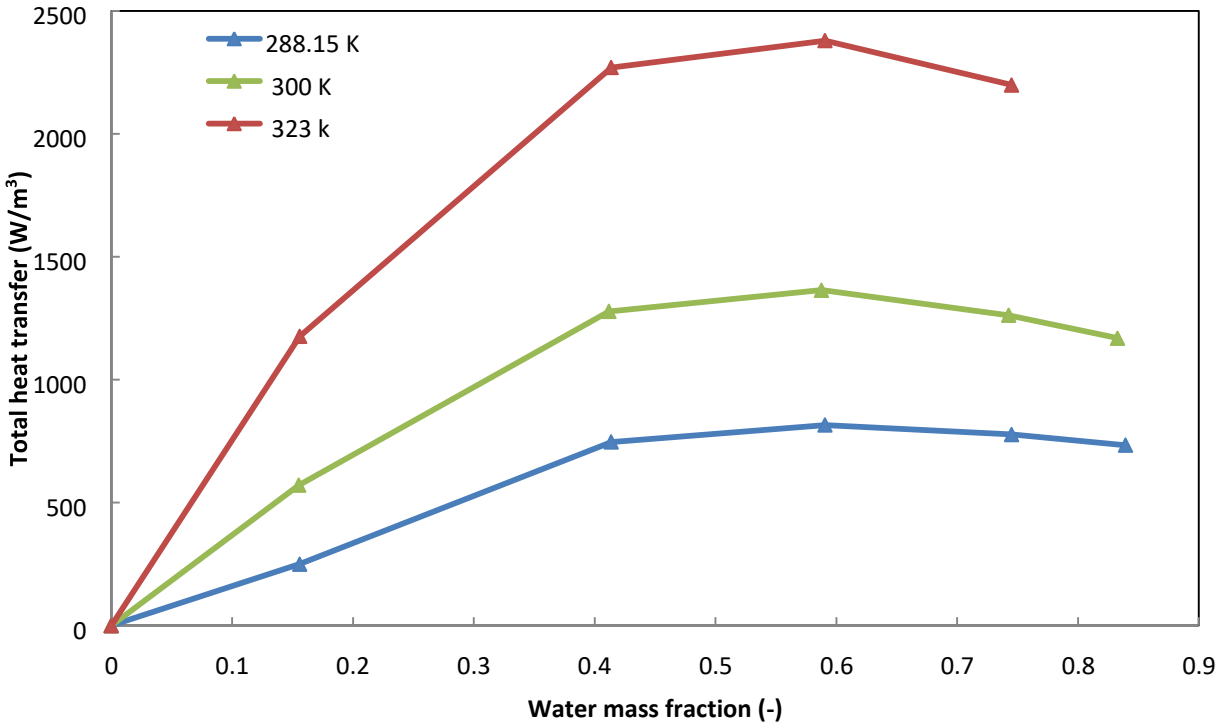

Figure5-42: Volumetric heat transfer (W) at an upstream stagnation pressure of 10.3 barg (150 psig) at 5 mm piston lift and different inlet water temperature

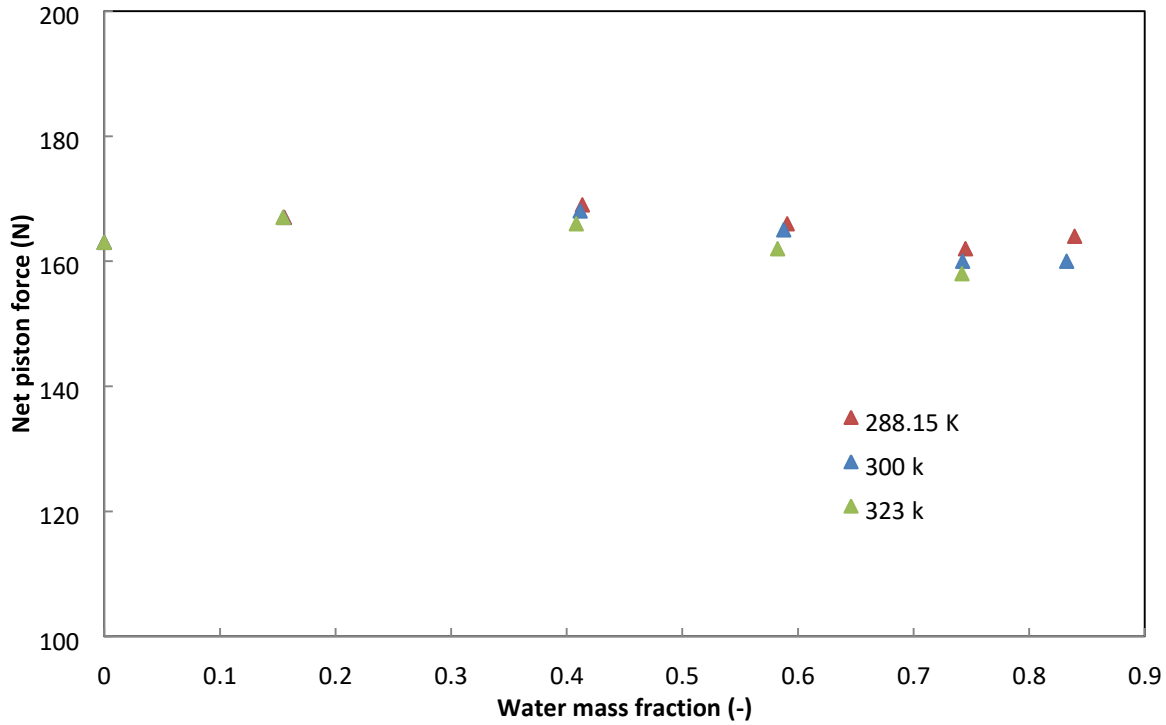

Figure5-43: Predicted net piston force at an upstream stagnation pressure of 10.3 barg (150 psig) at 5 mm piston lift

To look closer at the influence of heat transfer between the phases at the critical conditions of the flow, attention should be paid to Figures 5.44, 5.45, 5.46 and 5.47. Figure 5.44 shows contours of air static temperature at an upstream total pressure of 10.3 barg (150 psig) and a liquid mass fraction of 58%, with different inlet water temperature of 323K (a) and 288.15K (b), for a full lift of 5 mm. The figure presents the effect of the inlet water temperature on the air static temperature. It shows that the air static temperature increases with an increase in inlet water temperature due to relatively high thermal inertial of the water phase, which results in a volumetric heat transfer increase. Accordingly, the heat transfer between phases is now computationally evident, however, the effectiveness of this heat transfer is still of importance hence it may or may not be adequate in affecting the choking conditions. Figure 5.45 and 5.46 show contours of Mach number and velocity magnitude of air at an upstream total pressure of 10.3 barg (150 psig) and a liquid mass fraction of 58%, at a piston displacement of 5 mm, for inlet water temperature of 323K and 288.15K, respectively. The critical plane position (A) of Figure 5.45 indicates that the speed of sound is approximately 341 (m/s) whilst the critical plane position of Figure 5.46 indicates a speed of sound of approximately 329 (m/s). In fact, the difference between both speeds of sounds is definitely due to a difference in air temperature between the two critical plane locations, as shown in

Figure 5.44. Figure 5.47 shows contours of air density at an upstream total pressure of 10.3 barg (150 psig) and a liquid mass fraction of 58%, at piston lift of 5 mm, for inlet water temperatures of 288.15K (a) and 323K (b). The figure presents the influence of inlet water temperature and the associated heat transfer between the phases on the air density at the choking plane location. The figure shows that the air density decreases with the water inlet temperature increase. At the critical plane location of Figure 5.47 (a), the air density is 6.43 $(\mathrm{kg/m^3})$, whilst it is 5.22$(\mathrm{kg/m^3})$ at the critical plane position of 5.47 (b). According to Eq.5.42 the resulting air mass flowrate will be decreased, with an increase in heat transfer between the two phases resulting from an inlet water temperature increase. In other words, the reduction in air density due to an increase in inlet water temperature could compensate for the increase in speed of sound.

To conclude, the resulting volumetric heat transfer between the phases is believed to be not sufficient enough to significantly affect the choking conditions. Therefore the noticeable disagreement between the two numerical approaches in terms of air mass flow prediction could be mainly attributed to the slip velocity.

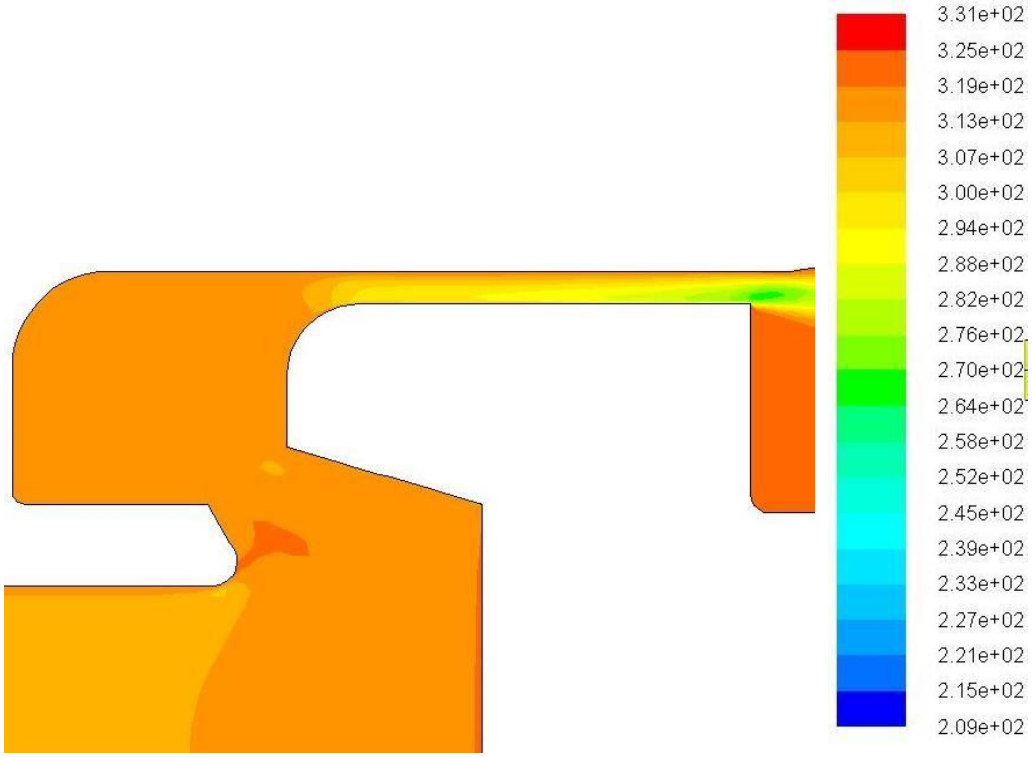

(a) At inlet water temperature of 323K

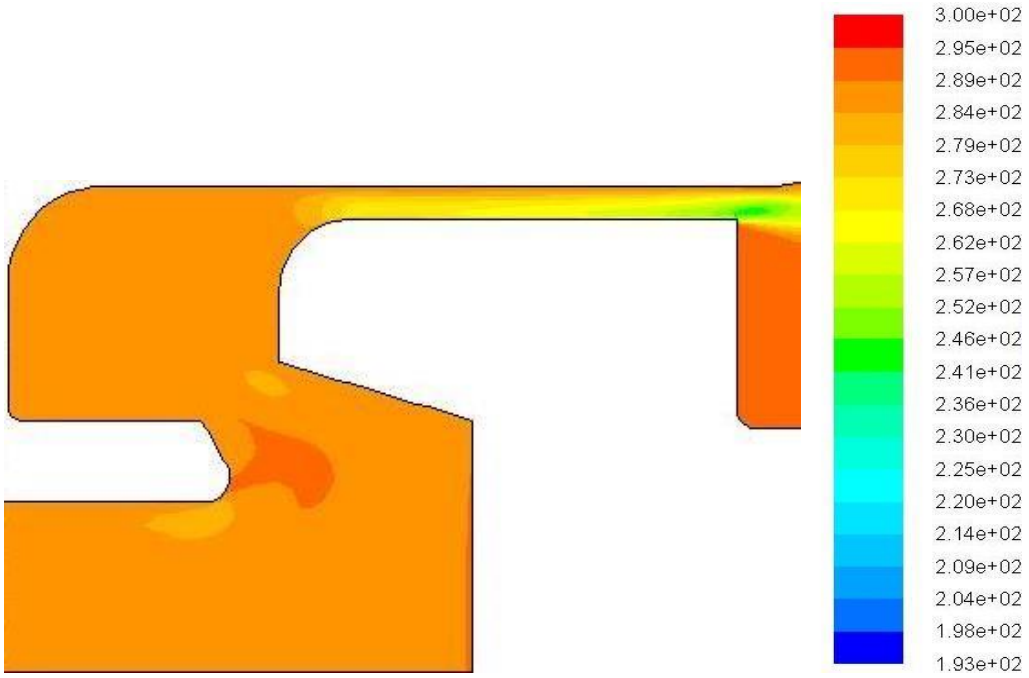

(b) At inlet water temperature of 288.15K

Figure5-44: Contours of static temperature of air at an upstream stagnation pressure of 10.3 barg (150 psig) and a liquid mass fraction of 58%, at 5 mm lift, for different inlet water temperature (a) and (b)

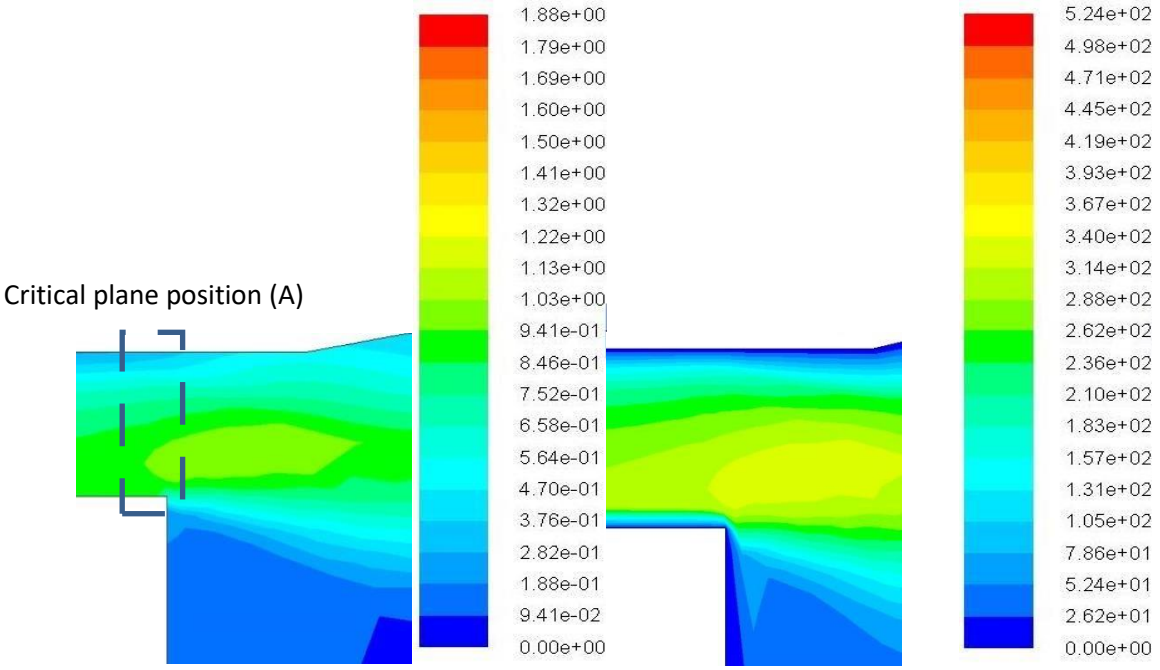

(a) Contours of Mach numbers (-) (b) Contours of velocity magnitude (m/s)

Figure5-45: Contours of Mach number and velocity magnitude of air at an upstream stagnation pressure of 10.3 barg (150 psig) and a liquid mass fraction of 58%, at 5 mm lift, at an inlet water temperature of 323K

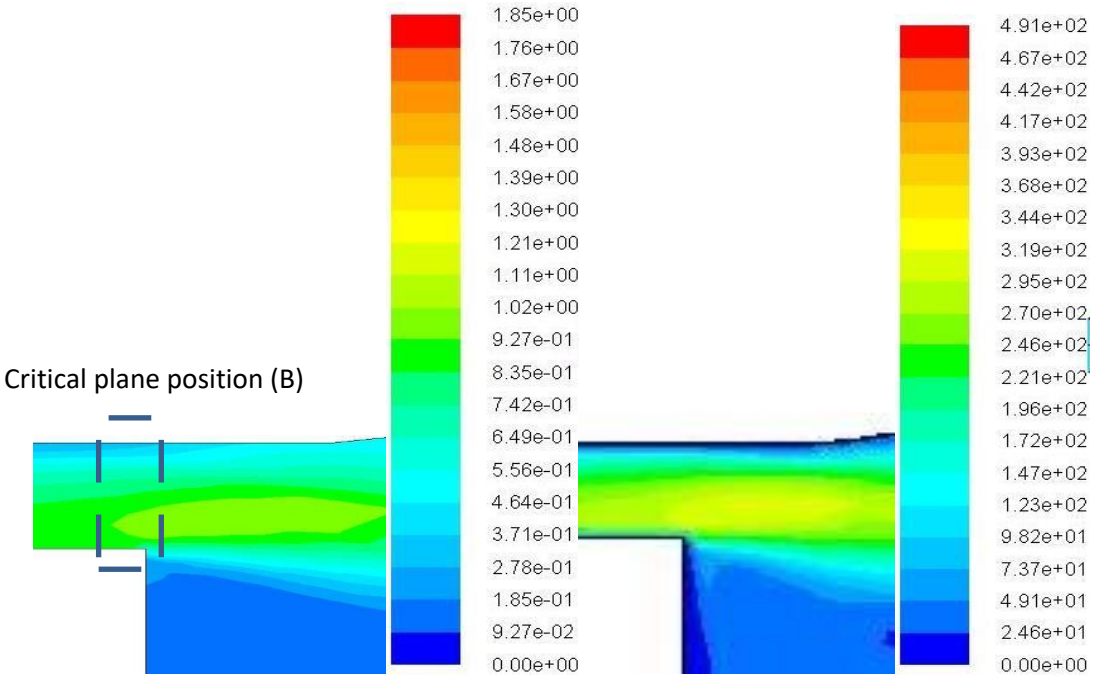

(a) Contours of Mach numbers (-) (b) Contours of velocity magnitude (m/s)

Figure5-46: Contours of Mach number and velocity magnitude of air at an upstream stagnation pressure of 10.3 barg (150 psig) and a liquid mass fraction of 58%, at 5 mm lift, at an inlet water temperature of 288.15K

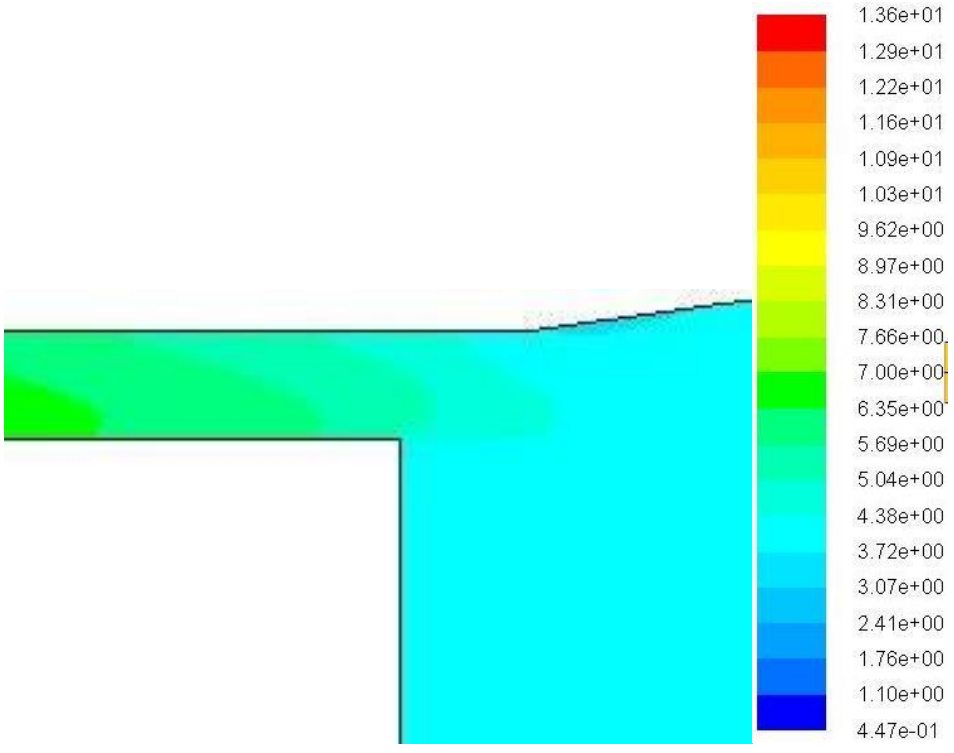

(a) At an inlet water temperature of 288.15K

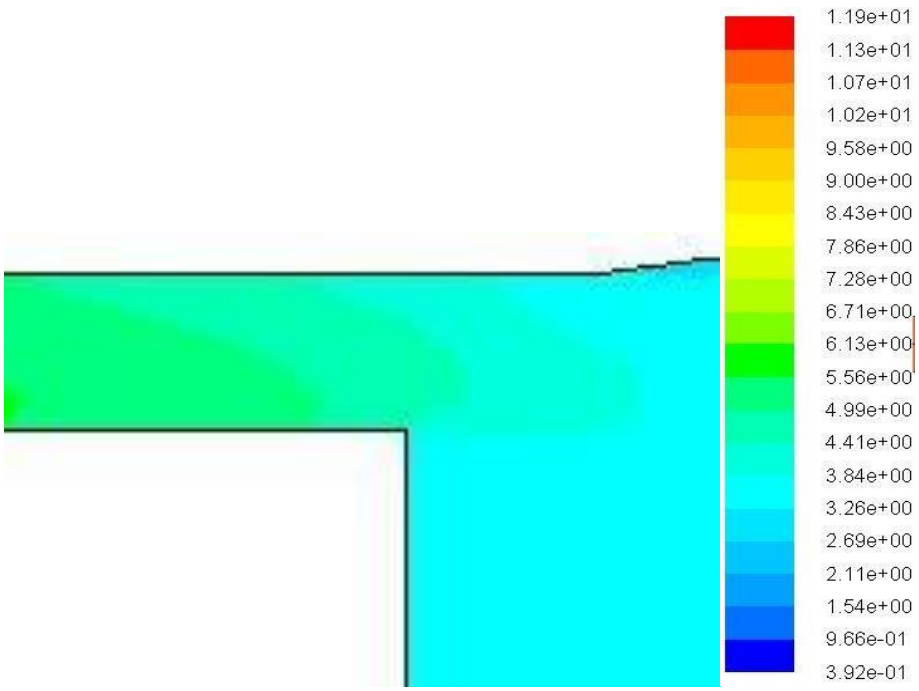

(b) At an inlet water temperature of 323K

Figure5-47: Contours of density of air at an upstream stagnation pressure of 10.3 barg (150 psig) and a liquid mass fraction of 58%, at 5 mm lift, for different inlet water temperature (a) and (b)

5.5.4 Homogenous Equilibrium Model (HEM)

This model was proposed by Darby [84] and given by the following equation:

0 5

$$G_{0} = \rho_n \left(-2 \int_{P_0}^{P_n} \frac{dp}{\rho_m}\right) . \quad (5.37)$$

Where, $\rho_n$and P_n are the mixture density and pressure at the valve outlet, respectively.

$$\rho_n = \alpha\rho_{air,outlet} + (1-\alpha)\rho_{water} \quad (5.38)$$

$$\rho_m = \alpha\rho_a + (1-\alpha)\rho_w \quad (5.39)$$

I

n

t

h

i

s
m
o
d
e
l
w
h
e
r
e
t
h
e
s
l
i
p
v
e
l
o
c
i
t
y
e
q
u
a
l
s
o
n

e
$(S = 1)$
f
o
r
t
h
e
c
a
s
e
o
f
a
h
o
m
o
g
e
n
o
u
s
f
l
o
w
a
s
s
u
m

p
t
i
o
n
,
w
h
i
l
e
x
r
e
p
r
e
s
e
n
t
s
t
h
e
a
i
r
m
a
s
s
f
r

action, α denotes the homogeneous volume

fraction of the air phase as:

$$\alpha = \frac{x}{x+(S(1-x)\frac{\rho_a}{\rho_w}} \tag{5.40}$$

The mixture mass flowrate is determined by using the following expression:

$$\dot{m} = k_{da}\, G_0\, A \tag{5.41}$$

k_{da} denotes the gas discharge coefficient and has been experimentally determined. According to Darby's work [84], this measured discharge coefficient was found to be close to unity in most safety valves carrying choked gases (about 0.975). This justifies the assumption that the choking point at full lift is the nozzle throat area, which is the basis for the determination of the mass flux. The critical flowrate is achieved at the maximum value of the mass flowrate at the outlet static pressure range. As a result of having a low water volume fraction for the range of water mass flowrates examined, the mixture critical pressure ratio was found to be close to the single phase air flow critical pressure ratio.
Consequently, the critical pressure ratio of the single phase flow was applied instead.

Figure 5.48 compares the predicted air mass flow by both the mixture and the Euler-Euler model against the experimental data, the HEM of Darby and the ISO standard ISO-4162-10 adopted the HNE-DS model proposed by Diener and Schmidt [87] for selection of safety relief valves used for two phase flow; at a piston lift of 5 mm and an upstream inlet pressure of 10.3 barg (150 psig) for a range of water mass fractions. Furthermore, the HNE-DS model has been also adopted for non-flashing two phase flows of air/water of this study based on the model equations presented in Appendix G. The figure shows that the two fluid approach is the most accurate and reliable model amongst the models examined. From the figure, the air mass flowrate predicted by the HEM developed by Darby is relatively acceptable compared to the CFD mixture model even though both models still underpredict the flow discharged with a maximum discrepancy of about 15%, particularly at medium to high liquid mass fractions. Furthermore, the predicted air mass flowrate by the analytical model of Darby is considered to be the closest to the mixture model with 8% underpredictions of the discharged flowrate. The figure also shows that the HNE-DS model significantly overpredicts the mass flow discharged from the valve under two phase flow conditions. In addition, this supports the

work of Elmyyah [88] who concluded that the HNE-DS model would overpredict the mass flow discharge particularly in this type of safety relief valves.

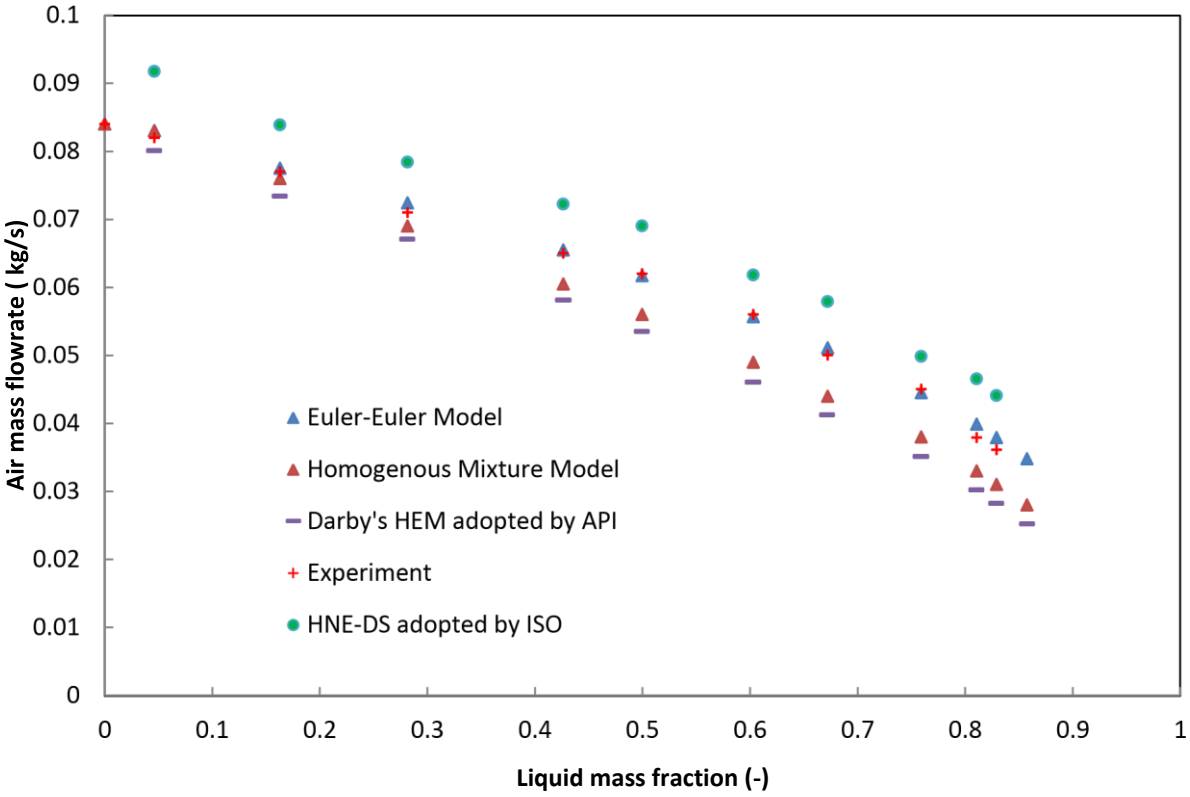

Figure5-48: Comparison between experimental data and the CFD predictions and the analytical model of Darby at an upstream stagnation pressure of 10.3 barg (150 psig) at 5 mm piston lift

5.6 Discussion

5.6.1 Flow-Lift Characteristics

Figure 5.49 experimentally presents the air mass flowrate against the piston position at both single phase and different water mass fraction. From the figure, the air flow-lift characteristics in the two phase flow behave similar to the air flow-lift characteristics in the single phase flow. This suggests that both single phase and mixture two phase flows have similar critical plane locations. As it can be noticed, there is an obvious reduction in the air mass flowrates with more water flowing through the valve.

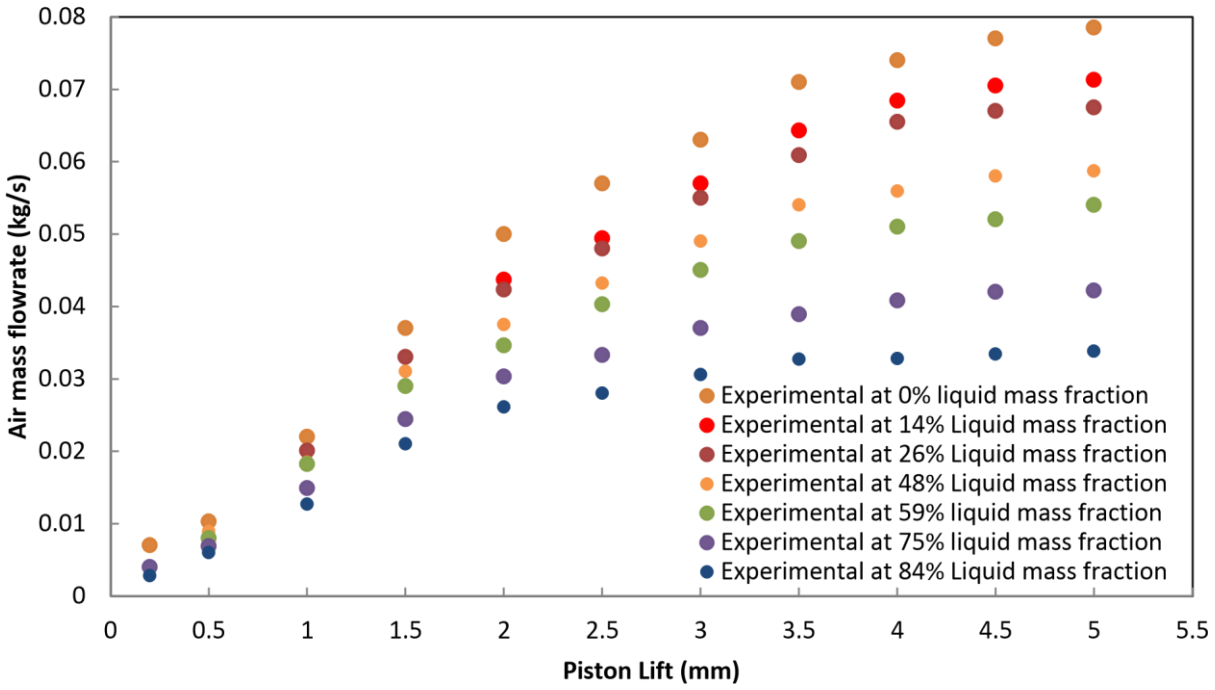

Figure5-49: The influence of the water flowrate on the air flowrate at an upstream stagnation pressure of 10.3 barg (150 psig)

This lower discharged air flow due to more water encountered into the valve could be justified by simply examining the one dimensional continuity equation of the flow at the choking plane where the Mach number of unity occurred.

$$\dot{m}_{air} = \alpha \rho v A \tag{5.42}$$

As the maximum discharged flowrate through the valve satisfies the critical mass flowrate for a wide range of pressure ratio, there should be a critical location with a flow area named the critical area $(A = A_c)$ which is constant for any water flowrate. In this critical plane, the flow velocity is equal to the speed of sound $(v = c)$hence a Mach number of one $(M = 1)$ is incurred therefore the air mass flowrate will be volume fraction dependent.

Figure 5.50 exhibits the water volume fraction at the choking location at a 3 mm piston lift and an upstream pressure of 10.3 barg (150 psig) for different inlet water volume fractions of 5% and 0.2%. From both cases (a) and (b) presented here, there is an indication of an annular flow (film flow) particularly at the piston front face even though the flow is still modelled as

dispersed. Noticeable, at a low inlet water volume fraction of 0.2% the water droplets do not affect the flow area available for the air to flow freely which leads to relatively higher air mass flowrates.

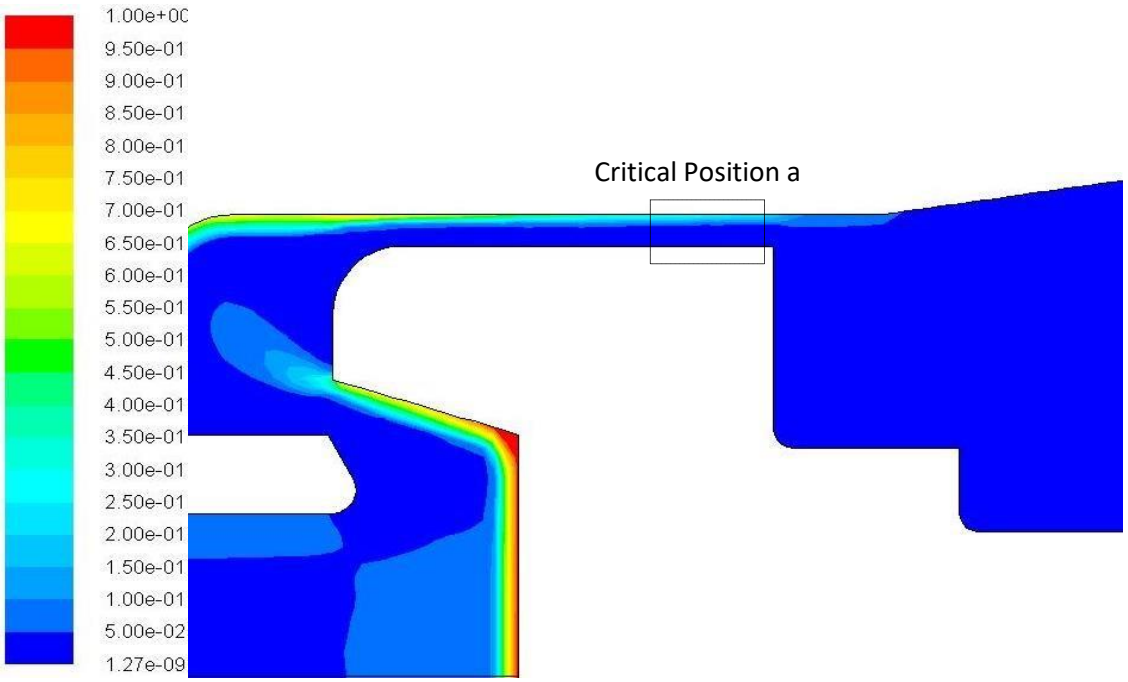

(a) Water mass fraction of 84% (5% inlet water volume fraction)

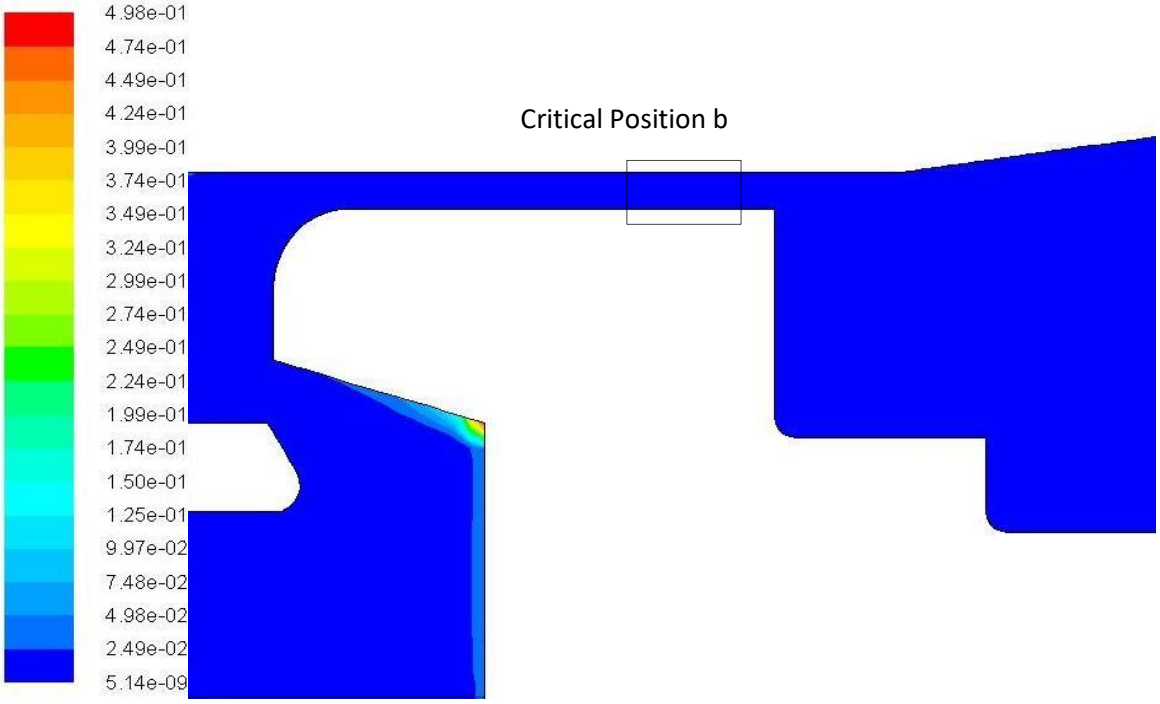

(b) Water mass fraction of 18% (0.2% inlet water volume fraction)

Figure5-50: Water volume fraction at a piston lift of 3 mm and an upstream pressure 10.3 barg (150 psig)

Figure 5.51 shows the deviation of the predicted mass flowrate by the Euler-Euler modelfrom the experimental data at an upstream inlet pressure of 10.3 barg (150 psig) for piston lifts of 1 mm and 5 mm. From the figure, the two fluid model apparently overpredicts the mass flowrate with a maximum discrepancy of 8% particularly at low lifts which might result from an improper mesh particularly at the piston seat where the geometry is more complicated to be represented exactly. On the other hand, the predicted results are in very good agreement with the experiment at 5 mm lift in particular with a maximum discrepancy of 4%, as shown in Figure 5.51.

To conclude, the predicted mass flowrates by the Euler-Euler model are in very good agreement with the experimental data, however, the aforementioned prediction deviations from the experiment particularly at high liquid mass fractions might be accounted for by different flow regimes and water dispersion.

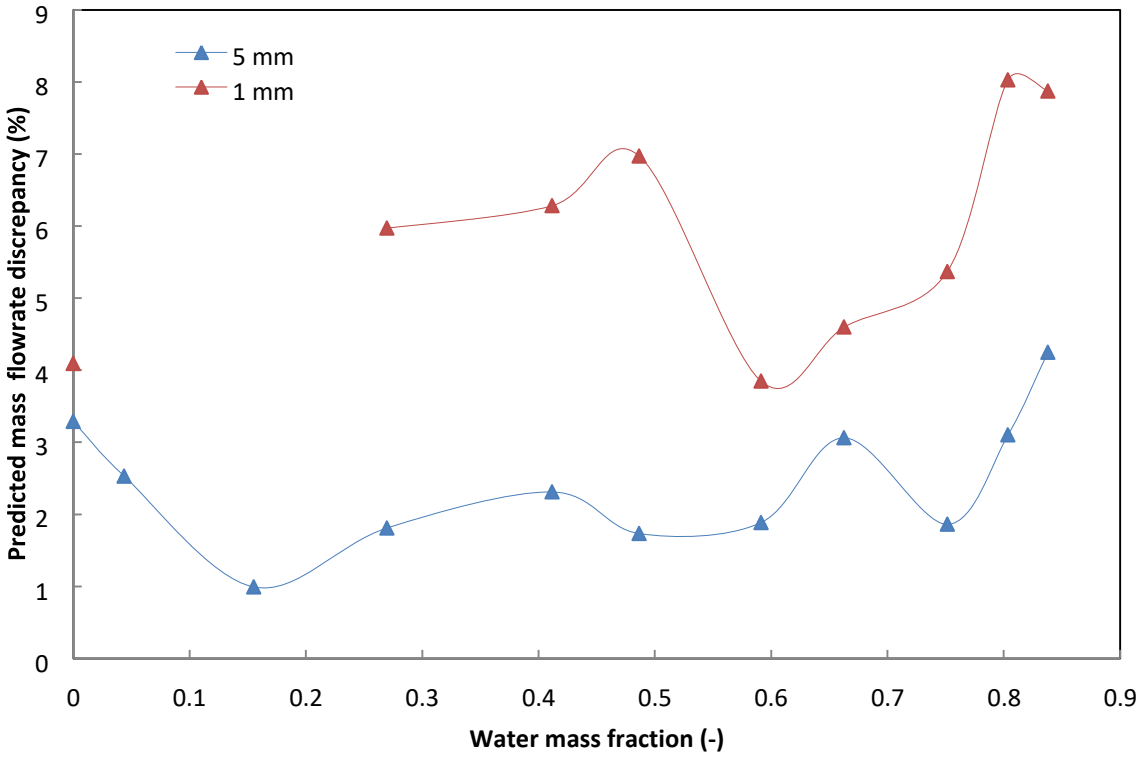

Figure5-51: Deviation percentage of the CFD predicted results from the experimental data at an upstream stagnation pressure of 10.3 barg (150 psig) for piston lifts of 1 mm and 5 mm

5.6.2 Force-Lift Characteristics

Figure 5.52 presents the force-lift characteristics at an upstream pressure of 13.8 barg (200 psig) and different liquid mass fractions. The figure shows that the piston force increases with piston lifts. This behaviour of the forces exerted on the piston valve could be classified into two stages: first, in the interval between 0.2mm to approximately 2mm lift; second, the interval of lift beyond the 2 mm lift up to a 5 mm lift where the valve is fully opened. In the first stage, there is a non-linear with slightly decreasing rate of net force. In the second stage, however, a steady increase of the net force is observed that ends with a fairly constant magnitude. Furthermore, the main difference in these two stages is dominated by some factors such as the flow area, choking plane position, resulting mass flowrates and back pressure. These factors play an important role in defining these stages and have been discussed in detail in Section 4.7.4.1. The figure shows that the single phase force, where the liquid mass fraction is 0%, has the lowest magnitude particularly at lower piston lifts in the range 0.2 to 1.5 mm. After these piston lifts, the single phase force increases with a relatively higher rate of the net force but its magnitude does not exceed the force of certain two phase flow conditions. In other words, for the higher lifts stage, the single phase force is noticeably below the two phase flow force particularly at two phase flow conditions that hold a liquid mass fraction of up to 25%. The net piston forces are determined by the pressure and piston surface shear forces. The viscous shear force is found to be very small in general, and acts only on the piston side face; in this case the magnitude is less than 0.9 N hence its influence on the net piston force is neglected.

The net piston force is mainly dependent upon the pressure magnitude and distribution on the piston surfaces particularly at the piston front face. In single phase flow conditions, the pressure value and distribution on the piston front face is only influenced by the air mass flowrate at a constant upstream pressure applied to all piston lifts. In two phase flow conditions, however, the pressure value and distribution is different as the second phase of the liquid does affect the magnitude and distribution of the pressure. An increase in the water content under two phase flow conditions leads to an increase in the pressure value on the piston front face which results in higher net forces. In the meantime, the air mass flowrate

decreases with an increase in the water mass flowrate as shown in Figure 5.49 and results in a net piston force decrease as shown in Figure 5.52.

To conclude, there are two factors in which the piston net force might be affected: surface pressure increase due to an increase in water flowrates and a pressure decrease due to decrease in the air flow. For two phase flow conditions at low lifts a small decrease in air flowrate due to an increase in water flowrate is encountered. This results in a net piston force increase, as shown in Figure 5.52. However, increase in the back pressure due to an increase in water flowrate results in higher forces exerted on the piston back face which leads to a reduction in the net piston force. This is mainly reliant on the adjusting gland of the valve which will be discussed in Section 5.6.3.

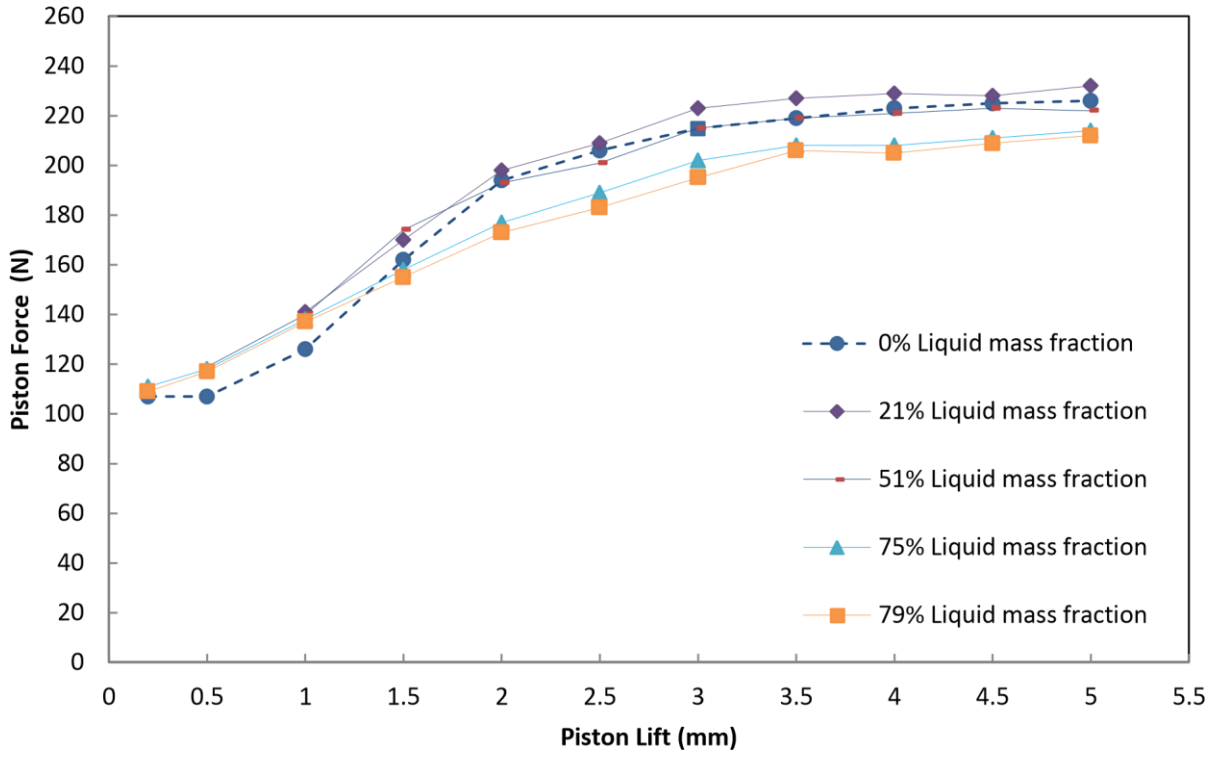

Figure5-52: Force-lift characteristics at an upstream stagnation pressure of 13.8 barg (200 psig) for various water mass fractions, with the modified gland

In terms of the pressure value, Figure 5.53 shows the predicted pressure distribution on just half of the piston front face at 2 mm lift and an upstream pressure of 13.8 barg for different water mass fractions. The pressure distribution pattern in all cases are fairly similar but with

different magnitudes. The two phase flow conditions show higher pressure values distributed all over the outer area of the front face of the piston while lower pressure values can be seen on the inner area of the piston front face and the piston edges. In fact, two thirds of the area is exposed to a higher pressure magnitude which leads to a higher force exerted on the piston front face under two phase flow conditions. The latter concept of obtaining higher front face forces should logically have introduced a higher net piston force particularly for the first stage of the force-lift characteristics. Although the pressure magnitude on the piston front face is relatively higher particularly at high liquid mass fractions, there is a reduction in the net piston force due to an increase in the piston back pressure. This increase in the piston back pressure is shown in Figure 5.54, which shows that the back pressure at an upstream pressure of 6.9 barg (100 psig) for piston lifts of 1 mm and 5 mm with the modified gland in place. The figure presents a comparison between the back pressure predicted by the CFD and the measured back pressure. As shown from the figure, there is a maximum discrepancy of approximately 8-10% between the experimental and the CFD back pressure. This maximum discrepancy appears particularly at higher lifts and higher liquid mass fractions. The figure also indicates that the back pressure acting on the piston increases when the piston lifts further and with the increase in the water mass fraction. This means that modelling of the gland is very important thus its influence on the back pressure and the associated piston forces will be discussed in Section 5.6.3.

Comparisons between the results of force-lift predicted by the Euler-Euler model and the experimental data are shown in Figures 5.33, 5.34, 5.35 and 5.36. These comparisons have been explained in detail in section 5.4.2. Accordingly, a maximum discrepancy of about 27N was found at two phase flow conditions for high liquid mass fractions at high piston lifts, which gives 16% overprediction of the net force. However, one of the significant reasons for the experimental results to deviate from the CFD predictions is believed to be due to the back pressure associated with the modified gland and the downstream flow regime. Although similar experimental method of single phase back pressure measurement is used for the two phase flow back pressure measurement, there is still inconsistency or even greater with the two phase flow conditions. The aforementioned maximum discrepancy between the experimental and predicted back pressure might be attributed to: firstly the proper representation of the gland geometry and the associated mesh issues through the simulation,

and secondly the buckling issues associated with the length of the tube which is mainly restricted to the lengths of the remaining components of the rig particularly the PVC T junction. Other issues can affect the experimental measurements such as alignment of the rig as it could result in friction force; however, it has been frequently checked.

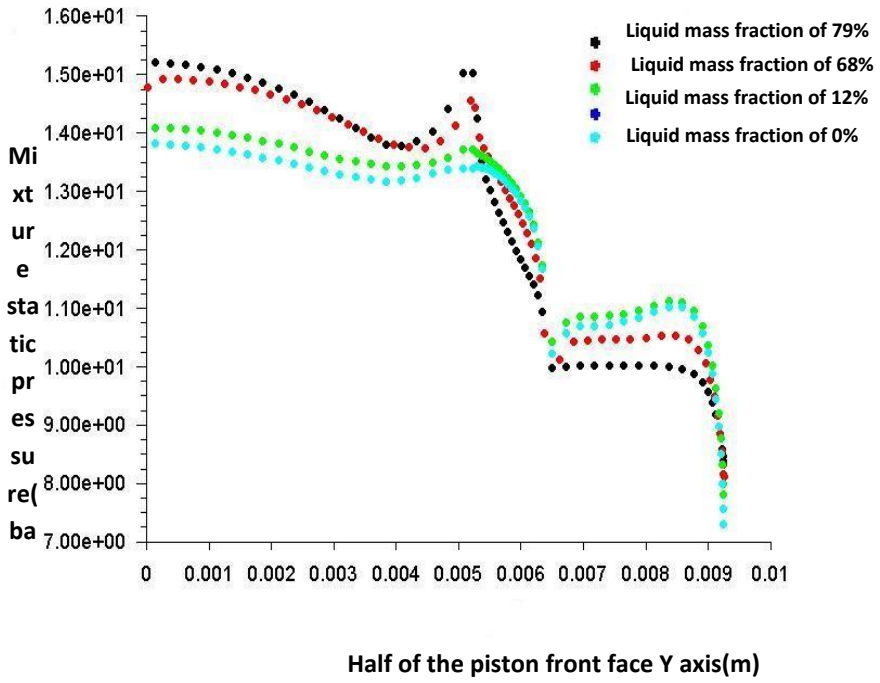

Figure5-53: Pressure distribution on piston face (half) at an upstream stagnation pressure of 13.8 barg (200 psig) and 2 mm piston lift

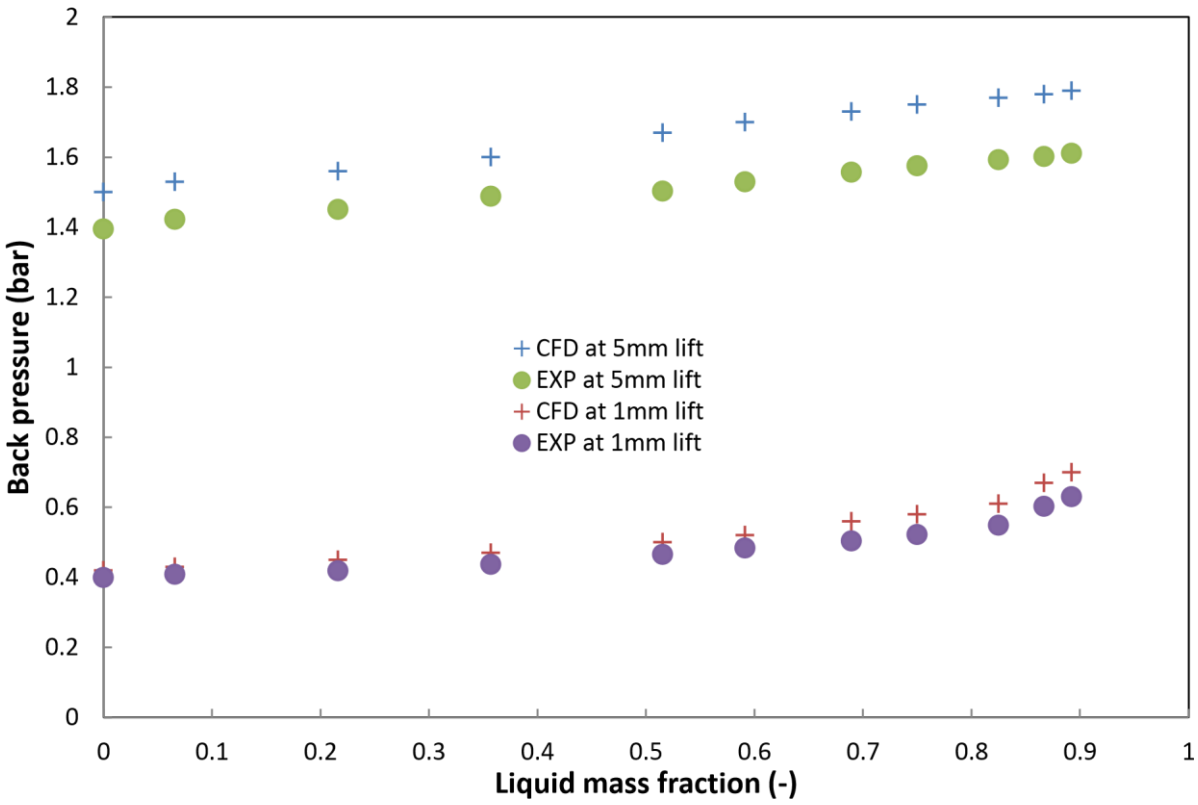

Figure5-54: Piston back pressure at an upstream stagnation pressure of 6.9 barg (100 psig) and piston lifts of 1 mm and 5 mm, with gland

5.6.3 Effect of the gland

Figures 5.13 and 5.14 compare the behaviour of the net piston force for the valve examined with and without the modified gland in place. The figures show clearly that higher net forces exerted on the piston valve can be obtained when the modified gland is removed and vice versa. However, the compression and expansion of the flow inside the valve and the occurrence of a shock wave downstream of the piston are mainly subjected to the adjusting gland of the valve (modified gland). To understand these effects the back pressure has been examined at different two phase flow conditions. Figure 5.55 shows the piston back pressure at a test pressure of 10.3 barg (150 psig) and different liquid mass fraction at a piston lift of 3 mm. The figure presents higher back pressure magnitudes with the modified gland in place due to a lower flow area and a greater restriction to the discharged flow. Hence the higher back pressure associated with the modified gland in place leads to a greater piston back face force, which results in a lower net force exerted on the piston valve.

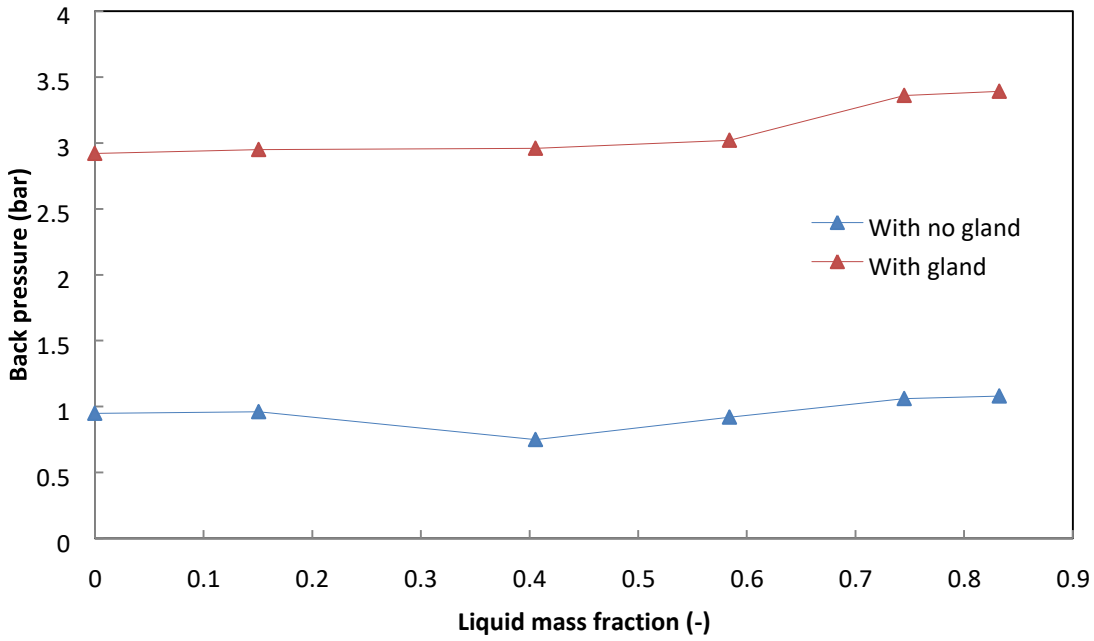

Figure5-55: Effect of the gland on back pressure at an upstream stagnation pressure of 10.3 barg (150 psig) and different inlet water mass fraction at 3mm lift

Figure 5.56 shows the back pressure-lift curve for the valve with no gland at an upstream pressure of 8.28 barg (120 psig) and different inlet water mass fractions. The Figure indicates that an increase in water quantity can result in an increase in the back pressure with higher magnitudes as soon as the piston lifts further. Although there is a relatively higher back pressure at lower piston lifts (0.2 – 2 mm) with high liquid mass fractions, as indicated in Figure 5.56, the net piston force under these conditions is still greater than the single phase force, as indicated in Figure 5.52. This can be justified as the piston front face at these circumstances would be exposed to a higher pressure magnitude, as shown in Figure 5.53, which will compensate for the effect of the back pressure. On the other hand, the back pressure will offset the increase in the pressure on the piston front face, to produce a lower net piston force at liquid mass fractions beyond approximately 40% at high piston lifts, as shown in Figure 5.54.

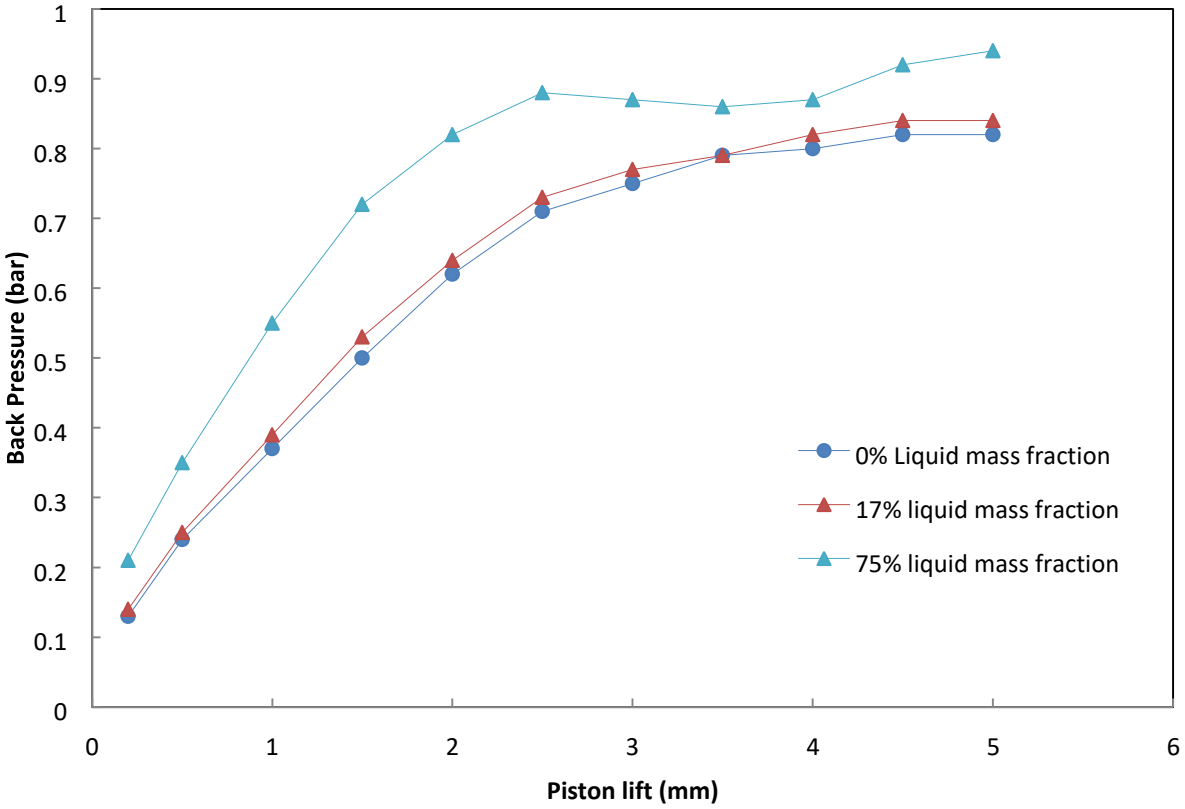

Figure5-56: Back pressure-piston position at an upstream stagnation pressure of 8.28 barg (120 psig) and different inlet water mass fractions, with no gland

Figure 5.57 shows the back pressure and piston force at different upstream inlet pressure of 8.28, 10.3 and 13.8 barg (120, 150 and 200 psig) as liquid mass fraction varies from 0 to 0.89 at a piston lift of 2 mm with the gland removed. As it can be seen, the higher upstream pressure magnitude applied provides a higher back pressure and a higher piston force. The figure also shows that with an increase in water quantity the back pressure will increase slightly until a decrease occurs at a certain liquid mass fraction which varies with the test pressure applied. The back pressure reduction results in a slight increase in the piston force, as shown in Figure 5.57. After that, an increase in the back pressure is noticeable with water quantity increase hence a reduction in net piston force occurs. In addition, the behaviour of the net piston force for the valve with the modified gland in place is similar to the behaviour of the net piston force when the modified gland is removed but with different magnitudes.

However, it is reckoned that the reduction in back pressure occurs due to the position of the downstream shock wave associated with the flow expansion. In other words, for each liquid

mass fraction case encountered the reduction in back pressure, the shock wave occurred downstream of the piston back face might exist further away from the piston back face, if it is compared to the other cases. This allows the flow to further expand from the piston back face and results in lowering the back pressure hence a higher net piston force results. It is noted, this sudden drop in the back pressure exists only with the removal of the modified gland at approximately 0.5 liquid mass fractions.

A similar study was carried out by Elmayyah [88], who did conclude that the flow is very sensitive to the flow path geometry. Therefore, a closer examination on how the back pressure can be influenced by the flow path geometry, and regions of compression and expansion of the flow associated with the modified gland should be addressed. This was achieved by looking at some contours of back pressure and Mach number with the modified gland in place and with no modified gland, as indicated in Figures 5.58 and 5.59, respectively. Although the removal of the modified gland is not practical, it is worth presenting here to draw the attention of the designers to the sensitivity of the flow to the flow path geometry. The two cases are presented here as case A for the valve with the modified gland and case B for the valve without the modified gland.

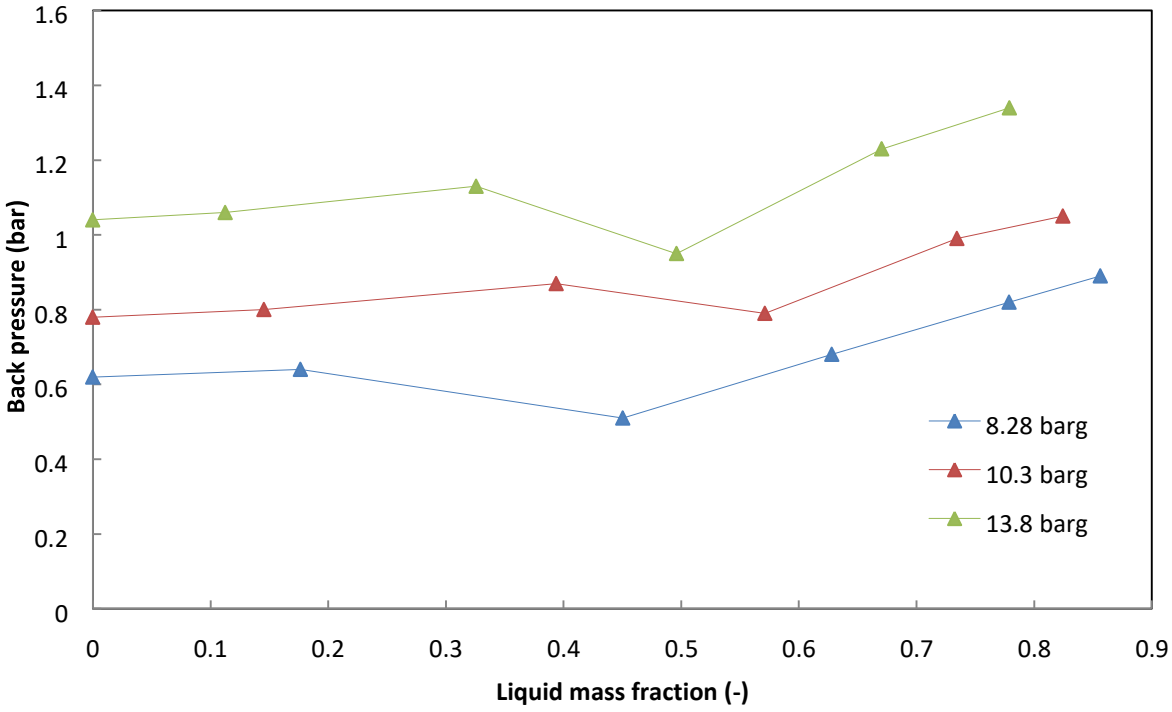

(a) Back pressure-liquid mass fraction

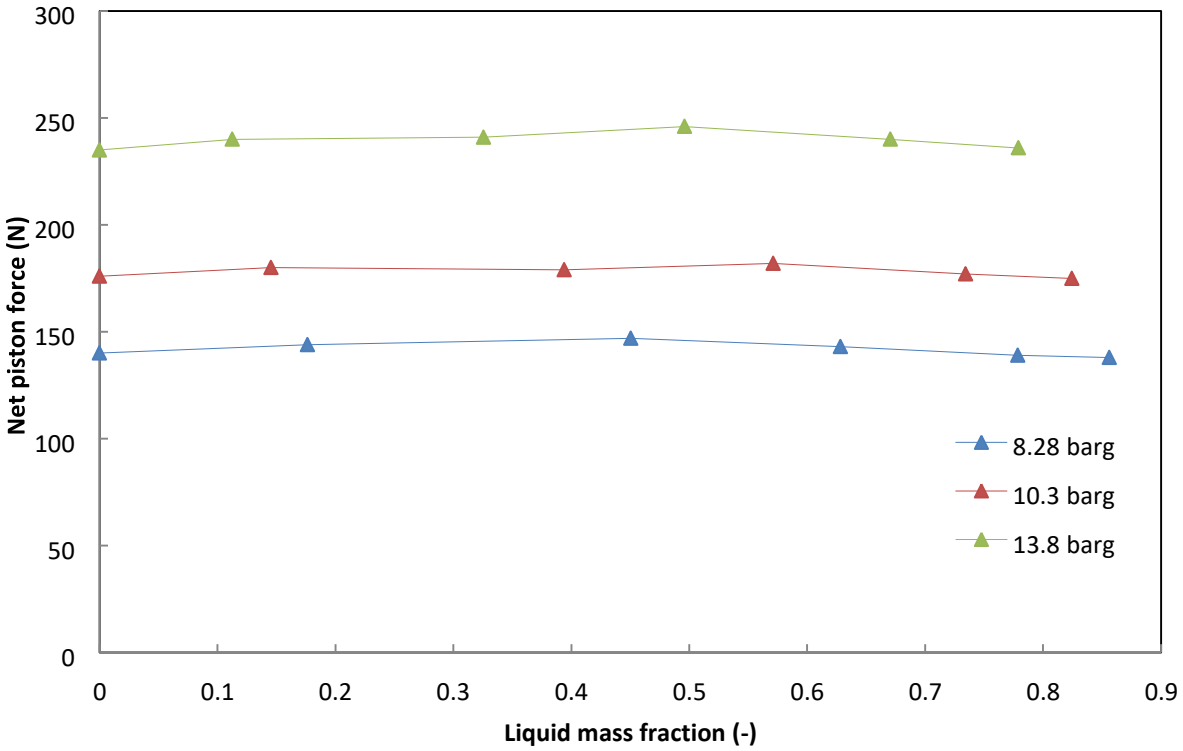

(b) Force-liquid mass fraction

Figure5-57: Back pressure and force at different upstream stagnation pressures and different inlet water mass fractions at 2 mm lift, with no gland

Figure 5.58 presents case A which investigates the static pressure and Mach number downstream of the piston, at an upstream pressure of 13.8 barg and a liquid mass fraction of 52% at a piston lift of 3.5 mm for the valve with the modified gland in place. Figure 5.59 exhibits case B which addresses the static pressure and Mach number downstream of the piston at the same two phase flow conditions and piston lift of the previous case of A but now with no modified gland. It is apparent that the pressure magnitude and pressure distribution on the piston back face are different in both cases. Although the compression waves of both cases exist at the same location; close to the end of the passageway between the piston and the valve body, the wave in case A is found to be less stronger than in case B. In both cases the flow undergoes an expansion downstream of the choking location (critical plane). From both cases, the direction of the flow expansion is significantly different. In the case A, the flow accelerates in parallel to the inclined wall of the valve for a short distance then a compression occurs as the flow is trapped by the existence of the modified gland, as indicated in Figure 5.58. This is followed by another expansion of the flow downstream of the modified gland. As

a consequence, this ensures a higher level of back pressure acts on the piston back face, as shown in Figure 5.58.

In case B, as indicated in Figure 5.59, the flow accelerates supersonically downstream of the piston but now towards the piston rod instead of the inclined wall of the valve. This results in a very high pressure gradient in the expanding wave collides with a compression wave over a relatively long distance. Therefore a standing shock wave associated with the aforementioned collisions can be identified. With the removal of the modified gland, however, the flow expands freely as there is comparatively no restriction this time, which leads to lowering the pressure magnitude acting on the piston rear face that affects the net force exerted on the piston.

The plot of the static pressure and the Mach number values along the valve walls indicates the shock wave establishment. Figures 5.60 and 5.61 exhibit the presence of the shock wave at nearly 0.041 m from the valve inlet, where the pressure suddenly rises and the Mach number drops from supersonic flow to subsonic flow. In addition, there is another strong shock wave noticed at the outlet of the valve and should be remedied by an attachment of a sudden expansion.

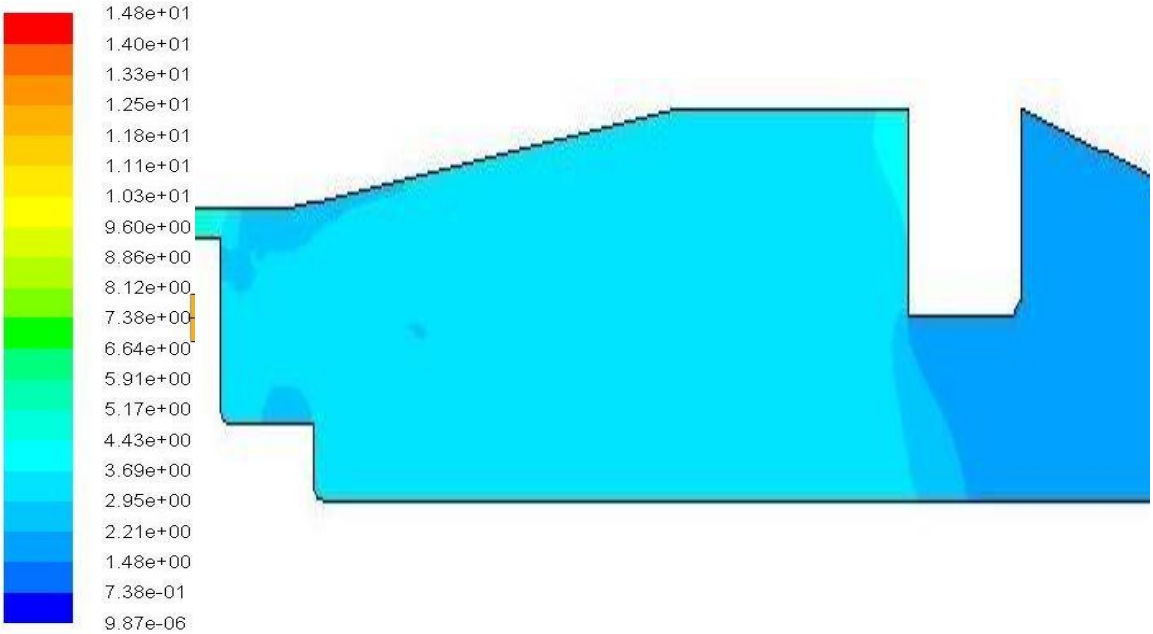

(a) Static pressure (barg)

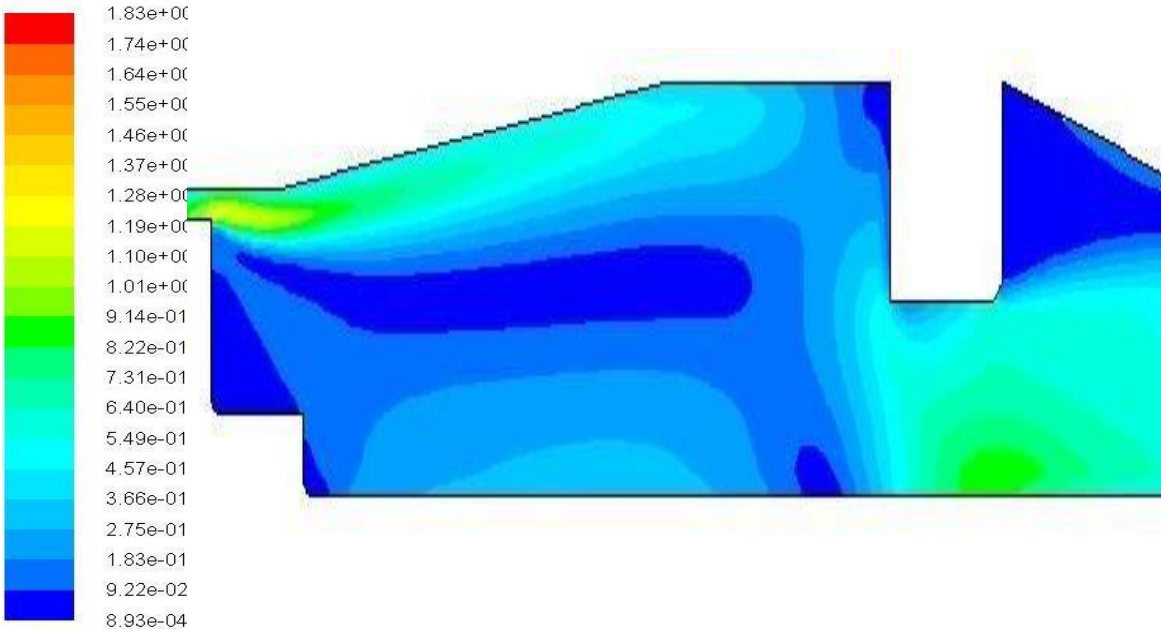

(b) Mach number (-)

Figure5-58: Contours of static pressure and Mach number at an upstream stagnation pressure of 13.8 barg (200 psig) and a liquid mass fraction of 52% at a piston lift of 3.5 mm, with gland (Case A)

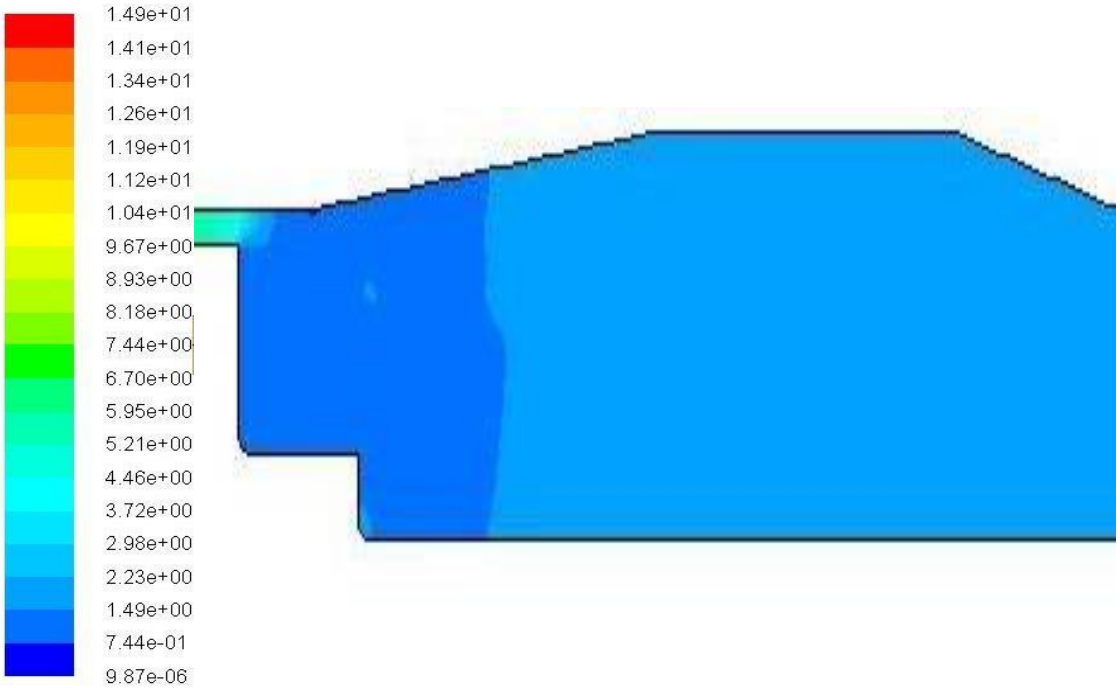

(a) Static pressure (barg)

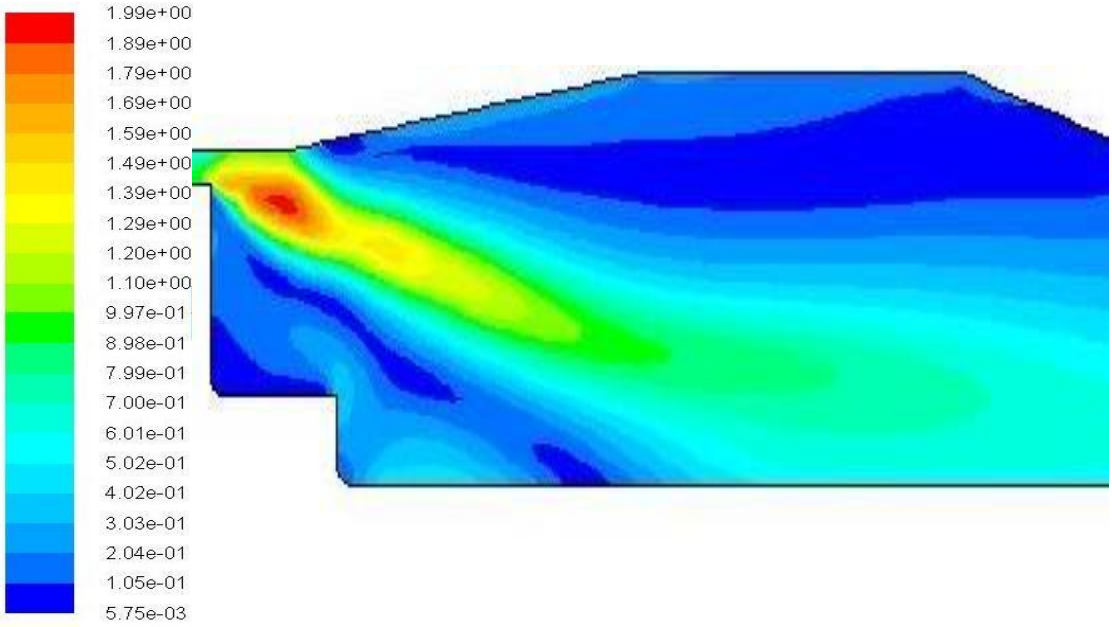

(b) Mach number (-)

Figure5-59: Contours of static pressure and Mach number at an upstream stagnation pressure of 13.8 barg (200 psig) and a liquid mass fraction of 52% at a piston lift of 3.5 mm, with no gland (Case B)

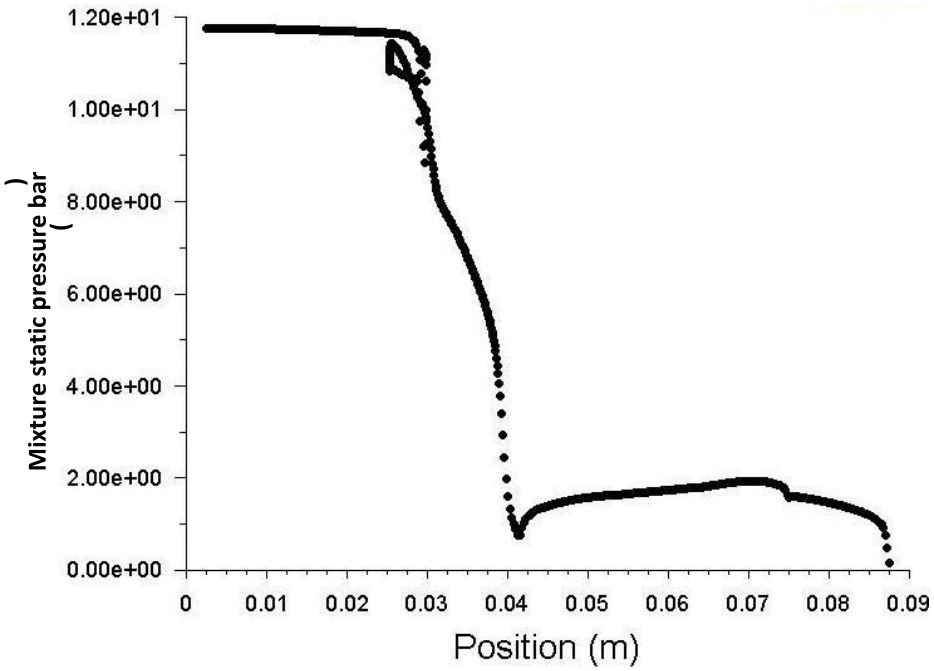

Figure5-60: Static pressure at the valve walls for an upstream total pressure of 13.8 barg (200 psig) and a liquid mass fraction of 52% at a piston lift of 3.5 mm, with no gland

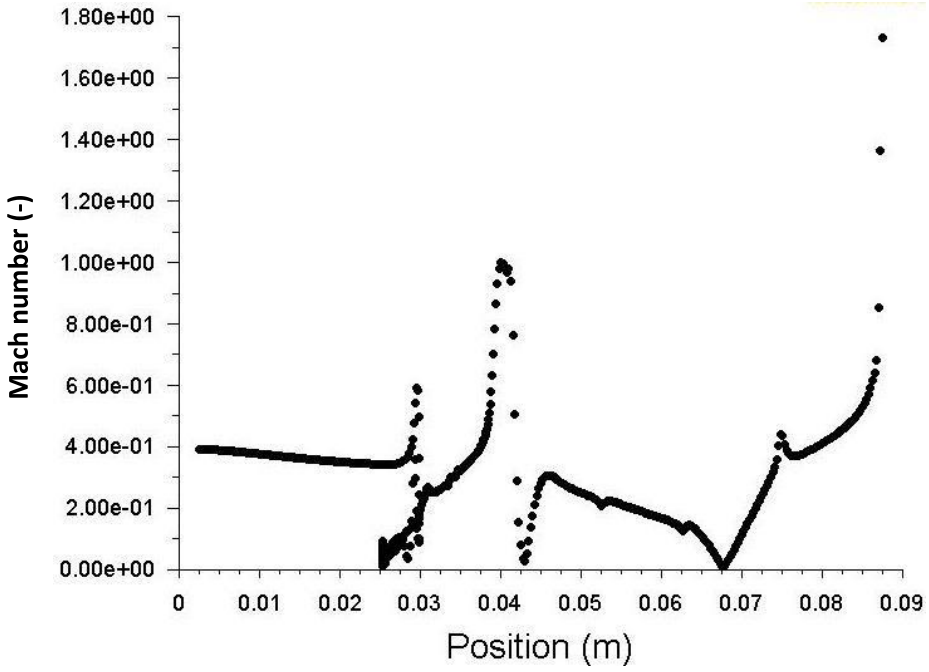

Figure5-61: Mach number at the valve walls for an upstream total pressure of 13.8 barg (200 psig) and a liquid mass fraction of 52% at a piston lift of 3.5 mm, with no gland

5.7 Scaling Approach for the Safety Relief Valve under Steady-State Two Phase Flow Conditions

The general approach of design and analysis of the safety relief valve applied to single phase flow conditions in Chapter 4, has been extended to two phase flow conditions. This is by means of normalising the flow-lift and force-lift characteristics of the cases of two phase flow conditions presented previously in this Chapter. For two phase flow conditions, the influence of the liquid content should be taken into consideration along with the changes in operation pressure and temperature. The normalised air flowrate and the piston force under two phase flow conditions will be discussed in the following section.

With regards to the normalised flow-lift characteristics, the pressure and the valve seat area were used to identify the flow-lift characteristics for single phase flow conditions at the available working pressures based on Eq.4.17. However, the same equation was implemented to determine the flow-lift characteristics for two phase flow conditions existing in this study. As a consequence, all two phase flow-lift curves achieved do not seem to collapse onto one

curve. In addition, the resultant flow-force curves were of about 48% uncertainty. Therefore the influence of the liquid mass fraction on the air flow-lift characteristics of two phase flows found to be of significance as discussed in section 5.7. To avoid the mentioned uncertainty particularly in air flowrate predictions under the two phase flow conditions tested in this study, the work of Elmayyah [88] was adopted to ensure less deviation in air flowrates. Thus an additional term based on an exponential approximation was added to Eq.4.17 to account mainly for the effect of the liquid content.

This term derived by Elmayyah [88] is$(e^{0.7\,x_{liquid}})$ was found to be successfully applied.

The normalised air mass flowrate scaling parameter would become as follows:

$$\dot{m}_N = \frac{\dot{m}}{P_0\ A_{seat}} \sqrt{T_0} e^{0.7\,x_{liquid}} \tag{5.43}$$

Where x_{liquid}denotes the liquid mass fraction (the water content in the mixture).

Using the above formula of 5.43 will reduce the maximum uncertainty in air flowrate predictions to approximately 12%. Hence Figure 5.62 shows the normalised air flow-lift characteristics for a wide range of two phase flow conditions. If a mean curve is created, this might reduce the maximum uncertainty of predicted air mass flowrate to about 6%.

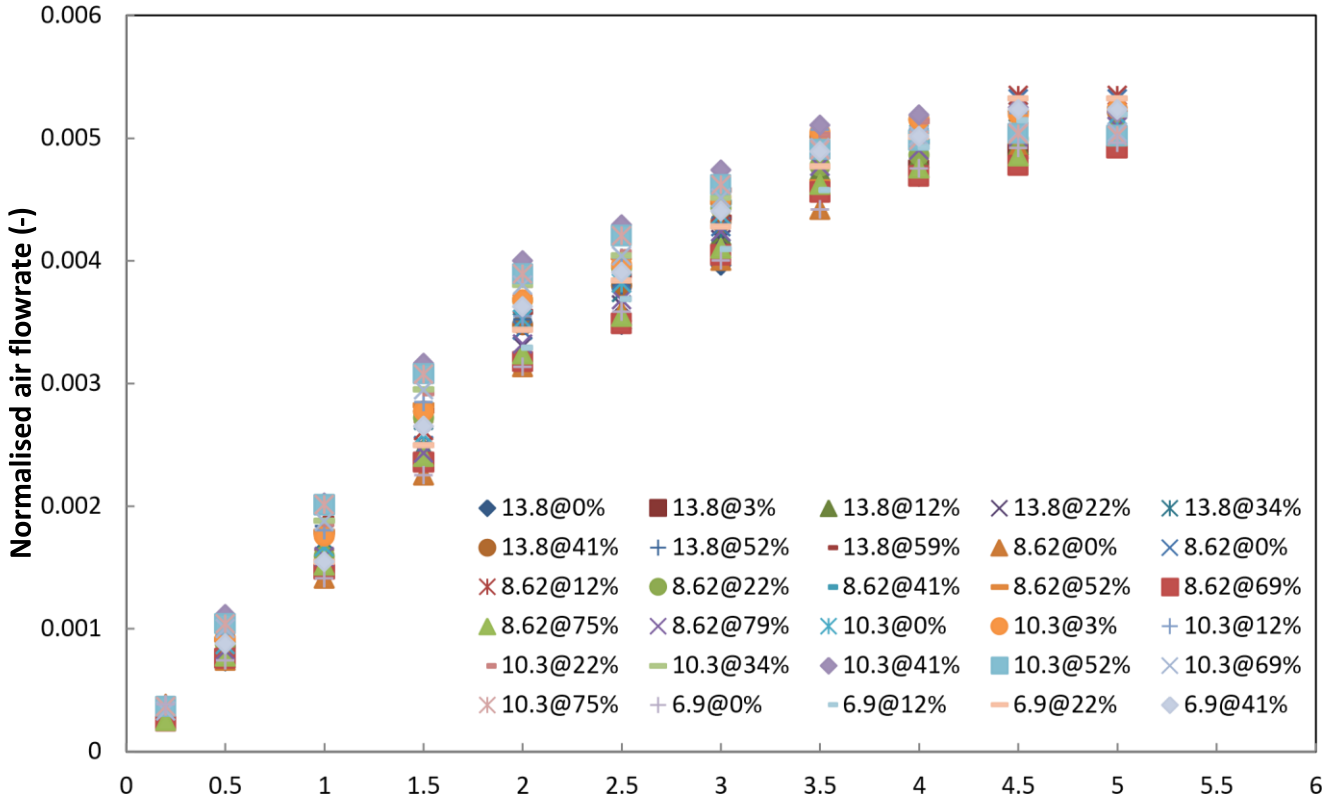

Piston lift (mm)

Figure5-62: Normalised flow-lift characteristics at different upstream inlet pressures and various liquid mass fractions

As far as the normalised force under two phase flow conditions is concerned, the normalised force-lift characteristics are obtained at all pressures by using Eq.5.44 that was applied for single phase flow conditions.

The following expression is used to identify the normalised force:

$$F_N = \frac{F}{(P_0 - P_{atm})\, A_{seat}} \tag{5.44}$$

The force characteristics under liquid injection conditions are shown in Figures 5.13 and 5.14for variations in liquid mass fractions at fixed lifts and again in Figures 5.16, 5.17 and 5.18for variation in piston lift. These figures show that the forces acting on the valve disc will decrease as the liquid mass flow increases. However previous studies conducted by Elmayyah [88] showed that the water mass flowrate has no significant effect on force-lift characteristics. In this study, the change is relatively minor for the cases shown and leads to an approximate reduction of less than 12% in force. This largely supports the results of Narabayashi et al [104].While the influence of the liquid on the forces is not considered significant from these cases, it is possible that more significant effects could result when considering the interaction of the disc force and spring forces. Figure 5.63 shows the normalised force-lift characteristics at all working pressures tested in this study with a maximum deviation of about 16%. The figure presents the data with a typical spring line included; the intersection of the curves is the steady state operating point for the valve at the corresponding pressure. This figure shows that for the observed variations in force–lift characteristics due to the considered liquid injection effects the intersection of the spring line can vary between 1.5 mm and 4 mm and for a variable two phase inlet condition would lead to notable oscillation in the disc if these variations were to occur. On the other hand, if a mean curve is obtained, the maximum uncertainty of predicted forces will be of about 8%.

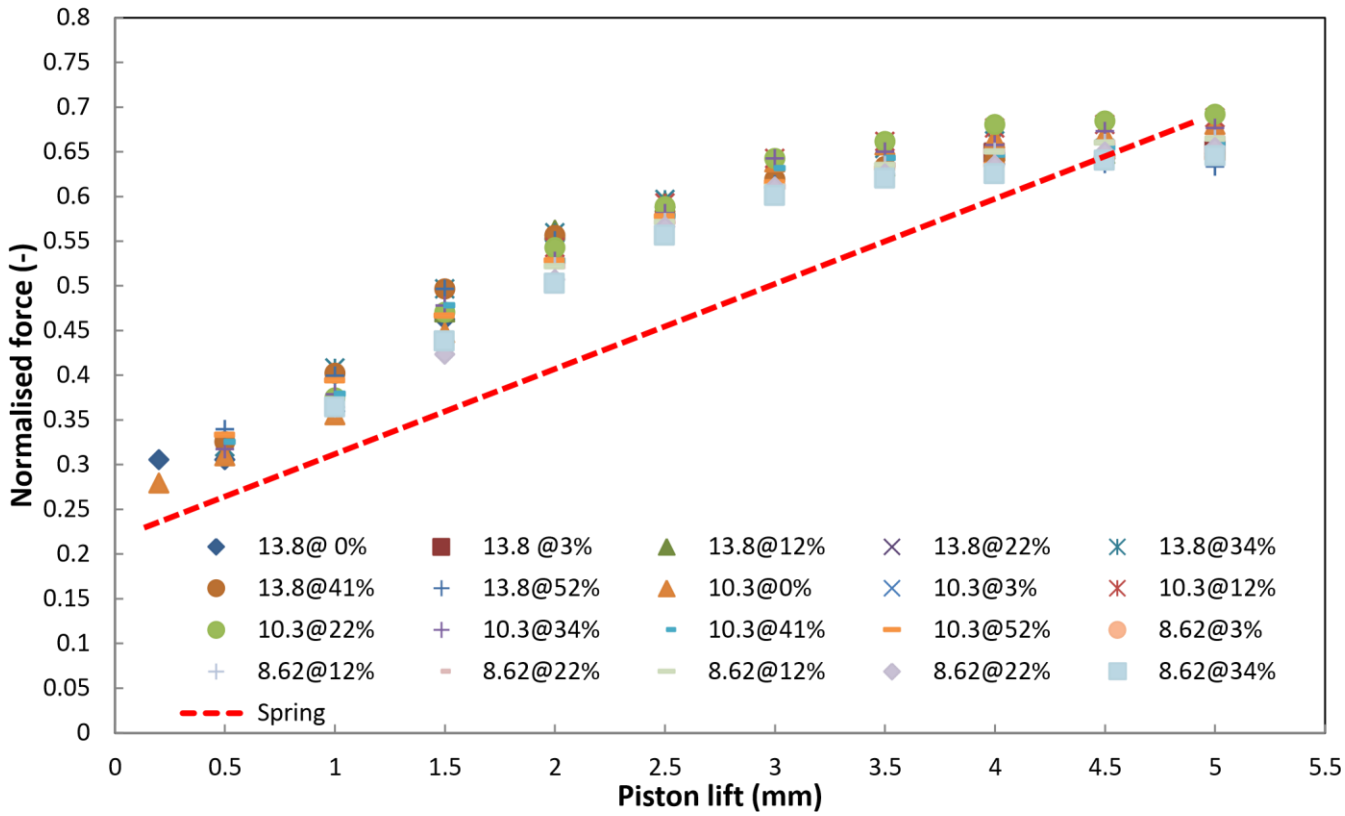

Figure5-63: Normalised force-lift characteristics at different upstream pressures and various liquid mass fractions

Chapter Six

6 Compressible Two-Phase Flashing Flow of Steam-Water Mixture

6.1 Modelling of the phase change process in safety valves; preliminary steps

In a wide variety of engineering systems such as heat transfer, power, transport or chemical engineering systems, the topic of two-phase flows whose optimal design and safe operation are of great scientific interest, becomes progressively significant.

The concept of critical flow conditions is fundamentally simple. In single phase gas flows, the critical condition is associated with a certain location in the flow domain where the Mach number is unity (gas velocity = acoustic velocity in the gas phase) and occurs at the smallest cross-section. The critical flowrate or choked flowrate is usually independent of downstream conditions. The mass flowrate increases until it reaches a maximum magnitude then remains constant even for a further decrease in the downstream pressure “backpressure”. The choked flow “critical flow” is far more complicated when encountered in two phase flows, hence the assumptions of isentropy and homogeneity assumed for single phase flows are no longer applicable. It is argued that there is a rapid change in the critical region, whose relaxation time for mass, heat and momentum transfer is of importance.

The modelling of flows in safety valves where phase change processes dominate has been carried out primarily with simplified models with very little effort devoted to using CFD based approaches. This chapter presents preliminary steps to investigate the basis process and the ability of the two fluid model to predict the phase exchanges occurring in the valves. To simplify the problem the study investigates the flows occurring under non-equilibrium conditions in a converging-diverging nozzle depicted in Figure 6.1. Specifically, the ability of established mechanical and thermal non-equilibrium two phase multi-dimensional modelling approaches to predict the critical two-phase flow conditions of steam-water through an existing converging-diverging nozzle are investigated. To overcome the essential difficultly of model validation, well-presented data based on the work of Charless [150] was used to assess the two fluid modelling approach. Details of the 2D converging-diverging nozzle used in this study, the modelling approach implemented, computational grid, boundary conditions and solution strategy and results and validation of the CFD model; will be presented in the following sections.

6.2 Convergent-Divergent Nozzle Details

According to what has been stated previously, it would be of interest to detail the converging-diverging nozzle used for this study. The following explanation of the apparatus and associated nozzle was cited in the study of Charless [150], whose experimental apparatus is schematically shown in Appendix D. In general, the rig has four main sections, which are: the air, steam and hot water supply, condenser and the test section. The test section consists of three major parts: a stagnation chamber, a spray chamber and a rectangular cross-section two-dimensional nozzle. The test rig was constructed to work under various flow conditions including single phase air, mixtures of air-water and steamwater. With regards to measuring systems, different devices were fitted to the rig to measure liquid and gas flowrates, inlet pressure and temperature and pressure distribution along the nozzle. A calorimeter was provided to ensure that steam delivered to the test section must be at the saturated state to avoid the occurrence of the more complicated process of the homogenous nucleation.

An important design objective of Charless's experimental programme was to achieve steam nozzle flow without the occurrence of nucleation, droplet growth and condensation shock, but ensure two phase non equilibrium conditions by the injection of the saturated liquid droplets. This was attempted by controlling the steam inlet condition and the steam

expansion by designing appropriate diverging section. As will be discussed later this was only partially achieved. It should be noted that the so-called “condensation shock” was expected somewhere in the divergent part of this supersonic nozzle, therefore considerable attention was paid by Charless to specification of the half-angle in the divergent portion of the nozzle to eliminate its occurrence on the nozzle.

Figure 6.2 depicts a detailed drawing of the nozzle. The nozzle was made of two blocks that were machined together from 1 inch thick brass plate. Nineteen pressure taps of 0.0625 inch diameter and 0.5 inch length were separately spaced 0.5 inch along the nozzle. These taps were connected to manometers through 0.125 inch flare fittings that were accommodated by a larger diameter threaded over the outer length of the taps. Ten of these taps were fitted into one block whilst the remaining taps in the other. The first and second tap was drilled in the straight section of the nozzle, one in each block; hence they were chosen as reference pressures.

A cross-section of the complete nozzle was cited in the work of Charless [150], as shown in Figure 6.3. Both ends of the nozzle blocks were attached to flanges made from brass. 0.25 inch brass back-up plates were used to hold the glass side-walls, made from 1 inch thick tempered Pyrex plate, against the nozzle blocks. To provide a good seal along the length of the nozzle, however, the glass was separated from the nozzle blocks by utilizing 0.03125 inch thick rubber gasket material. The gasket was placed in a 0.020 inch deep groove that machined into the upper and lower surface of the blocks. There was a difficulty in sealing the surface between the glass plates and the end flanges, therefore a 0.0625 deep groove was machined into the flange surfaces then filled with RTV-112 silicone rubber sealant.

As far as the flow domain is concerned, it is of importance to provide details of the nozzle contour. As illustrated in Figure 6.2, it consists of two straight sections that were connected by two circular arcs. The radii in the converging and diverging portions of the nozzle found to be R_1= 1.961 inch and R_2=0.283 inch, respectively. The angles in the converging and diverging parts of the nozzle were 29^{0}-58’ and 6^{0}-4’, respectively. In addition, the areas of the inlet, throat and exit of the nozzle were found to be 4.8498^2 inch, 0.7524^2 inch and 1.7815^2 inch, respectively. The nozzle assembly was held together by using braces and tierods, to ensure adequate sealing pressure over all contact surfaces.

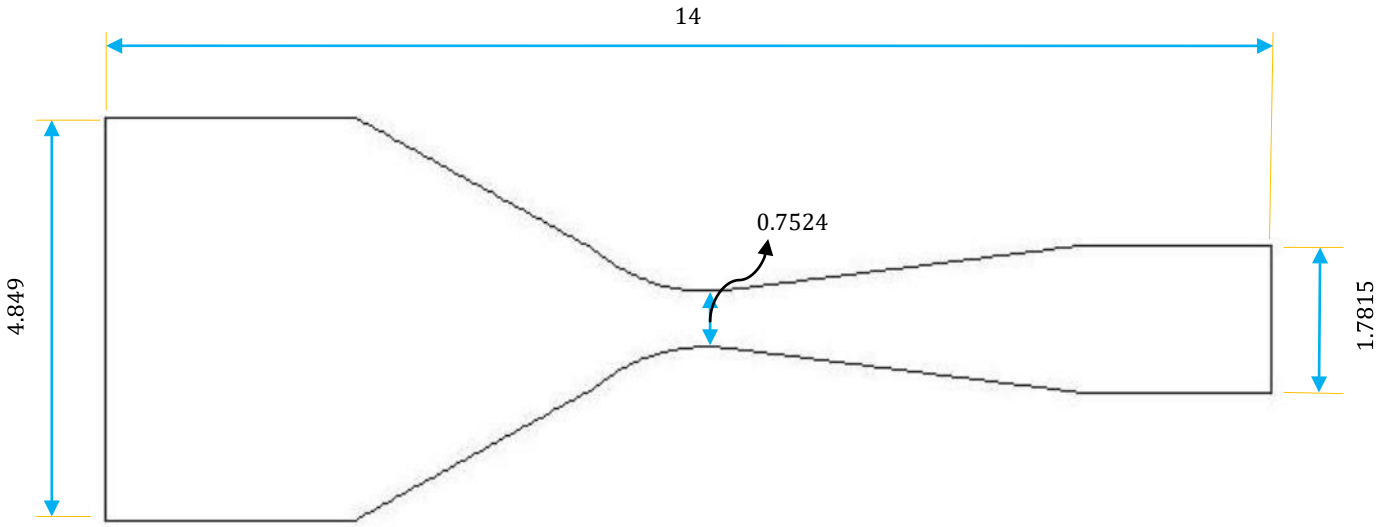

Figure 6-1: Dimensions of the nozzle (in inches)

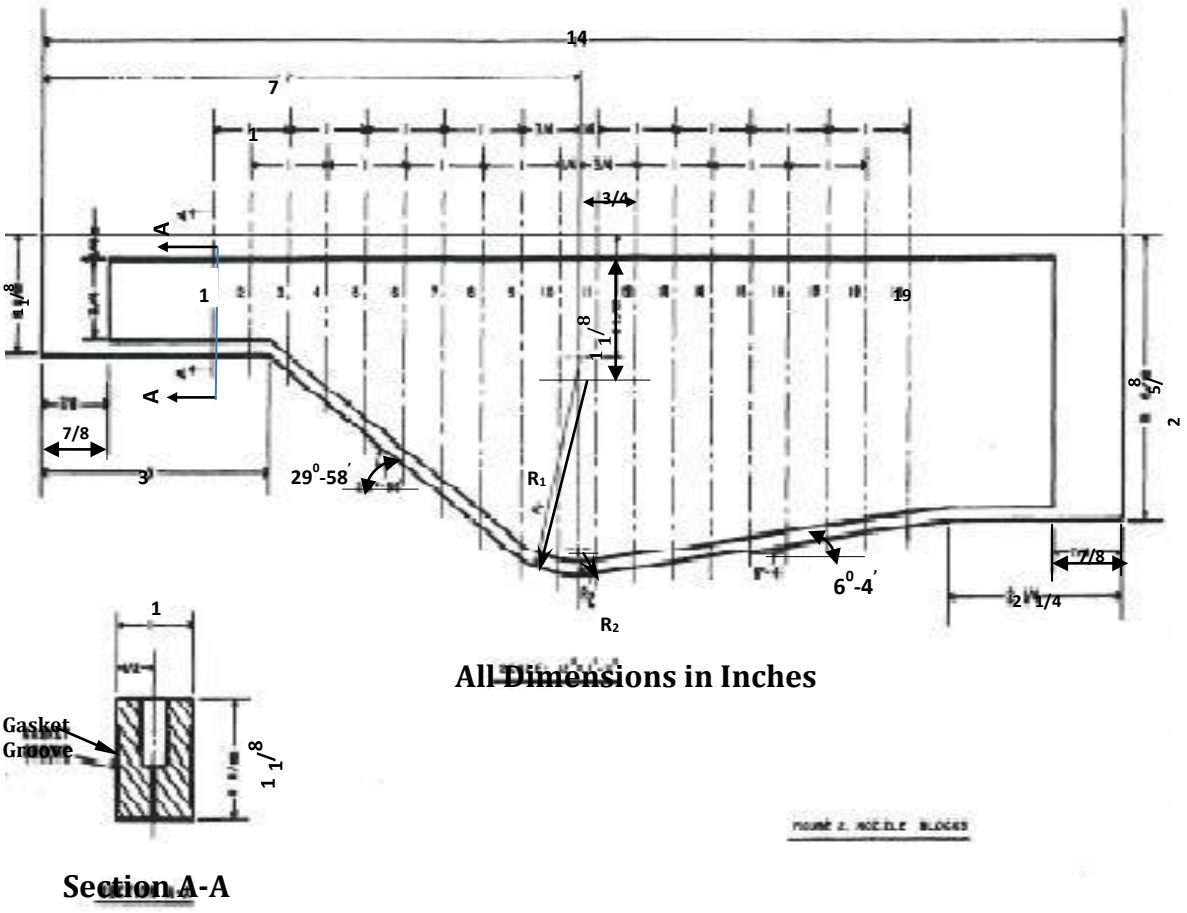

Figure6-2: A schematic diagram of the nozzle block [150]

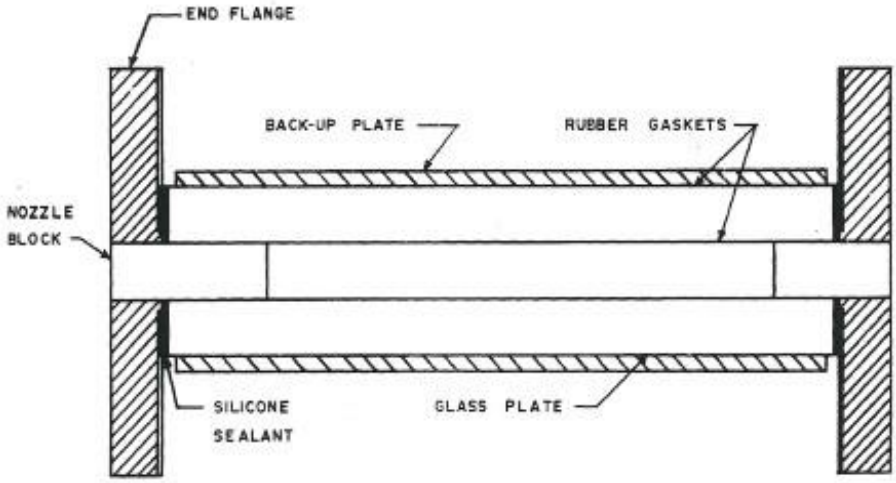

Figure6-3: A cross-section of the nozzle assembly [150]

6.3 CFD Modelling Approach

In this study both phases of the steam-water mixture were treated as a continuum based on the two fluid Euler-Euler approach. The second phase of water droplets is represented via equations that are developed in the form of volume averaged properties. The EulerianEulerian approach consists of a set of transport equations (continuity, momentum and Energy) for each phase and interfacial equations (drag, lift, slip and heat and mass transfer) to represents the nature of the interactions between phases.

6.3.1 Two Phase Flow model (Euler-Euler Model)

A pressure-based Eulerian-Eulerian multi-phase model was investigated to address thermal and mechanical non equilibrium effects of two phase flow conditions of high-speed supersonic turbulent steam-water mixtures. The numerical model was based on a full Navier-Stokes viscous flow solution procedure. The governing equations of the model are those previously described in Section 5.3.1, which are based in the Fluent 6.3 User Guide [126]. Standard models are used in all cases with interfacial drag determined by the drag coefficient model of Schiller and Naumann, [127] and the interfacial heat transfer based on the Ranz and Marshall's work [128]. A simplified approach to two phase turbulence is chosen based on a k-

ε mixture approach [126]. The so-called near-wall treatment was based on the standard wall functions, which are applied in terms of flow mean velocity and temperature for momentum and energy transport, respectively [126].

However, additional modelling to account for the mass transfer processes is required. The second term in the right hand side of Eq.6.1 is acquired based on the chosen mechanism; however, in the present case condensation may occur due to steam expansion resulting from the pressure drop along the fluid domain and supercooling conditions. Simultaneously there might be evaporation of the existing water droplets and depends on the degree of superheating as the pressure decreased. The liquid-vapour mass transfer is governed by the following vapour transport equation:

$$\frac{\partial}{\partial t}(\alpha\rho_v) + \nabla \cdot \left(\alpha\rho_v \overline{V}_v\right) = (\dot{m}_{l\to v} - \dot{m}_{v\to l}) \tag{6.1}$$

Where v is vapour phase, α is the vapour volume fraction, ρ_v is the vapour density, $\overline{V}_v$ is the vapour phase velocity and $\dot{m}_{l\to v}\ and\ \dot{m}_{v\to l}$ is the rate of mass transfer due to evaporation or condensation and has units of *(*kg/s/m^3). The mass transfer depends on the following temperature regimes as follows:

If $T_l > T_{sat}$

$$\dot{m}_{l\to v} = coeff * \alpha_l\rho_l * \frac{(T_l - T_{sat})}{T_{sat}} \quad \text{(Evaporation)} \tag{6.2}$$

If $T_v < T_{sat}$

$$\dot{m}_{v\to l} = coeff * \alpha_v\rho_v * \frac{(T_v - T_{sat})}{T_{sat}} \quad \text{(Condensation)} \tag{6.3}$$

However, the $coeff$ is a coefficient that needs to be fine-tuned and can be interpreted as a relaxation time. This coefficient can be theoretically quantified based on the so-called

accommodation coefficient and the physical characteristics of the gas particularly at near equilibrium conditions [126]. This also requires the interfacial area density to be identified. Establishing a value for the accommodation coefficient is not trivial and is usually achieved by matching experimental data. In this study the value was chosen to be 0.25 and was based on the work of Charless [150] who adopted the value from the work of Hickman [153]. Thus it was chosen to be 0.25 for both evaporation and condensation.

With regards to modelling of the interfacial heat transfer as described in Subsection 5.3.1.1.3, this requires the calculation of the Nusselt number and the Prandtl number. The latter dimensionless numbers depend mainly on the determination of the thermal conductivity and viscosity of steam phase. Therefore, thermal conductivity k_V w/m.k) and viscosity μ_V (kg/m.s) of the steam were determined based on the kinetic theory, according to the following correlations:

$$k_V = \frac{15}{4}\frac{R}{M_w}\mu_V \left[4\frac{C_p M_w}{15\,R} + \frac{1}{3}\right] \tag{6.4}$$

Where:

$M_w$is the molecular weight (kg/kmol), R is the universal gas constant (J/mol. K) and C_p is specific heat (kj/kg.k).

$$\mu_V = 2.67e-6\,(\frac{\sqrt{M_w \mathrm{T}}}{\sigma^2 \Omega_\mu}) \tag{6.5}$$

$$\Omega_\mu = \Omega_\mu(\mathrm{T}^*) \tag{6.6}$$

$$\mathrm{T}^* = \left(\frac{\mathrm{T}}{\epsilon/K_B}\right) \tag{6.7}$$

Where: The Lennard-Jones parameters, σ " characteristic length" (Angstrom) and ϵ/K_B "energy parameter" (K), are inputs to the kinetic theory calculation and for steam found to be 2.605 and 572.4, respectively [153].

6.3.2 Computational Grid

The nozzle geometry is presented as a 2D planar model with an unstructured mesh type as shown in Figure 6.4 that contains approximately 11486 elements with an approximate size of 1 mm, based on a triangular and quadratic cell type. The mesh is generated based on proximity and curvature advanced sized function with a fine relevance centre as well as a fine span angle centre. The generated mesh is also examined based on a mesh metric methodology of skewness and found to be 0.52 as a maximum value in only 92 elements all over the flow domain. An investigation into grid independence was performed where the results from the standard mesh (11486 cells) were compared with those of a mesh 2 times more dense with 23270 cells. The results are shown in Figure 6.5 and indicate that the 11486 cell mesh is grid independent as far as the mass flowrate is concerned. However, the 23270 cell mesh was found to give better mass flowrates predictions, with approximately 0.75-1.2% greater mass flowrate, than the standard mesh (11486 cells). Nevertheless, the standard mesh of 11486 cells was adopted for all cases due to delivering numerical solutions with less convergence time.

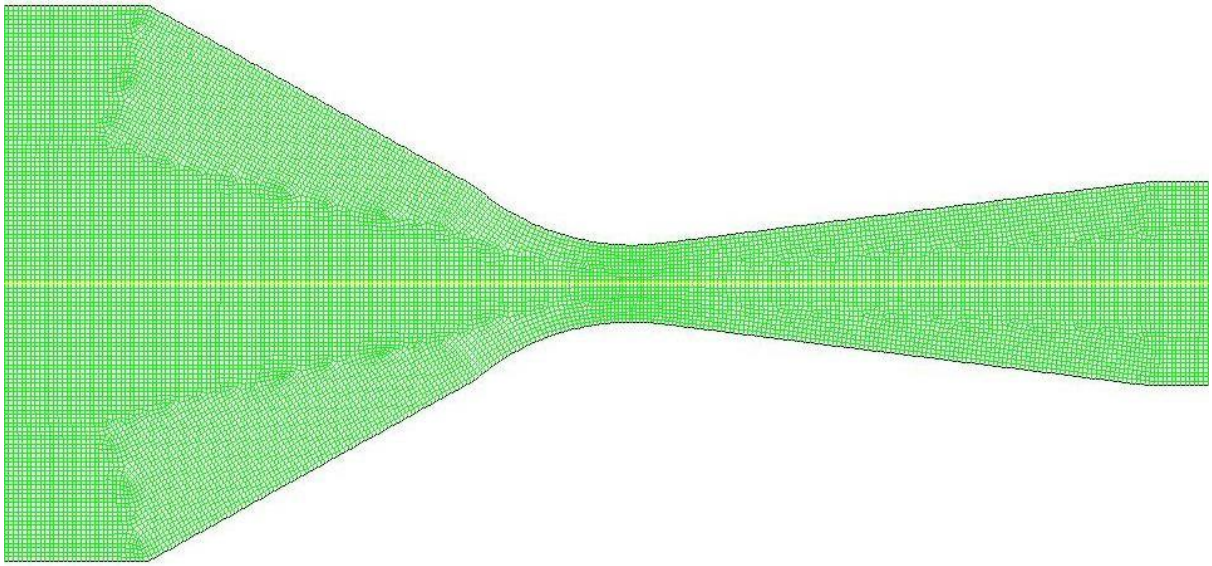

Figure6-4: The 2D convergent grid (The fluid domain)

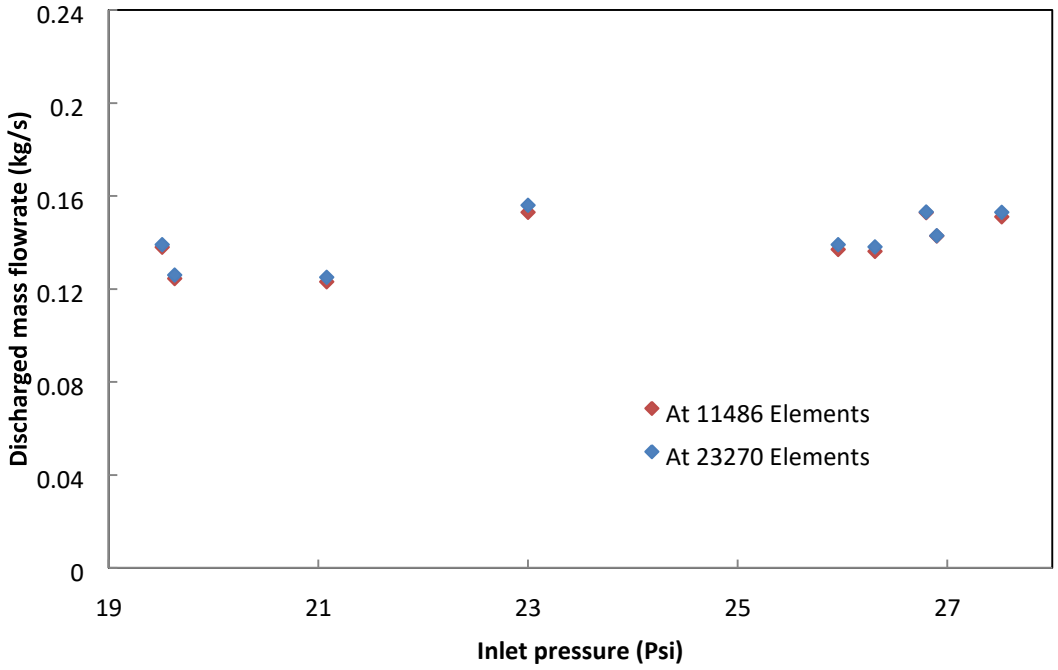

Figure6-5: Mesh independence study, CFD mass flowrates based

6.3.3 Boundary Conditions and Solutions Strategy

The two phase mixture of steam-water comprises steam at pressure P and saturated temperature T_v, and spherical droplets of water with a constant diameter D_d at saturated temperature T_L. There are three main zones in the computational domain; the inlet, specified as a pressure-inlet, the outlet specified as a pressure-outlet and the interior-fluid represented by the whole domain as a steam/water mixture. Other zones are considered as walls. At the inlet-pressure boundary condition, the total pressure of the mixture is specified in each case separately according to the experimental data. The testing pressure was in the range of 13.28 – 20.34 Psi (0.92-1.4 bar) for single phase flows of steam, 19.51-27.52 Psi (1.34-1.89 bar) for two-phase flow of steam-water mixtures, and 37.14-54.63 Psi (2.56-3.76 bar) for two-phase flow of air-water mixtures. The steam and liquid temperatures are set at the corresponding experimental values and are generally close to saturated conditions of the total pressure specified in the experiment. The liquid mass fraction has different values (from 0 to 0.36). As the mixture turbulence multiphase model is employed an initial guess values of κ and ϵ are set to be 0.1 (m^2/s^2) and 0.1 (m^2/s^3), respectively. The pressure-outlet boundary is set at atmospheric pressure. Also, initial values of κ and ϵ and the volume fraction of the water are to be equal to those of the pressure-inlet zone. The zones representing the walls are considered as stationary walls. The inlet pressure boundary has been used to apply both the inlet steam and water conditions. A uniformly distributed two phase flow has been assumed to represent the experiments and the one-dimensional homogenous equilibrium model for the determination of the inlet volume fraction, which is based on a mono-dispersed single diameter droplet size modelling. Each inlet cell is set to the experimental inlet saturated pressure and temperature, and a volume fraction established to inject an appropriate amount of liquid corresponding to a test condition. The volume fraction was calculated based on the theory of homogenous void fraction of Eq.6.8 and found to deliver self-consistent results. In addition, Eq.6.9 is used to calculate the gas mass fraction.

$$\alpha=\left[1+\frac{(1-x)}{x}\frac{\rho_G}{\rho_L}\frac{U_G}{U_L}\right]^{-1} \tag{6.8}$$

Where

x : denotes the gas mass fraction

$$x=\frac{m_G}{m_G+m_L} \tag{6.9}$$

While, m_G and m_L are the mass flowrates of the gas and the liquid, respectively.

This adequately sets the phase inlet boundary conditions to those in practice but does not directly correspond to the test conditions where a liquid inlet mass flow combined with a steam pressure inlet would have intuitively been more representative. As mentioned in the previous study of two-phase air-water flow, this was found not to give physically correct results and is believed to be a code related issue. With regards to the solution strategy, the solution method used was the steady-state pressure-based solver for segregated iterative procedure of the popular phase coupled SIMPLE method to resolve the pressure-velocity coupling in the flow. A Green-Gauss cell based spatial discretization for the gradient was implemented and a second order upwind spatial discretization for the density, momentum, turbulent kinetic energy, turbulent dissipation rate and energy gradient terms, whereas the volume fraction was discretized based on a first order upwind scheme to ensure a more stable convergence. In addition, the solution is initialized by a hybrid initialization method to obtain accurate results, then being controlled by lowering the under-relaxation factors. The energy equation was not solved for the first 100 iterations, to ensure initial stability. In terms of convergence criteria, all cases have converged with threshold values in the order of 10^{-7} for all variables except for mass continuity which was in the order of 10^{-4}. In addition, the convergence time for all cases was around 37 mins on 8GB desktop PC consisting of 4 parallel processors with 11486 element proximity and curvature mesh adopted. However, the above calculation procedure was repeated for further validation purposes using the airwater mixtures from the work of Charless [150].

6.4 Euler-Euler CFD Model Results and Validation

The following results are presented on the basis of examining the predictive capability of the two-fluid model for critical single and two phase flow conditions on the convergingdiverging nozzle illustrated above. Tables 6-1, 6-2 and 6-3 present test conditions of the working fluid, which vary from single phase to two phase flow conditions.

Table 6-1: Summary of Air-Water Data:

Run	Upstream inlet pressure (Psi)	Inlet temperature of air and water (K)	Inlet air mass fraction(-)
Air-water_1	52.14	302.66	0.915
Air-water_2	50.84	302.72	0.894
Air-water_3	54.63	290.11	0.901
Air-water_4	37.14	293.11	0.867
Air-water_5	41.19	290.28	0.861
Air-water_6	47.90	290.17	0.882
Air-water_7	47.64	290	0.899
Air-water_8	39.66	290.72	0.898
Air-water_9	49.90	289.22	0.908

Table 6-2: Summary of Steam-Water Data:

Run	Upstream inlet pressure (Psi)	Inlet temperature of steam and water (K)	Inlet steam mass fraction(-)
steam-water_1	21.08	383.61	0.788
steam-water_2	19.63	381.5	0.727
steam-water_3	26.90	391	0.871
steam-water_4	26.31	390.33	0.890
steam-water_5	27.52	391.72	0.834
steam-water_6	25.96	389.89	0.873
steam-water_7	26.80	390.88	0.795
steam-water_8	23	386.22	0.680
steam-water_9	19.51	381.28	0.641

Table 6-3: Summary of Single-Phase Steam Data:

Run	Upstream inlet pressure (Psi)	Inlet temperature of steam(K)
steam_1	14.98	396.94
steam_2	18.51	398.83
steam_3	13.28	391.39
steam_4	17.77	390.61
steam_5	17.44	393.22
steam_6	20.34	387.67

steam_7	**14.48**	**378.89**

Figure 6.6 shows the critical mass flowrate of single-phase flow of superheated steam at different upstream inlet pressures that lie in the range of 13-21 Psi (0.9 –1.45 bar). The figure indicates that an increase in upstream inlet pressure leads to the critical mass flowrate increase. The figure also exhibits a comparison on steam mass flowrate between experimental data of Charless [150] and the current two fluid model. However, in the same figure, the two fluid model of Euler-Euler CFD model underpredicts the mass flowrate of steam with a maximum discrepancy of about 8.3% for the range of upstream inlet pressures investigated.

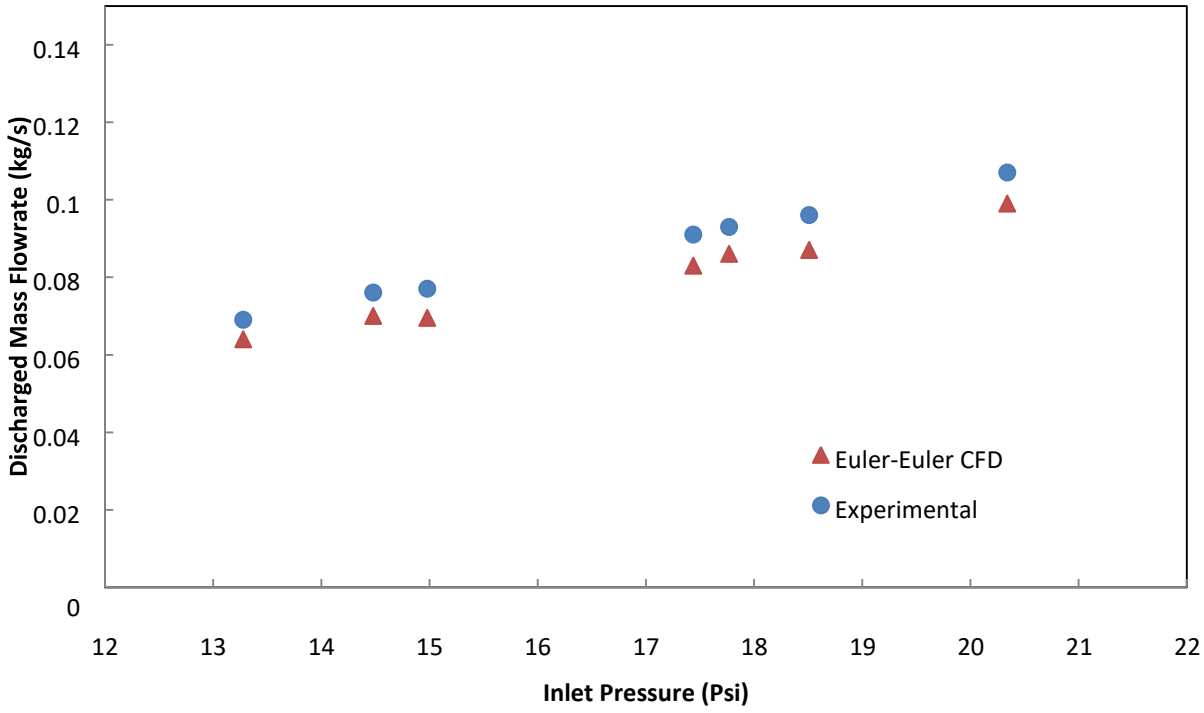

Figure6-6: A comparison between experimental data and CFD Euler-Euler model for predictions of mass flow discharge for single phase flow of superheated steam at different upstream pressures

Figure 6.7 presents the total mass flowrate of two-phase flow of steam-water mixtures at different upstream inlet pressures of 19-28 Psi (1.31-1.93 bar) and various water mass fractions of 0-0.36, which are specified in the Euler-Euler CFD model cases according to experimental data tabulated in the Charles's work [150]. However, the total mass flowrates

predicted by the mechanical and thermal non-equilibrium Euler-Euler CFD model fall within the range of experimental data with a maximum deviation of around 4-5% , for the given inlet pressure range.

Further verification to the predictive capability of the two fluid model of Euler-Euler CFD can be achieved by examining the critical mass flow predictions of two phase flow of air-water through the converging-diverging nozzle. Figure 6.8 shows the total mass flow discharge of two phase flow of air-water mixture for a pressure range of 37-54 Psi (2.55 – 3.72 bar) and for the same liquid mass fraction range used for the above mentioned two-phase flows of steam-water mixture. Again, the two fluid model of Euler-Euler CFD underpredicts the total mass flow discharge within 4-5%, for the range of upstream inlet pressures studied here.

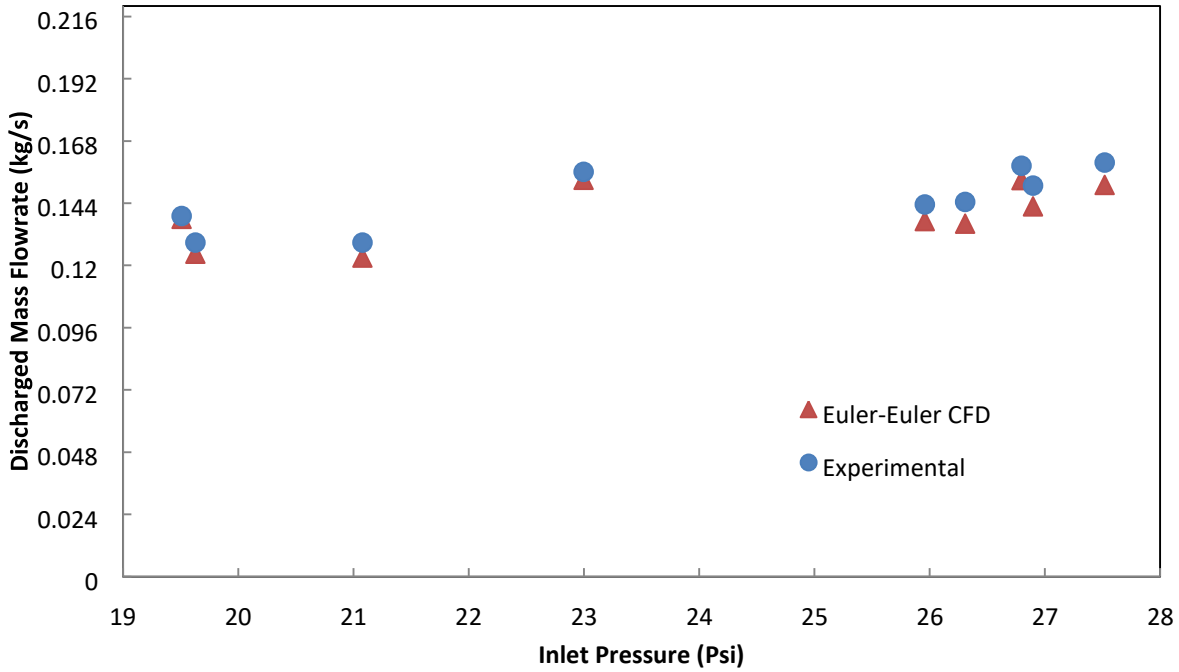

Figure6-7: A comparison between experimental data and CFD Euler-Euler model for predictions of total mass flow discharge of two phase flow of steam-water at different upstream pressures

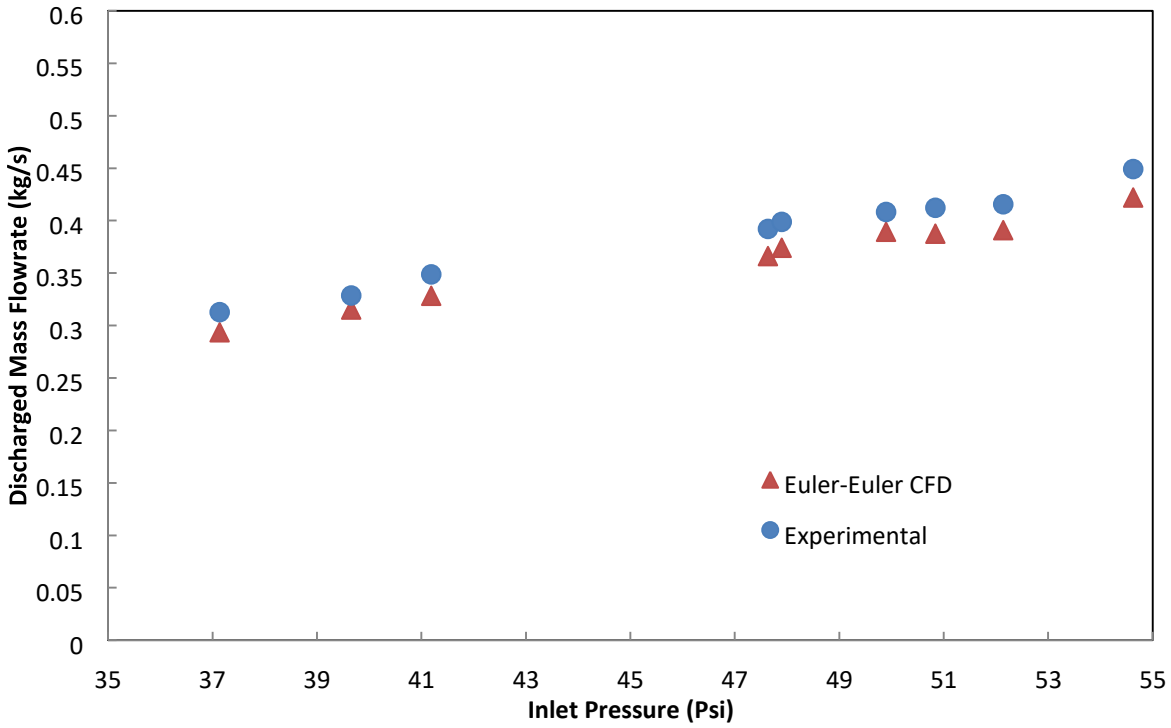

Figure6-8: A comparison between experimental data and CFD Euler-Euler model for predictions of total mass flow discharge of two phase flow of air-water at different upstream pressures

Figure 6.9 presents the contours of Mach number of steam-water mixture at an upstream inlet pressure of 21.08 Psi (1.45 bar) and an inlet liquid mass fraction of 0.212 whereas the critical flow (choking) conditions obviously appear close to the nozzle throat or might be slightly further downstream of the nozzle throat. This latter concept of critical conditions occurrence would obey the “internal Raleigh flow theory” whenever sufficient heat transfer between the phases has incurred.

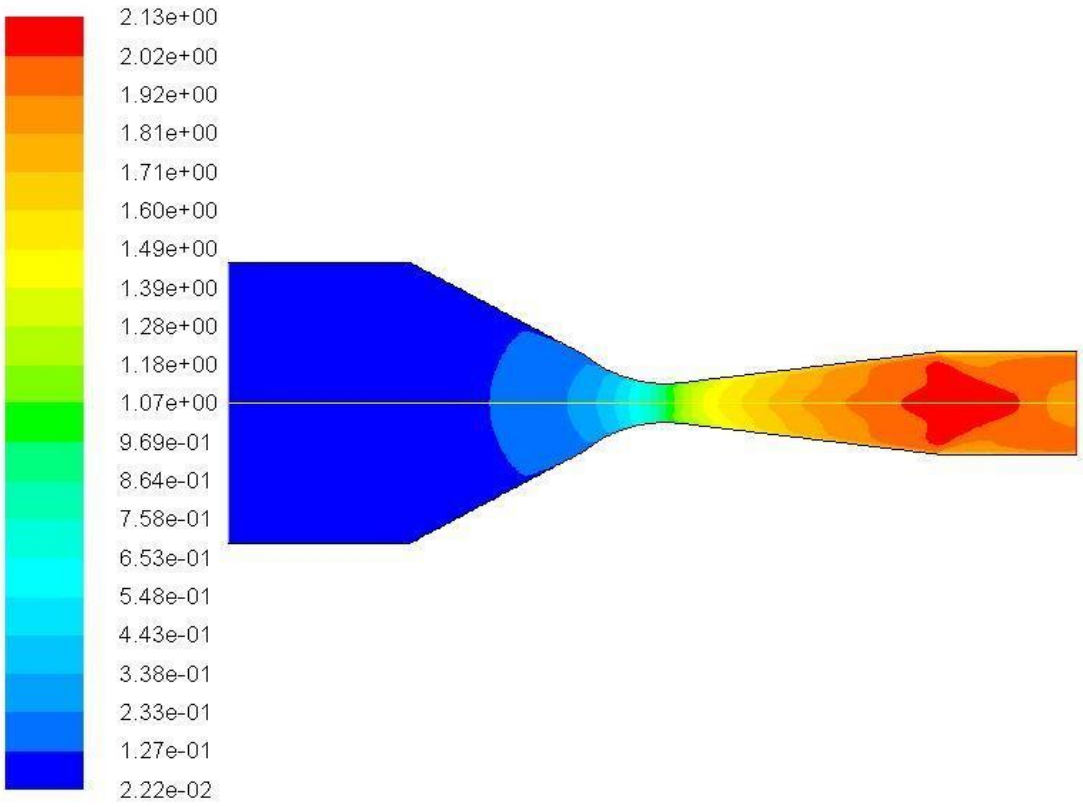

Figure6-9: Contours of Mach number at upstream pressure of 21.08 Psi (1.45 bar) and an inlet liquid mass fraction of 0.212

Figure 6.10 shows the static pressure contours of steam-water mixture at an upstream inlet pressure of 27.52 Psi (1.90 bar) and an inlet liquid mass fraction of 0.166. The figure presents a compression stage which occurs in the converging part of the nozzle, followed by further expansion to near atmospheric conditions as the flow passes the nozzle throat towards the diverging portion of the nozzle. However, there is a slight increase in pressure that is apparent at the end of the diverging section, as shown in Figure 6.10. This might result from a condensation shockwave. In addition, the static pressure along the centreline of the nozzle is presented in Figure 6.11. The figure shows a sudden risen in pressure at the end of the diverging portion of the nozzle. This sudden increase in the pressure vanishes as the flow expands further to an atmospheric pressure at the nozzle exit.

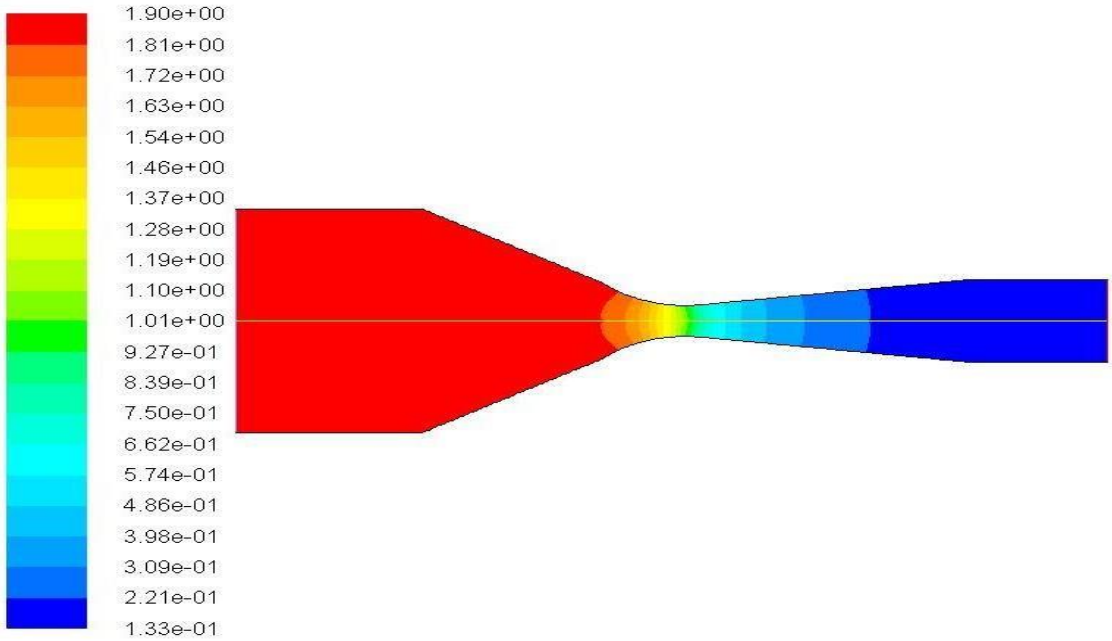

Figure6-10: Contours of static pressure (bar) at an upstream pressure of 27.52 Psi (1.90 bar) and an inlet liquid mass fraction of 0.166

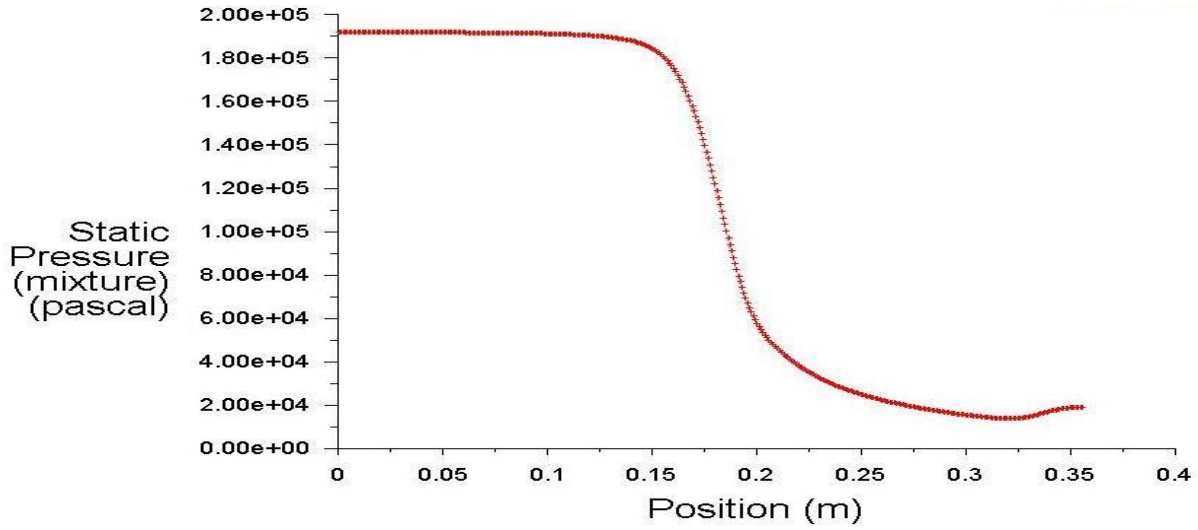

Figure6-11: CFD static pressure of the mixture at an upstream pressure of 27.52 Psi (1.90 bar) and an inlet liquid mass fraction of 0.166

However, the mechanical non equilibrium between the steam and water phase is now evident therefore the assumption of homogenous mixture flow is no longer applicable, as shown in Figure 6.12. The figure presents the magnitude velocity of the steam and water predicted along the nozzle, at an upstream inlet pressure of 27.52 Psi (1.9 bar) and an inlet mass fraction

of 0.166. The figure shows that both phases are at mechanical equilibrium conditions when the mixture flows up to the end of the first straight portion of the nozzle prior to the converging section. After that, each phase flows at a different velocity magnitude with a higher value recorded for the steam phase. The velocity of the steam found to be around three times of the water phase, owing to the rapid expansion of the steam through the nozzle as well as the higher inertia of the water.

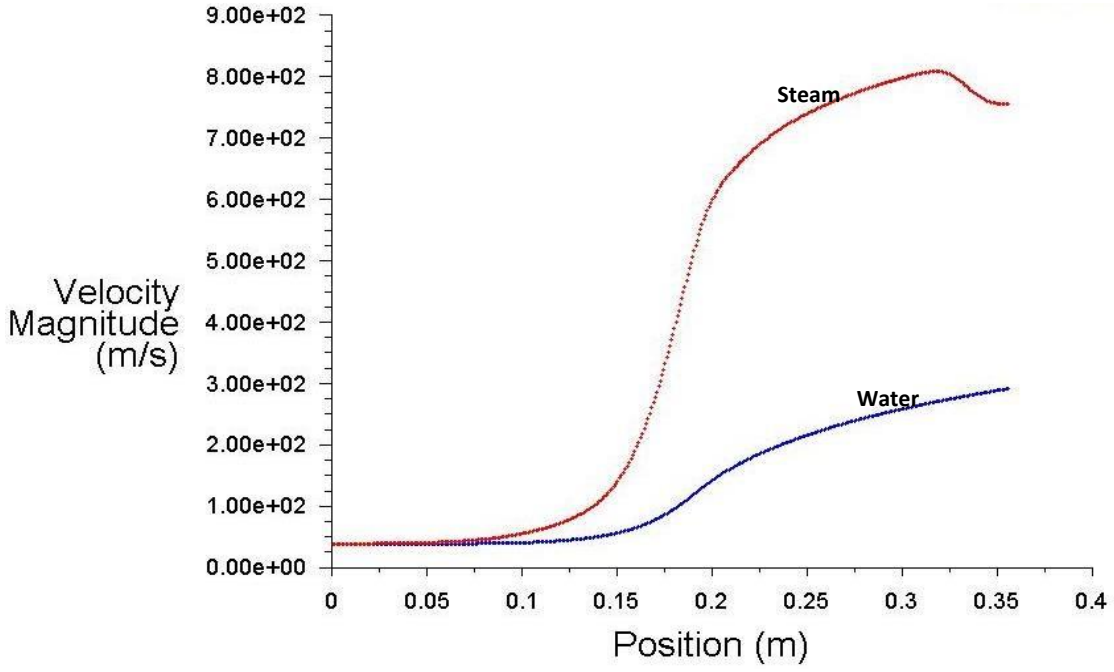

Figure 6-12: CFD velocity magnitude of steam and water at an upstream pressure of 27.52 Psi (1.90 bar) and an inlet liquid mass fraction of 0.166

With regards to the thermal non equiliburium associated with heat transfer between the two phases due to a tempertaure difference, Figure 6.13 shows the predicted static temperature of both phases and the saturation temperature along the nozzle , for an inlet upstream pressure of 27.52 Psi (1.9 bar) and a liquid mass fraction of 0.166. According to the figure, thermal equiliburium conditions of the steam-water mixture can be observed from the predicted temperature. The temperatures of both phases are equal particularly at the nozzle inlet up to a location close to the throat where the steam phase would begin to rapidly expand, as depicted in Figure 6.13. The water temperature predicted by the twofluid model of the Euler-Euler CFD is always higher than the the steam temperature due to the high thermal inertia of the water phase as well as the fast expansion of the steam phase particularly at the diverging portion of the nozzle. The saturation temperature is predicted in

the nozzle based on a piecewise linear method instead of assuming a constant value. In addition, Figure 6.13 indicates significant thermal non-equilibrium; superheating of the water by up to 50K and subcooling of the steam by 80K. These predicted values appear greater than what would be expected from the literature discussing similar process. For example, Gerber and Kermani [136] prediction indicates that thermal non equilibrium of the order of 30K is sufficient to nucleate and result in water/steam returning to near equilibrium conditions. The results suggest that the models used in a simple two fluid approach are insufficient to represent the processes. Unfortunately no experimental data is currently available to help improve the model. Clearly further effort is required to investigate these issues.

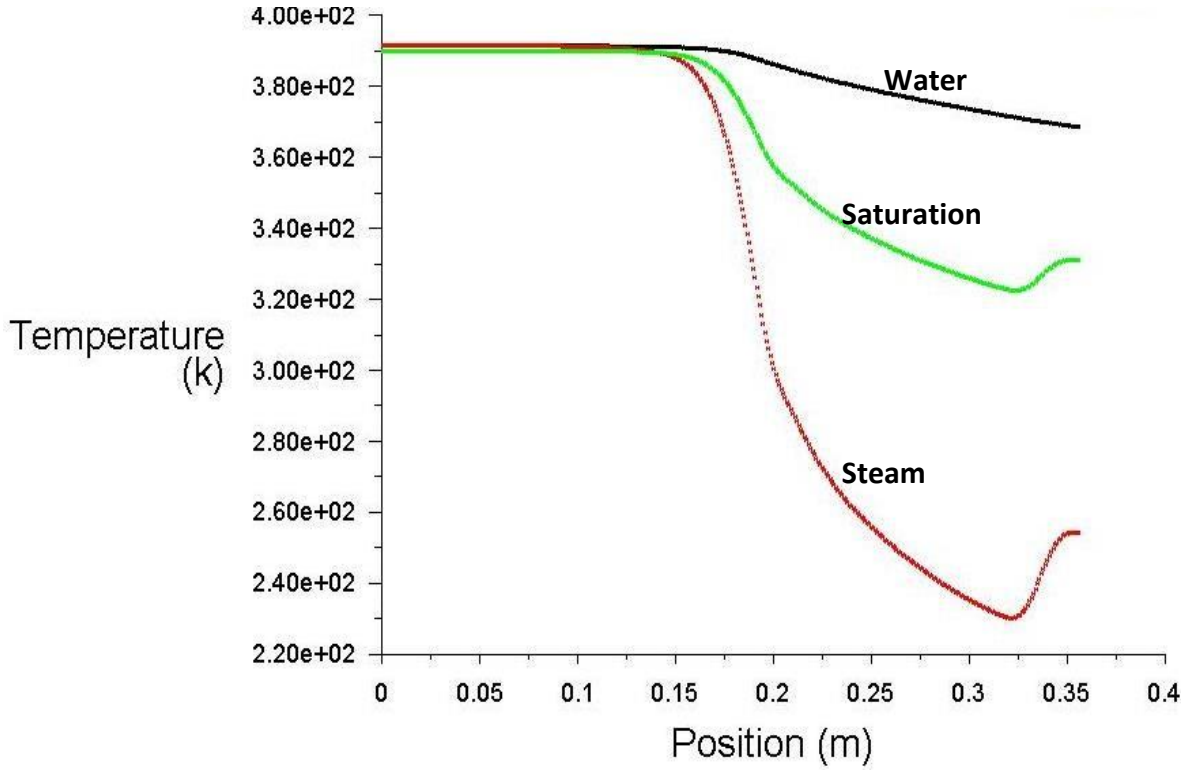

Figure 6-13: CFD Static temperature of steam and water, and saturated temperature at an upstream pressure of 27.52 Psi (1.90 bar) and an inlet liquid mass fraction of 0.166

However, the heat transfer included in this study is modelled based on the Ranz-Marshall correlation. For details of the model, refer to subsection 5.3.1.3. It is worth mentining here that the relative Reynold's number calculated according to Eq.5.8 would justify the use of the Ranz-Marshall correlation, as the maximum Reynold's number does not exceed 4000 in this study, as illiustrated in Figure 6.14. As far as the amount of heat transfered from the water phase whose temperature is higher to the steam phase is concerned, the total volume integral heat transfer was calculated from Eq.5.13 based on the inlet upstream pressure of 27.52 Psi

(1.9 bar) and liquid mass fraction of 0.166, and found to be 1229.6 W. Having this amount of heat inside the nozzle and assuming no heat would be dissipated through the wall to the envirnmoment, is insufficient to bring the steam phase back to the saturation temperature once more. This is based on a steam mass flowrate of 0.1228 kg/s with a specific heat of 2014 J/kg.k, hence the increase in temperature will be of 4.97K. The main reason for this less amount of heat might be attributed to the volumetric heat transfer coefficient according to Eq.5.14, which was found to be inadequate due to the very small liquid volume fraction contained in the nozzle, as shown in Figure 6.15. The figure shows that the majority of the water phase flows along the wall of the converging section of the nozzle, whilst very small magnitudes of water volume fraction can be seen over the remaining flow domain.

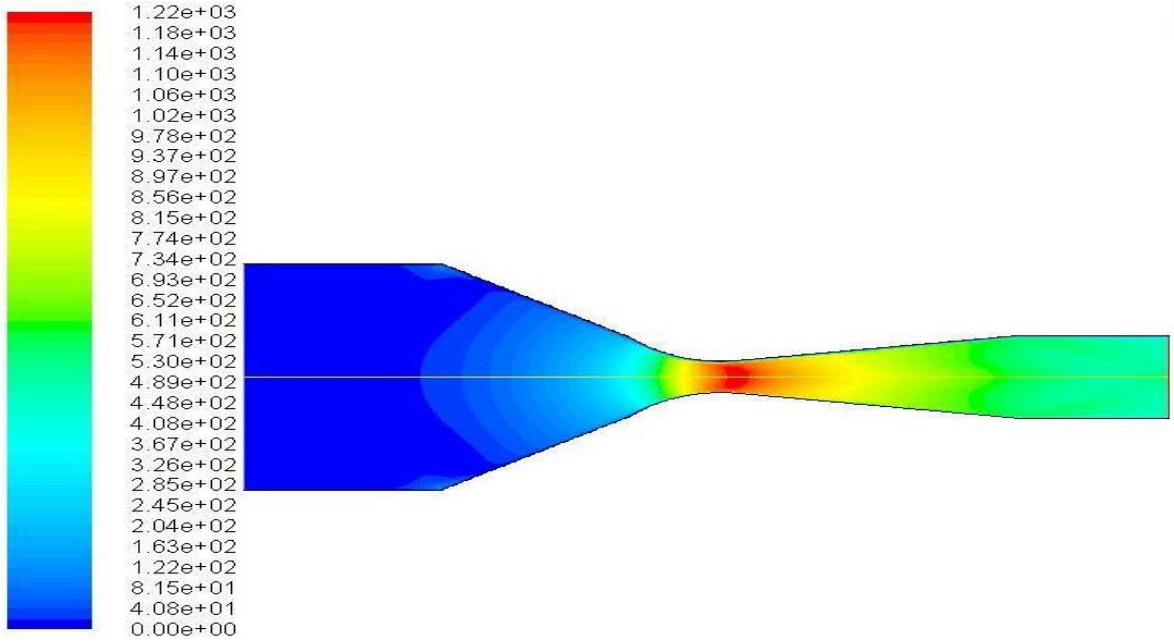

Figure 6-14: Contours of Reynolds number at an upstream inlet pressure of 27.52 Psi (1.9 bar) and an inlet liquid mass fraction of 0.166

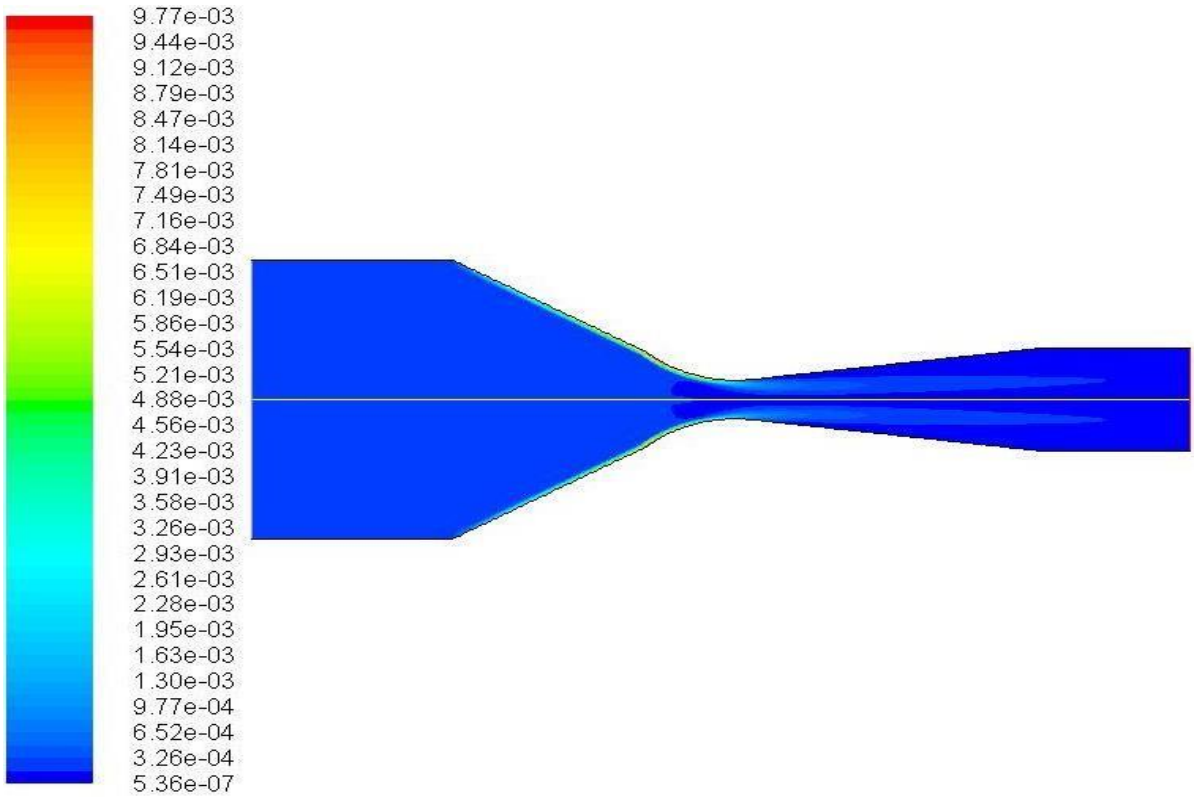

Figure 6-15: Contours of water volume fraction at an inlet upstream pressure of 27.52 Psi (1.9 bar) and an inlet liquid mass fraction of 0.166

In addition, further investigation was achieved in terms of thermal and velocity response times of the existing droplets to examine the time dependence of the characteristics of the water droplet compared to the carrier phase of steam. The velocity response time (τ_V) and thermal response time (τ_T) were identified based on Eq.6.10 and Eq.6.11 and found 116 and 48 (ms), respectively, whilst this water droplet takes no more than 4.2 (ms) to leave the nozzle based on its averaged velocity.

$$\tau_V = \frac{\rho_d d_p^2}{18\mu_c} \quad (6.10)$$

$$\tau_T = \frac{C_d \rho_d d_p}{12 k_c} \quad (6.11)$$

As far as the mass transfer process in the converging diverging nozzle is concerned, for all available cases in the work of Charless [150], the rate of mass transfer between phases was based on kinetic energy theory model of Hertz-Knudsen [151]. It is of importance to define the evaporation-condensation mechanism of mass transfer between the two phases of steam

and water through the mixture. Although the homogenous nucleation process of condensation was neglected in the Charles's work [151], the kinetics of interphase mass transfer at a droplet surface is considered. In addition, the steam phase is assumed to be pure therefore the portion of mass transfer due to diffusion is no longer existing, which significantly appears only in the air-water mass transfer process of Charles's work. According to the above equations of 6.2 and 6.3, the rates of water evaporation and steam condensation were predicted by implementing the two-fluid model of Euler-Euler CFD, as graphed in Figure 6.16 and 6.17, respectively. As can be noticed from Figure 6.13, the water temperature is almost above the saturation temperature, which augments evaporation while the steam is sub-cooled resulting in condensation.

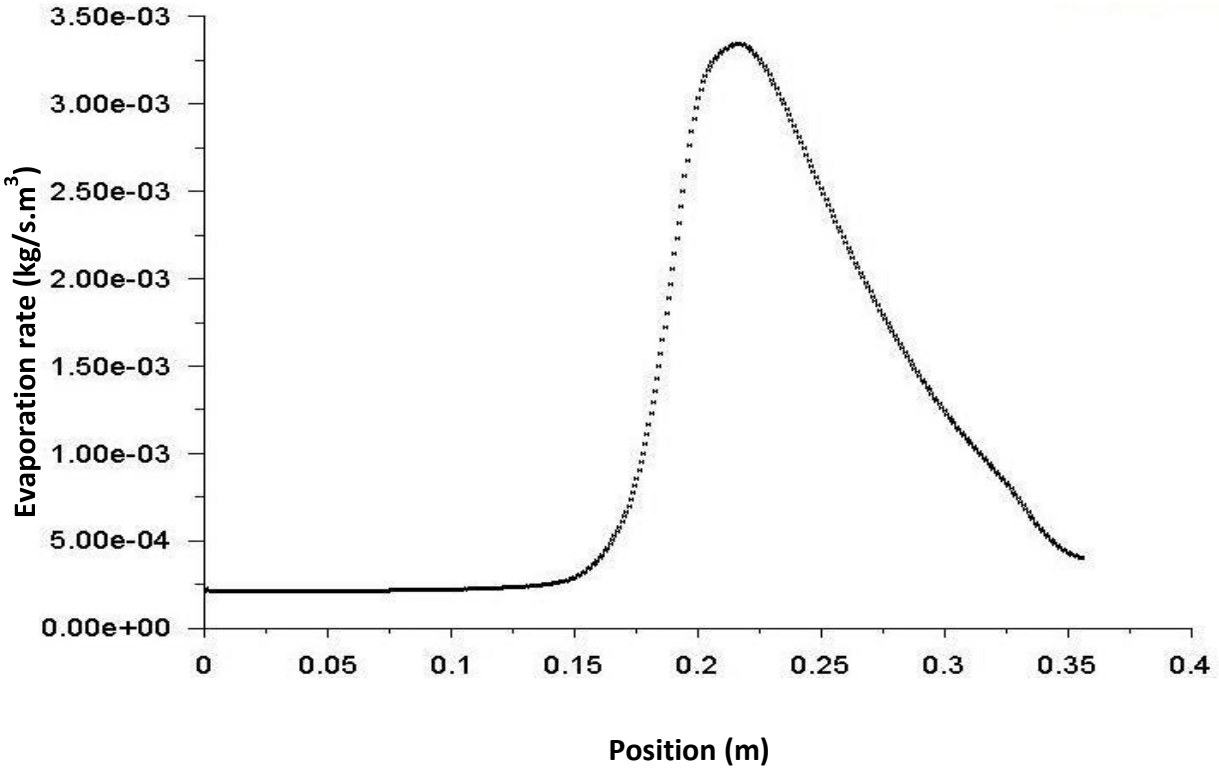

Figure 6-16: The evaporation mass transfer rate at an upstream pressure of 27.52 Psi (1.9 bar) and an inlet liquid mass fraction of 0.166

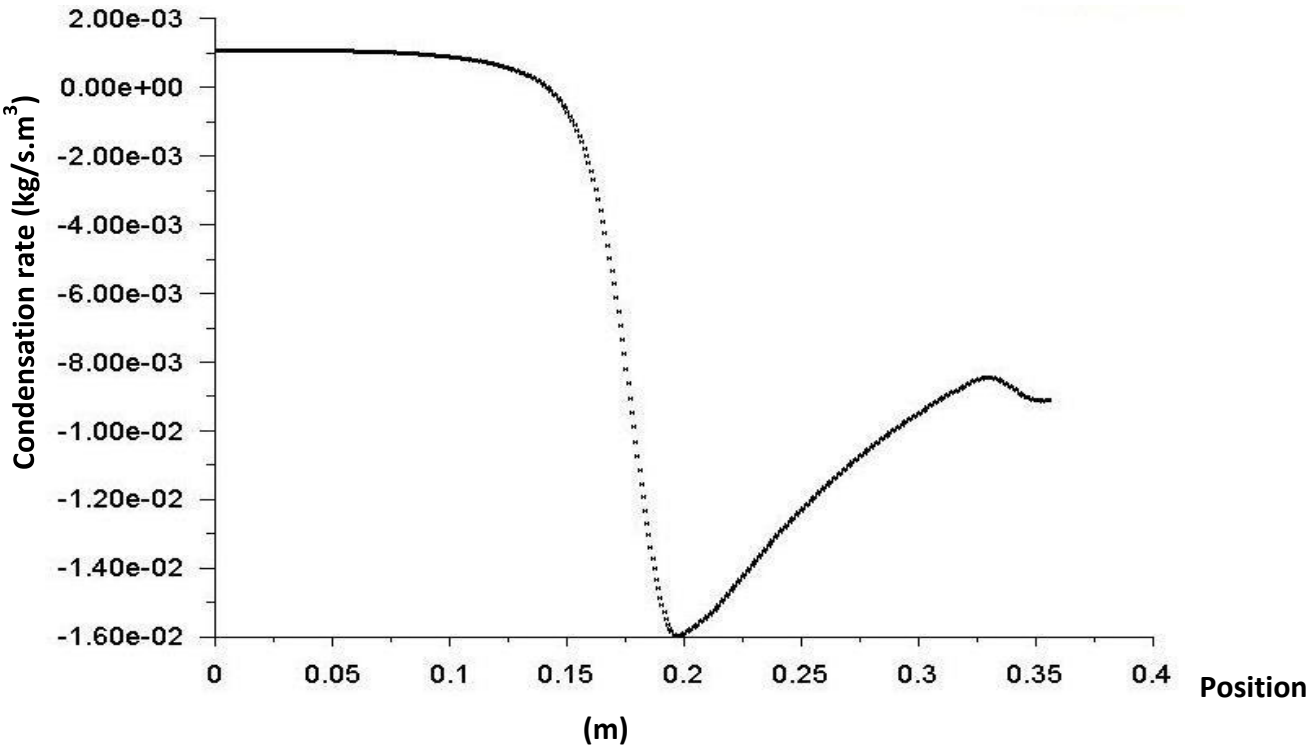

Figure 6-17: The condensation mass transfer rate at an upstream pressure of 27.52 Psi (1.9 bar) and an inlet liquid mass fraction of 0.166

The results of mass transfer rates between the two phases for all different cases are tabulated, as shown in Table 6.4. The predicted CFD results of the mass transfer indicate no significant rates can be seen under these two phase flow conditions of steam-water mixture. However, from the work of Charless [150], it was mentioned that "roughly 2-3% of the mass flowrate of liquid was converted into steam". In fact, this was based on some assumptions that were the interface pressure considered to be the saturated pressure, and a grossly simplified model of droplet breakup was adopted to investigate the influence on the overall flow.

However, the CFD Euler-Euler model developed for this study is based on a single droplet diameter; hence the droplet breakup process was not taken into consideration for modelling simplification purpose as well as a difficulty in adopting it through the current ANSYS FLUENT CFD code. Therefore, the very significant disagreement between the model of Charless and the two fluid model approach in terms of predicting the so-called reverse mass transfer rate of evaporation and condensation might be attributed to the latter assumption of the single droplet diameter. This is in addition to the liquid volume fraction in the fluid domain, which

is found to be very small, hence results in less evaporation rate. The steam density would also influence the condensation rate as it is small compared to the liquid density. However, the small values of mass transfer rates presented in Table 6.4 can be attributed to the balance between the evaporation and condensation according to the vapour transport equation of 6.1. In addition, the positive mass transfer rate denotes the occurrence of the evaporation, whilst the negative magnitude refers to the condensation process.

Table 6-4: The predicted mass transfer rates on two phase flows of steam-water mixture at different upstream inlet pressures and different inlet liquid mass fractions:

Upstream inlet pressure (Psi)	Inlet liquid mass fraction (-)	Total volume integral mass transfer rate ($kg/s.m^3$)(m^3)
19.51	0.36	-6.957E-8
19.63	0.273	-2.678E-7
21.08	0.212	-1.665E-7
23	0.32	-4.219E-7
25.96	0.127	-2.787E-8
26.31	0.11	-2.534E-8
26.8	0.205	-4.778E-8
26.9	0.129	9.277E-9
27.52	0.166	4.162E-8

6.5 Issues relating non prediction

Different mass transfer mechanisms can be addressed, i.e. the steam nucleation and the droplet growth and the flashing evaporation. The homogenous nucleation and the associated droplet growth based on the work of Gerber and Kermani [136], as well as the flashing evaporation based on the work of Moneeb et al [162] can be investigated for steam flows in a safety valve or a nozzle, and will be the proposal of future work. These will be included in the two fluid model of the CFD fluent code through the so-called user defined functions (UDFs) to account for the mass transfer rate on the mass

conservation equation. The latter concept of mass transfer rate will be automatically accounted in both the momentum and energy conservation equations of the two fluid model approach. In addition, investigation of high pressure upstream inlet conditions will be of interest. Studies of the film flows in accelerating devices i.e. nozzles and safety relief valves will be also of importance.

Chapter Seven

7 Conclusions and Future Work

7.1 Summary

A computational fluid dynamic approach has been implemented to examine the behaviour of single phase air flow and two phase air-water flow conditions in a conventional spring loaded safety relief valve. This computational approach has been also used to investigate two phase steam-water flow conditions in a convergingdiverging nozzle. The CFD approach is developed based on a two dimensional axisymmetric grid convergence to represent the fluid domain in the safety relief valve. A computational grid two dimensional planar based has been used to represent the fluid domain in the converging diverging nozzle. The CFD model results have shown a good predictive capability. In spite of an experimental approach has been established for examining safety relief valve under single and two phase flow conditions, experimental data and a homogenous non equilibrium model were available for the CFD model validations. For the safety relief valve testing, flow-lift and force-lift characteristics have been achieved both experimentally and computationally at different test pressures. A design approach for the safety relief valve tested has been adopted based on normalising the flow-lift and force-lift characteristics at all available working pressure. It is of importance to clarify that this study is limited to a present experimental facility based on an in-house rig, hence the upstream inlet pressure is in the range of 4.8 to 13.8 barg and liquid mass fraction lies in the range of 0 to 0.87. The steam-water mixture studies are subjected to the flow conditions of upstream pressure of (1.31 to 1.92 barg) and a liquid mass fraction of (0 to 0.36), as mentioned in the work of Charless [150].

7.2 Single Phase Studies Conclusions

- The study of the highly compressible single phase flow of air through the safety valve has paved our way towards understanding two phase flows.

- The study has evidenced that the adjusting gland has no influence on the critical (choking) mass flowrate predicted. The only effect of the gland is on the back pressure and the associated piston force. Therefore, having the gland in place will reduce the net piston force due to a relatively high back pressure.

- For the valve with low lifts (0-2 mm) and fixed test pressure, the air flow rate is dependent on the flow area between the piston front face and the valve seat where the critical plane (choking location) occurs.

- For the valve with high lifts (lift>2 mm) and fixed test pressure, the air flow rate is governed by the flow area of the passageway around the piston where the choking plane occurs.

- The 2D axisymmetric model developed in this study based on a RANS and k-ε turbulence model found to be adequate in air mass flowrate and piston force predictions.

- In terms of the model accuracy of predictions, the mass flowrate found to be overpredicted with almost maximum 2-3% whilst the piston force found to be also overpredicted with maximum 6%. The piston force prediction is mainly relied on the accurate representation of the valve geometry and the adjusting gland.

- The computational fluid dynamic (CFD) has been a very good tool to identify and analyse the physical and thermal properties of the flow inside the safety relief valve. The CFD predictions give details of the trends observed in valve flow and force characteristics along with the interaction with valve geometry, which are very important in terms of effective designs.

- Flow-lift and force-lift characteristics have been achieved experimentally by using the in-house test rig facility, and computationally by using the CFD. Obtaining these characteristics allow the use of scaling parameters to normalise the flowlift and force-lift characteristics and have a CFD approach to safety valve design.

7.3 Two Phase Air-Water (Frozen Flow) Studies Conclusions

- The behaviour of two phase flows of air-water mixtures namely frozen flow in a conventional spring loaded safety relief valve has been investigated experimentally and theoretically. An experimental approach has been established

for testing the safety relief valve based on an in-house test rig facility, which has been developed to generate and measure the two-phase flows of air-water conditions. Air and water mass flowrate, pressures, temperature and piston position (lift) have been measured.

- The valve flow-lift and force-lift characteristics at different working pressures and liquid mass fraction have provided significant help in understanding the two phase flow behaviour and in the validation of the CFD.

- The flow-lift characteristics of two phase mixtures found to have a similar behaviour to single phase flow characteristics particularly with low lifts.

- For all cases of two phase flows tested in this study, a very obvious reduction in air mass flowrate has been observed when the water mass flowrate increase. This is, however, due to an increase in water volume fraction, which occupies more volume in the flow domain than the air phase.

- Despite the adjusting gland has shown no impact on the mass flowrate, it has provided a significant effect on the back pressure, hence the resultant piston force.

- The water mass fraction imposes a small influence on the piston force. This largely supports the results of Narabayashi et al [104].

- A two dimensional axisymmetric model has been used to represent the valve geometry instead.
- A two-fluid model of Euler-Euler CFD with a k-Ɛ mixture model to account for the flow turbulence has been developed based on homogenous mechanical and thermal non equilibrium assumptions. Accordingly, the two phases are assumed to be run at different velocity and different temperature. The Euler-Euler model has shown to give good predictions of mass flowrate and piston force. It terms of accuracy, the CFD of two-fluid model of Euler-Euler found to overpredict the

flowrate with maximum uncertainty of about 4-8%, whilst the piston force has been also overpredicted with maximum uncertainly of approximately 19% particularly at higher lifts, higher liquid mass fractions. However, the turbulent drift force was included to account for the interphase turbulent momentum transfer and found to predict less mass flowrates and higher net piston forces therefore it was disabled.

- The Euler-Euler CFD model has shown the capability to give better understanding to the flow behaviour, physical and thermal properties as well as the choking plane and the shock waves inside the valve.

- The Euler-Euler CFD model has been compared against the CFD homogenous equilibrium mixture model and the analytical equilibrium homogenous model developed by Darby [84]. As the reference is the mass flowrate experimental data, the homogenous mixture model has been in very good agreement with the two-fluid model for low liquid mass fractions. However, for medium to high liquid mass fractions, the homogenous mixture model has shown to underpredict the mass flowrate with a maximum discrepancy of about 16%.

- The above comparison gives evidence that the thermal and mechanical equilibrium assumptions on two phase flows are no longer applicable. Therefore, the slip and the temperature difference between the air and water phases have been computationally investigated.

- It is worth mentioning here that the CFD mixture model of the Fluent based with a model to account for the slip has been implemented. Unfortunately, the CFD mixture model with the slip model included has shown no convergence for all the cases. Thus it has been of significance to run it without the slip model to ensure its convergence then to be used for calibration.

- The critical velocity has been identified by using both models of the two-fluid model of Euler-Euler CFD and the CFD homogenous mixture model. The results

have shown that the two-fluid model of Euler-Euler CFD predicts higher velocity magnitude for medium to high liquid mass fractions, hence gives high critical mass flowrate. In fact, this has been found as a reliable reason to justify the above mentioned discrepancy between the two CFD models in the prediction of mass flowrate.

- The effect of heat transfer based on Ranz-Marshall model has been computationally addressed in this study. This has been achieved by having different inlet water temperature to enhance heat transfer between phases. An increase in inlet water temperature has shown no significant change in air mass flowrate predicted. It has been argued that the heat transfer between phases at experimental conditions particularly for inlet water temperature of 288K may not be sufficient to affect the critical flow conditions.

- To account for the uncertainty of flow regime occurs; a single diameter droplet size (i.e. mono dispersed) has been hypothesised at the inlet of the valve and multiple solutions for a range of droplet diameters have been obtained. For the reference case, a 10 µm diameter has been postulated and the effect of droplet sizes between 5 and 35 µm has been investigated. It was found that 1 µm would match homogenous conditions. In the absence of breakup and/or coalescence of the droplet, however, the number of droplets that are generated by the spray nozzle will be in the order of $10^{11.}$

- Flow-lift and force-lift characteristics have been obtained experimentally by using the in-house test rig facility, and computationally by using the CFD.

  Obtaining these characteristics have led to establishing a design approach for safety relief valves based on scaling parameters to normalise the flow-lift and force-lift characteristics. The normalised flow-lift characteristics have collapsed into one curve with maximum uncertainty of about 12%, whilst the normalised force-lift characteristics have also collapsed into one curve with maximum uncertainty of 16%. On the other hand, if mean curves of the normalised flow-lift

and force-lift characteristics are created, the above mentioned uncertainties would be reduced to half of their magnitudes.

7.4 Two Phase Steam-Water (Flashing Flow) Studies Conclusions

- The study has been considered as an initial attempt in modelling a two phase flow of steam-water mixtures.

- The study was intended to investigate the behaviour of two phase flow of steamwater mixtures through a safety relief valves. However, lack of experimental facility has prevented us from tackle it; hence the study has been conducted on a converging-diverging nozzle with data available.

- A two dimensional planar model has been adapted to represents the flow domain of the nozzle geometry.

- A two fluid model of Euler-Euler CFD to account for mechanical and thermal non equilibrium between phases with a k-Ɛ mixture model to account for the flow turbulence has been developed to examine the behaviour of the two phase flow of steam-water mixtures in the converging-diverging nozzle.

- The CFD model has included a model to account for the mass exchange between phases (model for mass transfer).

- The CFD model has been validated against experimental data provided by Charless [150]. The work of Charless has been for a small scale of a steam-water system as the working pressure was in the range of 19 Psi to 27.5 Psi (1.31 – 1.92 bar) and a liquid mass fraction lies in the range between 0 and 0.36.

- ❖ The critical mass flowrate has been determined by the two-fluid model and shown to be in good agreement with the experimental data with a maximum discrepancy of about 6%.

- ❖ The CFD model has shown that the mechanical and thermal non equilibrium conditions between phases are evident.

- ❖ The evaporation and condensation rates have been computationally obtained based on a kinetic theory of the vapour transport equation. The saturation temperature has been computed based on a piecewise-linear procedure.

- ❖ The evaporation and condensation model of the existing fluent code shows no significant mass transfer rate predicted.

- ❖ The sensible heat transfer between phases has been calculated based on the Ranz-Marshall model and found to be not sufficient to change the critical flow conditions in the nozzle.

- ❖ The two fluid model shows inconsistency in terms of predicting the flow physics on the divergent part of the studied nozzle.

7.5 Key outcomes of study with respect to manufacturers' requirement and needs

- ❖ According to the manufacturer, the safety relief valve studied in this thesis is mainly implemented for single phase flow conditions; however, in this study the work is being extended to examine the valve under two phase flow conditions.

- The two phase flow studies of this thesis could help the valve's supplier knowing that their product has been assessed for a wide range of flow regime conditions, where evaporation/condensation processes possibly occur.

- Product development by a valve manufacturer relies on experimental work and is a time consuming trial and error approach. Therefore developing and applying physical models and numerical methods based on CFD techniques for such very complex flows in safety relief valves would reduce the associated experimental costs.

- As the valve, examined in this thesis, has a flow path through the valve, the performance is very sensitive to piston back pressure as the valve components (spring, spring holders, spring adjusting) are exposed to the fluid flow. Therefore the CFD simulations will be of significance and provide detailed quantification and visualisations of the valve internal flow hence the impact of geometry variations in valve design could be assessed before the manufacturing process. This is not easily accessible through experimental techniques.

7.6 Future Work

- Different turbulence models should be investigated.

- Different flow regimes should be modelled as the annular film flow is now evident.
- Transient two phase flow conditions should be examined to improve the existing safety relief valve design approach.

- The dynamic behaviour of the safety relief valves should be computationally investigated.

- The mass transfer modelling approach should be extended to cover a wide range of operation conditions, hence to model the homogenous nucleation and the associated droplet growth, and the flashing evaporation in valves and nozzles.

- The experimental facility developed for two phase flow of air-water mixtures should be modified to cover a wide range of working pressures and liquid mass fraction.

Bibliography:

1. B. Föllmer, and A. Schnettler, "Safety Relief Valves According New Requirments of En (PED) Versus AD/TRD or ASME," *Tech. Rep.*, (2004).

2. I. S. Grinberg, and I. R. Krichker, "Design Method for Safety Valves with Pressure Applied Above the Seat," *Chemical and Petroleum Engineering*, Vol. 9, No. 8, Pp. 696698, (1973).

3. P. R. Sterland, "Understanding The Behaviour of Relief Valve," *IMechE*, Vol. C373/84, Pp. 57-62, (1984).

4. D. K. Sharma, "State-of-The-Art Design of Spring Loaded Safety Valves." *Joint Conference of the Pressure Vessels and Piping, Materials, Nuclear Engineering and Solar Division.* (1981).

5. G. J. Parker, "'Pop' Safety Valves: A Compressible Flow Analysis," *International Journal of Heat and Fluid Flow*, Vol. 6, No. 4, Pp. 279-283, Dec. (1985).

6. P. L. Betts, and J. Francis, "Design Of High-Lift Pressure Relief Valves with NonAdjustable Blowdown for Gas/Steam." *Journal of Process Mechanical Engineering, Vol*. 209, No. Part E, (1995).

7. P. L. Betts, and J. Francis, "Pressures beneath the Disc of a Compensated Pressure Relief Valve For Gas/Vapour Service Pressure Relief Valve for Gas/Vapour Service," *Journal of Process Mechanical Engineering*, Vol. 211, Pp. 285-289, (1997).

8. J. Francis, "Zone Modeling of High Lift Safety Relief Valves Subject to Choked Compressible Flow," *Proceeding of The 3rd International Seminar On Fire and Explosion Hazards*, Pp. 795-806, (2001).

9. L. Gerhard, J. Broedermann, and T. Scheele, "Pressure Relief of High Pressure Devices" *Chemical Engineering & Technology* 30, No. 6: 695-70, (2007).

10. J. Schmidt, W. Peschel, and A. Beune, "Experimental and Theoretical Studies on High Pressure Safety Valves: Sizing and Design Supported By Numerical Calculations (CFD)," *Chemical Engineering & Technology*, Vol. 32, No. 2, Pp. 252-262, (2009).

11. S. Sethi, and L. S. Ying, "A Simulation Model to Predict Performance Characteristics of a Safety Relief Valve." In Proc. *1st Summer Computer Simulation Conference, Vancouver, Canada*, Pp. 800-806, (1993).

12. S. Sethi, and A. Sabit, "Predicting the Fluid Flow through a Pressure Relief Valve Using The CFD Code Phonics," Vol. 26. *Proceeding of The 11th Annual Simulators Conference*, Pp. 229-235,(1994).

13. H. Berger, "Numerical Simulation of Gas Flow in Pneumatic Components," *Forschung Im Ingenieurwesen*, Vol. 58, No. 3, Pp. 67-74, Mar. (1992)

14. W. Dempster, and W. Elmayyah, "A Computational Fluid Dynamics Evaluation of a Pneumatic Safety Relief Valve." *The 13th International Conference On Applied Mechanics and Mechanical Engineering (Amme)*, May.(2008).

15. W. Dempster, C. K. Lee, and J. Deans, "Prediction of The Flow and Force Characteristics of Safety Relief Valves," *Proceedings Of Pvp2006-Icpvt-11 2006 ASME Pressure Vessels and Piping Division Conference*, Jul. (2006).

16. J. Bilanin, and M. E. Teske, "Modeling Flow through Spring Loaded Safety Valves," Vol. 190, *ASME PVP Conference. ASME*, Pp. 29-36,(1990)

17. D. Moncalvo, L. Friedel, B. Jörgensen, and T. Höhne, "Sizing of Safety Valves Using ANSYS CFX-Flo," *Chemical Engineering & Technology*, Vol. 32, No. 2, Pp. 247-251, (2009).

18. H.-D. Kim, J.-H.Lee, K.-A.Park, T. Setoguchi, and S. Matsuo, "A Study of the Gas Flow through an Lng Safety Valve," *Journal of Thermal Science*, Vol. 15, No. 4, Pp. 355-360, Dec. (2006).

19. R. D'alessandro, "Thrust Force Calculations for Pressure Safety Valves," *Proc. Safety Prog.*, Vol. 25, No. 3, Pp. 203-213, (2006).

20. S. Muschelknautz, and A. Wellenhofer, “Flow Reaction Forces Upon Blowdown of Safety Valves," *Chemical Engineering & Technology*, Vol. 26, No. 7, Pp. 797-803, (2003).

21. M. Manninen, V. Taivassalo, and S. Kallio,“On The Mixture Model for Multiphase Flow,”*Technical Report, Technical Research Centre of Finland,* (1996).(Cited in [88])

22. J. E. Funk, "Poppet Valve Stability," *Journal of Basic Engineering*, Pp. 207-212, Jun. (1964).

23. B. Follmer, "Oscillating Functioning of Safety Valves Generated By Their Inlet Geometry." International Symposium of Flow Visualisation, Sep. (1980).

24. J. Cremers, and L. Friedel, "Design Of Spring Loaded Safety Valves With Inlet and Discharge Pipe Against Chatter In The Case Of Gas Flow," *Chemical Engineering & Technology*, Vol. 26, No. 5, Pp. 573-576,(2003).

25. G. Macleod, "Safety Valve Dynamic Instability: An Analysis of Chatter," *Journal of Pressure Vessel Technology*, Vol. 107, Pp. 172-177, May (1985).

26. ISO 4126-1:2004 Safety Devices for Protection against Excessive Pressure. Safety Valves. International Organization for Standardization (ISO)." *Tech. Rep*., (2004).

27. ISO 4126-7:2004 Safety Devices for Protection against Excessive Pressure. Safety Valves. International Organization for Standardization (ISO)."*Tech. Rep*., (2004).

28. A. Beune, "Analysis of High-Pressure Safety Valves." *A Catalogue Record is Available from the Eindhoven University of Technology Library ISBN*: 978-90, (2009).

29. V. Dossena, F. Marinoni, F. Bassi, N. Franchina, and M. Savini, "Numerical and Experimental Investigation on The Performance of Safety Valves Operating with Different Gases” *International Journal of Pressure Vessels and Piping* 104: 21-29, (2013).

30. J. Schmidt, and P. Wolfgang, "Sizing and Operation Of High_Pressure Safety Valves" *Process and Plant Safety: Applying Computational Fluid Dynamics*: 69-94, (2003).

31. R. Darby, "The Dynamic Response of Pressure Relief Valves in Vapor or Gas Service, Part I: Mathematical Model" *Journal of Loss Prevention In The Process Industries"*, Volume 26, Issue 6 , Pages 1262-1268, ISSN 0950-4230, November (2013).

32. A. A. Aldeeb, R. Darby, and S. Arndt, "The Dynamic Response of Pressure Relief Valves In Vapor or Gas Service. Part Ii: Experimental Investigation." *Journal of Loss Prevention in the Process Industries* 31: 127-132, (2014).

33. R. Darby, and A. A. Aldeeb, "The Dynamic Response of Pressure Relief Valves In Vapor or Gas Service. Part Iii: Model Validation." *Journal of Loss Prevention in the Process Industries* 31: 133-141, (2014).

34. C.J. Hős, A.R. Champneys, K. Paul, and M. Mcneely, "Dynamic Behavior Of Direct Spring Loaded Pressure Relief Valves In Gas Service: Model Development, Measurements and Instability Mechanisms", *Journal Of Loss Prevention In The Process Industries*, Volume 31, Pages 70-81, Issn 0950-4230, September (2014).

35. F. Bassi, F. Cecchi, N. Franchina, S. Rebay, and M. Savini, "High-Order Discontinuous Galerkin Computation of Axisymmetric Transonic Flows In Safety Relief Valves." *Computers & Fluids* 49, No. 1: 203-213, (2011).

36. F. Bassi, A. Crivellini, V. Dossena, N. Franchina, and M. Savini, "Investigation of Flow Phenomena in Air–Water Safety Relief Valves By Means Of a Discontinuous Galerkin Solver." *Computers & Fluids* 90: 57-64, (2014).

37. V. Dossena, P. Gaetani, F. Marinoni, and C. Osnaghi, "On the Influence of Back Pressure and Size on the Performance of Safety Valves."*In ASME 2002 Pressure Vessels and Piping Conference*, Pp. 35-41.American Society Of Mechanical Engineers, (2002).

38. V. Dossena, F. Marinoni, S. Di Vincenzo, A. Boccazzi, and R. Sala, "High Pressure Fluctuations Induced By Safety Valves Operating With Liquids at Very Low Lift."In *ASME/JSME 2004 Pressure Vessels and Piping Conference*, Pp. 95-101.American Society Of Mechanical Engineers, (2004).

39. X. G. Song, Ji. H. Jung, H. S. Lee, D. K. Kim, and Y. C. Park, "2-D Dynamic Analysis Of A Pressure Relief Valve By CFD." In *Proceedings of the 9th Wseas int. Conference on Applied Computer and Applied Computational Science. ISBN*, Pp. 978-960, (2010).

40. X. G. Song, L. Wang, and Y. C. Park, "Transient Analysis of A Spring-Loaded Pressure Safety Valve Using Computational Fluid Dynamics (CFD)."*Journal of Pressure Vessel Technology* 132, No. 5: 054501, (2010).

41. X. G. Song, L. Cui, and Y. C. Park, "Three-Dimensional CFD Analysis of a SpringLoaded Pressure Safety Valve From Opening To Re-Closure," In *ASME 2010 Pressure Vessels and Piping Division/K-Pvp Conference*, Pp. 295-303. American Society of Mechanical Engineers, (2010).

42. X. G. Song, S.G. Kim, L. Wang, and Y. C. Park, "Transient Flow Analysis of Spring Loaded Pressure Safety Valve."In *ASME 2009 Pressure Vessels and Piping Conference*, Pp. 253-258.American Society Of Mechanical Engineers, (2009).

43. X. G. Song, Y. C. Park, and J. H. Park, "Blowdown Prediction of a Conventional Pressure Relief Valve with a Simplified Dynamic Model."*Mathematical And Computer Modelling* 57, No. 1: 279-288, (2013).

44. X. G. Song, L. Cui, M. Cao, W. Cao, Y. C. Park, And W. M. Dempster, "A CFD Analysis of The Dynamics of a Direct-Operated Safety Relief Valve Mounted on A Pressure Vessel." *Energy Conversion and Management* 81: 407-419, (2014).

45. C. Dumitrache, I. Calimanescu, and C. Comandar, "Naval Standard Safety Valve Design Using Cad Solutions." In *Applied Mechanics and Materials*, Vol. 658, Pp. 65-70. (2014).

46. J. Francis, And P. L. Betts, "Modelling Incompressible Flow in a Pressure Relief Valve." *Proceedings of the Institution of Mechanical Engineers, Part E: Journal of Process Mechanical Engineering* 211, No. 2: 83-93, (1997).

47. L. Thorén, And A. Budziszewski,"CFD Simulation of a Safety Relief Valve for Improvement of a One-Dimensional Valve Model in Relap5." (2012).

48. D. W. Sallet, W. Nastoll, R. W. Knight, M. E. Palmer, And A. Singh, "Experimental Investigation Of The Internal Pressure And Flow Fields In A Safety Valve." *Am. Soc. Mech. Eng., (Pap.) ;(United States)* 81, (1981).

49. D. W. Sallet, and G. W. Somers, "Flow Capacity and Response of Safety Relief Valves to Saturated Water Flow." *Plant/Operations Progress* 4, No. 4: 207-216, (1985).

50. P. M. Petherick, And A. M. Birk. "State-Of-The-Art Review of Pressure Relief Valve Design, Testing and Modeling."*Journal of Pressure Vessel Technology* 113, No. 1: 46-54, (1991).

51. A. Singh, "An Analytical Study of the Dynamics and Stability of a Spring Loaded Safety Valve." *Nuclear Engineering and Design* 72, No. 2: 197-204, (1982).

52. Mr.V.D.Rathod, Prof.G.A.Kada, And Mr.V. G. Patil, "Design And Analysis Of Pressure Safety Releas Valve By Using Finite Element Analysis" *International Journal Of Engineering Trends And Technology (IJETT)* – Volume 13 Number 1, ISSN: 2231-5381, Jul. (2014).

53. J. Francis, And P. L. Betts, "Backpressure in a High-Lift Compensated Pressure Relief Valve Subject To Single Phase Compressible Flow." *Journal of Loss Prevention in the Process Industries* 11, No. 1: 55-66, (1998).

54. J. Francis, And P. L. Betts, "Modelling Incompressible Flow in a Pressure Relief Valve." *Proceedings of the Institution of Mechanical Engineers, Part E: Journal of Process Mechanical Engineering* 211, No. 2: 83-93, (1997).

55. A. Beune, J. G. M. Kuerten, and M. P. C. Van Heumen, "CFD Analysis with Fluid–Structure Interaction of Opening High-Pressure Safety Valves."*Computers & Fluids* 64:
108-116, (2012).

56. A. Pateriya, and M. Khan,"Structural and Thermal Analysis of Safety Relief Valve" *International Journal of Pure and Applied Research in Engineering and Technology*, Review Article; Volume 3 (4): 7-13, (2014).

57. A. Pateriya, and M. Khan, "Structural and Thermal Analysis of Spring Loaded Safety Valve Using Fem." (2015).

58. G. Licskó, A. Champneys, and C. Hos, "Nonlinear Analysis of a Single Stage Pressure Relief Valve."*Int. J. Appl. Math* 39, No. 4: 12-26, (2009).

59. K. Patel, "CFD Analysis of a Pressure Relief Valve." *International Journal for Scientific Research & Development* 2, No. 04: 2321-0613, (2014).

60. A. Beune, J. G. M. Kuerten, and J. Schmidt, "Numerical Calculation and Experimental Validation of Safety Valve Flows at Pressures Up To 600 Bar." *AICHE Journal* 57, No. 12: 3285-3298, (2011).

61. M. S. Rajapati, and Dr. Dn. Raut, "Analysis of Pressure Relief Valve Using Matlab Simulink." In *37th National & 4th International Conference on Fluid Mechanics and Fluid Power, December* (2010).

62. A. Murrone, and P.Villedien, "Numerical Modeling of Dispersed Two-Phase Flows". *Aerospace Lab Journal*, (2011).

63. M. Ishii, "Thermo-Fluid Dynamic Theory of Two-Phase Flow". Volume 22 Of Direction
Des Etudes Etrecherchesd'électricité De France. Eyrolles, Paris, (1975).

64. C.W. Hirt and B.D. Nichols "Volume of Fluid (Vof) Method for the Dynamics of Free Boundaries". *Journal of Computational Physics*, 39: Pp. 201–225, (1981).

65. M. Sussman, M. Smereka and S. Osher “A Level-Set Approach for Computing Solutions to Incompressible Two-Phase Flows”. *Journal of Computational Physics*, 114, Pp. 146– 159, (1994).

66. R. Saurel and R. Abgrall “A Multiphase Godunov Method for Compressible Multifluid and Multiphase Flows”. *Journal of Computational Physics*, 150, Pp. 425-467, (1999).

67. M.R. Baer, J.W. Nunziato, “A Two-Phase Mixture Theory for the Deflagration-To-Detonation Transition (DDT) In Reactive Granular Materials”. *Journal of multiphase Flows*, 12, Pp. 861-889, (1986).

68. A.K. Kapila, R. Menikoff, J.B. Bdzil, S.F. Son and D.S. Stewart “Two-Phase Flow Modelling of DDT In Granular Materials: Reduced Equations”. *Phys. Fluid*, Vol. 13, Pp.
3002-3024, (2001).

69. A. Murrone and H. Guillard “A Five Equation Reduced Model for Compressible Two Phase Flow Problems”. *Journal Of Computational Physics*, 202, Pp. 664–698, (2005)

70. M. Reocreux, “Contribution Al’etude Des Debits Critiques En Ecoulementdipdasiqueeauvapeur”, Ph.D. *Thesis*, Universitescientifique ET Medicale De Grenoble, (1974).

71. L. Friedel, “Two-Phase Pressure Drop Model For Safety Valves”, Eur. *Two-Phase Flow Group Meeting,Trondheim*,(1987).

72. Z. Bilicki and J. Kestin, “Proc. Roy. Sot. London Ser. A”, 482, 379, (1990).

73. P. Downar-Zapolski, “An Influence of the Thermodynamic Disequilibrium on the Pseudo-Critical Flow of One-Component Two-Phase Mixture”, Ph.D. *Thesis, Institute for Fluid Flow Machinery, Gdansk*, (1993).

74. V. Feburie, M. Giot, S. Granger and J.M. Seynhaeve, *Int. J. Multiphase Flow*, 19, 541, (1993).

75. F. Menter, “CFD Best Practice Guidelines For CFD Code Validation For Reactor Safety Applications,” Ecora Fiks-Ct-2001-00154, (2002).

76. T. Höhne, D. Moncalvo, and L. Friedel, “Analysis Of Safety Valve Characteristics Using Measurements and CFD Simulations” Leser Gmbh & Co. Kg, *Technischesbüro and Tu Hamburg-Harburg, Institut Für Strömungsmechanik*, (1999).

77. B. Shannak, “Mixture Loss Coefficient of Safety Valves Used In Nuclear Plants”. *Department Of Mechanical Engineering, Al-Balqa Applied University, Al-Huson University College, Al-Huson*, P.O. Box 50, Jordan, May (2009).

78. G. Boccardi, P. R. Bubbico, and B. Mazzarotta , “Two Phase Flow Through Pressure Safety Valves Experimental Investigation and Model Prediction”. *Chemical Engineering Science*, September (2005).

79. G. Boccardi, P. R. Bubbico, and F. Di Tosto, “Geometry Influence on Safety Valves Sizing In Two-Phase Flow”. *Journal of Loss Prevention in the Process Industries,* January (2008).

80. L. Bolle, “Experimental and Theoretical Analysis of Flashing Water Flow through A Safety Value”. *Journal of Hazardous Materials,* April (1996).

81. L. Bolle, P. Downar-Zapolski, J. Franco, and J. M. Seynhaeve, “Flashing Water Flow through a Safety Valve”. *Journal of Loss Prevention in the Process Industries*, (1996).

82. M. S. Brennan, “Multiphase CFD Simulations of Dense Medium and Classifying Hydro-
Cyclones”. Third International Conference on CFD in the Minerals and Process Industries CSIRO, Melbourne, Australia, December (2003).

83. M. Brennan, M. Narasimha, and P. Holtham, “Multiphase Modelling Of Hydrocyclones Prediction of Cut Size”. *Minerals Engineering*, April (2007).

84. R. Darby, “On Two-Phase Frozen and Flashing Flows in Safety Relief Values: Recommended Calculation Method and the Proper Use of the Discharge Coefficient”. *Journal of Loss Prevention in the Process Industries*, July (2004).

85. H. Derlien and L. Friedel, “Accuracy of Safety Valve Two-Phase Mass Flow Capacity Sizing”. *Chemical Engineering and Technology*, (2006).

86. R. Diener and J. Schmidt, “Extended Omega-Method Applicable for Low Inlet Mass Flow Qualities”. *Ludwigshafen, Germany*, June (1998).

87. H. Derlien and L. Friedel, “Reproductive Accuracy of Generic Omega Parameter Safety Valve Two Phase Critical Mass Flow Models Based on Water and Refrigerant R 134a Data”. *Chemical Engineering and Technology*, (2007).

88. W. Elmayyah, “Theoretical and Experimental Investigations of Multiphase Flow in Safety Relief Valves,” *A Thesis Presented For The Degree of Doctor of Philosophy. Department Of Mechanical Engineering, University Of Strathclyde Glasgow*, May (2010).

89. H. K. Fauske, “Sizing Rupture Disks For Two Phase Flow”. *Technical Report*, (1988).

90. H. K. Fauske., “A Practical Approach to Certifying the Capacity of Pressure Relief Valves In Two Phase Flow Service”. *Technical Report*, October (2002).

91. S. Ghorai and K. Nigam, “CFD Modeling of Flow Profiles and Interfacial Phenomena in
Two-Phase Flow in Pipes”. Chemical Engineering and Processing, January (2006).

92. ISO 4126-10 Safety Devices for Protection Against Excessive Pressure – Part 10: Sizing Of Safety Valves and Connected Inlet and Outlet Lines for Gas/Liquid Two Phase Flow *International Organization for Standardization (ISO). Technical Report*, (2004).

93. A. Kendoush, “Thermohydraulic Effects of Safety Relief Valves”. *Experimental Thermal and Fluid Science*, July (1999).

94. S.C. K. De Schepper, G. J. Heynderickx, and G. B. Marin, "CFD Modeling of All Gas Liquid and Vapour Liquid Flow Regimes Predicted By the Baker Chart". *Chemical Engineering Journal,* May (2008).

95. T. Lenzing, L. Friedel, J. Cremers, and M. Alhusein, "Prediction of the Maximum Full Lift Safety Valve Two-Phase Flow Capacity". *Journal of Loss Prevention in the Process Industries,* September (1998).

96. T. Lenzing, L. Friedel, and M. Alhusein, "Critical Mass Flow Rate in Accordance with the Omega-Method of Diers and the Homogeneous Equilibrium". *Journal of Loss Prevention in the Process Industries,* November (1998).

97. J. C. Leung, "A Generalized Correlation for One-Component Homogeneous Equilibrium
Flashing Choked Flow". *AICHE Journal,* (1986).

98. J. C. Leung, "A Theory on the Discharge Coefficient for Safety Relief Valve". *Journal of Loss Prevention in the Process Industries,* July (2004).

99. D. Moncalvo, and L. Friedel, "Reproductive Accuracy of Safety Valve Two Phase Mass Flow Capacity Models in Case of Air/Water, Resp., Viscous Liquid Flow Duty". *Forschungimingenieurwesen,* May (2005).

100. D. Moncalvo,and L. Friedel, "Influence of The Liquid Phase Physical Properties on the Void Fraction At The Inlet of a Full-Lift Safety Valve". *Chemical Engineering and Technology,* (2009).

101. M. Narasimha, M. Brennan, and P. Holtham, "Numerical Simulation of Magnetite Segregation in a Dense Medium Cyclone". *Minerals Engineering,* August (2006).

102. M. Narasimha, M. Brennan, P. Holtham, and T. Napiermunn, "A Comprehensive CFD Model of Dense Medium Cyclone Performance". Minerals Engineering, April (2007).

103. M. Narasimhaa, M. S. Brennanb, P. N. Holthamb, and T. J. Napier-Munn. Science

Direct - Minerals Engineering: “A Comprehensive CFD Model Of Dense Medium Cyclone Performance”. *Minerals Engineering*, (2007).

104. T. Narabayashi, H. Nagasaka, M. Niwano, and Y. Ohtsuki, “Safety Relief Valve Performance for Two-Phase Flow”. *Journal of Nuclear Science and Technology*, (1986).

105. K. Pougatch, M. Salcudean, E. Chan, and B. Knapper, “Modelling of Compressible Gas-Liquid Flow in a Convergent-Divergent Nozzle”. *Chemical Engineering Science*, August (2008).

106. J. Schmidt, and S. Egan, “Case Studies Of Sizing Pressure Relief Valves for TwoPhase Flow. *Chemical Engineering and Technology*, (2009).

107. H. Staedtke, “Gas-Dynamic Aspects of Two-Phase Flow: Hyperbolicity, Wave Propagation Phenomena, and Related Numerical Methods”. *Willyvch Verlag Gmbh and Co. Kgaa, Weinheim,Book,* September (2006).

108. K. Takase, H. Akimoto, and N. Leonid, “Results Of Two-Phase Flow Experiments with an Integrated Ingress-Of-Coolant Event (Ice) Test Facility for Iter Safety”. *Topilski B A Japan Atomic Energy Research Institute, Tokai-Mura, Ibaraki-Ken Japan B IterGarching Joint Work Site*, Boltzmannstrasse 2, D-85748 Garching, Germany, (1998).

109. Q. K. Tran and M. Reynolds,“Sizing Of Relief Valves For Two Phase Flow In Bayer Process”. *Technical Report*, (2002).

110. H. Yoon, M. Ishii, and S. Revankar, "Choking Flow Modeling With Mechanical and Thermal Non-Equilibrium," *International Journal Of Heat and Mass Transfer*, Vol. 49, No. 1-2, Pp. 171-186, Jan. (2006).

111. H. Yoon, M. Ishii, and S. Revankar, "Choking Flow Modeling With Mechanical NonEquilibrium For Two-Phase Two-Component Flow," *Nuclear Engineering and Design*, Vol. 236, No. 18, Pp. 1886-1901, Sep. (2006).

112. C. Mccorquodale, “Investigation into Two Phase Flow Through Safety Valves”*Department Of Mechanical Engineering, University Of Strathclyde Glasgow*, May (2010).

113. V. Kourakos, “Experimental Study and Modeling Of Single- and Two-Phase Flow In Singular Geometries and Safety Relief Valves” *P H D. D I S S E R T A T I O N* To Obtain The Title Of Doctorate Of Science In Engineering. *Faculté Des Sciences Appliquées of the Universitélibre De Bruxelles, Belgium*, October (2011).

114. V. Kourakos, P. Rambaud, J. M. Buchlin, and S. Chabane. "Flowforce in a Safety Relief Valve under Incompressible, Compressible, and Two-Phase Flow Conditions (Pvp2011-57896)." *Journal of Pressure Vessel Technology* 135, No. 1: 011305, (2013).

115. W. Dempster, and W. Elmayyah, “*Two Phase Discharge Flow Prediction In Safety Valves”.International Journal of Pressure Vessels and Piping*, 110. Pp. 61-65. ISSN 0308-0161, (2013).

116. N. I. Kolev, “*Multiphase Flow Dynamics 2 Thermal and Mechanical Interactions”*, 3rd Edition, Springer, ISBN 978-3-540-69834, (2007).

117. H. Lemonnier, and E. S. Camelo-Cavalcanti, “Droplet Size and Velocity at the Exit of a Nozzle with Two Component near Critical and Critical Flow”, *National Heat Transfer Conference*; Atlanta, Ga (United States); 8-11 Aug (1993).

118. T. W. Alger, “Droplet Phase Characteristic in Liquid-Dominated Steam-Water Nozzle Flow”, *PhD Thesis*, Lawrence Livermore Laboratory, University Of California, (1978).

119. F. Mayinger, "Two-Phase Flow Phenomena with Depressurization—Consequences for the Design and Layout of Safety and Pressure Relief Valves." *Chemical Engineering and Processing: Process Intensification* 23, No. 1 (1988): 1-11, (1988).

120. K. H. Ardron, and R. A. Furness, "A Study of the Critical Flow Models Used in Reactor Blowdown Analysis." *Nuclear Engineering and Design* 39, No. 2: 257-266, (1976).

121. K. H. Ardron, "A Two-Fluid Model for Critical Vapour-Liquid Flow." *International Journal of Multiphase Flow* 4, No. 3: 323-337, (1978).

122. E. Elias, and G. S. Lellouche, "Two-Phase Critical Flow." *International Journal of Multiphase Flow* 20: 91-168, (1994).

123. G. B. Wallis, "Critical Two-Phase Flow." *International Journal of Multiphase Flow* 6, No. 1: 97-112, (1980).

124. C. F. Schwellnus, and M. Shoukri, "A Two_Fluid Model for Non_Equilibrium Two_Phase Critical Discharge." *The Canadian Journal of Chemical Engineering* 69, No. 1: 188-197, (1991).

125. R. Dagan, E. Elias, E. Wacholder, and S. Olek, "A Two-Fluid Model for Critical Flashing Flows in Pipes." *International Journal of Multiphase Flow* 19, No. 1: 15-25, (1993).

126. Fluent 6.3 User Guide, (2006).

127. L. Schiller, and Z. Naumann, Z. Ver. Deutsch. Ing.. 77. 318. (1935)

128. W. E. Ranz, and W. R. Marshall, “Vaporation From Drops, Part I”, *Chem. Eng. Prog*.. 48(3). 141–146, March (1952).

129. R. Billet, “*Evaporation Technology”*, Vch, Weinheim, (1989).

130. S. Leuthner, A. H. Maun, S. Fiedler, and H. Auracher, “Heat and Mass Transfer in Wavy Falling Films of Binary Mixtures”, *Int. J. Thermal Sci*., 38(11) Pp. 937-943, (1999).

131. A. Oron, S. H. Davis, and S. G. Bankoff, “Long-Scale Evolution of Thin Liquid Films”. *Rev.Mod. Phys*., 69(3) Pp.931-980, (1997).

132. J.W. Palen, Q. Wang, and J. C. Chen, “Falling Film Evaporation of Binary Mixtures”, *AICHE Journal*, 40(2) Pp. 207-214, (1994).

133. R. Krahl, M. Adamov, M. L. Aviles, and E. Bansch, “A Model for Two-Phase Flow with Evaporation”, *Weierstrab-Institut Fur Angewandte Analysis Und Stochastik (Wias),* ISSN 0946-8633, (2004).

134. K. Karkoszka, “Mechanistic Modelling of Water Vapour Condensation in Presence Of Non-Condensable Gases”, *Doctoral Thesis*, School Of Engineering Sciences, Department Of Physics, Div. Of Nuclear Reactor Technology, Stockholm, (2007).

135. W. E. Dunn, "Modeling of Two-Phase Flows In Horizontal Tubes." *Urbana* 51: 61801, (1996).

136. A. G. Gerber, and M. J. Kermani, "A Pressure Based Eulerian–Eulerian Multi-Phase Model for Non-Equilibrium Condensation in Transonic Steam Flow." *International Journal of Heat and Mass Transfer* 47.10: 2217-2231, (2004).

137. Y. Yang, and S. Shen, "Numerical Simulation on Non-Equilibrium Spontaneous Condensation in Supersonic Steam Flow." *International Communications in Heat and Mass Transfer* 36.9: 902-907, (2009).

138. A. G. Gerber, and A. Mousavi, "Application of Quadrature Method of Moments to the Poly-Dispersed Droplet Spectrum in Transonic Steam Flows With Primary and Secondary Nucleation." *Applied Mathematical Modelling* 31.8: 1518-1533, (2007).

139. D. A. Simpson, and A. J. White, "Viscous and Unsteady Flow Calculations of Condensing Steam In Nozzles." *International Journal of Heat and Fluid Flow* 26.1: 7179, (2005).

140. A. Guha, and J. B. Young, "Time-Marching Prediction of Unsteady Condensation Phenomena Due To Supercritical Heat Addition.” 167-177, (1991).

141. F. Bakhtar, and M. Piran, “Classical Nucleation Theory and Its Application to Condensing Steam Flow Calculations." *Proceedings of the Institution of Mechanical Engineers, Part C: Journal of Mechanical Engineering Science* 219.12: 1315-1333, (2005).

142. A. Guha, "Structure of Partly Dispersed Normal Shock Waves in Vapor_Droplet Flows." *Physics of Fluids A: Fluid Dynamics* 4: 1566, (1992).

143. A. Guha, "A Unified Theory of Aerodynamic and Condensation Shock Waves in Vapour_Droplet Flows with or without a Carrier Gas." *Physics of Fluids* 6: 1893, (1994).

144. X. Zhu, Z. Lin, X. Yuan, T. Tejima, Y. Niizeki, and N. Shibukawa, "Non-Equilibrium Condensing Flow Modeling in Nozzle and Turbine Cascade." *International Journal of Gas Turbine, Propulsion and Power Systems* 4, No. 3 (2012).

145. F-M. Ju, P-G. Yan and W-J. Han, "Numerical Investigation on Wet Steam NonEquilibrium Condensation Flow in Turbine Cascade." *Journal of Thermal Science* 21, No. 6: 525-532, (2012).

146. S. Senoo, and A. J. White, "Numerical Simulations of Unsteady Wet Steam Flows With Non-Equilibrium Condensation in the Nozzle and the Steam Turbine." In *ASME Joint Us-European Fluid Engineering Summer Meeting, Miami, Florida, Usa,* Pp. 757767, (2006).

147. J. Halama, F. Benkhaldoun, and J. Fořt, "Numerical Modeling of Two-Phase Transonic Flow." *Mathematics and Computers in Simulation* 80.8: 1624-1635, (2010).

148. A. Cioncolini, J. R. Thome, and C. Lombardi, “Algebraic Turbulence Modeling In Adiabatic Gas–Liquid Annular Two-Phase Flow.” *International Journal of Multiphase Flow,* Volume 35, Issue 6, Pages 580-596, June (2009).

149. A. Cioncolini, and J. R. Thome, "Algebraic Turbulence Modeling In Adiabatic and Evaporating Annular Two-Phase Flow." *International Journal of Heat and Fluid Flow* 32.4: 805-817, (2011).

150. G. Charless, “An Analytical and Experimental Study of the Flow of Air-Water and Steam-Water Mixtures in A Converging-Diverging Nozzle”, *PhD Thesis,* Engineering, Mechanical, Cornell University, (1968).

151. W. H. Lee, "A Pressure Iteration Scheme for Two-Phase Modeling". Technical Report La-Ur 79-975. Los Alamos Scientific Laboratory, Los Alamos, New Mexico. (1979). (Cited in [126]).

152. I. Tanasawa, "Advances in Condensation Heat Transfer". Advances in Heat Transfer. 21. 55–139. (1991). (Cited in [126]).

153. K. C. D. Hickman, "Maximum Evaporation Coefficient of Water," Eng. Design and Process Development, Vol.46, P. 1442, (1954). (Cited in [150]).

154. O. Hirschfelder, C. F. Curtiss, and R. B. Bird, "Molecular Theory of Gases and Liquids". John Wiley & Sons, New York. (1954). (Cited in [126]).

155. C. Crowe, M. Sommerfeld, and Y. Tsuji, "*Multiphase Flow with Droplets and Particles", Book,* Library of Congress Card Number 97-24341, United State of America, (1997).

156. R. M. Bruce, D. F. Young, and T. H. Okiishi, "Fundamentals of Fluid Mechanics", John Wiley & Sons, *Inc., 5th Edition*, (2004). (Cited in [88])

157. Http://Www.Spiraxsarco.Com/Resources/Pages/Steam-Engineering-Tutorials/Safety-Valves/Introduction-To-Safety-Valves.Aspx, January (2015).

158. Parcol S.P.A. Pressure Safety Relief Valves Technical Bulletin 3.1, Via Isonzo, 2*20010 Canegrate (Mi)- Italy, Issue 03*, (2011).

159. V.D. Rao, V.M. Krishna, K.V. Sharma, and P.V.J.M. Rao, "Convective Condensation of Vapor In The Presence of a Non-Condensable Gas of High Concentration In Laminar Flow In A Vertical Pipe", *Int. J. Heat Mass Transfer 51 (25– 26) 6090–6101*, (2008).

160. J. Kalová,"Termodynamickémodelovánípodchlazenévody." *PhD Thesis*. Czech Republic, (2012).

161. F. Bakhtar, and M. Piran, "Thermodynamic Properties of Supercooled Steam." *International Journal of Heat and Fluid Flow 1*, No. 2: 53-62, (1979).

162. H. A. Moneeb, H. Salmawy, A. H. El-Kholy, K. M. Shebl, and A. El-Lathy. "Computational and Experimental Study for Droplet Behavior under Flashing Condition." *In Tenth International Congress of Fluid Dynamics, Icfd10-Eg-3153.* (2010).

Appendices:

Appendix A: The Safety Relief Valve CAD Drawings

The Safety Relief Valve CAD drawings details studied in this thesis cannot be presented here as this will strictly require a permission from the valve's manufacturer.

For more information please conatct Dr. William Dempster at william.dempster@strath.ac.uk, or Moftah Alshaikh at Alsheak_2005@yahoo.com.

Appendix B: Details of the new modified tube used for back pressure measurement

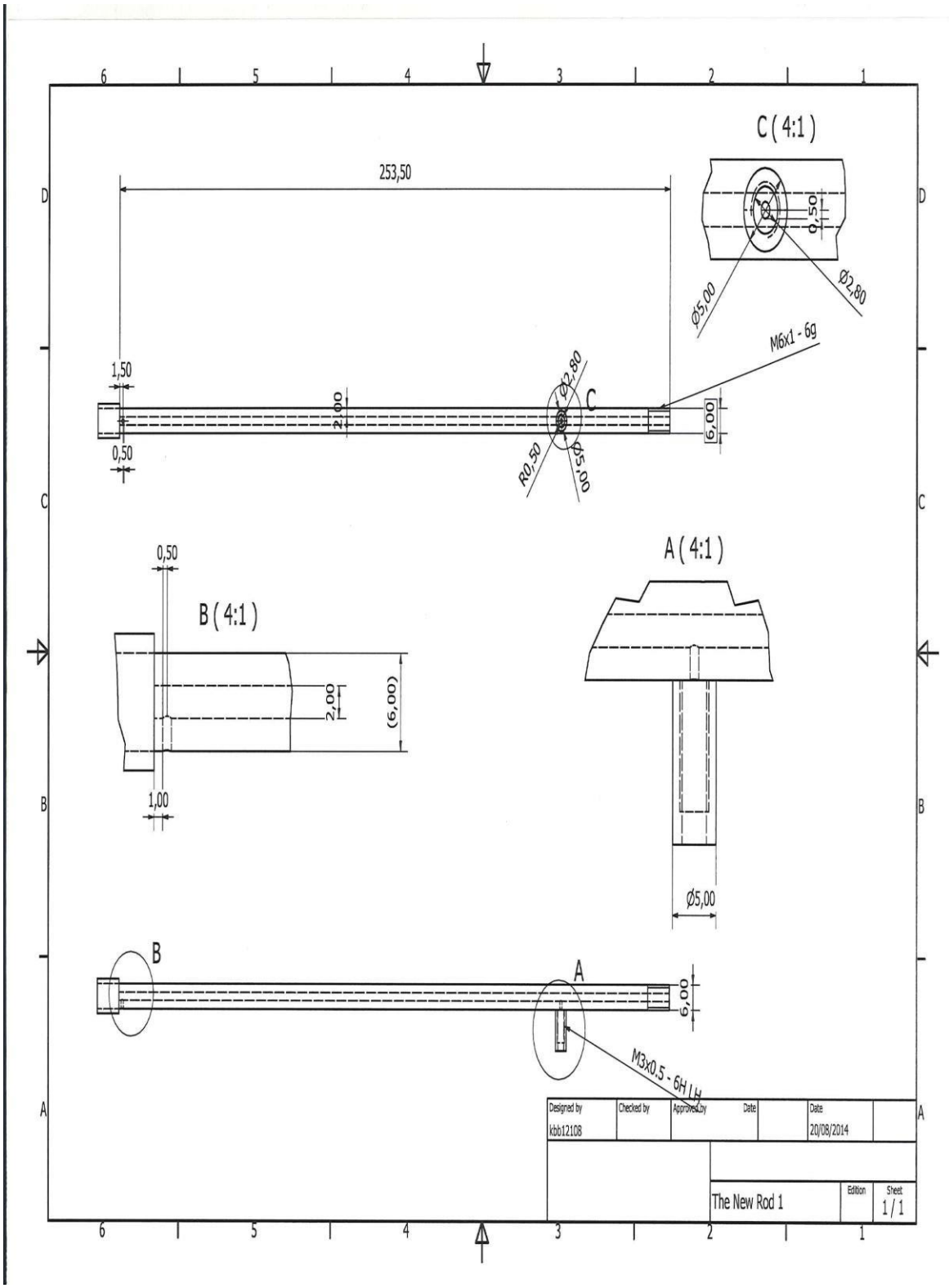

Appendix C: The dimension of the injection system " adapted from [112]"

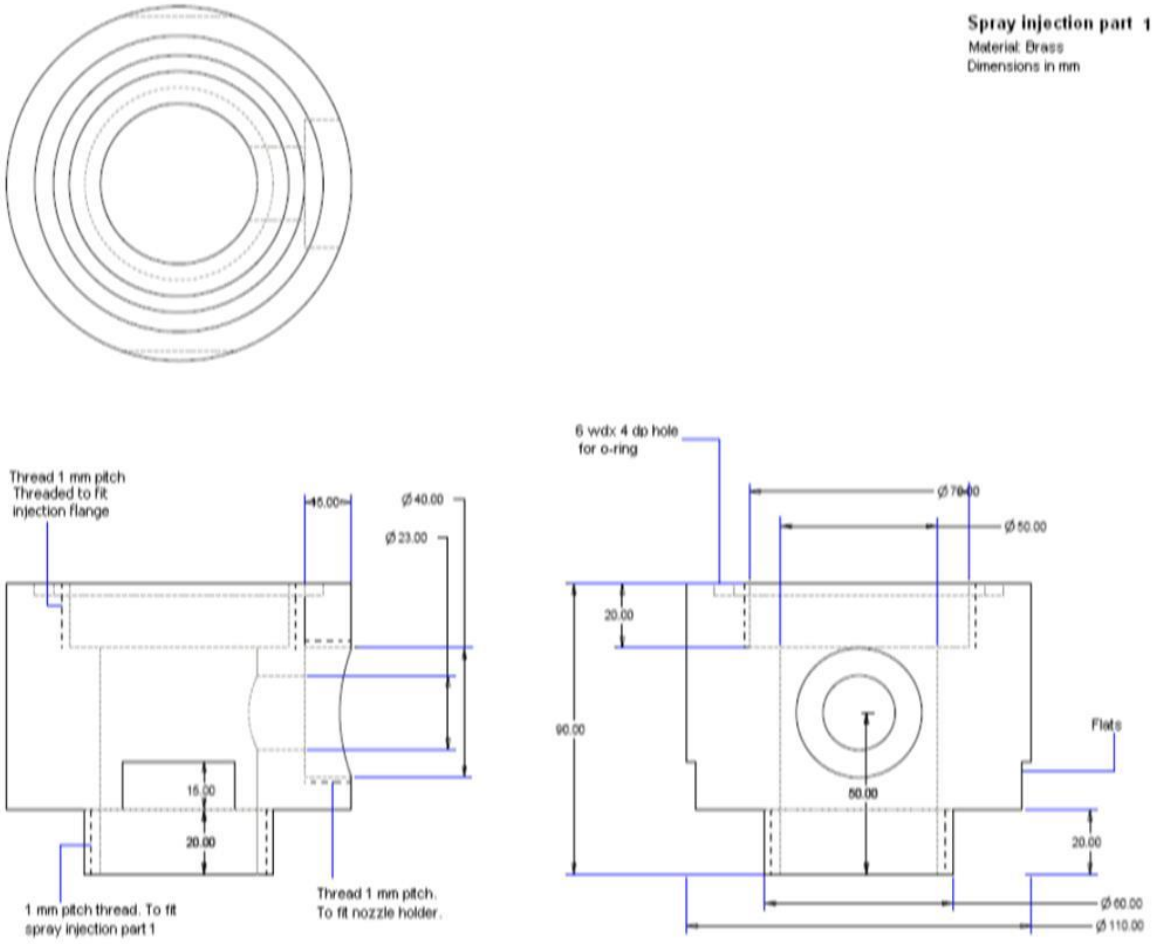

Spray injection part 2
Material: Brass
Dimensions in mm

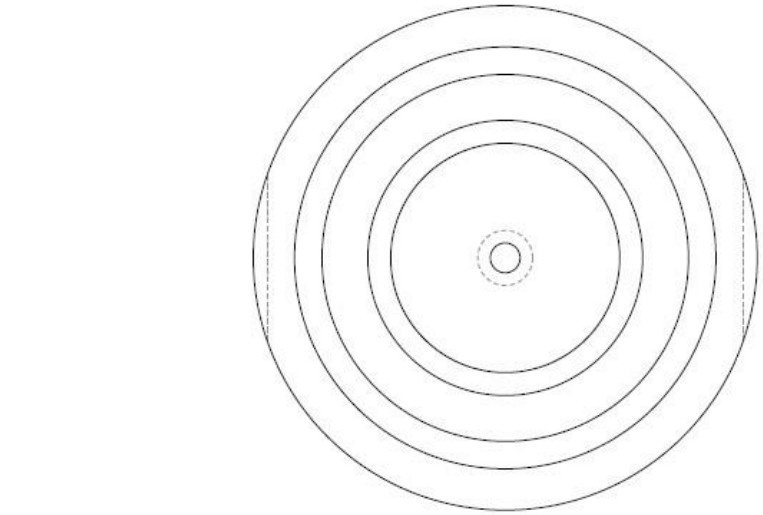

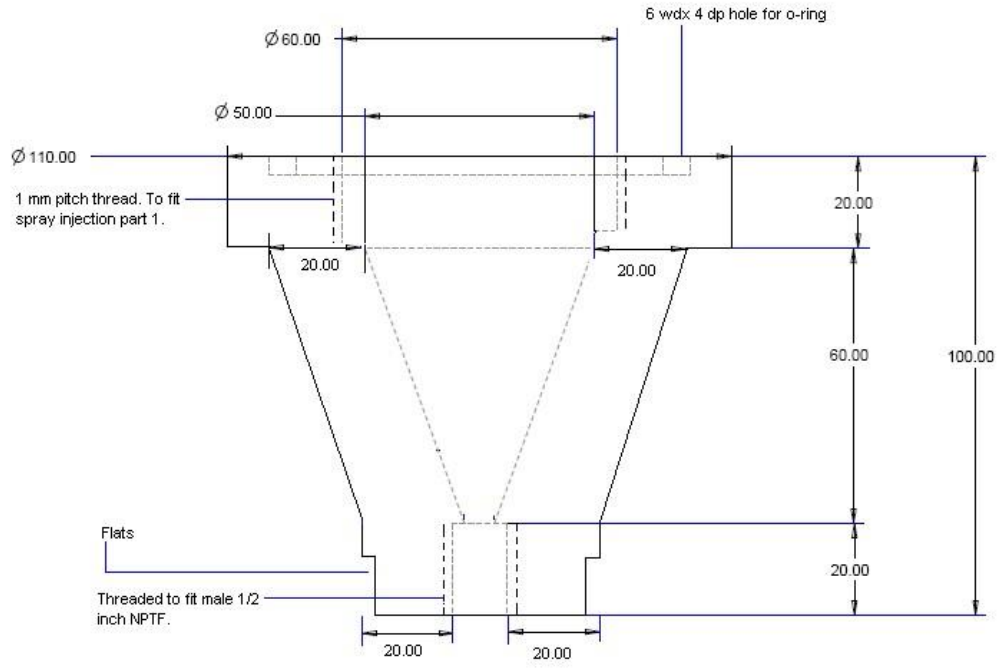

Appendix D:Details of Charless's experimental facility [150]

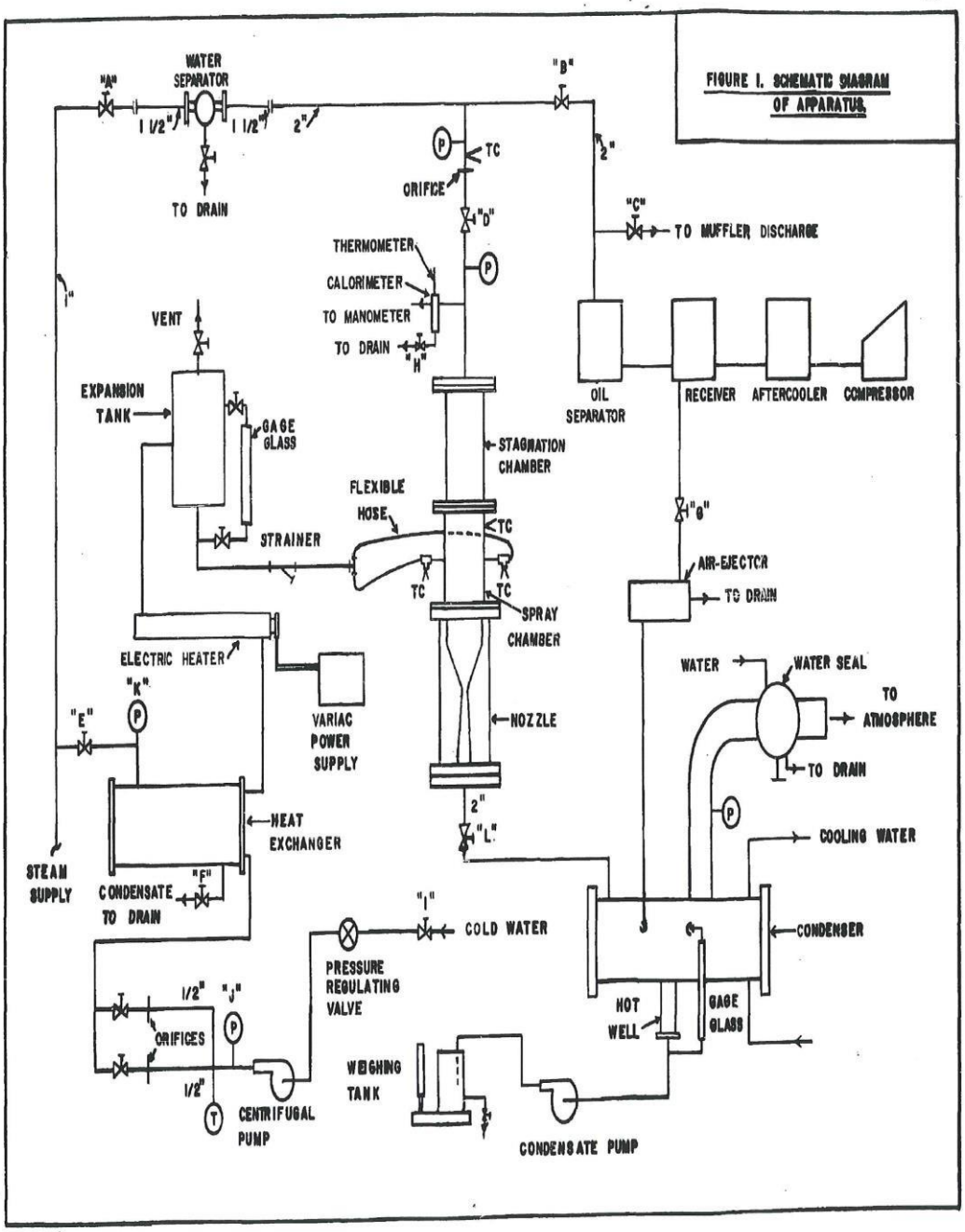

Appendix E:The dimensions of the modified gland

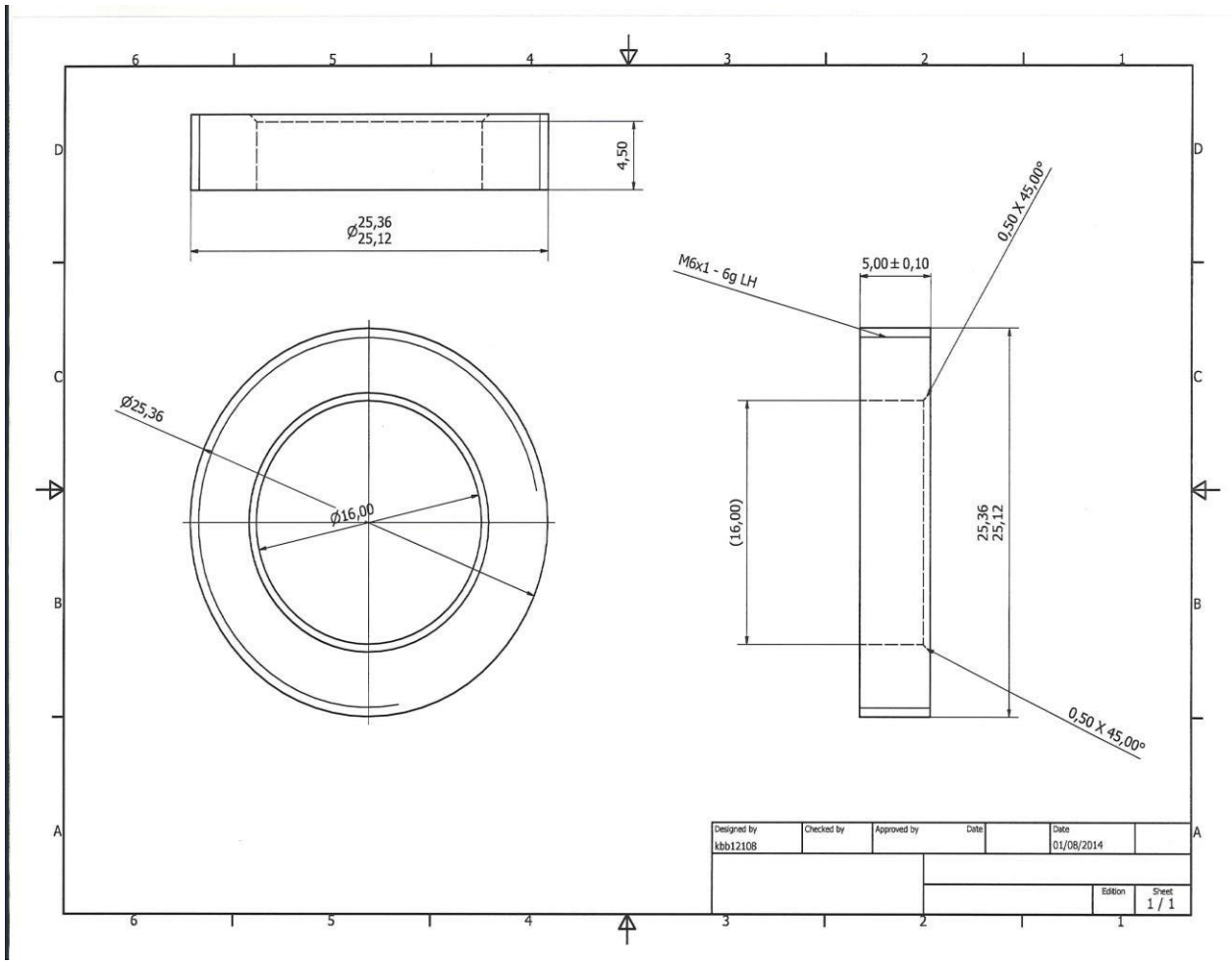

Appendix F: The magnitude of total pressure loss in the liquid injection nozzle upstream of the safety valve and how it might influence the results has been assessed and reported as the following:

A Case study: for two phase flow of air/water conditions at an upstream inlet total pressure (P_0) of 10.3 barg and a liquid mass fraction of 70%, at a valve lift of 5 mm with the adjusting gland in place.

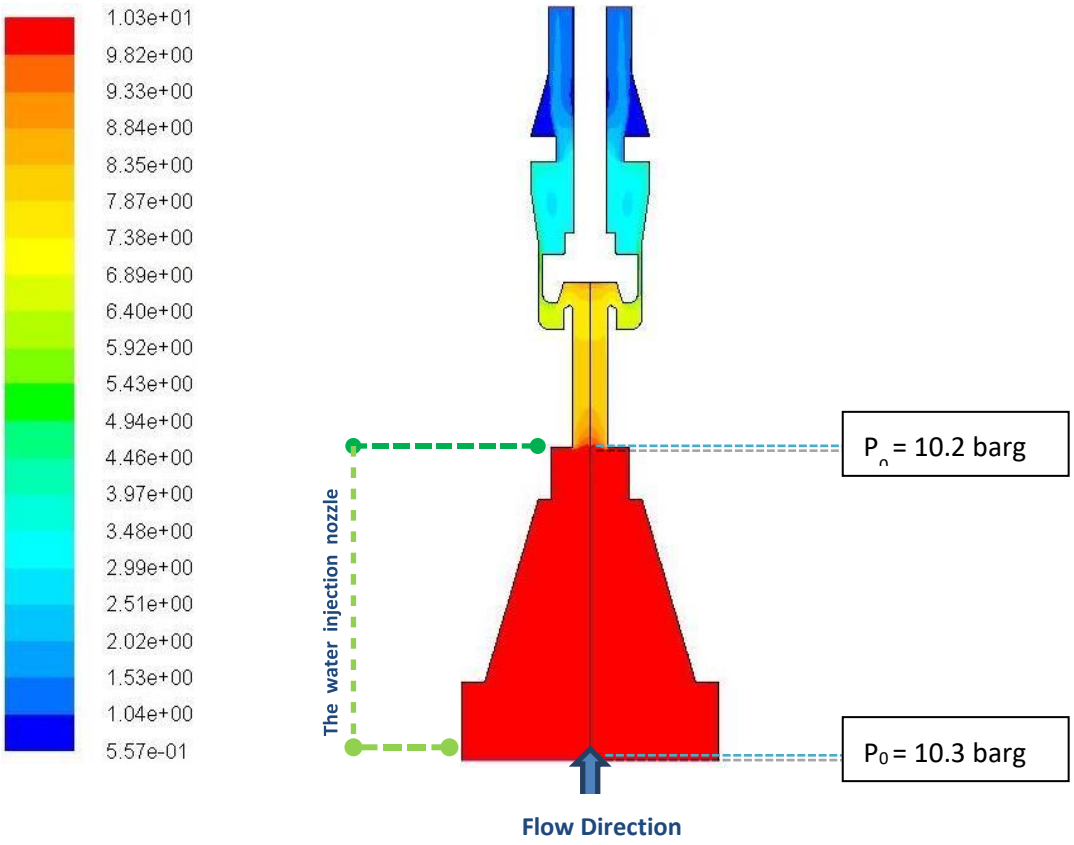

Figure F-1: Contours of total pressure at 10.3 barg and a liquid mass fraction of 0.7

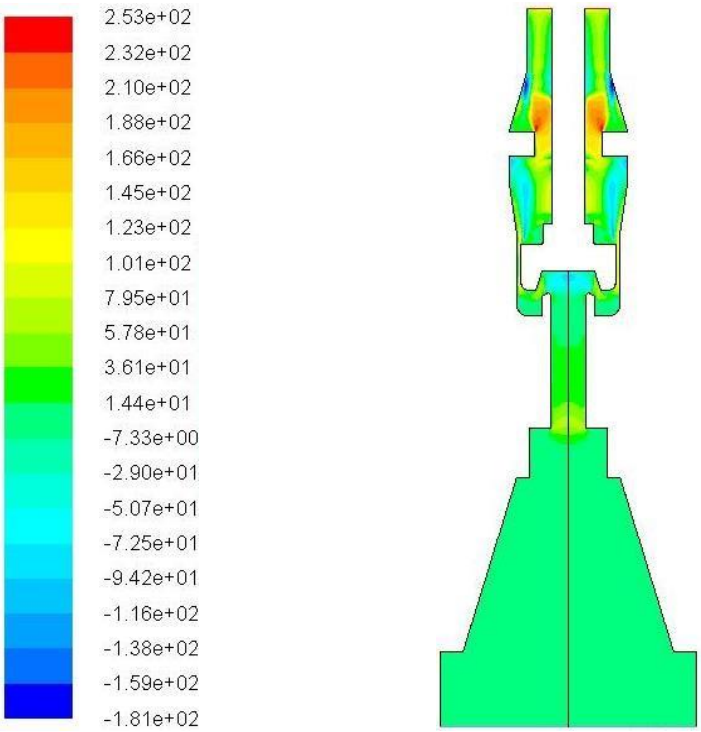

Figure F-2: Contours of slip (m/s) at 10.3 barg and a liquid mass fraction of 0.7

Figure F.1 shows contours of the stagnation pressure at an upstream inlet pressure of 10.3 barg and a liquid mass fraction of 0.7, and a 5mm piston displacement. As it can be seen from the figure there is a total pressure loss of approximately 0.98%, between the inlet of the water injection system and the inlet of the valve. The mass flow discharged and the associated net piston force exerted on the piston have been examined and found to be slightly influenced by how the inlet boundary conditions are represented. In other words, the above mentioned two phase flow conditions of the valve were tested for the valve with and without the water injection system. Figure F.2 presents contours of slip at an upstream inlet pressure of 10.3 barg and a liquid mass fraction of 0.7. The figure shows low slip velocity between the air and water in the converging section (which represents the water injection system). From the figure, the slip velocity in the water injector is in the range of 14-36 (m/s). However, the results of a comparison between CFD calculations based on the two scenarios of the valve and experimental results are presented in Tablef.1. With the water injection nozzle in place, the air mass flowrate is found to be slightly still overpredicted by approximately 3.5%, and the net piston force is also overpredicted by7.2%.

Therefore having the water injection nozzle modelled would improve the accuracy of predictions but increases computational time to achieve convergence (approximately more than 25 mins).

Table F.1: The flow and force results at an upstream inlet pressure of 10.3 barg and a liquid mass fraction of 0.7

Parameter	Valve with the water injection nozzle (CFD)	Valve withOUT the water injection nozzle (CFD)	Experimental
Air mass flowrate (Kg/s)	0.0561	0.0566	0.0542
Air mass flow Error (%)	3.5%	4.4%	-
Net piston force (N)	135	138	126
Net piston force Error (%)	7.2%	9.5%	-

Important Notes:

1. *The above total pressure (P_0)calculation is achieved according to the work of Guha [143], based on the following expression:*

$$\frac{P_0}{P_\infty} = \left[1 + \frac{1}{2}(\gamma - 1)M^2\right]^{\gamma/(\gamma-1)}$$

The value of γ is, in general, less than 1.32 which is the isentropic exponent for the gas phase alone. Therefore it has been considered for this calculation as 1.12 (mixture two –phase flows)

Where the equilibrium Mach number can be calculated as $M = V/a$, Hence the equilibrium speeds of sound (a) is given by $a = (\gamma(1 - x)R\,T)^{1/2}$

Where: x the mass fraction of dispersed phase, R specific gas constant, T gas temperature, V mixture velocity, P_∞ the upstream inlet pressure.

2. *This part of the corrections is added to the thesis through this appendix, with a short introduction is added to the relevant chapter in Section 5.3.3 , which explains the reason for checking such an issue as well as the justification for using no nozzle. However, all we are doing here is showing the effect of the nozzle for our boundary conditions. The actual effect of the real injector is not examined due to a difficulty in representing the second phase (the liquid phase) on the Euler-Euler two phase flow approach based on separate inlet boundary conditions (code coupling problems as stated clearly on the thesis), but alternatively it has been represented as a dispersed phase based on a liquid volume fraction.*

Appendix G: The HNED-DS model equations, as presented in [88]

Ideal mass flux

$$G = K_d\, C \sqrt{2\frac{P_o}{v_o}} \tag{A.2.1}$$

Discharge coefficient

$$K_d = \alpha_{seat}\, K_{dg} + (1 - \alpha_{seat})\, K_{dw} \tag{A.2.2}$$

$$\alpha_{seat} = 1 - \frac{v_l}{v_o \left[\omega\,(\frac{1}{\eta} - 1) + 1\right]} \tag{A.2.3}$$

Compressibility factor for non flashing flow

$$\omega = \frac{1}{\gamma}\,\frac{x.v_{go}}{v_o} \tag{A.2.4}$$

Critical pressure ratio η

$$0 = \eta_{crit}^2 + (\omega^2 - 2\omega)(1 - \eta_{crit})^2 + 2\omega^2 ln(\eta_{crit}) + 2\omega^2(1 - \eta_{crit}) \tag{A.2.5}$$

flow coefficient C

$$C = \frac{\sqrt{\omega\, ln(\frac{1}{\eta}) - (\omega - 1)(1 - \eta)}}{\omega\,(\frac{1}{\eta} - 1) + 1} \tag{A.2.6}$$

Where for critical flow,

$$\eta = \eta_{crit} \tag{A.2.7}$$

The mixture specific volume

$$v_o = x_o\, v_{go} + (1 - x_o) v_{lo} \tag{A.2.8}$$

Mass flow quality

$$x_o = \frac{\alpha_o \, v_{lo}}{(1-\alpha_o)\, v_{go} + \alpha \, v_{lo}} \tag{A.2.9}$$

Slip factor

$$\phi = \sqrt{\frac{v_o}{v_l}} \left\{ 1 + x_o \left[(\frac{v_{go}}{v_l})^{\frac{1}{6}} - 1 \right] \left[1 + x_o \left[(\frac{v_{go}}{v_l})^{\frac{5}{6}} - 1 \right] \right] \right\}^{-\frac{1}{2}} \tag{A.2.10}$$